

Diss. ETH Nr. 13436

MOLECULAR WEIGHT DISTRIBUTION AND GEL FORMATION IN EMULSION POLYMERIZATION

A dissertation submitted to the
SWISS FEDERAL INSTITUTE OF TECHNOLOGY ZURICH (ETHZ)
for the degree of
Doctor of Technical Sciences

Presented by

Alessandro Ghielmi

Dottore in Ingegneria Chimica, Politecnico di Milano,
born August 9, 1971
Citizen of Italy

Accepted on the recommendation of

Prof. Dr. M. Morbidelli, examiner

Dr. J. Congalidis, co-examiner

Dr. G. Storti, co-examiner

Zurich 1999

Contents

1	Introduction	1
1.1	Emulsion Polymers and Modeling of their Molecular Properties	1
1.2	This Work - Motivation and Outline	3
1.3	Emulsion Polymerization	5
2	Model Development and Results	11
2.1	Introduction	11
2.2	Kinetic Scheme and Basic Assumptions	12
2.3	Model Equations	15
2.3.1	Singly Distinguished Particles	15
2.3.2	Doubly Distinguished Particles	18
2.3.3	Polymer Formed by Monomolecular Termination	20
2.3.4	Polymer Formed by Combination	21
2.3.5	Evaluation of the Double Bonds in the Polymer Chains	22
2.3.6	Numerical Solution of the Model	23
2.4	Correct Inclusion of the Desorption Mechanism	23
2.4.1	Smith-Ewart Equations	25
2.4.2	Singly Distinguished Particles	26
2.4.3	Doubly Distinguished Particles	29
2.4.4	Terminated Chains	30
2.5	Model Results: Instantaneous Properties	30
2.5.1	Crosslinking Reaction	32
2.5.2	Propagation to TDB Reaction	37
2.6	Model Results: Cumulative Properties	41
2.6.1	Crosslinking Reaction	41
2.6.2	Propagation to TDB Reaction	45

2.7	Gelation: a Comparison with Flory's Statistical Theory	46
2.8	Conclusions	50
3	Fractionation Techniques for the Solution of Molecular Weight Distribution Equations	53
3.1	Introduction	53
3.2	Kinetic Scheme and Molecular Weight Equations	55
3.3	Model Solution	57
3.3.1	Detailed Solution	57
3.3.2	Overall Method of Moments	58
3.3.3	Partitioning According to the Number of Branches (PANB)	59
3.3.4	Numerical Fractionation	59
3.4	Gel Weight Calculation	62
3.5	Results and Discussion	63
3.5.1	Base Cases	63
3.5.2	Bimolecular Termination by Disproportionation	64
3.5.3	Bimolecular Termination by Combination	71
3.6	Conclusions	79
4	Effects of Compartmentalization on Molecular Weight Distribution and Gel Formation	81
4.1	Introduction	81
4.2	Model Summary	82
4.2.1	Correct Model	82
4.2.2	Approximate Model	82
4.3	Illustrative Calculations	84
4.3.1	Instantaneous Properties	84
4.3.2	Cumulative Properties	93
4.4	Analysis of the Assumption of Independence of the Two Lengths of a Pair of Chains	99
4.5	Case Studies	104
4.5.1	Styrene	105
4.5.2	Methyl Methacrylate	105
4.5.3	Vinyl Acetate	105

4.6	Singly Distinguished Particle Approach Adapted to the Features of Radical Compartmentalization	108
4.6.1	Concepts	108
4.6.2	Equation Development	111
4.6.3	Equation Solution in Terms of Moments	117
4.6.4	Results	118
4.7	Conclusions	123
5	Model Application to Experimental Systems - Vinyl Chloride and Vinyl Acetate	125
5.1	Introduction	125
5.2	Model for the Kinetics	126
5.2.1	Entry, Desorption and Bimolecular Termination Frequencies. Distribution of Radicals in the Particles	126
5.2.2	Monomer Concentration in the Particle Phase	128
5.2.3	Rate of Reaction	129
5.3	Vinyl Chloride Polymerization	130
5.3.1	Parameters	130
5.3.2	Results	130
5.4	Vinyl Acetate Polymerization	132
5.4.1	Parameters	132
5.4.2	Results	133
5.5	Conclusions	139
6	Model Application to an Experimental System - Butyl Acrylate	143
6.1	Introduction	143
6.2	The RC1 Reaction Calorimeter	145
6.2.1	The Instrument	145
6.2.2	The Energy Balance	146
6.3	Experimental	150
6.4	Data Evaluation	154
6.4.1	Conversion by Calorimetry	154
6.4.2	Conversion by Gravimetry	155
6.4.3	Polymer Particle Concentration	156
6.4.4	Average Number of Free Radicals per Particle	156

6.4.5	Parameters	158
6.5	Results and Discussion	158
6.5.1	Ab Initio Reactions - Kinetics	158
6.5.2	Ab Initio Reactions - Gel Formation	164
6.5.3	Seeded Reactions - Kinetics	167
6.6	Model Interpretation	173
6.6.1	Parameters	173
6.6.2	Model Results	176
6.7	Conclusions	184
	Conclusions	187
	Bibliography	191
	Notation	201
	Abbreviations	209
	Appendices	211
A	Model Solution	211
A.1	Numerical Fractionation	211
A.2	Fractionated Population Balance Equations	212
A.3	Fractionated Moment Equations	216
B	Relation Between Cumulated and Instantaneous Properties	223
C	Non-compartmentalized Model	225
D	Derivation of the Overall Moment Equations for a Bulk System	227
E	Fractionated CLD Equations for a Bulk System	229
F	Monomer Diffusion Limitations in Butyl Acrylate Emulsion Polymerization	231
G	Publications Derived from this Work	239
	Curriculum Vitae	241

Abstract

In this work a kinetic model for the molecular weight calculation of polymers produced in emulsion is developed. The model is original in that it accounts for active chain compartmentalization and at the same time for all branching mechanisms. Active chain compartmentalization is accounted for by using the concept of ‘doubly distinguished particle’ distribution. This distribution represents the length distribution of the pairs of chains belonging to the same particles. The branching mechanisms are described using the concept of ‘pre-life’, which represents the length of an active chain given by the monomer units which were added by propagation during previous growth periods. The pre-life concept had already been previously used for chain transfer to polymer, but it is extended to describe the very different step-growth mechanism related to crosslinking and terminal double bond propagation. The dimensionality of the problem is therefore not enhanced.

The population balance equations which result from the description of the molecular weight distribution are solved by means of the numerical fractionation (NF) technique. An analysis of the performances of NF is carried out by comparing to the results of a detailed model. It is shown that in some cases NF predicts the appearance of fictitious shoulders in the high molecular weight tail of the molecular weight distribution. In these cases, partitioning the polymer according to the number of branches gives very accurate solutions with limited numerical effort. A fast procedure is proposed to determine the number of branches to be used.

The nature of radical compartmentalization and its effects on the MWD are investigated. Compartmentalization is found to result in pairwise correlation of the lengths of the active chains belonging to the same particle for average number of radicals per particle typical of emulsion polymerization. This correlation needs to be accounted for in molecular weight modeling when combination is present. Approximate models neglecting this peculiar feature of compartmentalization may lead to large errors in the prediction of the polymer polydispersity, especially when branching and combination provide a mechanism which can lead to the formation of large branched chains (and eventually to gel). It is shown that the effect of compartmentalization is to delay this polydispersity increase and gel formation. This is due to the segregation of branched radicals in the particles, which prevents them from combining to form very large (gel) molecules.

The model is applied to describe literature molecular weight data from vinyl chloride and vinyl acetate emulsion polymerizations. In both cases it provides a deeper understanding of the mechanisms underlying these polymerization reactions.

Finally, butyl acrylate emulsion polymerizations experiments are analysed. This monomer system typically gives gel formation at very low conversions in bulk polymerization. Instead, gel is found to be formed in emulsion only at high conversions, above 70-80% conversion. This provides strong support for the validity of the model predictions.

Sommario

In questo lavoro viene sviluppato un modello per il calcolo del peso molecolare di polimeri prodotti in emulsione. L'originalità del modello risiede nel fatto che esso tiene conto della compartimentalizzazione delle catene attive e di qualsiasi meccanismo di ramificazione nel contempo. Della compartimentalizzazione delle catene attive si tiene conto facendo uso del concetto di distribuzione delle 'particelle doppiamente distinte'. Quest'ultima rappresenta la distribuzione delle lunghezze delle coppie di catene contenute nella stessa particella. I meccanismi di ramificazione sono descritti usando il concetto di 'vita pregressa', che rappresenta la lunghezza di una catena attiva data da quelle unità monomeriche aggiunte per propagazione in periodi di crescita precedenti. Il concetto di vita pregressa è stato usato in precedenza per la reazione di trasferimento a polimero, ma viene qui esteso a descrivere il diverso meccanismo di crescita discontinua dato dalle reazioni di 'crosslinking' e di propagazione a doppio legame terminale. La dimensione del problema non viene così aumentata.

Le equazioni di bilancio di popolazione che derivano dalla descrizione della distribuzione di peso molecolare sono state risolte utilizzando la tecnica di 'frazionamento numerico'. Un'analisi delle prestazioni di questa tecnica è stata condotta paragonando i risultati a quelli di un modello dettagliato. Si mostra che in alcuni casi il frazionamento numerico dà origine alla comparsa di spalle fittizie nella coda ad alti pesi molecolari della distribuzione di peso molecolare. In questi casi, frazionare il polimero secondo il numero di rami permette di ottenere soluzioni molto accurate con uno sforzo numerico ridotto. Un procedimento rapido viene proposto per determinare il numero di rami appropriato.

La natura della compartimentalizzazione dei radicali attivi e i suoi effetti sulla distribuzione di peso molecolare sono stati investigati. Si è trovato che la compartimentalizzazione ha come risultato la correlazione a coppie delle lunghezze delle catene attive appartenenti ad una stessa particella per valori del numero medio di radicali per particella tipici di una polimerizzazione in emulsione. Di questa correlazione è necessario tenere conto nella modellazione dei pesi molecolari qualora sia presente la terminazione per combinazione. Modelli approssimati che ignorano questa caratteristica specifica della compartimentalizzazione possono dare grandi errori nella predizione della polidispersità del polimero, specialmente quando la ramificazione e la combinazione costituiscono un meccanismo che può portare alla formazione di grosse catene ramificate (e infine di gel). Si mostra che la compartimentalizzazione ha l'effetto di ritardare questo incremento di polidispersità e la formazione del gel. Ciò è dovuto alla segregazione dei radicali ramificati

nelle particelle, di modo tale che la loro combinazione a formare molecole molto grandi (eventualmente di gel) viene impedita.

Il modello é stato utilizzato per interpretare dati di letteratura di polimerizzazioni in emulsione di cloruro di vinile e di acetato di vinile. In entrambi i casi esso fornisce una comprensione piú approfondita dei meccanismi che stanno alla base di queste reazioni di polimerizzazione.

Infine, si sono analizzate reazioni di polimerizzazione in emulsione di acrilato di butile. Questo monomero, polimerizzato in massa, dá tipicamente formazione di gel a conversioni molto basse. Al contrario, si é trovato che il gel si forma in emulsione solo ad alte conversioni, sopra il 70-80%. Ciò fornisce un valido supporto alla correttezza delle predizioni del modello.

Chapter 1

Introduction

1.1 Emulsion Polymers and Modeling of their Molecular Properties

Emulsion polymerization is a process of significant economical importance. Of the over 10^8 tonnes of polymers produced per year in the Western countries alone, about 15% are produced via emulsion polymerization [1]. Polymers made by this process include both commodity materials (e.g. synthetic rubber, latex paints and adhesives) and high added value products (e.g. diagnostic kits for biomedical application).

Nonlinear polymers are mostly encountered among commercial emulsion polymers. Typical examples are vinyl-divinyl systems such as butadiene homo or copolymers, polychloroprene and branched polymers such as polyvinylacetate and certain polyalkylacrylate and ethylene copolymers. In this case the emulsion technique, besides offering the usual advantages of low viscosity and no solvent use, constitutes sometimes a direct method for the buildup of crosslinked microspheres interesting for various applications [2].

The use of an emulsion polymerization for polymer synthesis strongly affects the properties of the final product. This is true not only due to the impurities, mainly emulsifier and buffer agent, which may be included in the polymer and which may constitute a drawback of the process, but also and especially because of the impact of the process on the molecular structure. As a matter of fact, it is well known that the mechanical, thermal and rheological properties of a polymer depend upon its microstructure, where this term includes molecular weight in all cases, composition and sequence distribution in the case of a copolymer, number and arrangement of branches or crosslinkages in the case of nonlinear chains. If the polymer is not constituted by chains identical in structure, as it normally happens, what counts is in principle the distribution of these properties, though often relation to average properties is sought for the sake of simplicity. In the case of gel containing polymers (with the gel defined as a polymer network formed as a result of

extensive branching or crosslinking, which is usually swollen by solvents but does not dissolve in non-destructive solvents) it has been reported that the amount of gel also influences a large number of properties of the polymer [3].

Considering the significant effect of the microstructure of the chains and of the eventual presence of gel on the properties of practical interest of the polymer, it is apparent that models including the calculation of the characteristics of the polymer on the microscale represent valuable tools for process development and optimization. In the frame of emulsion polymerization, a general model including branching mechanisms and gel formation and correctly accounting for the peculiar aspects of the emulsion reaction system is still missing.

The calculation of the molecular weight distribution (MWD) of linear polymers produced in emulsion has received considerable attention in the literature. After the works by Gardon [4] and Katz et al. [5] and the more general model developed by Min and Ray [6], a convenient and effective approach to the problem appeared in 1980 in a paper by Lichti et al. [7], where the concepts of ‘singly’ and ‘doubly distinguished particles’ were introduced in order to calculate the length distribution of the polymer chains, properly accounting for radical compartmentalization. With the term ‘compartmentalization’, the fact is indicated that in emulsion polymerization the radicals grow segregated in the polymer particles (see Section 1.3). This implies that the radicals growing in one particle cannot interact with those growing in another particle, which has a significant effect on the kinetic behavior and the molecular weights obtained. A solution to the problem of the MWD calculation which is substantially equivalent to that of Lichti et al., but based on the mathematics of Markov chains, was presented by Storti et al. [8]. More recently Clay and Gilbert [9] considered the case of rate coefficients depending on chain length.

With reference to branched and crosslinked polymers in homogeneous systems (bulk and solution polymerizations), a great number of models has been developed for the prediction of their microstructural properties, such as crosslinking densities and MWDs, and the possibility of gel formation. Following the works by Flory [10, 11, 12] and Stockmayer [13, 14], several statistical models appeared in the literature. More recently, greater effort has been devoted to the development of kinetic models. Such models can account for the fact that polymerizations are usually kinetically controlled, so that chains experiencing during the reaction different histories in terms of reaction conditions exhibit in general different structures. A rather exhaustive treatment by Hamielec and coworkers, involving the use of population balance equations (PBEs), permits both the calculation of molecular weights [15, 16, 17] and the prediction of gelation [18] in the presence of various branching

mechanisms.

The case of nonlinear polymers produced in emulsion is more complicated because the difficulties related to the description of the formation of nonlinear chains add on to the complexities related to the description of the heterogeneous emulsion polymerization system. No satisfactory kinetic model has been developed so far. In some cases [19, 20, 21] active chain compartmentalization is completely ignored. Arzamendi et al. [22, 23] developed a model which accounts for different rates of reaction in particles containing a different number of radicals, but fails in describing correctly the length of the chains produced through bimolecular termination by combination [24]. Accordingly, the effect of compartmentalization is only partially accounted for. A model for branched chains correctly describing radical compartmentalization through the distinguished particle approach developed by Lichti et al. [7], has been proposed by Ghielmi et al. [24]. This model, however, considers a single long-chain branching mechanism, namely chain transfer to polymer, and allows transport from the polymer particles to the water phase ('desorption' or 'exit') of active polymer chains of any length with the same rate, which is physically unreasonable.

An alternative approach proposed by Tobita et al. [25] for the MWD evaluation of polymers produced in emulsion is based on the Monte Carlo method. As it is typical for all models based on this method, this approach allows to manage very complex processes (such as the emulsion polymerization of nonlinear chains, accounting also for chain length dependent coefficients and non steady-state conditions) at the expenses of a rather significant computational effort. Moreover, such techniques make it often difficult to achieve an understanding of the physical meaning of the obtained results even in simple limiting cases where kinetic models admit analytical solutions.

1.2 This Work - Motivation and Outline

This work originates from the lack in the literature of a comprehensive kinetic model for the molecular weight calculation of polymers produced in emulsion, accounting at the same time for active chain compartmentalization and for the formation of nonlinear chains through the various possible branching mechanisms. As a matter of fact, a proper kinetic model existed only for linear chains [7]. Moreover, it is thought that the mechanism through which compartmentalization acts on the final MWD of the polymer requires better understanding, especially in the case of branched polymers.

The work is organized as follows. After recalling basic fundamentals on emulsion polymerization in the present introductory Chapter, a kinetic model is presented (Chap. 2),

which accounts for radical compartmentalization in the calculation of the molecular weight and branching distribution of a nonlinear polymer produced in emulsion. The approach adopted for the model development is analogous to that used by Ghielmi et al. [24]. However, the present model has a wider generality. All the known intermolecular mechanisms responsible for nonlinear chain formation are considered. In particular, inclusion of the crosslinking and propagation to terminal double bond (TDB) reactions is accomplished through a specific procedure, developed in this work, which takes advantage of the same description parameters already introduced for chain transfer to polymer [24]. Therefore, the complexity of the modeling is not enhanced.

Furthermore, a more acceptable description of radical desorption is adopted, which agrees with the common treatment of this mechanism in the literature [26, 27, 28, 29]. The model can therefore be safely applied to polymerization systems with significant rates of radical exit.

Some results of the model are shown in order to demonstrate its capabilities and features and to illustrate the effects of radical compartmentalization by comparison to a non-compartmentalized system (represented by a ‘pseudo-bulk’ model).

Besides developing more general and complete model equations, the approximate numerical techniques used for their solution are discussed and their reliability assessed (Chap. 3). This assessment is carried out referring to a bulk system, where accurate reference solutions are easier to obtain. However, the conclusions reached can be confidently extended to the emulsion system, due to the similar peculiar aspects exhibited by the approximate solution methods in homogeneous [30] and segregated [24] systems.

In Chap. 4 the developed model is used to better understand, also by comparing with a simplified model, the nature of radical compartmentalization. This is shown to consist in the presence in the polymerization locus of two radical populations with different characteristics, so that the active chains are pairwise correlated in length. This kind of knowledge on the features of compartmentalization is important because it permits to identify proper conditions for desired molecular weights. Moreover, it allows the development of simpler models which, besides accounting properly for the compartmentalization effects, allow more easily the inclusion of other effects, such as chain-length dependent rate coefficients, non-steady-state conditions, etc. The bases for the development of such a model are given.

In the final Chaps 5 and 6, the model is applied to the description of some emulsion polymerization systems of practical interest, namely vinyl acetate (VAc), vinyl chloride (VC) and butyl acrylate (BA). A comparison is made with experimental conversion, aver-

age molecular weight, MWD and gel fraction data. Molecular weight data for poly(vinyl chloride) (PVC) and poly(vinyl acetate) (PVAc) were taken from the literature, while gel fractions of poly(butyl acrylate) (PBA) were determined with the aim of providing meaningful data for the validation of the model presented in this work.

1.3 Emulsion Polymerization

In an emulsion polymerization process, water and emulsifier are added to the monomer species that must be polymerized. The surfactant molecules dispose themselves at the interface between the organic and the water phase and stabilize the monomer droplets which are formed by stirring. Thus, a heterogeneous system is formed where the continuous phase is the aqueous phase. To induce the beginning of the polymerization a water-soluble initiator is usually added (though addition of a lipophilic initiator is also possible [31]). Accordingly, polymerization is induced by radicals forming in the water phase and diffusing to the organic phase, where the polymerization occurs.

The course of a batch emulsion polymerization is usually represented through a three-interval scheme first proposed by Harkins [32]:

Interval I

At the beginning of the reaction, before the initiator is charged to the reactor, the system is constituted by monomer droplets suspended in the continuous water phase and stabilized by the surfactant. However, if enough surfactant has been added, and this is the usual case, other entities are also present in the system. These are very small aggregates, named micelles, constituted by surfactant molecules which dispose themselves with the hydrophilic part towards the water and the hydrophobic tail inwards. As the micelles are very small and numerous, thus presenting a very high surface per unit volume of emulsion, when a water-soluble initiator is introduced, the radical species formed in the water phase enter preferentially the micelles rather than the monomer droplets. Since some molecules of monomer swell the organic inside part of the micelle, as soon as a radical enters, polymerization starts inside the micelle. Accordingly, many of the micelles are transformed into very small polymer particles. These are swollen by the monomer diffusing from the monomer droplets through the aqueous phase (the monomer actually has a very small but finite solubility in water). The radicals keep on entering and polymerizing in the so-formed polymer particles and in the micelles rather than in the monomer droplets. As a consequence, more and more micelles are transformed into polymer particles and the

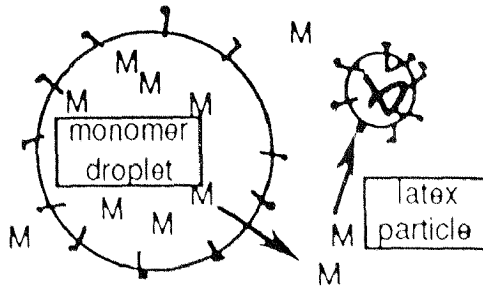


Figure 1.1: Diffusion of monomer from droplets to polymer particles through the aqueous phase.

polymer particles ('latex particles') keep growing while polymerization of the monomer diffusing from the droplets goes on (see Fig. 1.1, taken from ref. [1]).

After some time the micelles disappear completely, both because some are transformed into polymer particles and because an increasing amount of the emulsifier molecules which they are constituted of goes to stabilize the growing polymer particles. At this point interval I (also named 'nucleation stage') is over: the formation of new polymer particles stops and the polymerization carries on inside a constant number of polymer particles.

Besides micellar nucleation, which has been described here above, new particles may be formed through other mechanisms. For instance, if water dissolved monomer units are added by an initiating radical in the water phase to an extent where the formed oligomer becomes insoluble, this will collapse to give a polymer nucleus, which will be then stabilized by emulsifier molecules and swollen by the monomer. Therefore, a new particle is formed. The same kind of process may involve more oligomer chains. This kind of nucleation process, which we call 'homogeneous' since it occurs in the bulk of the water phase without the need for a micellar phase, can go on throughout the whole course of the polymerization until monomer is present in the water phase. Therefore, the statement that a constant number of particles is reached at the end of interval I is true only when this kind of nucleation is negligible. Usually, homogeneous nucleation is important for low emulsifier concentration polymerizations or for high solubilities of the monomer in the aqueous phase.

Interval II

In this second interval polymerization proceeds inside a constant number of polymer particles (in the absence of significant homogeneous nucleation) which are swollen by the monomer diffusing from the droplets through the water phase. As long as the monomer droplets exist, the system is in saturation conditions, and this implies a constant concen-

<i>Interval</i>	<i>Micelles</i>	<i>Monomer concentration</i>	<i>Particle number</i>	<i>Particle size</i>
I	present	constant	increasing	increasing
II	absent	constant	constant	increasing
III	absent	decreasing	constant	slightly decreasing

Table 1.1: Classification describing the time evolution of an emulsion polymerization

tration of monomer inside all phases, included the polymer particles (actually, this is the case also in interval I). Deviations from a constant value of the monomer concentration in the particle phase are due to particle size [4] and crosslinking density [33] effects. As the polymerization proceeds, the monomer droplets decrease in size and eventually disappear. At this point also interval II is over.

Interval III

This is the final stage. Virtually all the monomer is confined to the polymer particles, and its concentration decreases. The polymerization ends when the monomer is completely depleted. Unlike intervals I and II, where polymer particles grow in size because of the continuous migration of monomer from the droplets, in interval III they slightly decrease in size. This is due to the fact that the polymer density is higher than that of the monomer. Ordinary diameters of the polymer particles at the end of the process range from several tens to several hundreds of nanometers.

Table 1.1 summarizes the main characteristics of the three intervals of the emulsion polymerization process described above, and a representation of the three situations is given in Fig. 1.2 (taken from ref. [1]).

From the description above it appears that in an emulsion polymerization the reaction takes place in the polymer particles rather than in the much larger monomer droplets. This has a marked effect on the characteristics of the process and of the polymer chains produced compared to other polymerization processes, such as solution or suspension. Actually, it often happens that the polymer particles are so small that for most of the time no more than one radical grows in each particle. This prevents the active chains from coming together and terminating bimolecularly. The system can be conceived as constituted by many very tiny reactors in which the chains grow without stopping, at least until a new radical enters from the water phase (or a transfer event occurs). The

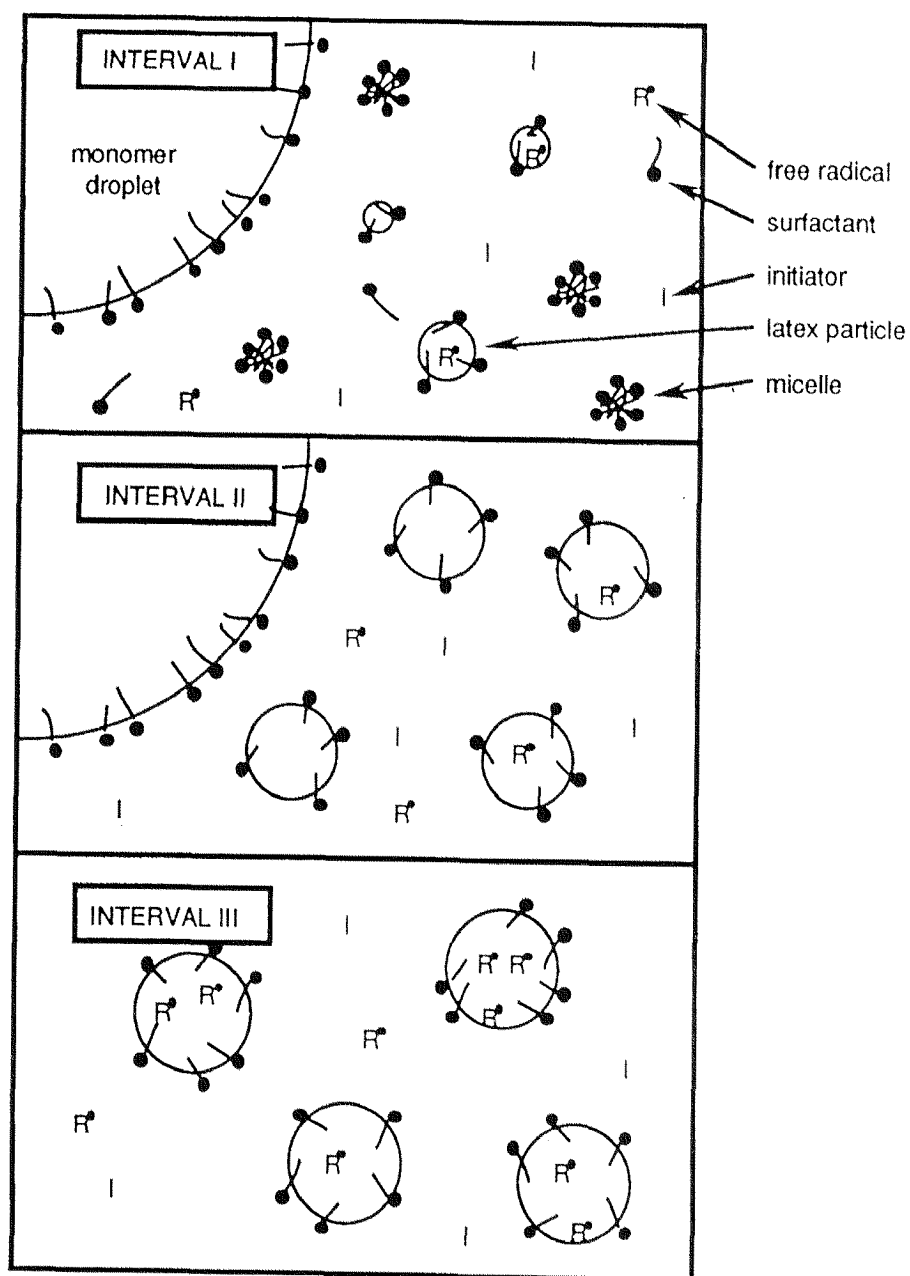


Figure 1.2: The three intervals of an emulsion polymerization.

chains are said to be 'compartmentalized' or segregated. This reduction of the termination rate has two main consequences: a high rate of the polymerization reaction and very high molecular weights of the produced macromolecules.

Seite Leer /
Blank leaf

Chapter 2

Model Development and Results

2.1 Introduction

The microstructural characteristics of main interest when dealing with a homopolymer are its molecular weight distribution and its branching or crosslinking distribution in the case of nonlinear polymers. The distribution of specific end-groups may also be of interest, especially for the extraction of mechanistic information, when analytical techniques sensitive to the presence of these groups are available for the characterization of the polymer (cf. e.g. [34]). Finally, the gel point of a polymerization system (i.e., the conversion at which a gel phase is formed) is a significant feature that needs to be known, both if a gel is desired or not.

The model presented in this chapter focuses on the calculation of the molecular weight and of the gel fraction. If the branching or crosslinking distribution is required, more detailed equations have to be written and solved, which must include a branching or crosslinking parameter. The principles of the development and solution of the equations stay however exactly the same, as will be shown in the following Chap. 3. In this chapter the calculation of only an average crosslinking density is performed, which is necessary for the prediction of the gel point and gel fraction according to the classical theory of Flory [35].

The same considerations hold for end-group calculation. If the distribution of an end-group with a specific functionality is required, it is enough to introduce a parameter representing the number of end-groups of this kind in the molecule. The number of equations will correspondingly increase by a factor equal to the maximum number of these end-groups in a chain (an iterative procedure may be required to determine this number) but the structure of the equations will not change.

In the present chapter the main concern is to show the principles of the development of molecular weight equations correctly accounting for active chain compartmentalization in

the presence of any possible intermolecular branching mechanism (which is the main aim of the whole work) rather than equations including all the possible features characterizing a chain. The extension of the equations to calculate branching or crosslinking and chain-end group distributions is considered conceptually trivial, though maybe intensive from a computational point of view.

2.2 Kinetic Scheme and Basic Assumptions

The model developed in this work is aimed to describe an emulsion polymerization reaction where one or more of the following mechanisms yielding nonlinear chains is present: chain transfer to polymer, crosslinking and propagation to TDB. Accordingly, the following kinetic scheme has been considered:

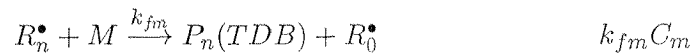
- radical entry in the particles frequency



- propagation



- chain transfer to monomer



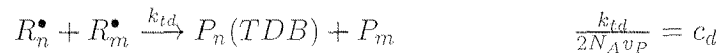
- monomolecular termination (desorption and burial)



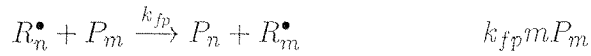
- bimolecular termination by combination



- bimolecular termination by disproportionation



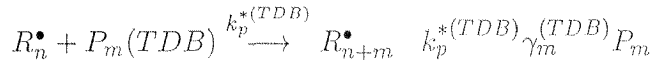
- chain transfer to polymer



- crosslinking



- propagation to terminal double bond



Here $P_m(TDB)$ represents a dead polymer chain of length m with a terminal double bond, generated either by a chain transfer to monomer or by a termination by disproportionation event. Distinction between TDBs originated by these two different mechanisms can be made if necessary. Next to each reaction, the corresponding frequency is given (all symbols are defined in the Notation).

Note that the crosslinking reaction can occur only when the fed monomer is at least bifunctional (e.g. a diene), thus producing polymer chains having double bonds all along, which can be attacked by a growing radical. This mechanism yields a radical which, through the usual propagation process, results in a single chain consisting of two long chains connected by a tetrafunctional unit (crosslinkage). The rate of crosslinking is proportional to the concentration of double bonds in the polymer chains, rather than to the concentration of the chains. The concentration of double bonds is in turn proportional to the concentration of polymerized monomer units through parameter γ_m , representing the ratio of the number of double bonds on chains of length m to the number of units polymerized in chains of the same length. When crosslinking is not active ($k_p^* = 0$), none of these double bonds are consumed and parameter γ_m assumes the integer value $f_u - 1$, with f_u the functionality of the reacting monomer, i.e., the number of unsaturations it contains. If crosslinking is active, γ_m decreases during the reaction from its initial value $f_u - 1$, due to the consumption of double bonds along the polymer chains. However, this decrease is generally rather small even for systems in which gel formation occurs. Accordingly, the use of a single chain length independent parameter $\gamma_m = \gamma$ (which varies during the reaction) can be considered a good approximation. The calculation of parameter γ is dealt with in the section regarding the model equations.

The rate of the propagation to TDB reaction can be treated similarly. This is in fact proportional to the concentration of the TDBs, which can be expressed as the concentra-

tion of the dead polymer chains P_m multiplied by the average number $\gamma_m^{(TDB)}$ of TDBs per terminated chain. Compared to γ_m , $\gamma_m^{(TDB)}$ might be more strongly dependent on chain length even at low polymerization degrees. However, in this work this dependence has been ignored and accordingly a single parameter $\gamma^{(TDB)}$ has been introduced, the value of which again may change during the polymerization process.

A remark should be made about the chain transfer to monomer reaction. According to the kinetic scheme adopted, the TDB is left on the dead chain, and the new formed radical does not have an unsaturation at its end. This happens when transfer of an atom from the β carbon of the reacting radical to the unsaturated monomer occurs. However, an atom (often hydrogen) abstraction from the monomer molecule may also take place, and the TDB is left on the new formed radical. Examples are given by the polymerization of vinyl chloride in the first case and of vinyl acetate and allyl monomers in the second one [36].

In the case where the TDB is subject to further polymerization, the two chain transfer to monomer mechanisms may lead to rather different polymer microstructures. For example, in the case where neither chain transfer to polymer nor crosslinking are present, the mechanism involving the transfer of a β -atom cannot possibly lead to chains having more than one TDB each, while chains with two TDBs (bifunctional macromolecules) can be produced when the second mechanism is active. The consequences on the MWD of the produced polymer can be rather significant. The existence of such bifunctional macromolecules in the reaction system can in fact lead to gel formation even in systems where both crosslinking and chain transfer to polymer are absent [18]. In the present model an average number $\gamma^{(TDB)}$ of TDBs is assumed for each chain and no distinction is made between chains with one, two, or more TDBs. Accordingly, cases where the chemical mechanisms can produce chains with more than one TDB should be considered with special attention. This can happen, for instance, in the already mentioned case of chain transfer to monomer through atom abstraction or in the case of chain transfer to monomer through a β -atom transfer coupled to chain transfer to polymer. In the case of a crosslinked polymer, propagation to TDB should not have a great influence, unless TDBs are much more reactive than the internal double bonds giving the crosslinkages.

From the kinetic scheme above it appears that multiradical activity on single polymer chains and intramolecular reactions (particularly cyclization) are ignored. The degree of polymerization of radicals entering from the water phase is considered negligible compared to that successively reached in the particles. Moreover, the rate constants for the various

reactions are assumed chain length independent and equal for the sol and the gel phase. Finally, the bimolecular termination rate constants c_c and c_d and the desorption frequency k_d are considered, at a given reaction time t_e , the same in all particles, i.e., particle volume monodispersion is assumed.

2.3 Model Equations

2.3.1 Singly Distinguished Particles

In order to compute the molecular weight of the dead polymer, the chain length distribution (CLD) of the active polymer must first be calculated. This is done by making use of the concept of distributions of the ‘singly distinguished particles’. In the general case of branched chains, this distribution is given by the fraction of particles $B'_i(t, t', n')$ containing i active chains, one of which, branched, was born at time t and is still growing at time $t + t'$. This chain is the ‘distinguishing chain’. The parameter n' , called ‘pre-life’, accounts for the length of the chain which is not due to the monomer units added by propagation in the last period of activity (following time t). Chain pre-life may be given by the length of the dead chain which yielded the distinguishing active chain after undergoing chain transfer to polymer or by the length of a dead chain incorporated in the growing chain through a crosslinking or a propagation to TDB reaction. In any case, it is related to monomer units bound to a polymer chain in a period which is previous to the current growth period.

Chain transfer to polymer and crosslinking (or propagation to TDB) are treated differently, since the first causes a growing radical chain to terminate and a new one to start, while the second is a step-growth process involving the addition, in a single propagation event, of a certain number of monomer units (given by those contained in the dead chain which is being incorporated) to the growing radical, without stopping its activity. Hence, when a dead chain of length n' undergoes chain transfer to polymer, a new radical having pre-life n' and current lifetime $t' = 0$ is born. Instead, when an active chain having pre-life n' and current lifetime t' gives a crosslinking (or propagation to TDB) reaction on a dead chain of length m' , its pre-life becomes $n' + m'$ and its current lifetime t' remains unchanged.

It is clear that a distinguishing chain with pre-life n' greater than zero is necessarily branched, since it has experienced a chain transfer to polymer, a crosslinking or a propagation to TDB reaction. On the other hand, linear distinguishing chains have zero pre-life. These last are represented by the distribution $N'_i(t, t')$, which coincides with the

distribution first introduced by Lichti et al. [7] for the calculation of the CLD of linear polymers produced in emulsion.

From the distributions $B'_i(t, t', n')$ and $N'_i(t, t')$ the CLD of the active polymer is readily calculated, since the length of the distinguishing chain is given by $n = n' + \alpha t'$, where $\alpha = k_p C_m$ is the frequency of the propagation reaction. This holds true (under the assumption of long chain) since k_p and C_m can be considered constant on a time interval typical of chain life.

The PBEs for the distributions of the singly distinguished particles are the following:

- *linear chains*

$$\begin{aligned} \frac{\partial N'_i(t, t')}{\partial t'} &= \rho N'_{i-1} - [\rho + ik_d + i(i-1)c + k_{fm}C_m + k_{fp}\sigma^{(1)} + k_p^*\gamma\sigma^{(l)}]N'_i \\ &\quad + ik_d N'_{i+1} + (i+1)icN'_{i+2}, \quad i = 2, \dots, N-2 \end{aligned} \quad (2.1)$$

- *branched chains*

$$\begin{aligned} \frac{\partial B'_i(t, t', n')}{\partial t'} &= \rho B'_{i-1} - [\rho + ik_d + i(i-1)c + k_{fm}C_m + k_{fp}\sigma^{(1)} + k_p^*\gamma\sigma^{(l)}]B'_i \\ &\quad + ik_d B'_{i+1} + (i+1)icB'_{i+2} + \int_0^{n'} k_p^*\gamma B'_i(t, t', n'-m)m^l D(t, m) dm \\ &\quad + k_p^*\gamma N'_i(t, t')n'^l D(t, n'), \quad i = 2, \dots, N-2 \end{aligned} \quad (2.2)$$

where $D(t, n)$ is the CLD of the dead polymer at time t . As it is usual for balances of this kind [24], minor modifications arise for $i = 1$, $i = N - 1$ and $i = N$, where N represents the maximum number of radicals in the same particle.

Eqs (2.1) and (2.2) are written considering all possible events producing or consuming a distinguishing linear or branched active chain, respectively, in a particle in state i (i.e., a particle containing i active chains). Some of these events involve directly the distinguishing chain under examination, giving birth to consumption terms. Others do not affect the distinguishing chain but only the state of the particle where this is located and may yield both production and consumption terms. Only the terms relative to the crosslinking and propagation to TDB reactions are discussed here, while all the others have been described in detail in [24]. The terms $-k_p^*\gamma\sigma^{(l)}N'_i$ and $-k_p^*\gamma\sigma^{(l)}B'_i$ in eqs (2.1) and (2.2), respectively, account for the consumption of the distinguishing chain due to its reaction with a double bond on a dead chain. The quantity $\sigma^{(l)}$ represents the l^{th} -order moment of the dead polymer, expressed as a molar concentration referred to the particle volume. When $l = 1$ these terms represent the crosslinking reaction, since the rate of reaction is first order

with respect to the concentration of the monomer units bound to the dead polymer, while when $l = 0$ they represent TDB propagation, the rate of which is first order with respect to the concentration of the dead chains (with $k_p^* = k_p^{*(TDB)}$ and $\gamma = \gamma^{(TDB)}$). When both mechanisms are present, two terms of this type should appear in every equation. However, here above and in the following, these two terms, which can be always treated identically, are condensed in a single one to make the equations more legible.

Note that no production terms appear in eq. (2.1) due to crosslinking, since this mechanism produces only branched radicals. Instead, in the balance for the branched chains two positive terms appear on the right-hand side, accounting for the crosslinking (or propagation to TDB) reaction of active chains of current lifetime t' with dead chains of length such that the resulting chains have pre-life equal to n' . The reacting radicals may be linear or branched. Here again, $l = 1$ for the crosslinking reaction and $l = 0$ for propagation to TDB.

Finally, note that in the above equations it is implicitly assumed that $N > 3$. Therefore, when $N \leq 3$ they must be properly modified.

The initial conditions of the integro-differential equations (2.1) and (2.2) involve all those mechanisms giving birth to a new active chain, hence not crosslinking and propagation to TDB, which are considered as events incorporating a dead chain in a pre-existing radical. In particular, radical entry from the water phase and chain transfer to monomer produce linear active chains of negligible length (conventionally assumed zero). Instead, chain transfer to a dead polymer chain of length n' produces a branched active chain with pre-life n' . Accordingly, the initial conditions for N'_i and B'_i are:

$$N'_i(t, t' = 0) = \rho N_{i-1}(t) + k_{fm} C_m i N_i(t) \quad (2.3)$$

$$B'_i(t, t' = 0, n') = k_{fp} i N_i(t) n' D(t, n') \quad (2.4)$$

where $D(t, n')$ is the chain length distribution of the dead polymer (so that $D(t, n') dn'$ represents the particle concentration of dead chains with length between n' and $n' + dn'$) and N_i is the fraction of polymer particles containing i radicals, given by the Smith-Ewart equations [37].

Eqs (2.1) and (2.2) for the singly distinguished particles with linear and branched distinguishing chain, respectively, can be rewritten in matrix form as follows:

$$\frac{\partial \underline{\mathbf{N}}'(t, t')}{\partial t'} = \underline{\mathbf{A}}(t) \underline{\mathbf{N}}'(t, t') \quad (2.5)$$

$$\frac{\partial \underline{\mathbf{B}}'(t, t', n')}{\partial t'} = \underline{\mathbf{A}}(t) \underline{\mathbf{B}}'(t, t', n') \quad (2.6)$$

$$+ \int_0^{n'} k_p^* \gamma \underline{\mathbf{B}}'(t, t', n' - m) m^l D(t, m) dm + k_p^* \gamma \underline{\mathbf{N}}'(t, t') n^l D(t, n')$$

where $\underline{\mathbf{N}}'(t, t')$ and $\underline{\mathbf{B}}'(t, t', n')$ are column vectors containing the $N'_i(t, t')$ and $B'_i(t, t', n')$ distributions respectively, and $\underline{\mathbf{A}}(t)$ is the band matrix arising from the coefficients of eq. (2.1) when $i = 1, N$.

2.3.2 Doubly Distinguished Particles

In order to account for polymer chains terminated by bimolecular combination, it is necessary to consider the distribution of pairs of chains belonging to the same particle, since two chains belonging to two different particles cannot obviously couple. The physical reasons for this requirement when modeling molecular weights are discussed in detail in Chap. 4. The distributions of the doubly distinguished particles are therefore introduced. In particular, in the case where both chains under examination are branched, the distribution $B''_i(t, t', t'', n', n'')$ is defined ($i \geq 2$), representing the fraction of particles containing i active chains, one of which was born at time t and was still growing at time $t + t'$, when a second chain was born. Both chains, called distinguishing chains, are still growing and are branched at time $t + t' + t''$. Parameters n' and n'' represent the pre-lives of the first and second-born chain respectively and have the same meaning as for the singly distinguished particles. Similar distributions are defined in the cases where at least one of the chains of the pair is not branched: $O''_i(t, t', t'', n')$ when only the first-born ('older') chain is branched, $Y''_i(t, t', t'', n'')$ when only the second-born ('younger') chain is branched and $N''_i(t, t', t'')$ when both chains are linear. In the following, only the PBE for $N''_i(t, t', t'')$ is written in detail, since, once the matrix of the coefficients of the relative system is defined, the balances for the other distributions can be written in a synthetic matrix form by simply adding some terms related to crosslinking. The equation describing distribution $N''_i(t, t', t'')$ is given by:

$$\begin{aligned} \frac{\partial N''_i}{\partial t''} = & \rho N''_{i-1} - [\rho + ik_d + i(i-1)c + 2k_{fm}C_m + 2k_{fp}\sigma^{(1)} + 2k_p^*\gamma\sigma^{(l)}]N''_i \\ & + (i-1)k_d N''_{i+1} + i(i-1)c N''_{i+2} \quad i = 3, \dots, N-2 \end{aligned} \quad (2.7)$$

As usual, minor modifications are required for $i = 2$, $i = N - 1$ and $i = N$.

As for the singly distinguished particles with linear distinguished chain, besides the terms accounting for entry, desorption, chain transfer and bimolecular termination, only a consumption term appears due to crosslinking, since a linear chain can just disappear as a result of its reaction with a double bond.

Eq. (2.7) can be written in matrix form as follows:

- *both chains linear*

$$\frac{\partial \underline{\mathbf{N}}''(t, t', t'')}{\partial t''} = \underline{\underline{\mathbf{D}}}(t) \underline{\mathbf{N}}''(t, t', t'') \quad (2.8)$$

where $\underline{\mathbf{N}}''(t, t', t'')$ is a column vector containing the $N_i''(t, t', t'')$ distributions and $\underline{\underline{\mathbf{D}}}(t)$ the $(N-1) \times (N-1)$ band matrix arising from the coefficients of eq. (2.7) when $i = 2, N$.

Since an active chain having pre-life $n' - m$ yields, when reacting by crosslinking or propagation to TDB with a dead chain of length m , a branched chain of length n' , the PBEs for $O_i''(t, t', t'', n')$, $Y_i''(t, t', t'', n'')$ and $B_i''(t, t', t'', n', n'')$ are given by:

- *older chain branched*

$$\begin{aligned} \frac{\partial \underline{\mathbf{O}}''(t, t', t'', n')}{\partial t''} &= \underline{\underline{\mathbf{D}}}(t) \underline{\mathbf{O}}''(t, t', t'', n') \\ &+ \int_0^{n'} k_p^* \gamma \underline{\mathbf{O}}''(t, t', t'', n' - m) m^l D(t, m) dm \\ &+ k_p^* \gamma \underline{\mathbf{N}}''(t, t', t'') n'^l D(t, n') \end{aligned} \quad (2.9)$$

where $\underline{\mathbf{O}}''(t, t', t'', n')$ is the column vector of the $O_i''(t, t', t'', n')$ distributions. The last two terms on the right-hand side account for the crosslinking reaction of the older chain (which might be branched or linear) of a pre-existing distinguishing pair, in order to give a branched older chain of pre-life n' (the younger chain being linear);

- *younger chain branched*

$$\begin{aligned} \frac{\partial \underline{\mathbf{Y}}''(t, t', t'', n'')}{\partial t''} &= \underline{\underline{\mathbf{D}}}(t) \underline{\mathbf{Y}}''(t, t', t'', n'') \\ &+ \int_0^{n''} k_p^* \gamma \underline{\mathbf{Y}}''(t, t', t'', n'' - m) m^l D(t, m) dm \\ &+ k_p^* \gamma \underline{\mathbf{N}}''(t, t', t'') n''^l D(t, n'') \end{aligned} \quad (2.10)$$

where $\underline{\mathbf{Y}}''(t, t', t'', n'')$ is the column vector of the $Y_i''(t, t', t'', n'')$ distributions. The last two terms on the right-hand side account for the the crosslinking reaction of the younger chain (which might be branched or linear) of a pre-existing distinguishing pair, in order to give a branched younger chain of pre-life n'' (the older chain being linear);

- *both chains branched*

$$\frac{\partial \underline{\mathbf{B}}''(t, t', t'', n', n'')}{\partial t''} = \underline{\underline{\mathbf{D}}}(t) \underline{\mathbf{B}}''(t, t', t'', n', n'')$$

$$\begin{aligned}
& + \int_0^{n'} k_p^* \gamma \underline{\mathbf{B}}''(t, t', t'', n' - m, n'') m^l D(t, m) dm \\
& + \int_0^{n''} k_p^* \gamma \underline{\mathbf{B}}''(t, t', t'', n', n'' - m) m^l D(t, m) dm \quad (2.11) \\
& + k_p^* \gamma \underline{\mathbf{Y}}''(t, t', t'', n'') n'^l D(t, n') \\
& + k_p^* \gamma \underline{\mathbf{O}}''(t, t', t'', n') n''^l D(t, n'')
\end{aligned}$$

where $\underline{\mathbf{B}}''(t, t', t'', n', n'')$ is the column vector of the $B_i''(t, t', t'', n', n'')$ distributions. The last four terms on the right hand side account for the crosslinking reaction of a chain (linear or branched) of a pre-existing distinguishing pair, in order to give a branched chain of the pre-life under examination (being the other chain already branched and of the desired pre-life).

Considering the possible mechanisms giving birth to a new younger chain of a pair of active chains, the following initial conditions can be written for systems (2.8) to (2.11) ($i = 2, N$):

$$N_i''(t, t', t'' = 0) = \rho N_{i-1}'(t, t') + k_{fm} C_m (i-1) N_i'(t, t') \quad (2.12)$$

$$O_i''(t, t', t'' = 0, n') = \rho B_{i-1}'(t, t', n') + k_{fm} C_m (i-1) B_i'(t, t', n') \quad (2.13)$$

$$Y_i''(t, t', t'' = 0, n'') = k_{fp} (i-1) N_i'(t, t') n'' D(t, n'') \quad (2.14)$$

$$B_i''(t, t', t'' = 0, n', n'') = k_{fp} (i-1) B_i'(t, t', n') n'' D(t, n'') \quad (2.15)$$

2.3.3 Polymer Formed by Monomolecular Termination

The dead polymer can be ideally subdivided into a portion terminated by any mechanism which does not alter the length of the active chain experiencing it, and another portion terminated by combination. The former termination mechanisms include, in addition to the strictly monomolecular ones (i.e., those the rate of which is first order with respect to the state of the particle), all the other mechanisms which are not monomolecular but which also do not affect the length of the active chain upon its death, namely disproportionation and instantaneous termination by entry in a particle in state N . For the sake of brevity, all these mechanisms will be referred to as monomolecular terminations in the following.

The polymer terminated by such monomolecular mechanisms can be further subdivided into two parts, the first linear and the other branched, represented respectively by distributions $S^M(t_e, t')$ and $G^M(t_e, t', n')$. These are the cumulative distributions at time t_e of the polymer chains terminated monomolecularly at any reaction time and which had current lifetime t' (and pre-life n' for branched chains) the moment they died. Accordingly, their length is $n = n' + \alpha t'$.

The PBE describing the time evolution of distributions $S^M(t_e, t')$ and $G^M(t_e, t', n')$ in a batch reactor is given by:

$$\begin{aligned} \frac{d[v_P S^M(t_e, t')]}{dt_e} = & \left\{ (k_d + k_{fm} C_m + k_{fp} \sigma^{(1)}) \sum_{i=1}^N N'_i(t_e - t', t') \right. \\ & + \frac{\rho}{N} N'_N(t_e - t', t') + 2c_d \sum_{i=2}^N (i-1) N'_i(t_e - t', t') \\ & \left. - [k_{fp}(\alpha t') + k_p^* \gamma(\alpha t')^l] S^M(t_e, t') \bar{n} \right\} \frac{1}{N_A} \end{aligned} \quad (2.16)$$

$$\begin{aligned} \frac{d[v_P G^M(t_e, t', n')]}{dt_e} = & \left\{ (k_d + k_{fm} C_m + k_{fp} \sigma^{(1)}) \sum_{i=1}^N B'_i(t_e - t', t', n') \right. \\ & + \frac{\rho}{N} B'_N(t_e - t', t', n') + 2c_d \sum_{i=2}^N (i-1) B'_i(t_e - t', t', n') \\ & \left. - [k_{fp}(n' + \alpha t') + k_p^* \gamma(n' + \alpha t')^l] G^M(t_e, t', n') \bar{n} \right\} \frac{1}{N_A} \end{aligned} \quad (2.17)$$

where v_P is the volume of a polymer particle and \bar{n} is the average number of free radicals per particle.

Note that the two equations are identical, except that in the equation for $S^M(t_e, t')$ no pre-life n' appears, and $N'_i(t_e - t', t')$ is used instead of $B'_i(t_e - t', t', n')$. The positive terms on the right-hand side of eqs (2.16)-(2.17) account for the dead polymer chains produced by monomolecular termination (i.e., desorption, chain transfer, entry in type N particles and disproportionation) of distinguishing chains belonging to singly distinguished particles.

Crosslinking appears only as a consumption mechanism, since no dead chains are formed through this reaction. It is worth noting that the corresponding negative term, which includes also chain transfer to polymer, requires the knowledge of the cumulative distribution of the dead polymer, a peculiarity of nonlinear polymers.

2.3.4 Polymer Formed by Combination

By considering the rate of coupling of the pairs of chains given by the distributions of the doubly distinguished particles, the PBEs for the distributions of the polymer terminated by combination can be derived. Four distributions are considered, $S^C(t_e, t', t'')$, $V^C(t_e, t', t'', n')$, $W^C(t_e, t', t'', n'')$ and $G^C(t_e, t', t'', n', n'')$, representing the dead polymer chains coming from pairs belonging to the $N''_i(t_e - t' - t'', t', t'')$, $O''_i(t_e - t' - t'', t', t'', n')$, $Y''_i(t_e - t' - t'', t', t'', n'')$ or $B''_i(t_e - t' - t'', t', t'', n', n'')$ distribution, respectively.

The relevant PBEs are:

$$\begin{aligned} \frac{d[v_P S^C(t_e, t', t'')]}{dt_e} &= \{2c_c \sum_{i=2}^N N_i''(t_e - t' - t'', t', t'') \\ &\quad - [k_{fp}(\alpha t' + 2\alpha t'') + k_p^* \gamma(\alpha t' + 2\alpha t'')^l] \\ &\quad \cdot S^C(t_e, t', t'') \bar{n}\} \frac{1}{N_A} \end{aligned} \quad (2.18)$$

$$\begin{aligned} \frac{d[v_P V^C(t_e, t', t'', n')]}{dt_e} &= \{2c_c \sum_{i=2}^N O_i''(t_e - t' - t'', t', t'', n') \\ &\quad - [k_{fp}(n' + \alpha t' + 2\alpha t'') + k_p^* \gamma(n' + \alpha t' + 2\alpha t'')^l] \\ &\quad \cdot V^C(t_e, t', t'', n') \bar{n}\} \frac{1}{N_A} \end{aligned} \quad (2.19)$$

$$\begin{aligned} \frac{d[v_P W^C(t_e, t', t'', n'')]}{dt_e} &= \{2c_c \sum_{i=2}^N Y_i''(t_e - t' - t'', t', t'', n'') \\ &\quad - [k_{fp}(n'' + \alpha t' + 2\alpha t'') + k_p^* \gamma(n'' + \alpha t' + 2\alpha t'')^l] \\ &\quad \cdot W^C(t_e, t', t'', n'') \bar{n}\} \frac{1}{N_A} \end{aligned} \quad (2.20)$$

$$\begin{aligned} \frac{d[v_P G^C(t_e, t', t'', n', n'')]}{dt_e} &= \{2c_c \sum_{i=2}^N B_i''(t_e - t' - t'', t', t'', n', n'') \\ &\quad - [k_{fp}(n' + n'' + \alpha t' + 2\alpha t'') + k_p^* \gamma(n' + n'' + \alpha t' + 2\alpha t'')^l] \\ &\quad \cdot G^C(t_e, t', t'', n', n'') \bar{n}\} \frac{1}{N_A} \end{aligned} \quad (2.21)$$

The positive production term on the right-hand side of eqs (2.18)-(2.21) accounts for the combination reaction between the two chains of the distinguishing pairs. The negative consumption term refers to the reactivation of the dead chains through chain transfer to polymer and crosslinking (or TDB propagation). In the case of chain transfer to polymer and crosslinking, since the rate of reaction is proportional to the number of monomer units in the dead polymer chains, each distribution is multiplied by the corresponding chain length. For propagation to TDB this dependence vanishes since $l = 0$.

2.3.5 Evaluation of the Double Bonds in the Polymer Chains

Some detail must be given about the calculation of quantities γ and $\gamma^{(TDB)}$ which appear in most equations derived in this section. Their evaluation can be performed from their definition:

$$\gamma = \frac{D_B}{\theta} \quad \gamma^{(TDB)} = \frac{T_{DB}}{n_T} \quad (2.22)$$

where D_B and T_{DB} are the total moles in the reaction locus of double bonds along the polymer chains and of TDBs, respectively, while θ and n_T are the total moles of polymerized monomer units and of polymer chains, respectively.

Quantities D_B and T_{DB} can be evaluated from simple overall balances taking into account the reactions forming and consuming double bonds along and at the end of the chains, respectively:

$$\frac{dD_B}{dt} = \left[k_p C_m (f_u - 1) - k_p^* \gamma \sigma^{(1)} \right] \bar{n} \frac{N_P V_w}{N_A} \quad (2.23)$$

$$\frac{dT_{DB}}{dt} = \left[c_d \sum_{i=2}^N i(i-1) N_i + k_{fm} C_m \bar{n} - k_p^*(T_{DB}) \gamma^{(T_{DB})} \sigma^{(0)} \bar{n} \right] \frac{N_P V_w}{N_A} \quad (2.24)$$

All symbols are defined in the Notation.

Quantities θ and n_T can be evaluated similarly from overall balances, accounting for the rate of polymerization for θ and of all the termination reactions and of the reactions reactivating dead chains for n_T .

2.3.6 Numerical Solution of the Model

All the equations derived above for the live and dead polymer distributions can be solved by means of the method of moments. However, it is well known that this method fails in correspondence of the gel point (i.e., the time or conversion at which a gel phase appears). Moreover, for a very wide polymer chain distribution, as might be that under examination, few moments are not enough for an accurate CLD reconstruction even before the gel point. Both these difficulties can be overcome by fractionating the heterogeneous polymer chain population into subsets or ‘generations’, each constituted by chains more uniform in length and degree of branching [30]. The moments of the distributions representing these narrower subpopulations do not diverge at the gel point and permit the reconstruction of the overall CLD of the sol phase before and after the gel point.

The rules adopted for the fractionation and the equations for the calculation of the distribution of each generation, yielding the results presented in the Model Results Section 2.6, are discussed in Appendix A.

2.4 Correct Inclusion of the Desorption Mechanism

In the previous Sections 2.2 and 2.3, exit (or desorption) of radicals from the particles to the water phase was accounted for in agreement with the development set forth in refs [7] and [24]. Therefore, desorption was considered to affect chains of any length with the same rate and to cause cessation of their activity, i.e., it was considered as a first order chain-length independent stoppage reaction (thus appearing also in the dead polymer balances). In fact, desorption is neither chain-length independent nor a termination mechanisms. It involves preferably short chains, which have a greater compatibility with the water phase and

diffuse more easily out of the particles, and does not have as a direct effect the termination of the active chain, which can in principle re-enter a particle and go on propagating. Casey et al. [29] have shown theoretically that desorption of radicals longer than one monomer unit is negligible, while there is experimental evidence suggesting that also longer oligomers can contribute to the overall rate of desorption [38]. Here, it is of interest to us to remove the obviously wrong assumption of chains of any length terminating by desorption and to introduce into the molecular weight equations the exit of oligomeric radicals only. To this aim, the approach developed by Asua et al. [28] has been followed. This is quite a general statistical approach considering the probability associated to the occurrence of various reactions, including desorption and re-entry of oligomer radicals, in the particle and water phases. In ref. [28], the desorbing species is assumed to be the monomeric radical generated by chain transfer to monomer. Inclusion of the exit (and re-entry) of longer oligomers could be accomplished by considering the corresponding probabilities for these species, but is not considered here. Moreover, equations for linear chains are developed, since the presence of branching mechanisms does not affect the general mechanism of desorption and can be immediately included.

With the aim of obtaining a final form of the molecular weight equations in which the elemental reactions determining the desorption rate are lumped in a single parameter, the rate coefficient k_d is introduced. This is the ordinary desorption parameter which appears in the Smith-Ewart equations, $k_d i$ representing the frequency of desorption of radicals from particles with i radicals, and $k_d \bar{n} N_P$ (where N_P is the total particle concentration) the overall rate of desorption. Coefficient k_d must then be related to the elemental rates of the reactions involving the desorbing species, i.e., the monomeric radicals generated by chain transfer. Therefore, we consider the possible fates of such a radical: when it is in a particle, the radical may desorb with a probability P_i (dependent upon particle state i) and, when it is in the water phase, the radical may react (i.e., not re-enter a particle as a monomeric radical) with a probability β . Probabilities P_i and β are obviously related to the rates of all the possible events the radical may undergo in each of the two phases. Since the overall rate of desorption is given, according to the definition of coefficient k_d , by $k_d \bar{n} N_P$, the frequency of re-entry (per particle) is given by $\rho_{re} = k_d \bar{n} (1 - \beta)$, i.e., by the frequency of desorption times the probability of re-absorption. Shortly, one has to consider that:

- a monomeric radical produced by chain transfer to monomer may desorb with probability P_i from a particle in state i ;

- a desorbed monomeric radical may re-enter with probability $(1 - \beta)$;
- a re-entered monomeric radical may re-desorb with probability P_i from a particle in state i .

In terms of frequencies:

- monomeric radicals produced by chain transfer to monomer desorb with a frequency $k_{fm}C_m i P_i$ from particles in state i ;
- desorbed monomeric radicals re-enter with a frequency $\rho_{re} = k_d \bar{n} (1 - \beta)$;
- re-entered monomeric radicals re-desorb with a frequency $\rho_{re} P_i$ from particles in state i .

Considering these frequencies in the singly and doubly distinguished particle equations, one can write the correct balances. However, to understand how to proceed, we rather re-derive the Smith-Ewart equations first. Namely, what we mean to do, is to obtain the ordinary expression for the Smith-Ewart equations, involving the lumping coefficient k_d , starting from the elemental mechanisms.

2.4.1 Smith-Ewart Equations

Considering the reactions producing and consuming a particle in state i leads to the following PBE:

$$\begin{aligned} \frac{dN_i}{dt} = & (\rho - \rho_{re} P_i) N_{i-1} - [(\rho - \rho_{re} P_{i+1}) + k_{fm} C_m i P_i + c i (i - 1)] N_i \\ & + k_{fm} C_m (i + 1) P_{i+1} N_{i+1} + c (i + 2) (i + 1) N_{i+2} \end{aligned} \quad (2.25)$$

where the entry frequency ρ can be decomposed into a contribution coming from the decomposition of the initiator and one from the re-entry of desorbed radicals: $\rho = \rho_I + \rho_D$. Note that ρ_D differs from ρ_{re} since it includes also the radicals which have propagated in the water phase after desorption. However, it can be computed analogously to ρ_{re} .

The various terms in eq. (2.25) can be explained as follows. A particle with i radicals is produced:

- by entry in a particle in state $(i - 1)$, as long as the radical does not re-desorb (note that entry of initiator-derived and oligomeric radicals is considered to be irreversible): term $(\rho - \rho_{re} P_i) N_{i-1}$;

- by chain transfer in a particle in state $(i + 1)$ followed by exit: term $k_{fm}C_m(i + 1)P_{i+1}N_{i+1}$;
- by combination in a particle in state $(i + 2)$: term $c(i + 2)(i + 1)N_{i+2}$.

A particle with i radicals is consumed by the same events occurring to the particle itself, which yields the term: $[(\rho - \rho_{re}P_{i+1}) + k_{fm}C_m iP_i + ci(i - 1)]N_i$.

To obtain the ordinary Smith-Ewart equations, one has to consider that the overall desorption rate from state i particles, given by definition by $k_d i N_i$, can be calculated from the rate of the radicals desorbing for the first time after a chain transfer event, plus the rate of the radicals re-desorbing after re-entry:

$$k_{fm}C_m iP_i N_i + \rho_{re}P_i N_{i-1} = k_d i N_i \quad (2.26)$$

Substituting the previous relation written for i and $(i + 1)$ in eq. (2.25) yields:

$$\begin{aligned} \frac{dN_i}{dt} = & \rho N_{i-1} - [\rho + k_d i + ci(i - 1)]N_i + k_d(i + 1)N_{i+1} \\ & + c(i + 2)(i + 1)N_{i+2} \end{aligned} \quad (2.27)$$

which is the ordinary Smith-Ewart equation.

This kind of derivation of the Smith-Ewart equations shows (see eq. (2.26)) that the term $-k_d i N_i$ accounts for the particles in state i disappearing by a chain transfer followed by a desorption but also for those i state particles which do not form from $(i - 1)$ state particles because of re-desorption after re-entry, and which have instead been counted in the ρN_{i-1} term (which admits irreversible entry of all radicals).

Note, finally, that eq. (2.26) permits, by summation over all particle states (and considering that $\rho_{re} = k_d \bar{n}(1 - \beta)$), to obtain an expression for k_d [28]. If one assumes $P_i = P_1 \forall i$, this expression reduces to [28]:

$$k_d = \frac{k_{fm}C_m P_1}{1 - (1 - \beta)P_1} \quad (2.28)$$

2.4.2 Singly Distinguished Particles

A similar approach can be applied to obtain the PBEs for the singly distinguished particles. Considering the reactions producing and consuming a singly distinguished particle in state i one can write:

$$\begin{aligned} \frac{\partial N'_i(t, t')}{\partial t'} = & (\rho - \rho_{re}P_i)N'_{i-1} - [(\rho - \rho_{re}P_{i+1}) + k_{fm}C_m(i - 1)P_i + k_{fm}C_m \\ & + ci(i - 1)]N'_i + k_{fm}C_m iP_{i+1}N'_{i+1} + c(i + 1)iN'_{i+2} \end{aligned} \quad (2.29)$$

This equation can be understood by considering that a singly distinguished state i particle is formed:

- by entry in an N'_{i-1} particle, as long as the radical does not re-desorb: term $(\rho - \rho_{re}P_i)N'_{i-1}$;
- by chain transfer followed by desorption of one of the i non-distinguishing radicals of an N'_{i+1} particle: term $k_{fm}C_m i P_{i+1} N'_{i+1}$;
- by combination of two of the $(i+1)$ non-distinguishing radicals of an N'_{i+2} particle: term $c(i+1)iN'_{i+2}$

and that it disappears:

- by entry in the N'_i particle, but not if the entered radical re-desorbs: term $-(\rho - \rho_{re}P_i)N'_i$;
- by chain transfer followed by desorption of one of the $(i-1)$ non-distinguishing radicals of the N'_i particle: term $-k_{fm}C_m(i-1)P_i N'_i$;
- by chain transfer of the distinguishing radical: term $-k_{fm}C_m N'_i$ (note that it is not necessary that the formed monomeric radical undergoes desorption as in the previous item);
- by combination of two of the i radicals of the N'_i particle: term $-ci(i-1)N'_i$.

The initial condition for eq. (2.29) is given by:

$$N'_i(t, t' = 0) = (\rho - \rho_{re}P_i)N_{i-1} + k_{fm}C_m i(1 - P_i)N_i \quad (2.30)$$

Eq. (2.30) follows from the fact that a chain of length zero in a state i particle is formed by entry in an N_{i-1} particle, as long as the entered chain does not re-desorb, and by a chain transfer to monomer in an N_i particle, as long as the formed monomeric radical does not exit the particle.

Going back to eq. (2.29), the aim is to lump the re-entry events and desorption probabilities into the single desorption parameter k_d . To this purpose one can consider the desorption rate of non-distinguishing chains from an $N'_i(t, t')$ particle: this is given by the frequency of desorption of $(i-1)$ radicals, $k_d(i-1)$, times the fraction of particles where the distinguishing chain is present, given by the quantity $N'_i(t, t')$ itself. The same quantity can be calculated as the rate of formation (through chain transfer and re-entry) of

$N'_i(t, t')$ particles containing a monomeric radical, times the probability for its desorption.

In a formula:

$$[k_{fm}C_m(i-1)N'_i + \rho_{re}N'_{i-1}]P_i = k_d(i-1)N'_i \quad (2.31)$$

As a check, note that integration of eq. (2.31) on t' from 0 to ∞ , recalling that $\int_0^\infty N'_i(t, t')dt' = iN_i(t)$, yields eq. (2.26).

In analogy to what done for the Smith-Ewart equations, substituting relation (2.31) written for i and $(i+1)$ in eq. (2.29) yields, after some manipulation:

$$\begin{aligned} \frac{\partial N'_i(t, t')}{\partial t'} &= \rho N'_{i-1} - [\rho + k_d(i-1) + k_{fm}C_m + ci(i-1)]N'_i \\ &\quad + k_d i N'_{i+1} + c(i+1)iN'_{i+2} \end{aligned} \quad (2.32)$$

If this equation is compared to eq. (2.1) (in the case of no branching), it can be seen that the two equations differ just by an $(i-1)$ factor instead of i multiplying the coefficient k_d in the consumption term for the N'_i . This accounts for the fact that a chain transfer event is enough to lose the distinguished chain (term $-k_{fm}C_m$), with no need for the formed monomeric radical to desorb. Since the k_d parameter accounts also for the chain transfer to monomer, multiplying it by i instead of $(i-1)$ would lead to count this event twice. Moreover, it must not be forgotten that the k_d parameter accounts for the ‘ineffective’ entry of monomeric radicals in the case of a successive re-desorption, and this cannot possibly involve the distinguishing chain, which is not a monomeric radical, since lengths zero are considered in the initial condition only. The initial condition eq. (2.30) can be re-written, by substituting eq. (2.26), as

$$N'_i(t, t' = 0) = \rho N_{i-1} + (k_{fm}C_m - k_d)iN_i \quad (2.33)$$

Subtracting the k_d coefficient from $k_{fm}C_m$ accounts for the fact that a zero-length active chain is not formed in the particle if desorption follows chain transfer to monomer or re-entry.

Finally, by introducing the parameter

$$f = k_{fm}C_m - k_d \quad (2.34)$$

one can write the balance and initial conditions for the singly distinguished particles as:

$$\frac{\partial N'_i(t, t')}{\partial t'} = \rho N'_{i-1} - [\rho + k_d i + f + ci(i-1)]N'_i + k_d i N'_{i+1} + c(i+1)iN'_{i+2} \quad (2.35)$$

$$N'_i(t, t' = 0) = \rho N_{i-1} + f i N_i \quad (2.36)$$

These equations are the same as those given in Section 2.3 in the case of linear chains but for a correction to the chain transfer to monomer term (coefficient f instead of $k_{fm}C_m$).

Eqs (2.35) and (2.36) coincide with those already reported by Lichti et al. [39]. However, besides offering a rigorous rather than an intuitive approach, the complete development here reported permits to recognize that coefficient f does not account only for the transfer events that do not result in desorption (as stated in ref. [39]) but also for re-desorption of re-entered monomeric radicals.

2.4.3 Doubly Distinguished Particles

To obtain the PBEs for the doubly distinguished particles, one can operate in complete analogy to the case of the singly distinguished particles.

The balance accounting explicitly for the desorption following chain transfer to monomer and re-entry is:

$$\begin{aligned} \frac{\partial N_i''(t, t', t'')}{\partial t''} = & (\rho - \rho_{re}P_i)N_{i-1}'' - [(\rho - \rho_{re}P_{i+1}) + \\ & k_{fm}C_m(i-2)P_i + 2k_{fm}C_m + ci(i-1)]N_i'' + \\ & k_{fm}C_m(i-1)P_{i+1}N_{i+1}'' + ci(i-1)N_{i+2}'' \end{aligned} \quad (2.37)$$

Then, the rate of desorption of non-distinguishing chains from doubly distinguished particles in state i is considered:

$$[k_{fm}C_m(i-2)N_i'' + \rho_{re}N_{i-1}'']P_i = k_d(i-2)N_i'' \quad (2.38)$$

As a check for this equation, note that integration of eq. (2.38) on t' and t'' from 0 to ∞ , recalling that $\int_0^\infty \int_0^\infty N_i''(t, t', t'')dt'dt'' = i(i-1)N_i(t)/2$, yields eq. (2.26).

Substituting eq. (2.38) in (2.37) gives:

$$\begin{aligned} \frac{\partial N_i''(t, t', t'')}{\partial t''} = & \rho N_{i-1}'' - [\rho + k_d(i-2) + 2k_{fm}C_m + ci(i-1)]N_i'' \\ & + k_d(i-1)N_{i+1}'' + ci(i-1)N_{i+2}'' \end{aligned} \quad (2.39)$$

This equation coincides with eq. (2.7) save for the fact that an $(i-2)$ factor appears instead of i next to the coefficient k_d in the consumption term for the N_i'' . Similar arguments hold as for the case of the singly distinguished particles.

Passing on to the initial conditions, these are given by:

$$N_i''(t, t', t'' = 0) = (\rho - \rho_{re}P_i)N_{i-1}' + k_{fm}C_m(i-1)(1 - P_i)N_i' \quad (2.40)$$

Taking advantage of eq. (2.31), this equation becomes:

$$N_i''(t, t', t'' = 0) = \rho N_{i-1}' + (k_{fm}C_m - k_d)(i-1)N_i' \quad (2.41)$$

Finally, by using parameter f defined by eq. (2.34), the PBEs and initial conditions for the doubly distinguished particles become:

$$\begin{aligned} \frac{\partial N_i''(t, t', t'')}{\partial t''} &= \rho N_{i-1}'' - [\rho + k_d i + 2f + ci(i-1)]N_i'' \\ &\quad + k_d(i-1)N_{i+1}'' + ci(i-1)N_{i+2}'' \end{aligned} \quad (2.42)$$

$$N_i''(t, t', t'' = 0) = \rho N_{i-1}' + f(i-1)N_i' \quad (2.43)$$

These equations are the same as those given in Section (2.3) in the case of linear chains but for a correction to the chain transfer to monomer term (coefficient f instead of $k_{fm}C_m$). Eqs (2.42) and (2.43) coincide with those already reported by Lichti et al. [39]. With respect to this, the same considerations hold as for the case of the singly distinguished particles.

2.4.4 Terminated Chains

While in the previous treatment (see the Kinetic Scheme in Section 2.2) desorption was considered a first-order termination mechanism, it is actually not a termination mechanism, and must therefore not appear as such in the terminated polymer equations. Eq. (2.17) for the polymer terminated monomolecularly must therefore be re-written without the term related to desorption. In the case of linear chains:

$$\begin{aligned} \frac{d[v_P S^M(t_e, t')]}{dt_e} &= \{k_{fm}C_m \sum_{i=1}^N N_i'(t_e - t', t') + \frac{\rho}{N} N_N'(t_e - t', t') \\ &\quad + 2c_d \sum_{i=2}^N (i-1)N_i'(t_e - t', t')\} \end{aligned} \quad (2.44)$$

Introducing parameter f defined by eq. (2.34), the equation above becomes:

$$\begin{aligned} \frac{d[v_P S^M(t_e, t')]}{dt_e} &= \{(k_d + f) \sum_{i=1}^N N_i'(t_e - t', t') + \frac{\rho}{N} N_N'(t_e - t', t') \\ &\quad + 2c_d \sum_{i=2}^N (i-1)N_i'(t_e - t', t')\} \end{aligned} \quad (2.45)$$

i.e., as for the live chain equations, the equation results identical to that given in Section 2.3, but for parameter f instead of the first-order rate coefficient for chain transfer to polymer, $k_{fm}C_m$.

2.5 Model Results: Instantaneous Properties

Before considering the model results in terms of instantaneous properties, it is worth discussing their actual physical meaning in the case where mechanisms reactivating dead

polymer chains (thus producing nonlinear chains) are present. When no such mechanism is active, i.e., in the case of linear chains, eqs (2.16)-(2.17) and (2.18)-(2.21) represent the characteristics of the polymer produced at a given reaction time which, integrated over the entire process time, provide the characteristics of the final product. Although this last aspect holds true also in the presence of chain transfer to polymer, crosslinking or TDB propagation, eqs (2.16)-(2.17) and (2.18)-(2.21) do not have in this case a clear physical meaning. They describe the production at a given time of dead branched chains, portion of which (i.e., the pre-life) formed at previous times during the process, and involve negative terms as well, corresponding to the reactivation of dead polymer chains. Therefore, in the case of branched chains, eqs (2.16)-(2.17) and (2.18)-(2.21) do not provide the characteristics of the polymer produced instantaneously. Nevertheless, when the instantaneous molecular weight properties are defined, just as in the case of linear chains, through the following equations:

- *instantaneous number average chain length*

$$M_n^i = \frac{d(v_P \sigma^{(1)})}{d(v_P \sigma^{(0)})} \quad (2.46)$$

- *instantaneous weight average chain length*

$$M_w^i = \frac{d(v_P \sigma^{(2)})}{d(v_P \sigma^{(1)})} \quad (2.47)$$

- *instantaneous polydispersity ratio*

$$P_d^i = \frac{M_w^i}{M_n^i} \quad (2.48)$$

it can be shown that the relations linking these properties to the corresponding cumulated ones are independent of the polymer being branched or linear (see Appendix B). This means that, in the case of branched chains, the analysis of the instantaneous properties is still as significant with respect to the average values (M_n and M_w) and broadness (P_d) of the CLD of the polymer which is being produced as in the case of linear chains. Note that definitions (2.46)-(2.48) account for the fact that during an emulsion reaction polymer particles change in size.

The role of compartmentalization in emulsion polymerization systems where either a crosslinking or a propagation to TDB reaction is operative is illustrated through a series of simulations where the results obtained from the model here developed are compared to those given by a model neglecting active chain compartmentalization (though accounting for all other peculiarities of emulsion polymerization). This last model will be referred

Parameter	Value
C_m	$5.7 \cdot 10^{-3} \text{ mol cm}^{-3}$
k_d	$1.3 \cdot 10^{-3} \text{ s}^{-1}$
k_{fm}	$10 \text{ cm}^3 \text{ mol}^{-1} \text{ s}^{-1}$
k_{fp}	$0 \text{ cm}^3 \text{ mol}^{-1} \text{ s}^{-1}$
k_p	$2.6 \cdot 10^5 \text{ cm}^3 \text{ mol}^{-1} \text{ s}^{-1}$
k_p^*	$0 \div 5 \text{ cm}^3 \text{ mol}^{-1} \text{ s}^{-1}$
$k_p^{*(TDB)}$	$0 \div 2.6 \cdot 10^5 \text{ cm}^3 \text{ mol}^{-1} \text{ s}^{-1}$
k_{tc}	$1.16 \cdot 10^9 \text{ cm}^3 \text{ mol}^{-1} \text{ s}^{-1}$
k_{td}	$1.16 \cdot 10^9 \text{ cm}^3 \text{ mol}^{-1} \text{ s}^{-1}$
v_P	$1.21 \cdot 10^{-15} \text{ cm}^3$
γ	1
$\gamma^{(TDB)}$	0.517
$\sigma^{(0)}$	$2.38 \cdot 10^{-7} \text{ mol cm}^{-3}$
$\sigma^{(1)}$	$3.22 \cdot 10^{-3} \text{ mol cm}^{-3}$
$\sigma^{(2)}$	$105.3 \text{ mol cm}^{-3}$

Table 2.1: Numerical values of the model parameters used for the calculation of instantaneous properties. The moments $\sigma^{(k)}$ of the dead polymer are referred to the particle volume.

to as a ‘non-compartmentalized’ model and is simply obtained by forcing the moment equations derived for homogeneous polymerizations, reported in Appendix C, to describe the heterogeneous emulsion system. The comparison between the two models has been performed by imposing the same active chain concentrations ($\bar{n} = R^\bullet N_A v_P$, where \bar{n} is the average number of radicals per particle and R^\bullet the radical concentration in the non-compartmentalized case).

The numerical values of the parameters used for these calculations, corresponding to a typical free-radical polymerization, are summarized in Table 2.1.

2.5.1 Crosslinking Reaction

The crosslinking reaction has been first considered. Its effect on the molecular weight properties has been analyzed by calculating the instantaneous polydispersity ratio and weight average chain length as a function of \bar{n} at increasing values of the crosslinking kinetic constant, represented by the dimensionless parameter $q^* = k_p^* \gamma \sigma^{(1)} / c$, being $\sigma^{(1)}$ the first order moment of the overall dead polymer CLD and $c = c_c + c_d$ the pseudo-first order rate constant for bimolecular termination in the particles. These results have been generated by letting the radical entry parameter ρ vary and solving numerically [40] the Smith-Ewart equations in order to obtain the active chain distribution in the polymer particles N_i , which is then used for computing both the average number of radicals \bar{n} as well as the instantaneous molecular weight properties.

In order to achieve a better physical insight in the behavior of the systems considered, the two cases of bimolecular termination by combination and disproportionation are considered separately. The extent of the bimolecular termination reaction has been assumed the same in the two cases, i.e., the same value of the parameter c has been used. Moreover, in both cases, chain transfer to monomer is also present (see Table 2.1).

Fig. 2.1 shows the results relative to the case where the only active bimolecular termination mechanism is combination. So as to understand better the physical meaning of these results, it should be noted that for very low \bar{n} values monomolecular terminations prevail, while as \bar{n} increases bimolecular termination (by combination in this case) becomes more relevant and eventually dominant at \bar{n} values as large as about 2-3. The case of a non-compartmentalized system, represented by the dashed curves in Fig. 2.1, is first considered. In the case of linear chains, i.e., $q^* = 0$, it can be seen from Fig. 2.1(a) that the instantaneous polydispersity decreases with \bar{n} from 2 to 1.5, which are the typical instantaneous polydispersity values corresponding to monomolecular termination and bimolecular termination by combination, respectively. This happens because combination couples the lengths of the active chains, with the result of making the dead chain population more uniform. When the crosslinking reaction is introduced ($q^* > 0$), the polydispersity values increase compared to linear chains. This is mainly due to the peculiar feature of crosslinking, which involves preferably the longer dead chains, thus causing a further increase in their length which makes the chain population more wide. Accordingly, at a given value of \bar{n} , the polydispersity ratio is higher the higher the value of q^* . Observing the shape of the dashed P_d^i versus \bar{n} curves at increasing q^* values, it is interesting to note that these pass from a monotonically decreasing to a maximum exhibiting behavior (which would eventually become monotonically increasing at even higher q^* values). Such a maximum is the result of two counteracting tendencies. The first is a polydispersity increase caused by crosslinking for increasing \bar{n} values. The second effect is the decrease in polydispersity related to the presence of termination by combination, which has already been discussed for linear chains; this effect is stronger at higher \bar{n} values, where combination is dominant. The first of the two mentioned effects, absent in the case of linear chains, becomes more and more relevant at increasing values of the crosslinking rate.

The effect of compartmentalization can be well understood by comparing the continuous curves to the results (dashed curves) relative to the non-compartmentalized system discussed above. First of all, in a compartmentalized system bimolecular terminations are unfavoured, and larger \bar{n} values are needed (compared to a non-compartmentalized system) for these to prevail over monomolecular terminations. This explains, in Fig. 2.1(a),

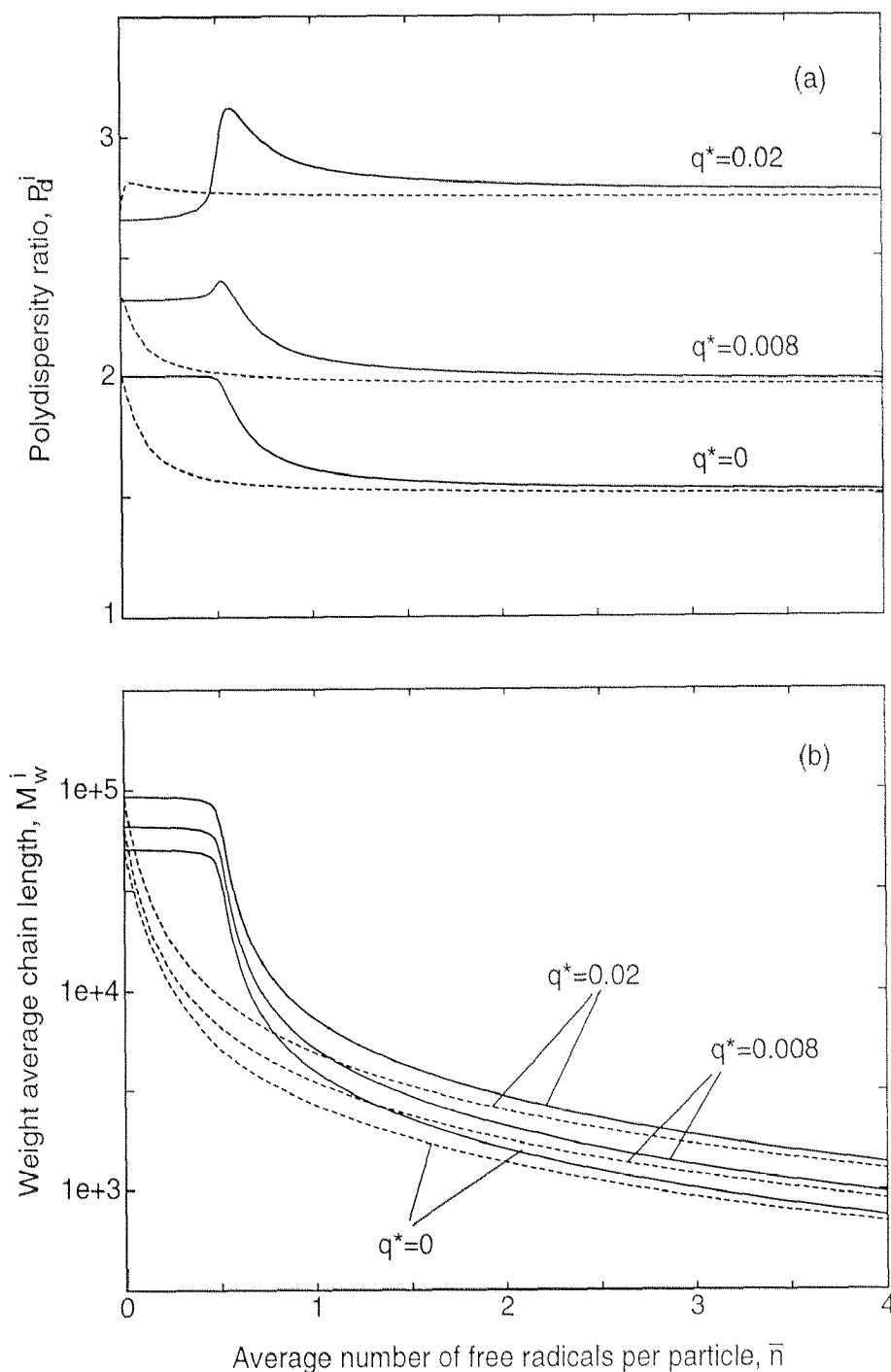


Figure 2.1: Polydispersity ratio (a) and weight average chain length (b) as a function of the average number of active chains per particle, \bar{n} , in the presence of bimolecular termination by combination. Parameter values as in Table 2.1 but with $k_{td} = k_p^{*(TDB)} = 0$ and three different values of q^* ($= k_p^* \gamma \sigma^{(1)} / c$). — : compartmentalized model; --- : non-compartmentalized model.

the almost horizontal portion of the continuous curves at low \bar{n} values, which is similar to that discussed earlier in the context of long-chain branching [24]. A second effect of compartmentalization is the modification it induces in the polydispersity behavior in a small range of \bar{n} values around 0.5, where the transition from monomolecular to bimolecular termination control occurs. This is the same (although much enhanced) trend highlighted for the non-compartmentalized system but delayed to larger \bar{n} values due to radical compartmentalization. At increasing \bar{n} values, pseudo-bulk conditions (i.e., conditions where compartmentalization is no longer effective) are approached and combination plays the same role as in a non-compartmentalized system, thus reducing polydispersity. Summarizing, the P_d^i versus \bar{n} behavior in the compartmentalized system can be explained on the same basis as for the non-compartmentalized case, but correcting it for the delay in bimolecular terminations prevailing (pseudo-bulk conditions being approached) and for the peculiar interaction between compartmentalization and bimolecular termination at \bar{n} around 0.5.

It should be noted that the two models (compartmentalized and non-compartmentalized) provide the same results both at large and at very small values of \bar{n} . This is an expected result, since, at both extremes, the effect related to active chain compartmentalization vanishes. This is because at high \bar{n} values the number of radicals in all particles is so large that these behave as mini-bulks, while at very low \bar{n} values all bimolecular events tend to disappear also in a non-compartmentalized system, and consequently compartmentalization does not play any role. The practical relevance of giving a correct description of compartmentalization is clear when comparing the solid and the dashed curves in Fig. 2.1 at intermediate values of \bar{n} (i.e., around $\bar{n} = 0.5$, which is a typical value for many emulsion reactions): significant differences arise in the polydispersity ratio, and the weight average chain length can be underestimated by even one order of magnitude when compartmentalization is neglected (Fig. 2.1(b)).

Similar simulations are shown in Fig. 2.2 for the case where bimolecular termination occurs through disproportionation. Starting once again from the non-compartmentalized system (dashed curves), it appears that in the case of linear chains ($q^* = 0$) the instantaneous polydispersity (Fig. 2.2(a)) remains constant and equal to 2 at all \bar{n} values, i.e., both when monomolecular and bimolecular terminations are dominant. This is due to the already discussed nature of the disproportionation mechanism, which maintains the length of the active chain upon termination. Since, as discussed above, polydispersity tends to increase at increasing \bar{n} values in the presence of crosslinking, monotonically increasing curves are obtained for $q^* > 0$.

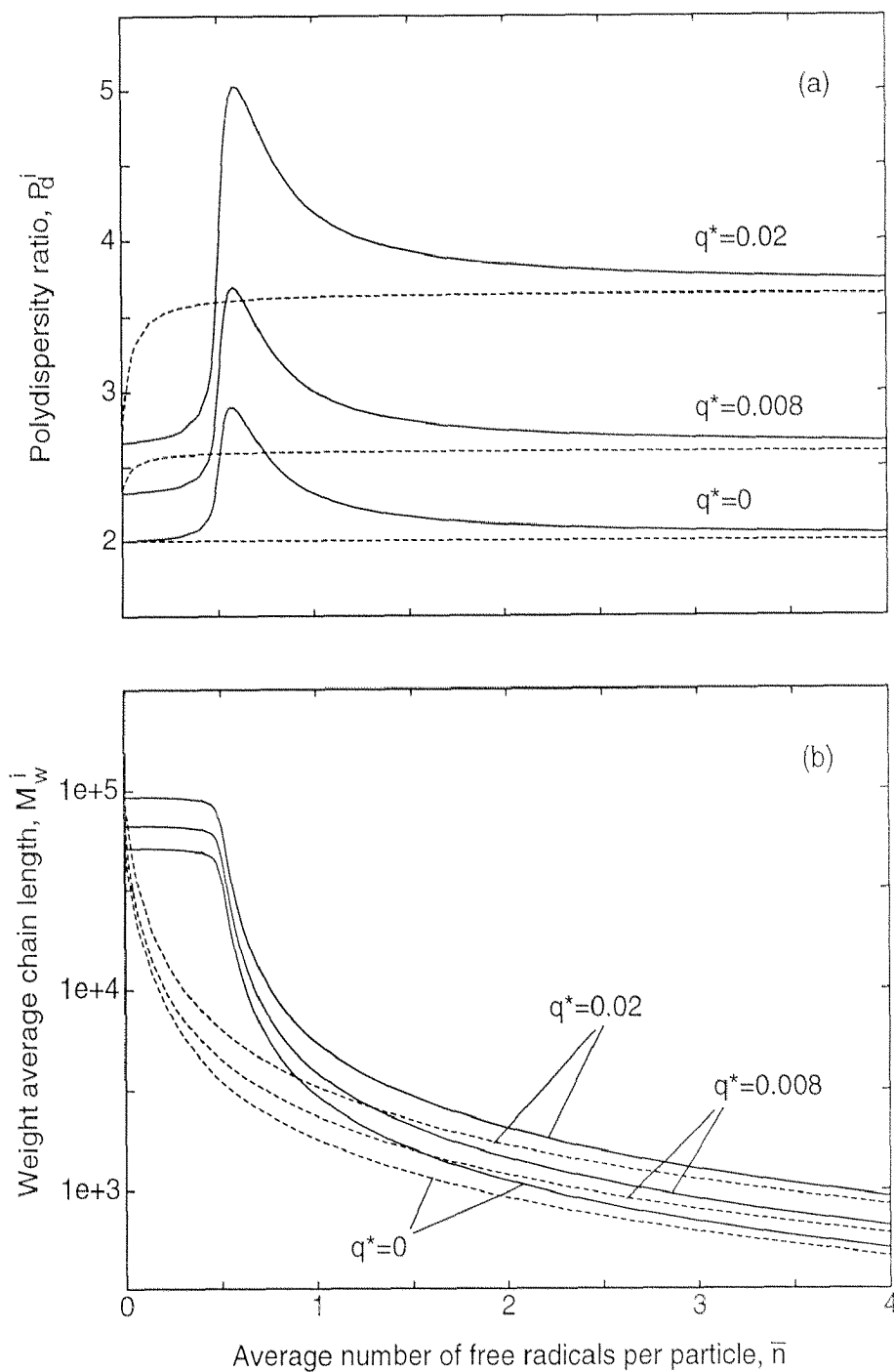


Figure 2.2: Polydispersity ratio (a) and weight average chain length (b) as a function of the average number of active chains per particle, \bar{n} , in the presence of bimolecular termination by disproportionation. Parameter values as in Table 2.1 but with $k_{tc} = k_p^{*(TDB)} = 0$ and three different values of q^* ($= k_p^* \gamma \sigma^{(1)} / c$). — : compartmentalized model; --- : non-compartmentalized model.

The effect of compartmentalization is best illustrated by comparing the solid to the dashed curves in Fig. 2.2. In the case of linear chains, it can be seen that disproportionation causes an enhancement in polydispersity (Fig. 2.2(a)) which leads to a maximum located at about $\bar{n} = 0.5$. This is a peculiar effect of disproportionation in compartmentalized systems, which appears when instantaneous termination by disproportionation involves short radicals incoming from the water phase, leading to polydispersity values as large as four [7]. The maximum in Fig. 2.2(a) for $q^* = 0$ is actually lower than four because of the presence of another termination mechanism (see Table 2.1). The presence of the crosslinking reaction (solid curves at $q^* > 0$) enhances the polydispersity values at all \bar{n} values. However, this effect appears to be stronger around $\bar{n} = 0.5$ and the maxima are even more pronounced than in the linear case.

As for the case of termination by combination, the practical importance of a correct description of compartmentalization (at least in the interval $0 < \bar{n} < 2$), both when considering polydispersity and average chain length, appears from the differences between the solid and the dashed curves in Fig. 2.2.

Finally, it is worth comparing the results of this section with those reported earlier for chain branching occurring through chain transfer to polymer (see Figs 3 and 5 of ref. [24]). The comparison is straightforward since the definitions and values of all parameters, included the moments of the CLD of the preformed dead polymer (see Table 2.1), have been chosen the same. As expected, it appears that the crosslinking reaction is more effective in increasing polydispersity and weight average chain length than the chain transfer to polymer reaction.

2.5.2 Propagation to TDB Reaction

In order to illustrate the role of the propagation to TDB reaction on the instantaneous molecular weight properties of polymers produced in compartmentalized systems, the polydispersity ratio has been calculated as a function of \bar{n} for increasing values of the rate of propagation to TDB. This is represented by the dimensionless parameter $q^{*(TDB)} = k_p^{*(TDB)}\gamma^{(TDB)}\sigma^{(0)}/c$, where $\sigma^{(0)}$ is the zeroth order moment of the overall dead polymer CLD. As for the crosslinking reaction, the two cases of bimolecular termination by combination and disproportionation have been considered separately.

Fig. 2.3 considers the case where bimolecular termination occurs by combination, while in Fig. 2.4 the only active bimolecular termination mechanism is disproportionation. A comparison with Figs 2.1(a) and 2.2(a), where all conditions are the same except for the branching mechanism, i.e., crosslinking instead of TDB propagation, leads to some imme-

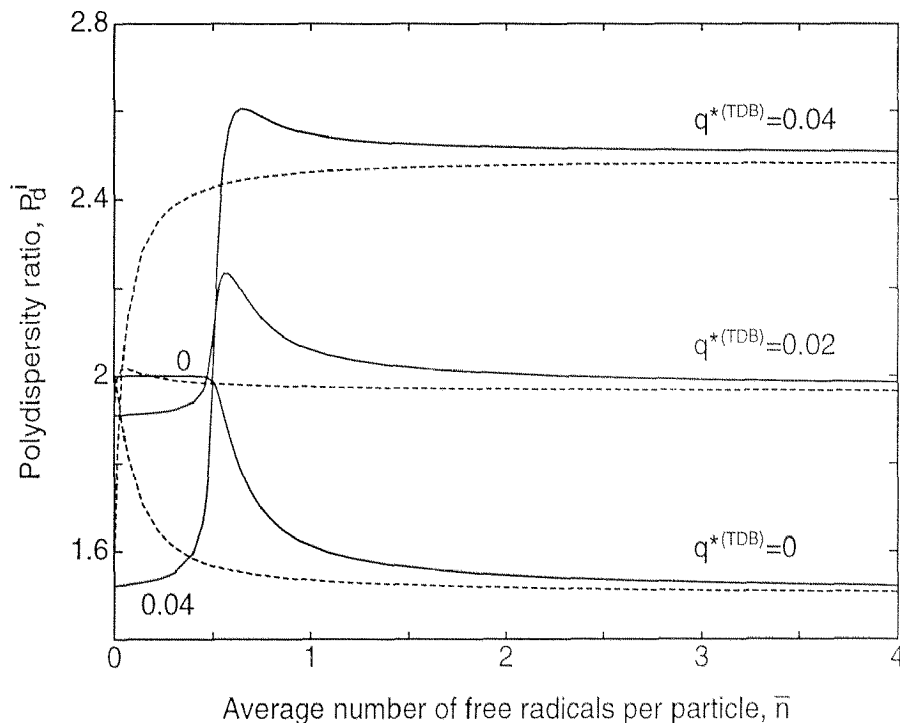


Figure 2.3: Polydispersity ratio as a function of the average number of active chains per particle, \bar{n} , in the presence of bimolecular termination by combination. Parameter values as in Table 2.1 but with $k_{td} = k_p^* = 0$ and three different values of $q^{*(TDB)}$ ($= k_p^{*(TDB)} \gamma^{(TDB)} \sigma^{(0)} / c$). — : compartmentalized model; --- : non-compartmentalized model.

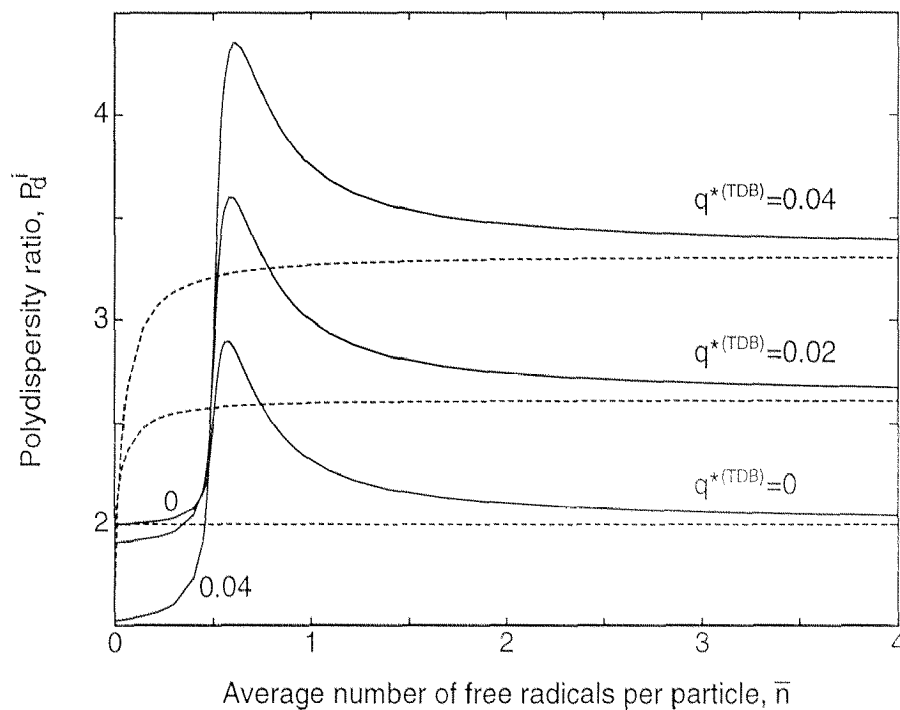


Figure 2.4: Polydispersity ratio as a function of the average number of active chains per particle, \bar{n} , in the presence of bimolecular termination by disproportionation. Parameter values as in Table 2.1 but with $k_{tc} = k_p^* = 0$ and three different values of $q^{*(TDB)}$ ($= k_p^{*(TDB)} \gamma^{(TDB)} \sigma^{(0)} / c$). — : compartmentalized model; --- : non-compartmentalized model.

diate considerations. First of all, it is apparent that the crosslinking reaction produces a much stronger increase in the polydispersity ratio than propagation to TDB at equal reaction rates, i.e., $q^* = q^{*(TDB)}$. This is because, although the two mechanisms are similar in the sense that both involve the addition of a free radical to an unsaturated polymer molecule, the rate of the crosslinking reaction is proportional to the length of the dead chain, while the rate of propagation to TDB is independent of its length (at least when neglecting steric effects and diffusive limitations). Accordingly, the crosslinking reaction involves preferably the longer dead chains and increases further their length. This obviously makes the polymer CLD wider.

On the other hand, the qualitative behavior of the polydispersity curves in Figs 2.3 and 2.4, such as the presence of the maxima both in the case of combination and disproportionation, is similar to that observed earlier in the context of Figs 2.1 and 2.2 and can be understood through the same arguments. Only one minor difference appears in the region of very low \bar{n} values, where polydispersity decreases for increasing rates of TDB propagation.

The results shown above suggest that the propagation to TDB reaction, often neglected in describing the kinetics of polymerization systems, has actually a significant effect on the molecular weight properties of the produced polymer. The values of the kinetic parameters used in Figs 2.3 and 2.4 are in fact representative of real systems. For instance, the value $q^{*(TDB)} = 0.04$, which leads to a remarkable polydispersity increase (more than 50% compared to linear chains at high \bar{n}), results from assuming the TDB as reactive as the monomer ($k_p^{*(TDB)} = k_p$) and $\gamma^{(TDB)} = 0.517$, i.e., slightly more than half the dead chains with one TDB.

The simulations shown in Figs 2.3 and 2.4 have been repeated in the presence of chain transfer to polymer (with $q = k_{fp}\sigma^{(1)}/c = 0.04$), in order to illustrate the interaction between the two branching mechanisms. The obtained polydispersity versus \bar{n} curves are shown in Figs 2.5 and 2.6 in the cases of bimolecular termination by combination and disproportionation, respectively. It is apparent that the presence of chain transfer to polymer significantly enhances the ability of the propagation to TDB reaction to increase the polydispersity. The role of the propagation to TDB mechanism is qualitatively the same as in the case discussed above, where it is the only branching mechanism operative. However, in the case where chain transfer to polymer is present, the effect of TDB propagation becomes quantitatively stronger. There is in fact a synergic action of the two mechanisms, since the TDB propagation can join together two macromolecules which have grown already to a large size due to repetitive chain branching reactions.

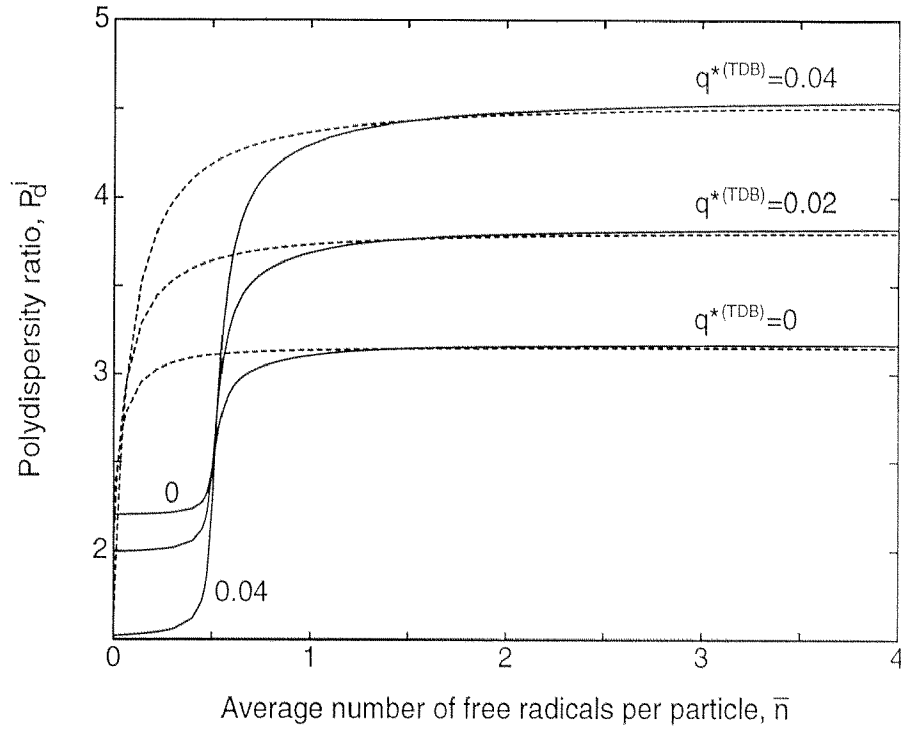


Figure 2.5: Polydispersity ratio as a function of the average number of active chains per particle, \bar{n} , in the presence of bimolecular termination by combination. Parameter values as in Table 2.1 but with $k_{td} = k_p^* = 0$, $q = k_{fp}\sigma^{(1)}/c = 0.04$ and three different values of $q^{*(TDB)}$ ($= k_p^{*(TDB)}\gamma^{(TDB)}\sigma^{(0)}/c$). — : compartmentalized model; - - - : non-compartmentalized model.

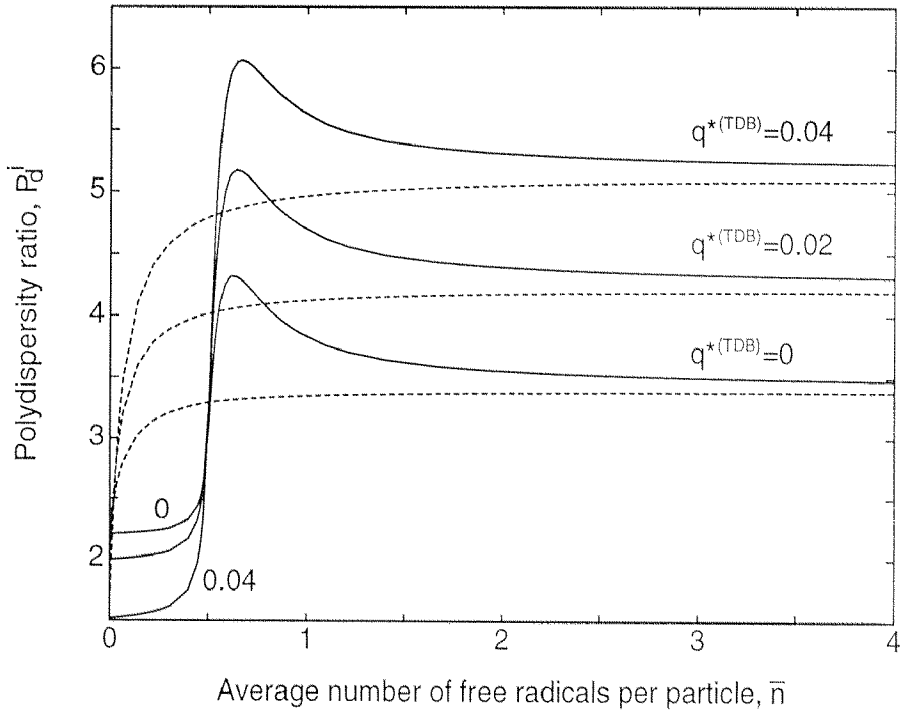


Figure 2.6: Polydispersity ratio as a function of the average number of active chains per particle, \bar{n} , in the presence of bimolecular termination by disproportionation. Parameter values as in Table 2.1 but with $k_{tc} = k_p^* = 0$, $q = k_{fp}\sigma^{(1)}/c = 0.04$ and three different values of $q^{*(TDB)}$ ($= k_p^{*(TDB)}\gamma^{(TDB)}\sigma^{(0)}/c$). — : compartmentalized model; - - - : non-compartmentalized model.

All the results reported above both for the crosslinking and the propagation to TDB reaction indicate that the role of chain compartmentalization on the MWD of a polymer produced in emulsion is important not only for linear chains [7] but also for branched polymers. As concluded earlier in the case of branched chains produced by chain transfer to polymer [24], using a model neglecting compartmentalization for calculating the MWD in an emulsion polymerization system can introduce significant inaccuracies, particularly in the range of values $0 < \bar{n} < 2$, which is typical of several systems of practical relevance.

2.6 Model Results: Cumulative Properties

The properties of the polymer which can be measured experimentally and which affect its end-use properties, i.e., those of interest in applications, are the cumulative ones. Therefore, the model described above for calculating the instantaneous MWD has been coupled to another model [41] which describes the evolution during the reaction of all quantities determining the MWD itself, i.e., monomer concentration in the particles, rates of radical entry and desorption, etc. This allows the description of the entire polymerization process and the calculation of the cumulative properties of the final product.

As for Section 2.5, which deals with the instantaneous properties, in the following we consider first the crosslinking and next the propagation to TDB reaction, this time with reference to the cumulative properties of the polymer. The two branching mechanisms have been considered separately in order to illustrate their peculiar features in affecting the molecular properties of the product. The interaction of different branching mechanisms, including the chain transfer to polymer reaction analysed in ref. [24], is indeed an interesting subject, which however has not been treated here.

2.6.1 Crosslinking Reaction

As mentioned above, the reported simulations have been performed using the numerical fractionation technique [30] which, as described in detail in Appendix A, requires the discretization of the CLD in appropriate subdistributions referred to as generations. In order to obtain reliable results the model requires the use of a sufficient number NG of branched generations, which can be determined by repeating the calculations with an increasing number of generations until no change in the results is observed. This procedure is illustrated in Fig. 2.7 with respect to the gel point and gel weight fraction for a seeded polymerization. It is seen that for increasing NG values convergence is achieved on the gel point at a reaction time equal to about 43 minutes (corresponding to 43% conversion). All kinetic constants, the characteristics of the seed and other necessary quantities used

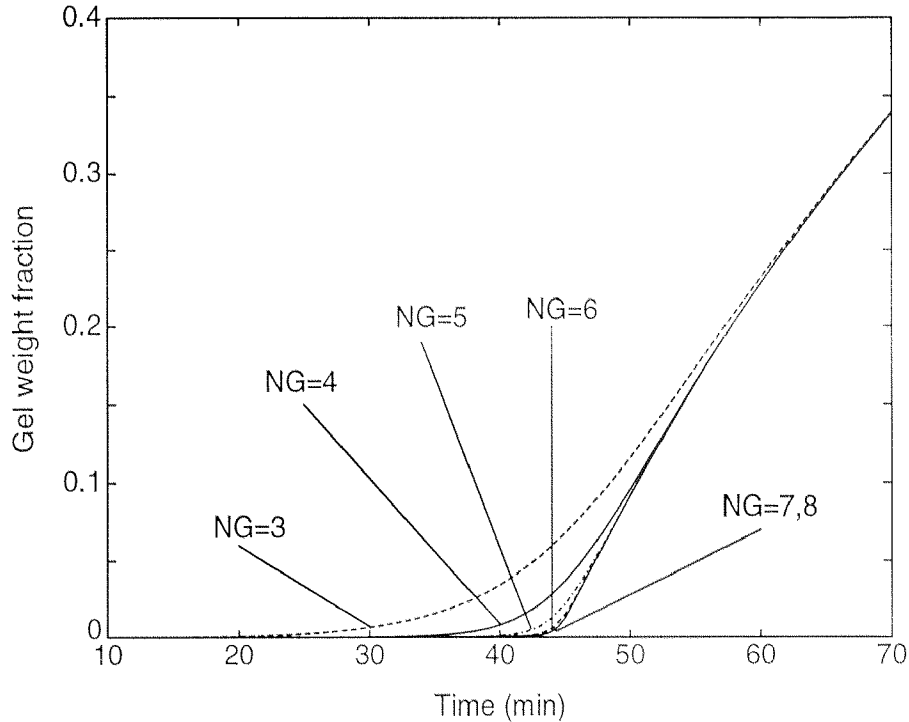


Figure 2.7: Gel weight fraction as a function of time for an increasing number of branched generations, NG . Parameter values as in Table 2.2, but with $k_p^{*(TDB)} = 0$.

in these calculations are reported in Table 2.2, with the only exception of $k_p^{*(TDB)}$ which has been taken equal to zero, so that crosslinking is the only source of nonlinearity for the macromolecules.

Once the optimal NG value is selected as the minimum at which convergence is achieved (i.e., $NG=7$ in the case shown in Fig. 2.7), calculations can be performed for all quantities of interest. In particular, molecular weight properties can be evaluated for the sol polymer fraction both before and after the gel point. The calculated number and weight average chain lengths of the sol, M_n and M_w respectively, are shown in Fig. 2.8 as a function of reaction time (solid curves). The qualitative behavior is similar to that observed in bulk [30] and in emulsion [24] for the case of gel formation due to the simultaneous presence of chain transfer to polymer and bimolecular combination. However, crosslinking is much more efficient in driving the system to gelation, and in fact gelation is reached at much lower conversions even for lower rates of the branching mechanism. Moreover, in this case bimolecular termination by combination is not necessary for the occurrence of gelation, since the mechanism connecting polymer molecules, thus ensuring a geometrical growth in the size of the chains which is needed for a very large size to be reached, is already provided by the crosslinking reaction. In other words, crosslinking on its own is sufficient

Parameter	Value	Meaning
B	0.939	Trommsdorff effect parameter [41]
C	3.875	Trommsdorff effect parameter [41]
$C_{m,w}^*$	$3.68 \cdot 10^{-6}$ mol cm ⁻³	monomer water concentration at saturation
D	-0.494	Trommsdorff effect parameter [41]
k_e	$2 \cdot 10^{-13}$ cm ³ s ⁻¹	entry rate constant
k_{fm}	9.07 cm ³ mol ⁻¹ s ⁻¹	chain transfer to monomer rate constant
k_{fp}	0 cm ³ mol ⁻¹ s ⁻¹	chain transfer to polymer rate constant
k_I	$1.18 \cdot 10^{-6}$ s ⁻¹	initiator decomposition rate constant
k_p	$2.59 \cdot 10^5$ cm ³ mol ⁻¹ s ⁻¹	propagation rate constant
k_p^*	10 cm ³ mol ⁻¹ s ⁻¹	crosslinking rate constant
$k_p^{*(TDB)}$	$2.59 \cdot 10^5$ cm ³ mol ⁻¹ s ⁻¹	TDB propagation rate constant
k_{tc}	$5.97 \cdot 10^9$ cm ³ mol ⁻¹ s ⁻¹	termination by combination rate constant
k_{td}	0 cm ³ mol ⁻¹ s ⁻¹	termination by disproportionation rate constant
$[I]_w^0$	$2.13 \cdot 10^{-6}$ mol cm ⁻³	initial molar concentration of initiator
M_n^{seed}	$1 \cdot 10^4$	seed number-average chain length
N_P	$1 \cdot 10^{14}$ cm ⁻³	seed particle concentration
P_d^{seed}	2	seed polydispersity ratio
M_m	104.2 g mol ⁻¹	monomer molecular weight
V_m	113.8 cm ³	total volume of charged monomer
$v_{P,0}$	$5 \cdot 10^{-16}$ cm ³	initial particle volume
V_w	1012.3 cm ³	total volume of charged water
η	1	initiator efficiency
ϕ_m^*	0.68	particle monomer volume fraction at saturation
ρ_m	0.878 g cm ⁻³	monomer density
ρ_p	1.05 g cm ⁻³	polymer density

Table 2.2: Numerical values of the model parameters used for the illustrative calculations of cumulative properties.

to yield chains of any generation order. In the same figure, the chain length averages are also reported in the absence of the crosslinking reaction, i.e., for linear chains (dashed lines), so as to highlight by comparison the effect of the crosslinking mechanism.

The entire weight CLD of the polymer, calculated at 40% conversion, a few percentages before gelation, is shown in Fig. 2.9 (solid line). This has been obtained by reconstructing the weight CLD of each generation from its first three moments (using the Schultz distribution [42]) and by then summing these up, each weighted on the ratio between the first order moment of the generation and the overall first order moment. In Fig. 2.9 these contributions are shown by the dashed curves, at least for the more representative generations. It can be seen that the crosslinking reaction produces a significant portion of polymer chains with very large degree of polymerization (branched generations $g = 1$ and $g = 2$ in the figure) which, by further growth and connection, rapidly lead to the formation of huge polymer networks, i.e., the gel.

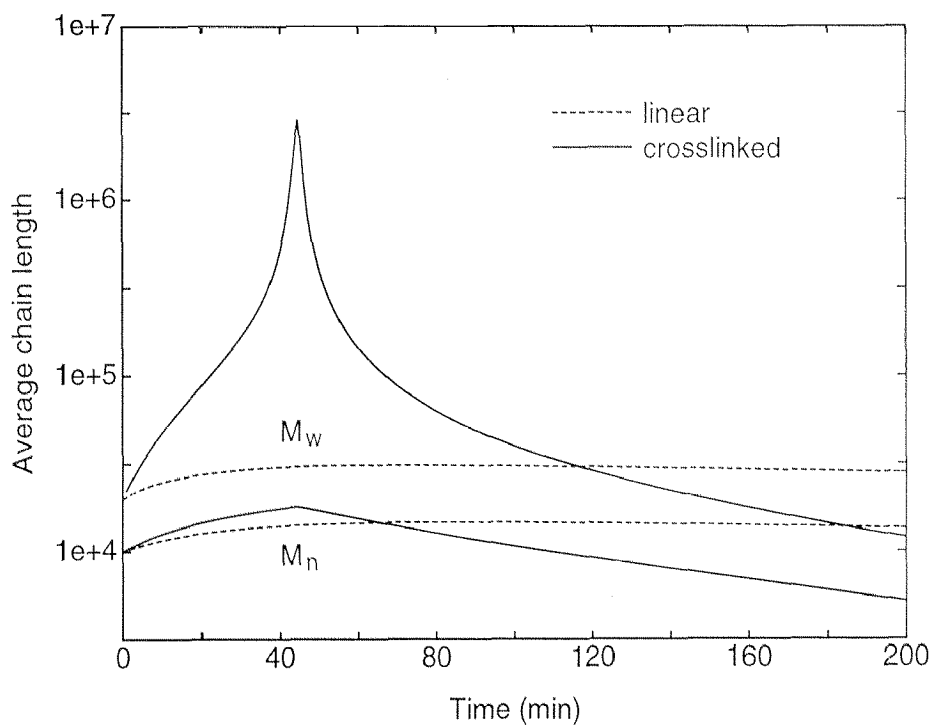


Figure 2.8: Number and weight average chain length as a function of time. Parameter values as in Table 2.2, but with $k_p^{*(TDB)} = 0$.

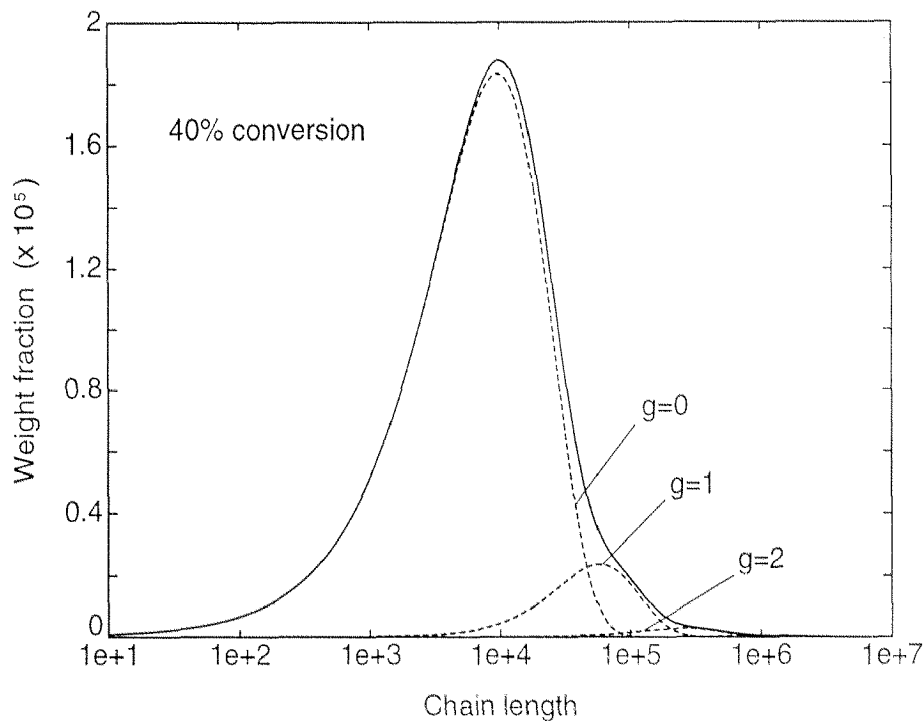


Figure 2.9: Overall weight chain length distribution at 40% conversion, just before the gel point, in the case of crosslinking as a branching mechanism. Parameter values as in Table 2.2, but with $k_p^{*(TDB)} = 0$.

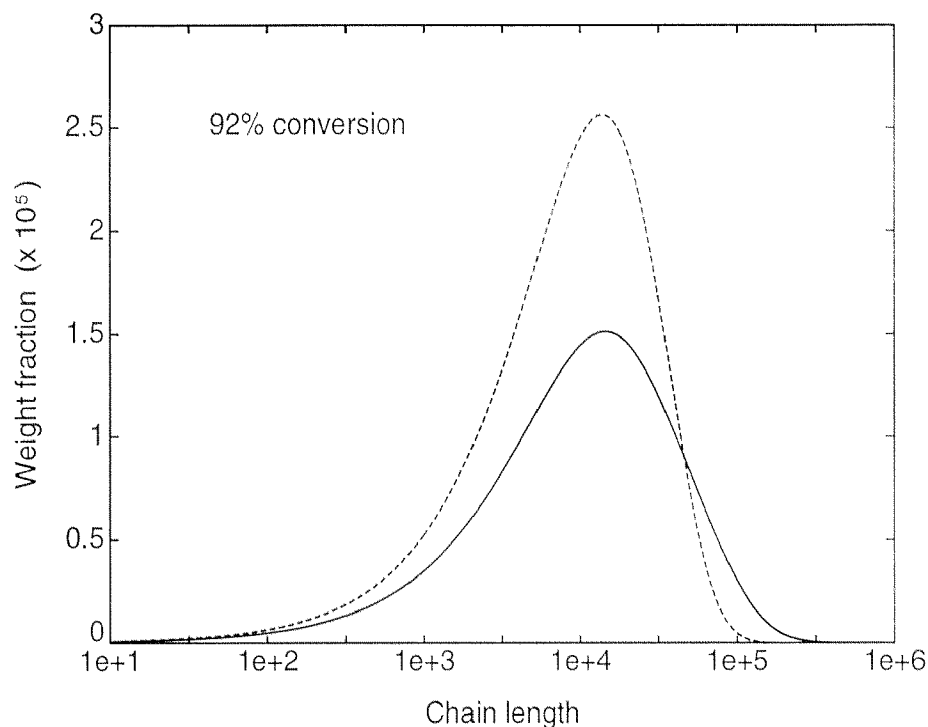


Figure 2.10: Overall weight chain length distribution at 92% conversion in the case of branching occurring through propagation to TDB (—) and no branching (- - -). Parameter values as in Table 2.2, but with $k_p^* = 0$.

It is worth noting that the possibility of using only three moments for the reconstruction of the CLD of each generation is due to the fact that these subdistributions are much narrower than the overall polymer chain distribution.

2.6.2 Propagation to TDB Reaction

The propagation to TDB reaction mechanism is present in several systems of practical interest, such as in the polymerization of vinyl acetate and of certain vinyl fluorides. In order to illustrate to what extent the CLD of a polymer produced in emulsion may be affected by the presence of the propagation to TDB reaction, two simulated CLDs are shown in Fig. 2.10. The solid curve refers to the case where TDB propagation is present, the dashed curve to that where it is absent (linear chains). The parameters used in the simulations are summarized in Table 2.2, except for the crosslinking kinetic constant k_p^* which is taken equal to zero. Note that the effect of TDB propagation is quite significant and cannot be neglected. The same marked effect of the propagation to TDB reaction has been observed also in the case where branching occurs already through another mechanism, namely chain transfer to polymer [43].

In Fig. 2.11, the weight CLD of the polymer produced in the presence of the propaga-

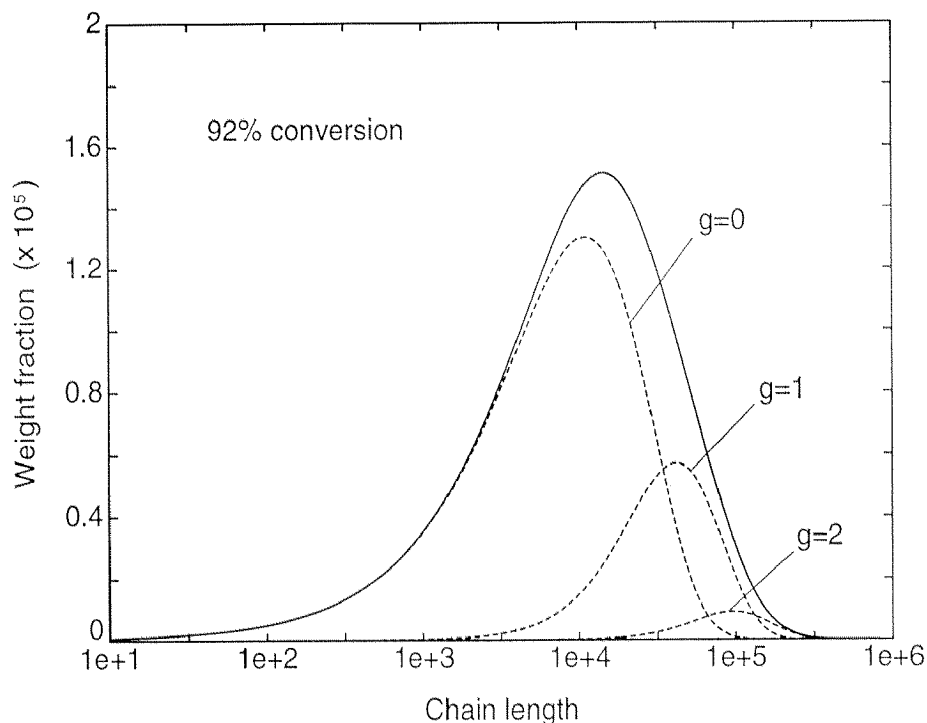


Figure 2.11: Overall weight chain length distribution at 92% conversion in the case of branching occurring through propagation to TDB. Parameter values as in Table 2.2, but with $k_p^* = 0$.

tion to TDB reaction shown in Fig. 2.10 is compared to the contributions of the individual generations (dashed curves). This shows more clearly the role played by the propagation to TDB reaction, which produces a relevant portion of high molecular weight branched chains (generations $g = 1$ and $g = 2$). However, the highest molecular weights produced are much smaller, even at far larger conversions, than those obtained in the case of crosslinking (see Fig. 2.9). Accordingly, no gel formation is predicted in this case for propagation to TDB. The lower efficiency of the propagation to TDB mechanism in approaching gelation as compared to crosslinking is due to the fact that the ability of the chains to combine with one another does not increase with their size. On the contrary, in the case of crosslinking, the larger a chain, the greater its expectancy for being involved in further crosslinking, i.e., for increasing further its size and complexity. This feature obviously favors the formation of the very large chains which the gel phase consists of [35].

2.7 Gelation: a Comparison with Flory's Statistical Theory

A comparison between the kinetic model developed in this chapter and Flory's statistical model [35] is performed with respect to the prediction of the gel point and the gel weight

fraction of the polymer in the case where a crosslinking reaction is present during the polymerization of a diene. The two models are quite different in nature, although they both refer to modest crosslinking densities, in the sense that no cyclizations are admitted. The model here developed is a kinetic model which describes in detail the formation of the nonlinear polymer chains as a result of all the involved chemical reactions. Gelation is determined as the point where chains of sufficiently large size and complexity are produced. According to the numerical fractionation technique, the critical size and complexity are given by the model itself, without any external assignment. On the other hand, Flory's model for gelation makes use of a criterion which, based on the topology of the macromolecular network (independently of the polymerization process through which this was obtained), states whether or not a gel has formed and to what extent. Neglecting the evolution of the polymerization process, this model is not able to account for the fact that some polymer chains might be more crosslinked than others, but the same crosslinking density is assumed for all chains, i.e., the polymer is supposed to be randomly crosslinked. This has a consequence also on the calculated CLD. Flory's criterion states that a gel appears when the following relation is verified:

$$\epsilon = \rho^* M_w^p = 1 \quad (2.49)$$

where ρ^* is the average crosslinking density and M_w^p the weight average chain length of the primary chains, defined as the linear chains which would be obtained if all crosslinkages were cut. The gel weight fraction, ω_g , is given by the following equation:

$$\omega_g = 1 - \sum_{n=1}^{\infty} \omega_n (1 - \rho^* \omega_g)^n \quad (2.50)$$

where ω_n is the weight CLD of the primary chains.

The application of this criterion requires the calculation of the distribution of the primary chains in the compartmentalized emulsion system. When the degree of crosslinking is not too high the primary chains can be thought of as the chains which would exist if all crosslinkages were severed or, alternatively, as the chains which would exist if no crosslinking were active, as suggested by Flory himself [44]. Accordingly, the quantities M_w^p and ω_n have been obtained using the model described above and setting the crosslinking reaction rate equal to zero. This does not affect the sense of our comparison, since the model adopted reduces to the description of linear chains in emulsion systems developed by Lichti et al. [7], obviously not accounting for gelation, which is instead predicted through eq. (2.49).

In order to solve eq. (2.50), the distribution ω_n has been expressed as a function of its moments through the approximation suggested by Hulburt and Katz [45]. If only the first three moments are used, this gives the number CLD as follows:

$$f(n) = \frac{\lambda}{M_n} p^{(\lambda)} \left(\frac{\lambda n}{M_n} \right) \sigma^{(0)} \quad (2.51)$$

where M_n and $\sigma^{(0)}$ are the number average chain length and the zeroth order moment of the distribution, respectively. The quantity λ and the function $p^{(\lambda)}$ are given by:

$$\lambda = \frac{1}{P_d - 1} \quad (2.52)$$

$$p^{(\lambda)}(z) = z^{\lambda-1} e^{-z}/(\lambda - 1)! \quad (2.53)$$

where P_d is the polydispersity of the distribution.

If the continuous form of eq. (2.50) is used:

$$\omega_g = 1 - \int_0^\infty \omega(n) (1 - \rho^* \omega_g)^n dn \quad (2.54)$$

observing that

$$\omega(n) = n f(n) / \sigma^{(1)}$$

and substituting the resulting analytic expression of $\omega(n)$ (which coincides with the Schultz distribution) in eq. (2.54), one finally obtains:

$$\omega_g = 1 - \frac{1}{\left[1 - \frac{M_n^p}{\lambda} \ln(1 - \rho^* \omega_g) \right]^{\lambda+1}} \quad (2.55)$$

which is the implicit expression for ω_g used in the following calculations. Of course, in this last equation not only M_n^p but also λ refers to the primary chain distribution.

The average crosslinking density ρ^* appearing in eqs (2.49) and (2.55) is calculated as $\rho^* = \nu/\theta$, where ν and θ are the moles of crosslinked and of total polymerized units in the system, respectively. The quantity ν is calculated through the following overall balance which counts all the crosslinking events:

$$\frac{d\nu}{dt} = 2k_p^* \gamma \frac{\theta \bar{n}}{v_P N_A} \quad (2.56)$$

All symbols are defined in the Notation. The coefficient 2 accounts for the fact that two crosslinked units are involved in every crosslinkage.

In Fig. 2.12 the gel weight fraction calculated by the two models is shown for various values of the crosslinking kinetic constant k_p^* . The solid lines refer to the kinetic model, while the dashed lines are the predictions of Flory's model (eq. 2.55). Note that some approximation may be involved in the use of eq. (2.55) because the weight CLD of the

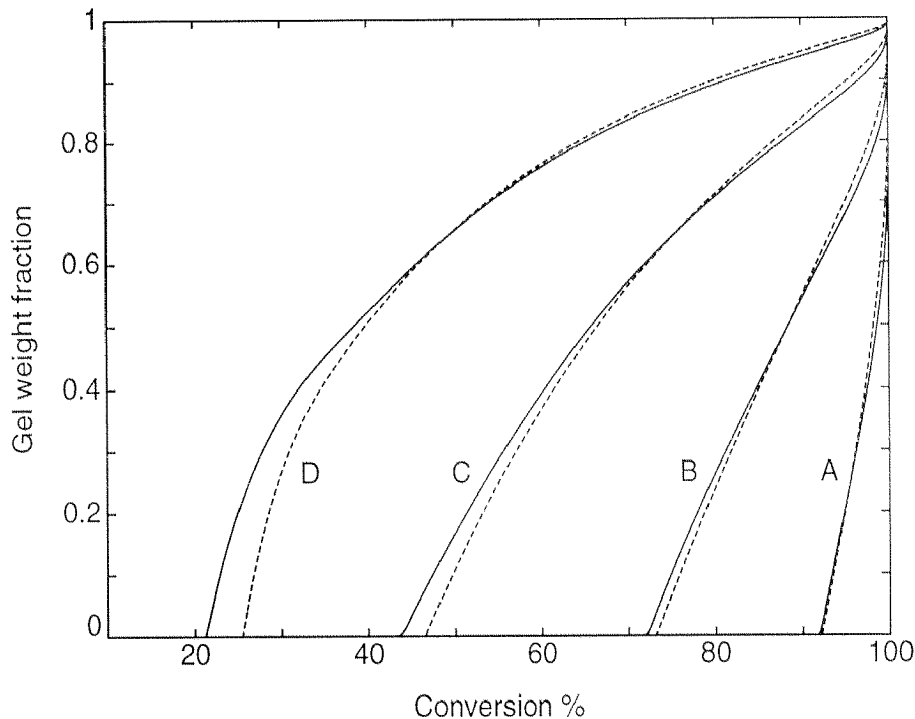


Figure 2.12: Gel weight fraction as a function of conversion at four different values of the crosslinking rate constant k_p^* . (A) $k_p^* = 2.5$ (B) $k_p^* = 5$ (C) $k_p^* = 10$ and (D) $k_p^* = 20 \text{ cm}^3 \text{ mol}^{-1} \text{ s}^{-1}$. All other parameter values as in Table 2.2, but with $k_p^{*(TDB)} = 0$. — : present model; --- : Flory's statistical theory.

primary chains has been reconstructed from its first three moments only. On the other hand, the gel point is that exactly predicted by Flory's theory through eq. (2.49).

It is remarkable that, even though the basic approach of the two models is entirely different, a fairly good agreement in the predictions both of the gel point and of the gel weight fraction is found. It is important to note that the kinetic model always predicts gelation at conversions lower than those given by Flory's model. This can be ascribed to the fact that in a real polymerization system there actually exists a distribution of crosslinking densities which causes gelation to occur somewhat earlier [44] than predicted by Flory's equation, which assumes random crosslinking, i.e., all chains equally crosslinked. The kinetic model instead does not make this assumption. The growth of the chains at different conversion degrees and their successive permanence in the reaction locus, which is the reason for the existence of a crosslinking density distribution among the primary chains [44] is accounted for in a correct manner by the use of the pre-life parameter. This justifies the earlier gelation predicted by the kinetic model in all cases.

Finally, it is worth noting that both models predict a small fraction of polymer remaining in the sol at total conversion, in agreement with other models reported in the

literature [21, 46].

2.8 Conclusions

In this chapter a kinetic model for the evaluation of the MWD of crosslinked and branched polymers produced in emulsion has been developed. The unique feature of this model is that the active chain compartmentalization, characteristic of emulsion polymerization, is accounted for in a rigorous way. This has been made possible by the introduction of a new coordinate in the PBEs of the active chains, the so-called chain pre-life. This parameter allows to account not only for the chain re-birth events typical of chain transfer to polymer [24], but also for the radical step-growth associated with the crosslinking and TDB propagation reactions. It is shown, by comparison with the results of a model neglecting compartmentalization ('non-compartmentalized' model), that significant errors in the prediction of the molecular weight properties of polymers produced in emulsion can be made when using models which do not account for active chain segregation in the particles.

The model has a rather wide generality and requires only some assumptions which are quite typical in nonlinear chain analysis: rate coefficients independent of chain length and a low crosslinking density, which implies that intramolecular reactions (primary and secondary cyclizations) and multiradical chains can be neglected. Although in this chapter we have focused mainly on the CLD, the model allows to calculate all the characteristics of the chains which may be of interest, such as branching and crosslinking density distributions (as shown in Chap. 3), the branch length distribution and so on. A description of the desorption mechanism in line with the current literature has been included in the CLD equations.

An analysis of the instantaneous properties of the polymer has been reported to highlight the effect of compartmentalization both in the case of linear and of branched chains. In all cases compartmentalization causes a delay in the bimolecular terminations becoming dominant at increasing radical concentrations. This results in a plateau in the polydispersity and average molecular weight curves at low radical concentrations, up to average numbers \bar{n} of active chains per particle of almost one half. In the presence of bimolecular termination by disproportionation, a peculiar maximum appears in the polydispersity curve around $\bar{n} = 0.5$, due to the formation of very short chains which can probably be hardly detected by ordinary MWD measurement methods, such as size exclusion chromatography. In the presence of a branching mechanism, maxima in polydispersity are

achieved around $\bar{n} = 0.5$ for intermediate branching rates also in the case of bimolecular termination by combination. The presence of these maxima is however not to be attributed primarily to compartmentalization, but to two counteracting tendencies: an increase in polydispersity at growing radical concentrations related to the presence of the branching mechanism, and a decrease due to the onset of termination by combination which, by chain coupling, tends to make the distribution more narrow. Compartmentalization, besides enhancing these maxima, has mainly the effect (once more related to the delay in the onset of bimolecular termination) of shifting them from very low \bar{n} values to $\bar{n} \simeq 0.5$.

Several simulations have been discussed in order to illustrate the role of crosslinking and TDB propagation on the polymer CLD and on the possible occurrence of gelation. It has been found that, although not always considered in polymerization reaction studies, the propagation to TDB reaction can have a significant effect on the CLD. This is expected to be the case of some important emulsion polymerization systems, such as vinyl acetate.

The model developed has been compared with Flory's statistical model in terms of gel point (i.e., the conversion at which a gel phase appears) and amount of gel produced as a function of conversion. These quantities are computed in Flory's model without describing the kinetics of branching in the system, but analyzing only the distribution of the so-called primary chains (which is equivalent to studying a linear polymerization) and deriving the characteristics of the gel from a statistical relation. The good agreement observed between the obtained results, in spite of the different nature of the two models, provides a significant support to the reliability of both.

Finally, it is worth noting that despite the conceptual difficulties, which make the derivation of the relevant PBEs a bit complex, the final form of the model equations to be solved is rather simple. In particular, the characteristics of the active chain population are given by the solution of linear systems of equations. The evaluation of the cumulative polymer properties involves instead the integration of a relatively small system of ordinary differential equations.

Seite Leer /
Blank leaf

Chapter 3

Fractionation Techniques for the Solution of Molecular Weight Distribution Equations

3.1 Introduction

For the solution of the MWD model for emulsion polymerization developed in this work a numerical method was chosen (see Chap. 2), namely numerical fractionation (NF), which is based on the partitioning of the polymer into classes of chains with similar dimensions. Within each class, the method of moments was applied for the calculation of the MWD. This procedure required the selection of a model distribution for the unknown MWD of each class which introduced an approximation in the solution. The target of the present chapter is primarily to verify the magnitude of this approximation. However, another fractionation strategy is also analysed, based on the subdivision of the chains according to the number of branches. This method is shown to give improved results (in the presence of chain transfer to polymer as a branching mechanism) when a detailed MWD is required and permits a straightforward calculation of the chain branching distribution. Therefore, this chapter also reaches the two additional aims of presenting a refined model solution and of showing how to include the branching distribution calculation in the model equations.

The whole analysis is carried out referring to a bulk system. This is done because the equations for such a system are simpler, and accurate reference solutions are obtained more easily. Nevertheless, the similar peculiar aspects exhibited by the approximate solution methods based on polymer fractionation in homogeneous [30] and segregated [24] systems assure that the conclusions reached can be extended to emulsion polymerization.

Considering free-radical polymerization in homogeneous systems, the modeling of the active and inactive species of all possible lengths in the reaction system leads to PBEs which consist of a very large set of ordinary differential equations with the reaction time as

the independent variable. The dimension of this system of equations varies according to the maximum chain length achieved in the reactor, which depends on the kinetic mechanisms and the kinetic constant values, the feed composition and all the other operating conditions of the reactor, and typically ranges from 10^3 to 10^5 or more.

A great variety of approaches has appeared through the years in the literature to solve this system efficiently. Significant examples are lumping [47], passage to continuous variable [48], the method of moments [49], and other methods of weighted residuals (including discrete weighted Galerkin [50] and discrete collocation methods [51]). Approaches of statistical nature, based on the mathematics of the Markov chains and on Monte-Carlo simulation [52], have also been used.

Of the methods above, some involve simplifying assumptions or reduction of the equations before their numerical solution. An example is given by the method of moments: in the presence of certain reaction mechanisms, such as chain transfer to polymer, this method requires the quasi-steady-state assumption (QSSA) for the active species to obtain a set of equations in closed form. If this assumption is not used, a closure equation has to be added to the system.

When considering accuracy and flexibility versus computational effort, excellent performances have been obtained using the discrete Galerkin h-p-method [53]. This provides in fact accurate solutions in the presence of comprehensive kinetic schemes, allows the treatment of complex reaction steps, e.g. chain-length dependent kinetics, and requires no model reduction. However, at least two situations may be illustrated where the application of this approach is not convenient.

The first situation is provided by those heterogeneous polymerization systems, such as emulsion polymerization, where the active chains grow segregated in the reaction loci and which are the object of the present work. It has been shown in the previous chapter that in such systems more internal coordinates than simply the chain length are required to describe completely the distribution of the active chains. Distributions with at least three internal coordinates (particle state and two chain lengths) must be considered. In problems of such a high dimensionality, using discrete methods on every variable becomes rather heavy. In this case less accurate methods may result more efficient and provide anyhow a satisfactory solution.

The second situation arises when evaluating the MWD in polymerization systems where the formation of a gel phase occurs, corresponding to the formation of chains of untreatably high lengths. In this case all solution methods fail unless the kinetic equations are modified in some way or an upper limit to the calculated chain length is imposed.

To deal with these situations, approximate methods have been adopted consisting of the subdivision of the overall polymer into classes, namely NF [30] and a method identifying the polymer chains according to the number of branches [54]. As already explained for NF, the basic idea of these methods is to subdivide a broad and complex distribution into a number of narrower distributions, the description of which can be made by simpler means. In such a way a single problem of difficult solution is decomposed into several sub-problems easier to solve. This simplification undoubtedly represents a great advantage when dealing with segregated systems [23, 24], where the starting problem is very complex. This explains the choice of NF as solution method for the emulsion polymerization MWD model developed in Chap. 2.

To test the potential and reliability of these approximate methods, reference solutions have been obtained through a numerical technique which, though computationally intensive, permits to calculate the correct MWD. Broad distributions originated by the presence of a branching mechanism, namely chain transfer to polymer, have been analysed. This reaction is responsible for the appearance of peculiar shoulders in the MWD profile obtained by NF [24, 30], which have been shown to be sensitive to the fractionation scheme adopted [23]. The question is whether these shoulders are produced in reality by the branching mechanism or are simply an artifact of the solution method, and, in the latter case, whether a different partitioning scheme (i.e., subdividing the polymer according to the number of branches) provides a better solution.

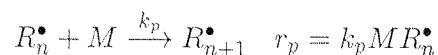
3.2 Kinetic Scheme and Molecular Weight Equations

A kinetic scheme constituted by classical free-radical polymerization steps has been considered, involving chain transfer to polymer as a source of chain branching:

- initiator decomposition rate



- propagation



- chain transfer to monomer



- chain transfer to modifier



- chain transfer to polymer



- bimolecular termination by combination



- bimolecular termination by disproportionation



where all symbols are defined in the Notation. On the right-hand side the expression for the rate of each reaction has been reported. All kinetic rate constants have been considered chain-length independent. Note that a R_0^\bullet molecule has been assumed to be formed by chain transfer to monomer instead of R_1^\bullet as usually considered. This has been done to make the following equations more compact and does not modify the final results due to the high chain lengths of the macromolecular species under examination. Finally, in the kinetic scheme above it is assumed that the polymer chains can have at most one active centre (monoradical assumption).

For the calculation of the concentrations of the active and terminated chains in a batch reactor, the following PBEs apply:

$$\begin{aligned} \frac{dR_n^\bullet}{dt} &= k_p M R_{n-1}^\bullet - [k_p M + k_{fm} M + k_{ft} T + (k_{tc} + k_{td}) \lambda_0 + k_{fp} \mu_1] R_n^\bullet \\ &\quad + k_{fp} \lambda_0 n P_n + \delta_{n,0} [(k_{fm} M + k_{ft} T) \lambda_0 + \mathcal{R}_I] \end{aligned} \quad (3.1)$$

$$\begin{aligned} \frac{dP_n}{dt} &= (k_{fm} M + k_{ft} T) R_n^\bullet + \frac{1}{2} k_{tc} \sum_{m=0}^n R_m^\bullet R_{n-m}^\bullet + k_{td} \lambda_0 R_n^\bullet \\ &\quad + k_{fp} \mu_1 R_n^\bullet - k_{fp} \lambda_0 n P_n \end{aligned} \quad (3.2)$$

where $\lambda_0 = \sum_{m=0}^{\infty} R_m^\bullet$ is the zeroth-order moment of the distribution of the active chains (i.e., the overall radical concentration), $\mu_1 = \sum_{m=0}^{\infty} m P_m$ is the first-order moment of the distribution of the terminated chains (i.e., the overall concentration of polymerized

monomer), $\delta_{n,0}$ is the Kronecker index and \mathcal{R}_I is the initiation rate ($\mathcal{R}_I = 2\eta k_I I$, with η an efficiency parameter).

3.3 Model Solution

In this section four numerical methods are described for solving the model eqs (3.1) and (3.2). The first method described is rather time consuming but provides the correct solution (at least in the frame of the QSSA, which is assumed valid by all methods considered). This solution is used as a term of comparison for testing the reliability of the approximate solutions provided by the other numerical techniques.

3.3.1 Detailed Solution

The rigorous solution of system (3.1)-(3.2) to obtain the CLD would require integration for all values of the chain length n up to values corresponding to negligible polymer chain concentrations. A simpler but equally accurate method can be developed by applying the QSSA to eq. (3.1) for the radical species, so that the differential system (3.1)-(3.2) reduces to the following algebraic-differential system:

$$R_n^\bullet = \frac{k_p M R_{n-1}^\bullet + k_{fp} \lambda_0 n P_n + \delta_{n,0} [(k_{fm} M + k_{ft} T) \lambda_0 + \mathcal{R}_I]}{k_p M + k_{fm} M + k_{ft} T + (k_{tc} + k_{td}) \lambda_0 + k_{fp} \mu_1} \quad (3.3)$$

$$\begin{aligned} \frac{dP_n}{dt} = & (k_{fm} M + k_{ft} T) R_n^\bullet + \frac{1}{2} k_{tc} \sum_{m=0}^n R_m^\bullet R_{n-m}^\bullet + k_{td} \lambda_0 R_n^\bullet \\ & + k_{fp} \mu_1 R_n^\bullet - k_{fp} \lambda_0 n P_n \end{aligned} \quad (3.4)$$

From system (3.3)-(3.4) it is seen that, as long as the moments λ_0 and μ_1 are known independently, the concentration of chains of length n depends only on that of chains of the same length or shorter. Accordingly, the CLD calculation can be truncated at any value of n , no matter how low, without introducing any error. The equations for the moments λ_0 and μ_1 can be derived by applying the method of moments to eqs (3.3) and (3.4), as described in the next section. The equations obtained are rigorous (in the frame of the QSSA) and allow an independent evaluation of the moments λ_0 and μ_1 , which can then be used to solve system (3.3)-(3.4).

It is worth noting that to obtain an accurate solution it is not necessary to solve eqs (3.3)-(3.4) for all n values up to the selected maximum value. In fact, eqs (3.4) for the terminated polymer can be integrated only for some selected values of n , while for the intermediate n values the concentrations P_n are obtained by low order interpolation. Here, parabolic interpolation was used. A convergence check with an increasing number

of nodes was performed for each simulated reaction to verify that the adopted number of nodes was sufficient.

3.3.2 Overall Method of Moments

The method of moments applied to the calculation of the CLD of a polymer typically consists of calculating integral properties of the distribution (the moments) and reconstructing it by selecting a model distribution and imposing that its moments are the same as those calculated. The k^{th} -order moments of the active and terminated chain distributions, $\lambda_k = \sum_{n=0}^{\infty} n^k R_n^{\bullet}$ and $\mu_k = \sum_{n=0}^{\infty} n^k P_n$, respectively, can be calculated by applying the moment operator $\sum_{n=0}^{\infty} n^k$ to eqs (3.1)-(3.2). When this is done, however, the resulting moment equations are not in closed form since, due to the presence of the chain transfer to polymer terms, the moments of order k of both the active and terminated chains depend on the moment of order $k + 1$ of the terminated polymer. If the QSSA assumption is applied, the following system of equations is obtained (see Appendix D):

$$\lambda_0 = \left(\frac{\mathcal{R}_I}{k_{tc} + k_{td}} \right)^{1/2} \quad (3.5)$$

$$\frac{d\mu_0}{dt} = (k_{fm}M + k_{ft}T)\lambda_0 + \left(\frac{1}{2}k_{tc} + k_{td} \right) \lambda_0^2 \quad (3.6)$$

and for $k \geq 1$:

$$\lambda_k = \frac{k_p M \sum_{j=0}^{k-1} \binom{k}{j} \lambda_j + k_{fp} \lambda_0 \mu_{k+1}}{k_{fm}M + k_{ft}T + (k_{tc} + k_{td})\lambda_0 + k_{fp}\mu_1} \quad (3.7)$$

$$\frac{d\mu_k}{dt} = k_p M \sum_{j=0}^{k-1} \binom{k}{j} \lambda_j + \frac{1}{2}k_{tc} \sum_{j=1}^{k-1} \binom{k}{j} \lambda_j \lambda_{k-j} \quad (3.8)$$

Note that, though the moment of order k of the active chains depends on the moment of order $k + 1$ of the terminated chains, the latter depends only on lower order moments of the active chains. This implies that, given a maximum moment order k_{max} , the system which calculates the moments up to $\mu_{k_{max}}$ for the terminated chains and up to $\lambda_{k_{max}-1}$ for the active chains, is in closed form. Accordingly, moments of any order can be calculated from eqs (3.5)-(3.8) in a rigorous manner (of course, in the limit of the QSSA).

Here, the distribution selected for the reconstruction of the CLD from its moments is a re-scaled Γ -distribution perturbed to the unknown distribution by a polynomial expansion in terms of associated Laguerre polynomials orthogonal to the Γ -distribution weighting function [45].

3.3.3 Partitioning According to the Number of Branches (PANB)

According to this method [54], each polymer chain is characterized not only by its length but also by the number of branches it bears. The following PBEs result:

$$\begin{aligned} \frac{dR_{n,b}^\bullet}{dt} &= k_p M R_{n-1,b}^\bullet - [k_p M + k_{fm} M + k_{ft} T + (k_{tc} + k_{td}) \lambda_0 + k_{fp} \mu_1] R_{n,b}^\bullet \\ &\quad + k_{fp} \lambda_0 n P_{n,b-1} + \delta_{n,0} \delta_{b,0} [(k_{fm} M + k_{ft} T) \lambda_0 + \mathcal{R}_I] \end{aligned} \quad (3.9)$$

$$\begin{aligned} \frac{dP_{n,b}}{dt} &= (k_{fm} M + k_{ft} T) R_{n,b}^\bullet + \frac{1}{2} k_{tc} \sum_{k=0}^b \sum_{m=0}^n R_{m,k}^\bullet R_{n-m,b-k}^\bullet + k_{td} \lambda_0 R_{n,b}^\bullet \\ &\quad + k_{fp} \mu_1 R_{n,b}^\bullet - k_{fp} \lambda_0 n P_{n,b} \end{aligned} \quad (3.10)$$

where $R_{n,b}^\bullet$ and $P_{n,b}$ represent the concentration of active and terminated chains, respectively, of length n and with b branches.

To obtain the overall polymer CLD, eqs (3.9)-(3.10) are solved to obtain the CLDs of the polymer chains for each number of branches b . Then, these are summed up over all possible branch numbers to obtain the desired quantity: $P_n = \sum_{b=0}^{\infty} P_{n,b}$.

The distributions $P_{n,b}$ are obtained by reducing eq. (3.9) for the radical species by means of the QSSA and by applying the moment operator $\sum_{n=0}^{\infty} n^k$ to the resulting system, in order to obtain the first three CLD moments for each number of branches (zeroth-, first- and second-order moments). The formulae and passages required to derive these moment equations are the same as those reported in Appendix D in the frame of the overall method of moments. From the first three moments, each distribution is reconstructed using a re-scaled Γ -distribution as model distribution [45]. With respect to this, the previous finding [55, 56] that the polymer fractions constituted by chains with a given number of branches follow a Γ -distribution in a randomly branched polymer suggests this to be a reasonable choice. Note that, unlike the overall moment eqs (3.7) and (3.8), the moment equations resulting in this case are not in closed form, i.e., the dependence of the terminated polymer moments on the next higher order moments cannot be eliminated. Accordingly, a closure equation is required. The following equation for the calculation of the third-order moment of the CLD of the terminated polymer with a given number of branches has been adopted:

$$\mu_{3,b} = \mu_{2,b} \left[2 \frac{\mu_{2,b}}{\mu_{1,b}} - \frac{\mu_{1,b}}{\mu_{0,b}} \right] \quad (3.11)$$

This closure formula is in agreement with the model distribution (re-scaled Γ -distribution) which has been chosen for the reconstruction of each CLD from its first three moments.

3.3.4 Numerical Fractionation

The concepts underlying the original version of NF proposed by Teymour and Campbell [30] have been explained in Appendix A in the frame of the solution of the emulsion

MWD model developed in Chap. 2. According to this method, the subdivision of the polymer into classes is not operated according to a structural feature of the chains (such as the number of branches in the PANB method) but is defined by the rules describing the transition of chains from one class to the other: these rules should assure that each class is made up by chains similar in size. The geometrical growth obtained passing from one generation to the following one provides an original insight into the physical process which leads to the formation of a gel. However, when regarding this fractionation strategy in the frame of a numerical method for accurate MWD evaluation, it probably results to be too coarse. This can be understood, for instance, by considering that a chain can keep adding branches within a certain generation without being transferred to the next higher. This results in broad generations which are difficult to describe numerically (even though much less than the original overall distribution).

To improve the description of the MWD, a refinement of the fractionation scheme has been proposed in the context of emulsion polymerization by Arzamendi and Asua [23]. The polymer is still subdivided into linear and branched chains, but the latter are subdivided as follows: each of the first n_b generations is constituted by chains having the same number of branches (coinciding with the generation index g), while for the generations $n_b + 1$ and higher the original rules allowing a geometrical growth in the chain dimensions are adopted. In other words, not only the linear chains but also chains with up to n_b branches are described separately, before introducing the fractionation developed by Teymour and Campbell.

The following transfer rules result in this case: the linear chains ($g = 0$) pass on to the first branched generation when they undergo chain transfer to polymer. Within the next n_b branched generations, transfer occurs either by chain transfer to polymer (to the next higher generation) or by combination (to the generation corresponding to the number of branches of the resulting chain or to generation $n_b + 1$ if the number of branches exceeds n_b). From generation $n_b + 1$ onwards, transfer to the next higher generation occurs when two chains of the same generation couple together through termination by combination. This generation transfer scheme is summarized in Table 3.1. In this table, $R_n^{\bullet(g)}$ and $P_n^{(g)}$ represent an active and a terminated chain, respectively, of length n and belonging to generation g . The parameter n_g indicates the number of branched generations in the sol phase. Accordingly, generation $n_g + 1$ corresponds to the gel phase (or better ‘pseudo-gel’ phase, where this term indicates everything which is lumped together with the gel phase into a single class).

This scheme allows a more detailed description of the moderately branched polymer

$0 \leq g_1 \leq n_b \ , \ \forall g_2$
$P_n^{(g_1)} + R_n^{\bullet(g_2)} \xrightarrow{k_{fP}} R_n^{\bullet(g_1+1)} + P_n^{(g_2)}$
$0 \leq g_1, g_2 \leq n_b$
$R_n^{\bullet(g_1)} + R_m^{\bullet(g_2)} \begin{cases} \nearrow P_{n+m}^{(g_1+g_2)} & \text{if } g_1 + g_2 \leq n_b \\ \searrow P_{n+m}^{(n_b+1)} & \text{if } g_1 + g_2 > n_b \end{cases} \xrightarrow{k_{tc}}$
$n_b + 1 \leq g_1 \leq n_g \ , \ \forall g_2$
$R_n^{\bullet(g_1)} + R_m^{\bullet(g_2)} \begin{cases} \nearrow P_{n+m}^{(g_1+1)} & \text{if } g_1 = g_2 \\ \searrow P_{n+m}^{(\max\{g_1, g_2\})} & \text{if } g_1 \neq g_2 \end{cases} \xrightarrow{k_{tc}}$

Table 3.1: Reactions giving transfer between generations.

which is instead lumped into the first very few branched generations (only one in the limit of no termination by combination) in the original version of NF.

According to the transfer rules summarized in Table 3.1, the PBEs (3.1)-(3.2) must be modified in order to account for the passage of chains between generations. The resulting ‘fractionated equations’ are reported in Appendix E. Note that when $n_b = 0$ these equations reduce to those corresponding to Teymour and Campbell’s original generation transfer scheme [30], which can therefore be considered as a special case of the fractionation scheme here adopted. In the following, we will refer to this special case as ‘classical NF’. Instead, when $n_g = n_b$ and the equation for $g = n_g + 1$ is neglected, the fractionation method considered reduces to the partitioning of the polymer based on the number of branches described in the previous Section 3.3.3, which does not account for the geometrical growth in size of the chains approaching gelation typical of the classical NF.

To solve the fractionated PBEs (cf. Appendix E), as for the method presented in Section 3.3.3, after reduction of the equations for the radical species by means of the QSSA, the method of moments has been applied in order to obtain the first three moments of each generation. Again, the resulting moment equations are not in closed form. The closure formula (3.11) is adopted within each generation to calculate the third-order moment as a function of the lower-order moments. This closure formula results from the re-scaled

Γ -distribution which has been chosen for the reconstruction of the CLD of each generation from its first three moments [45]. The overall CLD of the sol phase is obtained by summing up the contributions of each generation.

3.4 Gel Weight Calculation

From a mathematical point of view, a polymer molecule is identified as belonging to the gel phase when its dimensions are so large that the molecule can be considered infinite in size. Therefore, the formation of a gel phase in the polymerization system is revealed by the divergence of the second- and higher-order moments of the CLD. This implies that the overall method of moments fails at the gel point and provides no means of calculating the amount of gel or any other quantity beyond the gel point. On the other hand, for the other methods discussed above, integration can be carried out across the gel point without introducing any discontinuity. To this aim, it is sufficient to establish a maximum chain length, or number of branches, or any other feature related to molecular dimension, above which the polymer molecules are assumed to belong to the gel and are no longer simulated. This also permits, if this maximum size is selected so as to actually include all the molecules of the sol, to calculate correctly the amount of sol polymer (and thus of gel) and to have a complete description of the sol MWD. What ensures that this is possible, is that in the process of gel formation a gap appears between the gel, infinite in size, and the sol phase, where very large molecules may be present but still finite in size, so that they can be simulated (cf. e.g. ref. [30]).

In the case of the detailed solution method, it has been shown that the differential system can be truncated at any chain length without introducing any error in the CLD calculation up to that chain length. The sol CLD is thus calculated correctly up to any selected n_M value. Instead, for a correct evaluation of the amount of gel, the value of n_M must be taken so large as to have a negligible amount (in terms of weight and not only of number) of soluble chains that exhibit this chain length. This can be verified by examining the calculated weight CLD of the sol phase. The amount of gel μ_1^{gel} is then obtained by subtracting from the overall polymer μ_1 the amount of polymer in the sol phase, given by $\mu_1^{sol} = \sum_{n=0}^{n_M} nP_n$. Thus, the gel is considered to be made up of chains with a length greater than n_M .

In the case of the PANB method, a number of branches b_M can be selected, above which the polymer chain is considered to belong to the gel phase. The parameter b_M must be large enough so that the amount of soluble chains having this number of branches is

Parameter	Value
Kinetic parameters	
k_{fm}	$9.07 \cdot 10^{-2} \text{ l mol}^{-1} \text{ s}^{-1}$
k_{fp}	$5 \cdot 10^{-1} \text{ l mol}^{-1} \text{ s}^{-1}$
k_I	$1.18 \cdot 10^{-6} \text{ s}^{-1}$
k_p	$5 \cdot 10^2 \text{ l mol}^{-1} \text{ s}^{-1}$
k_{tc}	$0 \div 5.97 \cdot 10^6 \text{ l mol}^{-1} \text{ s}^{-1}$
k_{td}	$0 \div 5.97 \cdot 10^6 \text{ l mol}^{-1} \text{ s}^{-1}$
η	1
Initial concentrations	
I_o	$1 \cdot 10^{-3} \div 1 \cdot 10^{-1} \text{ mol l}^{-1}$
M_o	8.43 mol l^{-1}
T_o	0 mol l^{-1}

Table 3.2: Kinetic parameters and initial concentrations for the model simulations

negligible. The amount of gel can be calculated as $\mu_1^{gel} = \mu_1 - \sum_{b=0}^{b_M} \mu_{1,b}$, where $\mu_{1,b}$ is the amount of polymer constituted by chains with b branches.

In the case of NF, the index reflecting the dimension of the molecule is the generation index. Accordingly, a sufficiently large number of generations n_g has to be used to describe the sol phase. Teymour and Campbell suggest to check convergence of all quantities predicted by the model, and in particular the gel point, to verify that the number of generations selected for the description of the sol is large enough (note that this criterion can be applied also with the other solution techniques to check if the ‘dimension parameter’ has been taken large enough). The amount of gel can be calculated as $\mu_1^{gel} = \mu_1 - \sum_{g=0}^{n_g} \mu_1^{(g)}$, where $\mu_1^{(g)}$ is the amount of polymer belonging to generation g .

3.5 Results and Discussion

3.5.1 Base Cases

Two main case studies have been selected for comparing the results obtained through the various solution methods. In the first one, bimolecular termination is assumed to occur by disproportionation while in the second one it occurs by combination. In all cases chain transfer to polymer is present as a branching mechanism. Accordingly, in the second case the formation of a gel phase is possible, while in the first one the absence of a mechanism connecting chains together prevents the formation of the huge-sized molecules constituting such a phase. Within each case study, two different reaction rates, given by two different initiator concentrations, have been examined. All the values of the kinetic parameters and the initial concentrations selected for these simulations are reported in Table 3.2.

3.5.2 Bimolecular Termination by Disproportionation

For these simulations, the value of k_{tc} has been set to zero, i.e., bimolecular termination is assumed to occur only by disproportionation. Two reaction rates have been examined, corresponding to initial initiator concentrations $I_o = 1 \cdot 10^{-3} \text{ mol l}^{-1}$ and $I_o = 1 \cdot 10^{-1} \text{ mol l}^{-1}$.

The case of a lower reaction rate (lower initiator concentration) is first analysed. The distribution is calculated at 65% conversion through the four solution methods described above. In the case of NF, it is first calculated with $n_b = 0$, i.e., using the fractionation rules by Teymour and Campbell (classical NF). This is done because the classical method often predicts, in the presence of the mechanisms under consideration (chain transfer to polymer and disproportionation) a pronounced shoulder in the high molecular weight portion of the MWD or even a bimodal behavior, the existence of which in the real solution has to be checked. Fig. 3.1(a) shows a comparison between the results of the classical NF (solid curve) and the detailed solution method (dashed curve). It is apparent that the high molecular weight maximum is an artifact of the NF technique. By examining the contributions of the single generations to the overall CLD curve, as shown in Fig. 3.1(b), it can be observed that this maximum is due to the first branched generation, which is in fact a single generation containing all chains which are nonlinear. Teymour and Campbell's scheme does not in fact admit the transition to a second branched generation in this case, and the bimodality can therefore be related to the accumulation in the first branched generation of chains adding a growing number of branches. This observation has suggested the more detailed fractionation of the polymer chain population [23] discussed in Section 3.3.4.

Note that when chain branching occurs through different mechanisms, namely, terminal double bond propagation or crosslinking, this problem does not arise. This is because the branching mechanism joins two polymer chains together and is therefore directly responsible for the geometrical growth in chain size which rules the transfer between generations in the classical fractionation scheme. Thus, this scheme is enough to provide a good description of the branching process, which is not true in the case of chain transfer to polymer, where the branching mechanism is not a chain coupling mechanism. This is also suggested by the fact that the distributions calculated through the classical NF in the presence of terminal double bond propagation or crosslinking (and in the absence of chain transfer to polymer) do not exhibit the peculiar shoulders discussed here above (see Chap. 2 and ref. [43]).

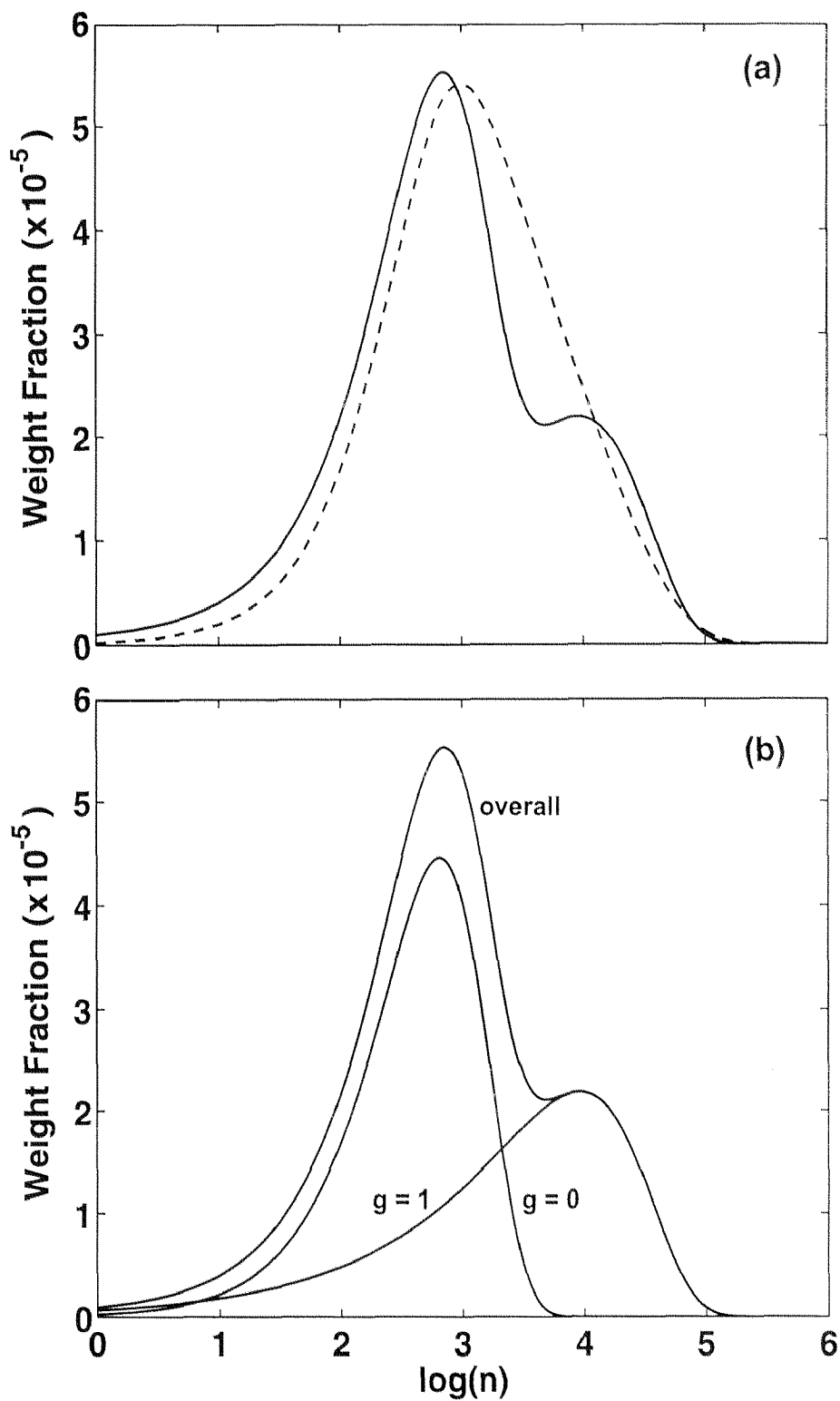


Figure 3.1: Chain length distribution at 65% conversion in the case of termination by disproportionation and low initiator concentration. (a) — : classical NF; --- : reference solution calculated by the detailed method; (b) classical NF with the contribution of the individual generations.

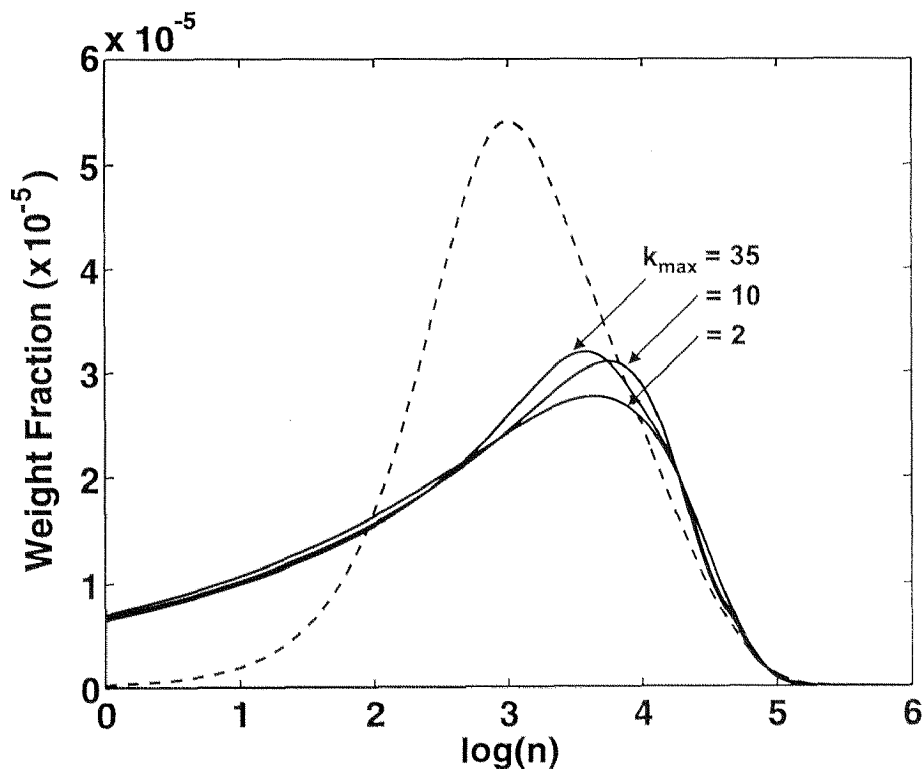


Figure 3.2: Chain length distribution at 65% conversion calculated by the overall method of moments for an increasing number of moments ($k_{max} = 2$ to 35) in the case of termination by disproportionation and low initiator concentration; --- : reference solution calculated by the detailed method.

In Fig. 3.2 the correct solution is used as a term of comparison for the solution obtained by the overall method of moments at an increasing number of moments (from $k_{max} = 2$ to $k_{max} = 35$, where k_{max} is the maximum order of the moments used for the reconstruction of the CLD). It can be seen that a very large increase of the maximum moment order corresponds to a limited improvement of the obtained solution, which is in any case very far from the ‘true’ solution. Increasing further the number of moments, severe oscillations begin to appear, in agreement with previous results reported in the literature using Laguerre polynomials [57, 58]. Therefore, when the full MWD is required, the overall method of moments fails to provide a satisfactory solution to the problem, at least with the model distribution chosen (perturbed Γ -distribution).

With the aim of testing to what extent a more detailed fractionation scheme can improve the accuracy of the solution, the CLD has been reconstructed using NF with increasing n_b values. The results are shown in Fig. 3.3(a), where values of n_b from 5 to 40 have been used (note that the value of $n_g - n_b$ is irrelevant to the result since with the considered reaction mechanisms the maximum generation which can be reached is $n_b + 1$). It can be observed that for increasing n_b values the high molecular weight maximum is

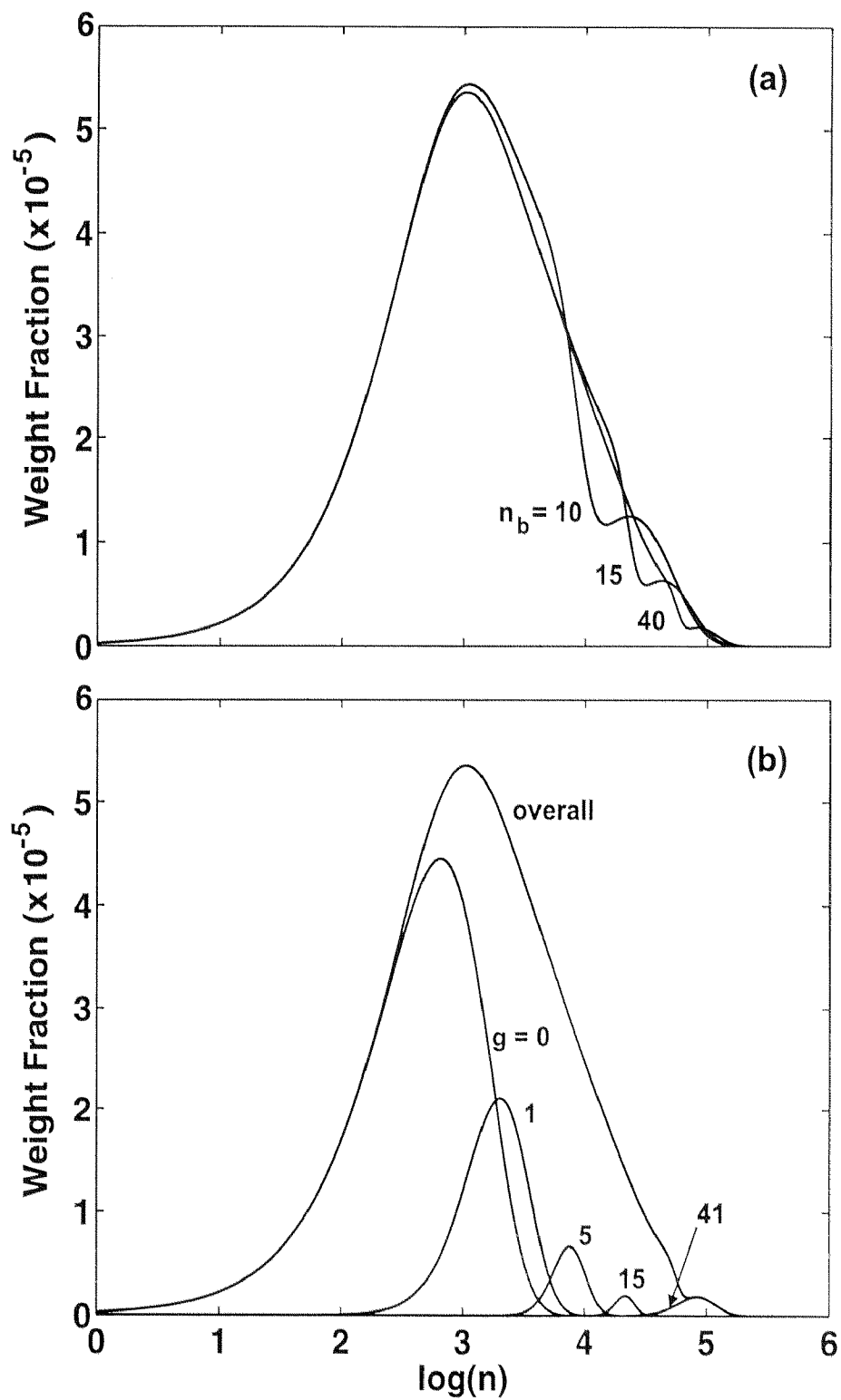


Figure 3.3: Chain length distribution at 65% conversion in the case of termination by disproportionation and low initiator concentration. (a) Refined NF for increasing n_b values; (b) refined NF (with $n_b = 40$) with the contribution of some of the generations.

shifted to higher chain lengths while its intensity is reduced. This maximum is due to the polymer chains accumulated in the last branched generation, constituted by polymer chains with more than n_b branches. This can be clearly seen in Fig. 3.3(b), where the contribution of some of the generations has been reported under the overall CLD for the case of $n_b = 40$. It is evident that, for increasing n_b values, the quantity of chains with more than n_b branches has to become negligible and the maximum has to disappear, while the polymer tends to be entirely subdivided into generations each constituted by chains with a given number of branches b . This suggests the more appropriate description to be given by the PANB method, as long as a large enough number of branches b_M is chosen. In fact, subdividing the chains according to the number of branches and selecting increasing b_M values, the calculated CLD approaches the ‘true’ solution. This is shown in Fig. 3.4, where the solution given by the PANB method is plotted for increasing b_M values (Fig. 3.4(a)) and at convergence to the correct solution (Fig. 3.4(b)). Therefore, in this case the PANB method results optimal when a detailed MWD profile is required.

If the number b_M is chosen large enough, so as to cover the entire molecular weight range, the PANB solution method also provides in a straightforward way a detailed characterization of the polymer in terms of branching. In fact, the concentration of polymer chains with a given number of branches b is provided by the zeroth-order moment $\mu_{0,b}$. This quantity is reported in Fig. 3.5(a) for the case under examination.

Another quantity of interest for a complete description of the branching properties of a polymer is the average number \bar{b}_n of branches per chain in chains of a given length n . This is given by:

$$\bar{b}_n = \frac{\sum_{b=0}^{b_M} b P_{n,b}}{\sum_{b=0}^{b_M} P_{n,b}} \quad (3.12)$$

For the case under examination, this function is plotted in Fig. 3.5(b). It is interesting to observe that the average number of branches increases linearly with chain length. This feature gives a hint on a possible way to quickly estimate the number of branches needed to cover the whole polymer CLD without seeking convergence on the CLD profile. In fact, from Fig. 3.1, it can be seen that, though yielding an incorrectly shaped CLD, the classical NF is able to predict correctly the maximum chain length reached in the system. Accordingly, the CLD can be first computed through the classical NF, which usually requires short computational times. Once the maximum chain length is known, and once the slope of the \bar{b}_n vs. n line is obtained by plotting eq. (3.12) with a low b_M value, extrapolation of this line to the maximum chain length gives an estimate of the b_M value required for the correct calculation of the CLD up to high chain length values. As a check

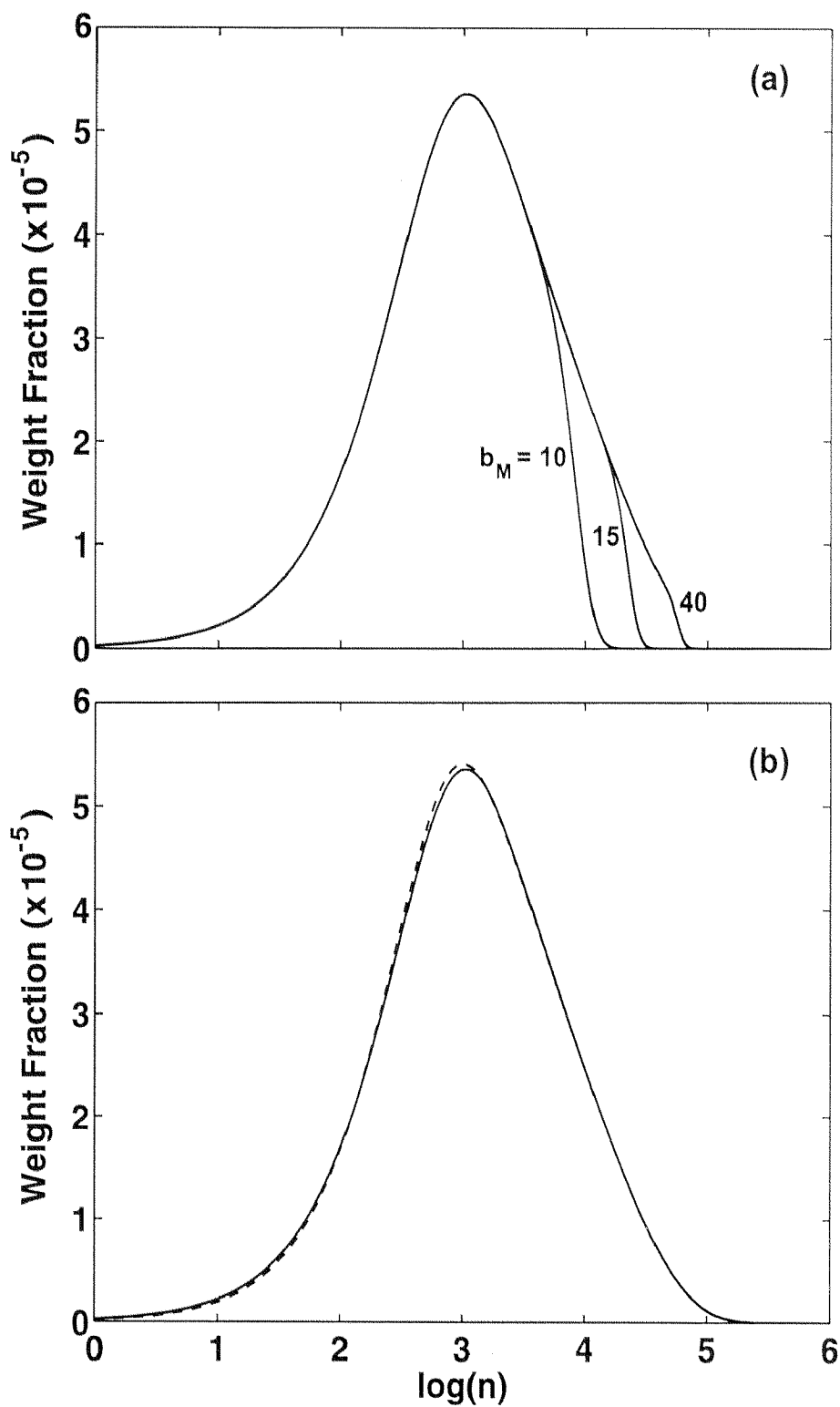


Figure 3.4: Chain length distribution at 65% conversion in the case of termination by disproportionation and low initiator concentration. (a) PANB method for increasing b_M values; (b) — : PANB method with $b_M = 145$; --- : reference solution calculated by the detailed method.

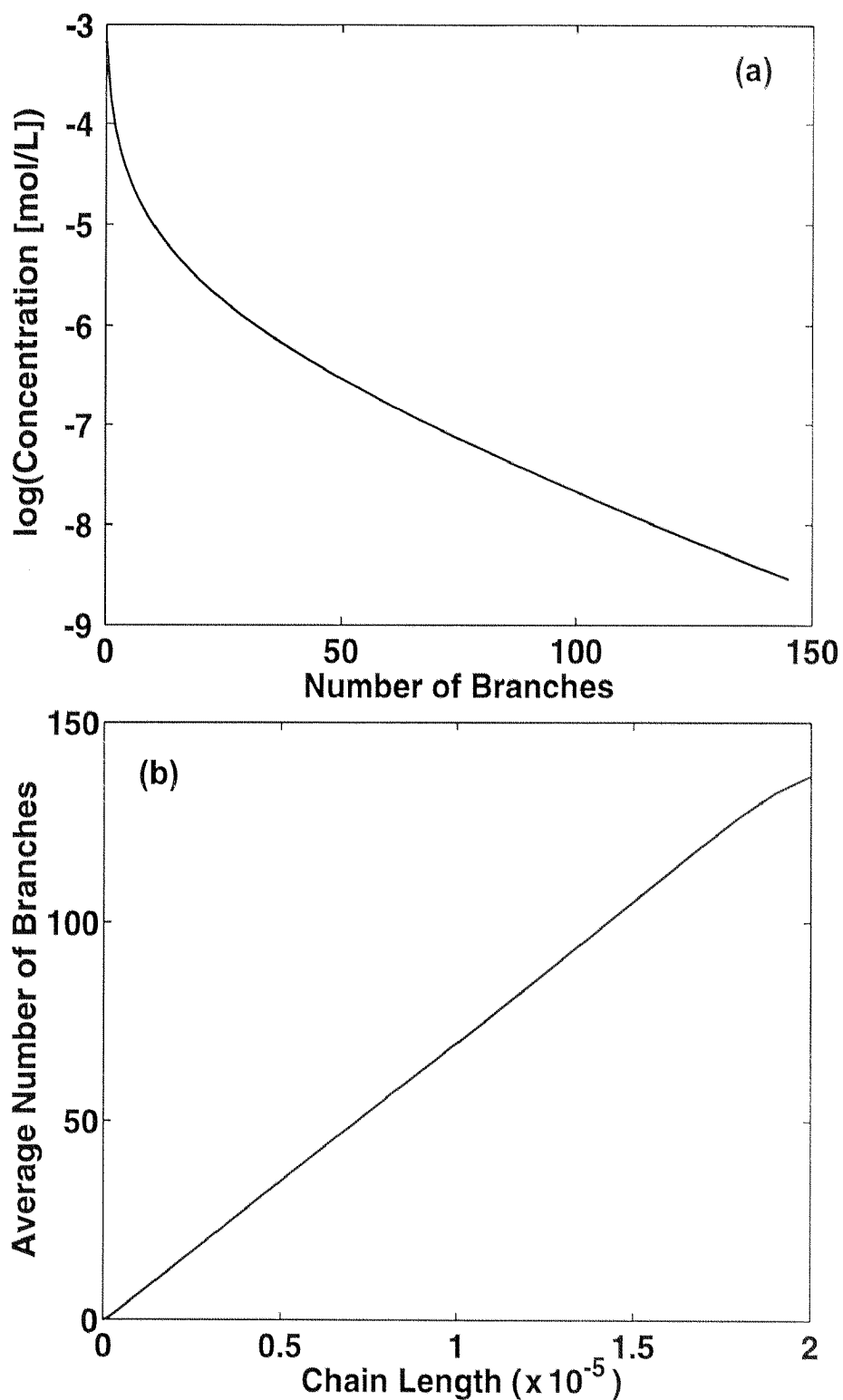


Figure 3.5: Branching properties at 65% conversion in the case of termination by disproportionation and low initiator concentration. (a) Concentration of chains as a function of the number of branches; (b) average number of branches per chain as a function of chain length.

of the method, note that the value of about 140 branches estimated from Fig. 3.5(b) to reach the maximum chain length $2 \cdot 10^5$ (see Fig. 3.1(a)), coincides with the value at which convergence on the CLD is achieved (see Fig. 3.4), i.e., it coincides with the minimum number of branches required for the correct solution.

A second case has been examined in which the reaction rate is enhanced by the use of a higher initial initiator concentration ($I_o = 1 \cdot 10^{-1} \text{ mol l}^{-1}$). The CLD obtained in this case by the classical NF is reported in Fig. 3.6 at 50% conversion (solid curve) and compared to the CLD given by the detailed solution method (dashed curve). In these conditions no bimodality is present and the dimensions of the shoulder are limited, so that the solution provided by the classical NF is not far from being satisfactory as it is, without the need for a more refined fractionation scheme. However, if a more accurate solution is required, this is provided by the PANB method (with $b_M = 80$), as in the case of a slow reaction rate previously examined.

The solution provided by the overall method of moments has also been analysed for comparison. In Fig. 3.7 it can be seen that this solution is nearer to the correct solution than in the case of low initiator concentration. This can be ascribed to the fact that the overall distribution is narrower. However, the solution given by the overall method of moments is still far from the correct solution even at very high moment orders. Therefore, also in this case the overall method of moments fails in providing a satisfactory CLD.

Summarizing, two cases have been examined, corresponding to two different reaction rates. In both cases the classical NF has been shown to give an improved MWD solution compared to the overall method of moments. However, it has also been shown that there exist situations where the classical NF gives birth to bimodalities or pronounced shoulders which do not appear in the true MWD. In this case, the refined NF technique proposed by Arzamendi and Asua [23] can be used as a quick way to verify whether the shoulders are an artifact of the NF solution method. It is enough to repeat the MWD calculation with a small n_b value, but greater than zero, and observe if the result changes. However, this technique does not remove the basic problem of the classical NF which, with the kinetic mechanisms considered, consists of the accumulation in the last generation ($n_b + 1$) of the chains with more than n_b branches. For a correct calculation of the MWD, the optimal solution method has been found to be the PANB method in both cases examined.

3.5.3 Bimolecular Termination by Combination

For these calculations, the value of k_{td} has been set to zero, i.e., bimolecular termination is assumed to occur only by combination. Two reaction rates have again been examined,

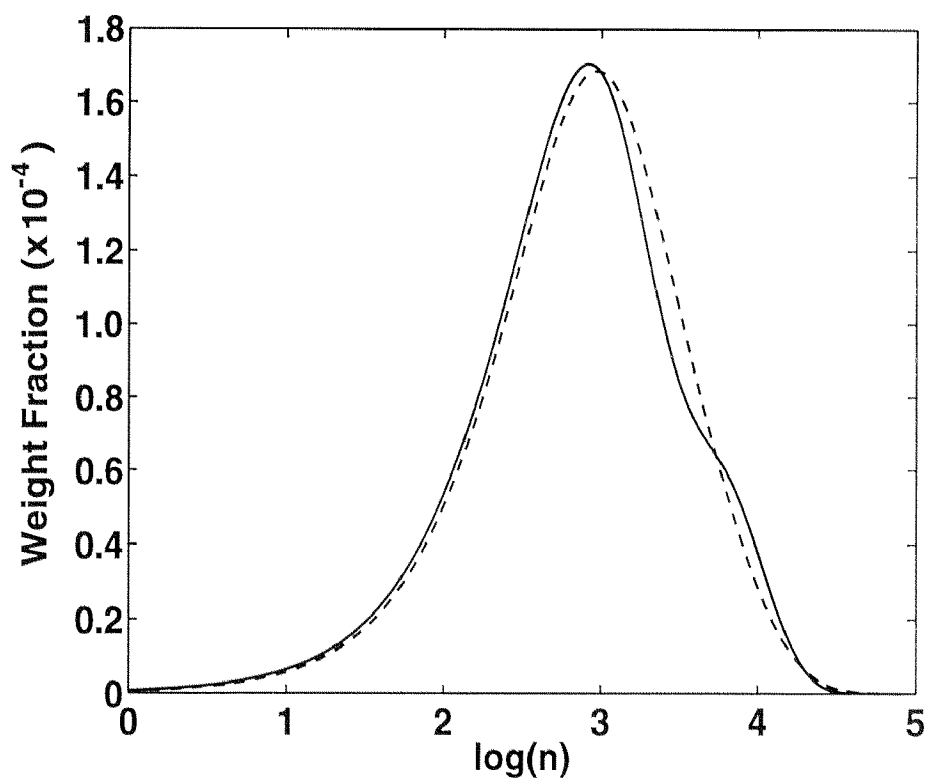


Figure 3.6: Chain length distribution at 50% conversion in the case of termination by disproportionation and high initiator concentration; — : classical NF; --- : reference solution calculated by the detailed method.

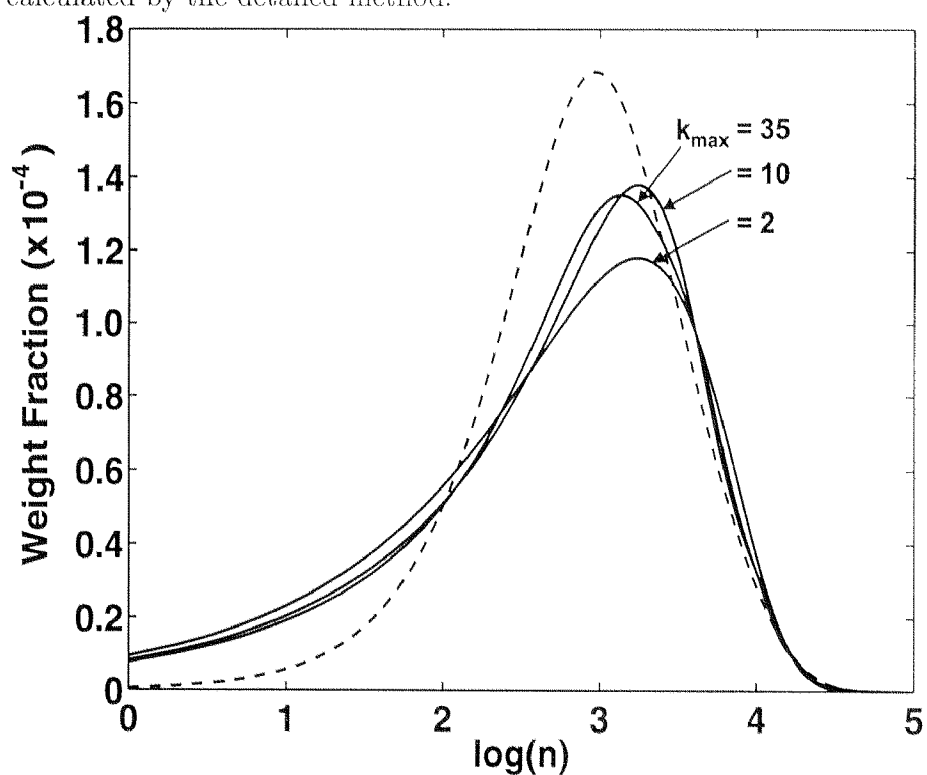


Figure 3.7: Chain length distribution at 50% conversion calculated by the overall method of moments for an increasing number of moments ($k_{max} = 2$ to 35) in the case of termination by disproportionation and high initiator concentration; --- : reference solution calculated by the detailed method.

corresponding to $I_o = 1 \cdot 10^{-1} \text{ mol l}^{-1}$ and $I_o = 1 \cdot 10^{-3} \text{ mol l}^{-1}$. Unlike the case of bimolecular termination by disproportionation, the presence of a mechanism connecting together chains which form branches through chain transfer to polymer can lead to the formation of a gel phase. In both cases examined gelation is in fact predicted by all four solution methods. In the case of the overall method of moments, the gel point is predicted as the instant where the second- and higher-order moments diverge and integration of eq (3.8) cannot be carried further. In the other cases, the amount of gel is calculated as discussed in Section 3.4.

The case of a lower reaction rate (lower initiator concentration) is first examined. In Fig. 3.8, the number- and weight-average chain lengths are reported as a function of conversion. The solid curve refers to the overall method of moments, while the dashed curve is the solution given by the NF (with $n_b = 0$, i.e., classical NF). Note that up to the gel point (vertical dotted line), which is predicted to be the same by the two methods, these provide exactly the same answer. This means that, though the fractionated equations require a closure formula, the average chain length values which they provide coincide with the rigorous values given by the overall method of moments. Additionally, while the overall method of moments fails at the gel point, NF permits the calculation of the average chain length values of the sol phase up to complete conversion.

Regarding the calculation of the complete CLD, the solution obtained from the overall method of moments at 65% conversion (just prior to gelation) is compared to the correct one in Fig. 3.9. Since the distribution is very wide, the overall method of moments provides a solution which is completely unsatisfactory. Moreover, increasing the maximum order of moments, oscillations already start to appear at $k_{max} = 3$.

In Fig. 3.10(a) the solution given by the classical NF (solid curve) is compared to the correct solution (dashed curve) at 65% conversion. The improvement in comparison to the overall method of moments is apparent. However, as in the case of bimolecular termination by disproportionation, it appears that NF is responsible for the arising of a marked shoulder at high molecular weights which does not exist in the true CLD. From Fig. 3.10(b), where the contributions of the single generations are reported under the overall CLD, it can be seen that the presence of the shoulder is due to the first branched generation. Although in this case the passage to the second generation is guaranteed by the presence of combination, the first branched generation still contains an accumulated amount of chains which have repeatedly added branches without being able to pass over to the second generation, as they didn't undergo a combination event with another branched chain. This problem can therefore be solved, as for the case of bimolecular termination by

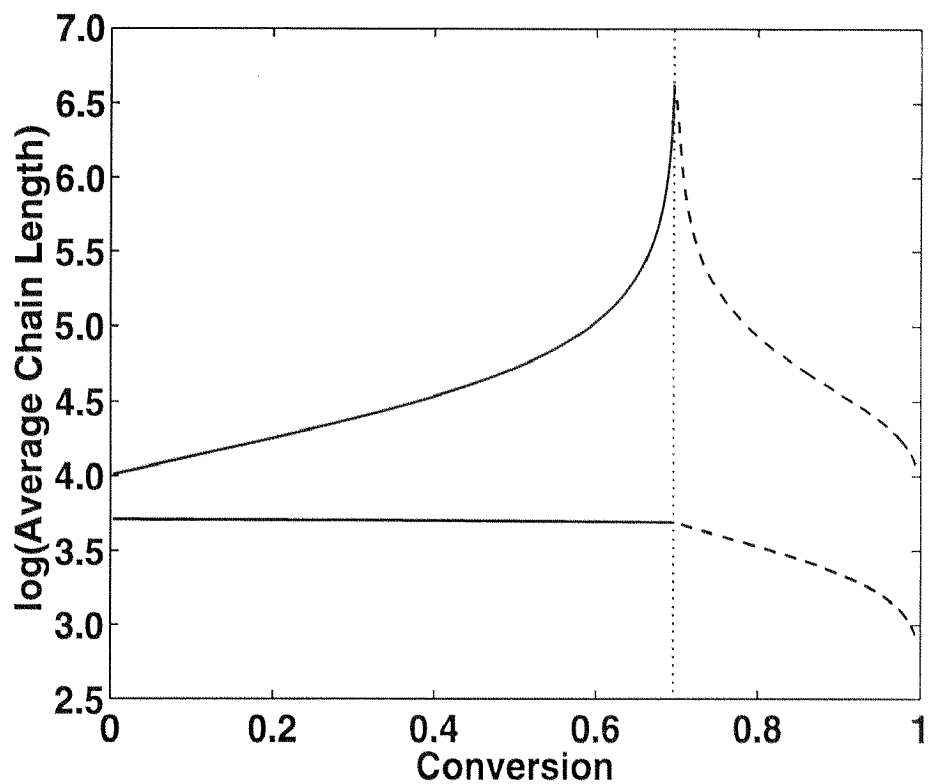


Figure 3.8: Number- and weight-average chain length as a function of conversion in the case of termination by combination and low initiator concentration; — : overall method of moments; --- : classical NF.

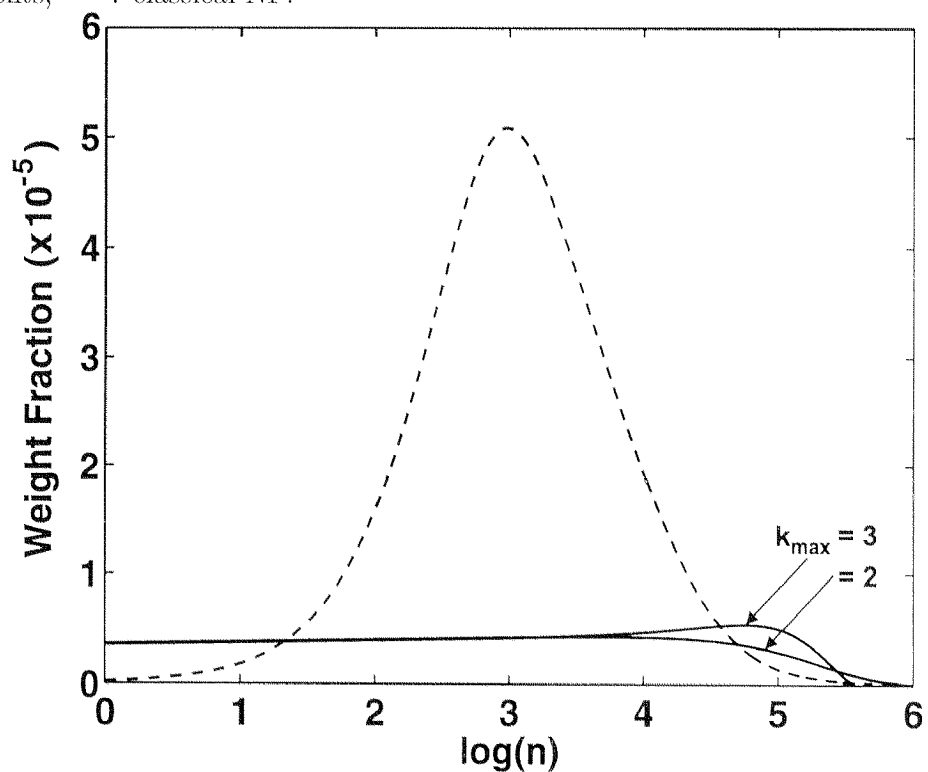


Figure 3.9: Chain length distribution at 65% conversion calculated by the overall method of moments for an increasing number of moments ($k_{max} = 2$ to 3) in the case of termination by combination and low initiator concentration; --- : reference solution calculated by the detailed method.

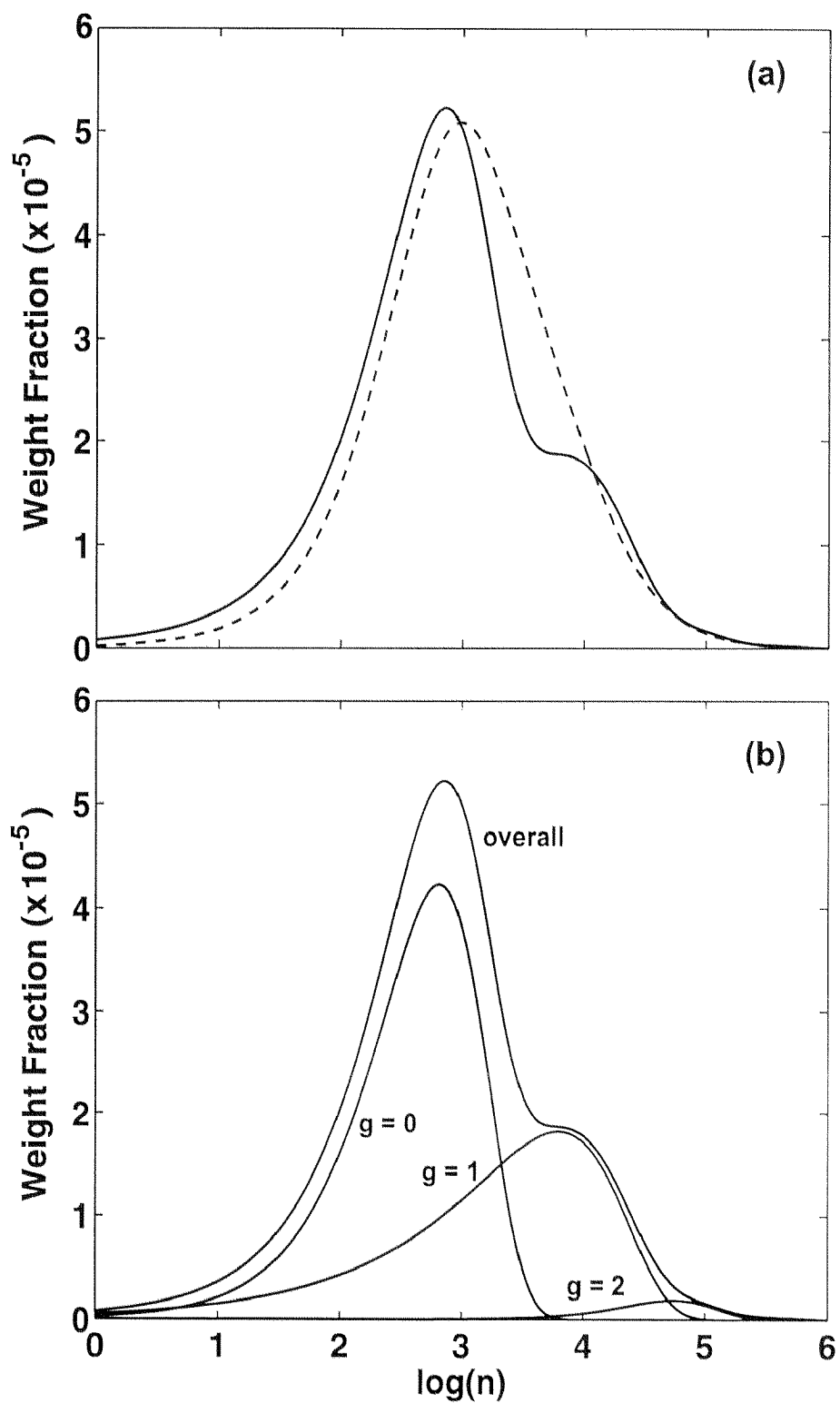


Figure 3.10: Chain length distribution at 65% conversion in the case of termination by combination and low initiator concentration. (a) — : classical NF; --- : reference solution calculated by the detailed method; (b) classical NF with the contribution of some individual generations.

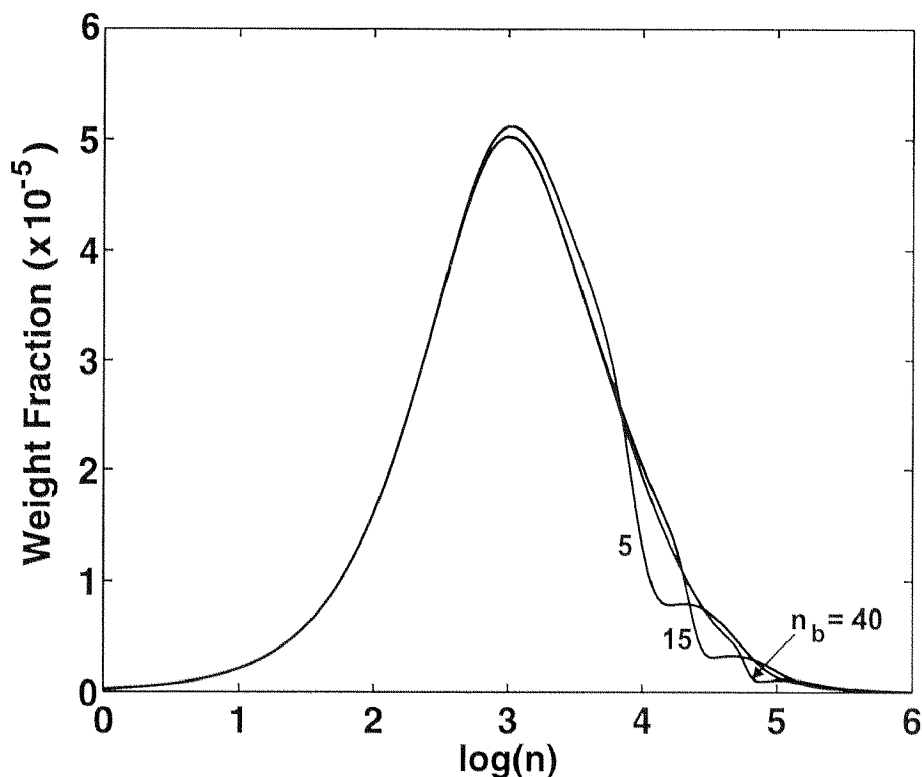


Figure 3.11: Chain length distribution at 65% conversion calculated by the refined NF technique for increasing n_b values ($n_b = 5$ to 40) in the case of termination by combination and low initiator concentration.

disproportionation, by operating a finer subdivision of the less branched chains according to the number of branches.

When this kind of partitioning is adopted, the marked shoulder actually tends to be reduced. This is shown in Fig. 3.11, where the CLD calculated for increasing n_b values is reported (with $n_g - n_b$, i.e., the Teymour and Campbell generations, fixed and equal to 6). Since for increasing n_b values, the polymer present in generation $n_b + 1$ (which is responsible for the shoulder) tends to disappear, and the same happens to the polymer belonging to the higher Teymour and Campbell generations, the description of these generations becomes redundant and one can more appropriately pass to the PANB solution method.

The solution given by the PANB method with $b_M = 160$ is reported in Fig. 3.12 (solid curve) and can be seen to be practically coincident with the correct solution (dashed curve). Therefore, also in this case the PANB method proves to be the most efficient when a detailed MWD is required. Moreover, as shown in the case of termination by disproportionation, it permits a complete description of the chain branching properties of the polymer. The number of branches $b_M = 160$ required to cover the whole MWD has been obtained through the extrapolation method discussed earlier in Section 3.5.2. It can be seen in fact from Fig. 3.10(a) that the classical NF provides a correct indication of the

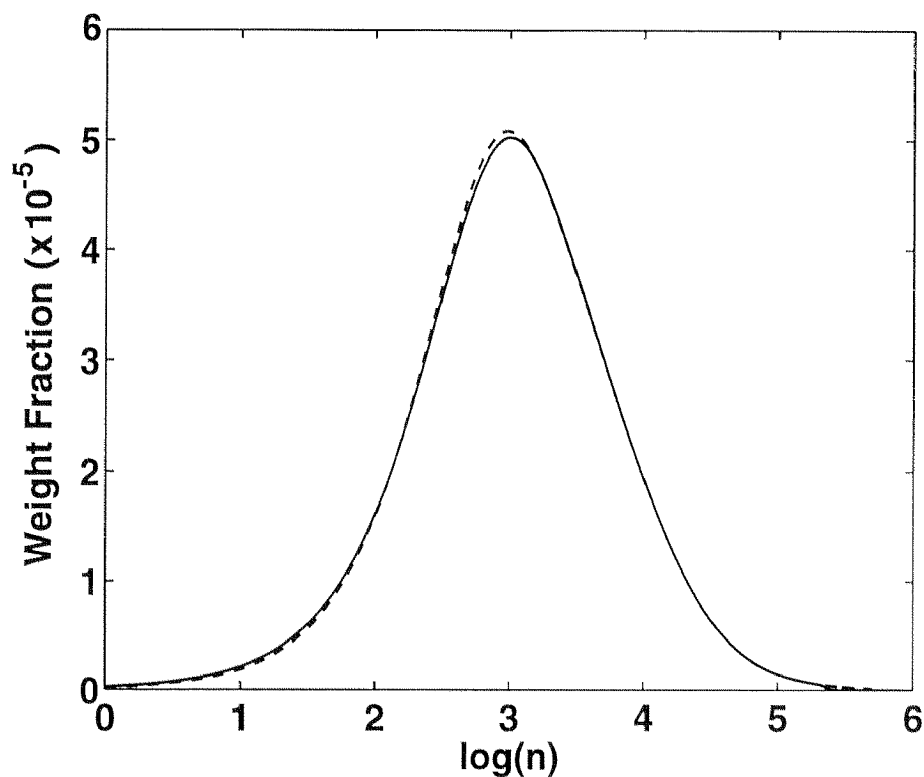


Figure 3.12: Chain length distribution at 65% conversion calculated by the PANB method with $b_M = 160$ in the case of termination by combination and low initiator concentration; --- : reference solution calculated by the detailed method.

maximum chain length in the system and it can be verified that the average number of branches vs. chain length relation is linear, as in the case of bimolecular termination by disproportionation.

The calculation of the CLD has been repeated at 80% conversion, after gelation has occurred, to examine the quality of the solution provided by the various methods after the gel point. Of course, no solution can be obtained by the overall method of moments, since the second- and higher-order moments diverge at the gel point. The detailed method has been shown in Section 3.3.1 to provide a correct solution to the PBEs (3.3)-(3.4) up to any selected chain length n_M . This is true for all conversions, no matter if a gel phase has formed or not. Therefore, the detailed solution method is able to provide a reliable reference solution also after the gel point. The requirement of a sufficiently large number of nodes at which the integration is performed has of course to be fulfilled.

In Fig. 3.13 the solution provided by the detailed method is used as a reference for the solutions given by the classical NF and PANB methods. The picture is unchanged compared to the pre-gel situation. The NF solution presents a shoulder that is an artifact of the method and the PANB technique provides a solution practically coinciding with the correct one. Accordingly, the PANB method proves to be an efficient and reliable method

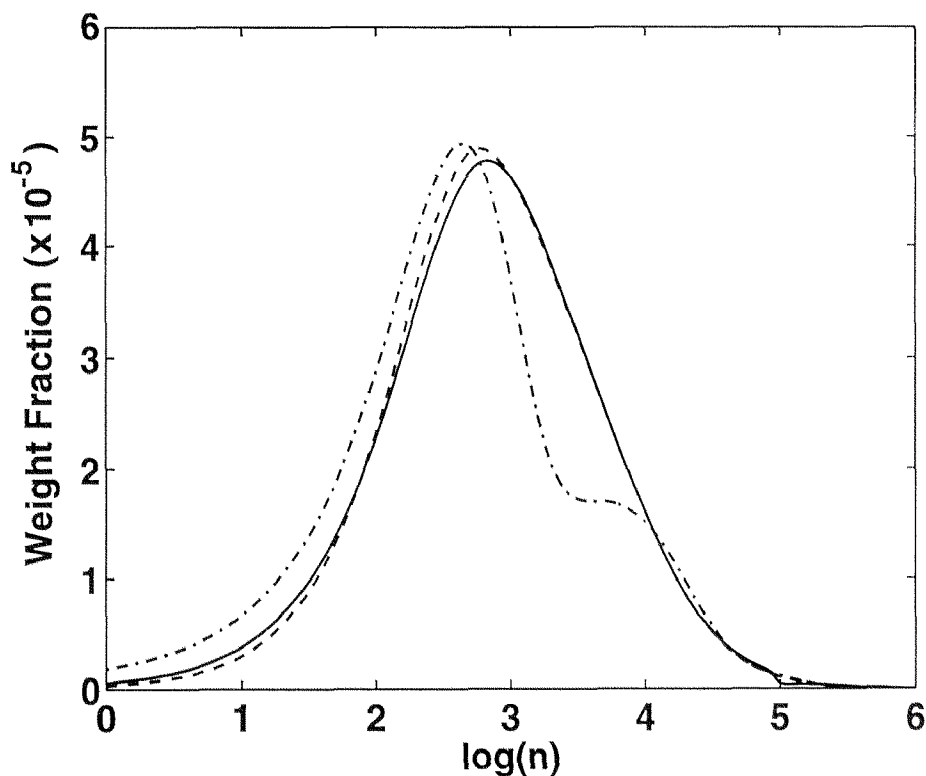


Figure 3.13: Chain length distribution at 80% conversion (after gel formation) in the case of termination by combination and low initiator concentration; — : PANB method ($b_M = 160$); - - : classical NF; - · - : reference solution calculated by the detailed method.

for the characterization of the soluble polymer fraction also in the post-gel period of the reaction.

Finally, the case with a larger initiator concentration has been investigated. In Fig. 3.14 the solution obtained by the classical NF at 50% conversion (just prior to gelation) is shown together with the solution given by the detailed method. The shoulder appears to be reduced in dimension and the solution is not far from being satisfactory. Once more, it can be shown that by adopting a finer subdivision of the polymer chain population, the solution can be further improved. A solution indistinguishable from the rigorous one can be obtained through the PANB method with $b_M = 180$.

As for the case of termination by disproportionation, two different situations have been examined, corresponding to two different reaction rates. In the case of higher reaction rates, the classical NF provides an acceptable solution. However, in the other case, where both the pre- and post-gel reaction periods have been investigated, a marked shoulder appears which is an artifact of the solution method, rather than a result of the reaction mechanisms. A reliable solution has instead been shown to be obtained in all cases when the polymer chains are subdivided according to the number of branches (provided that a sufficiently large number of branches is considered). This approach also has the advantage

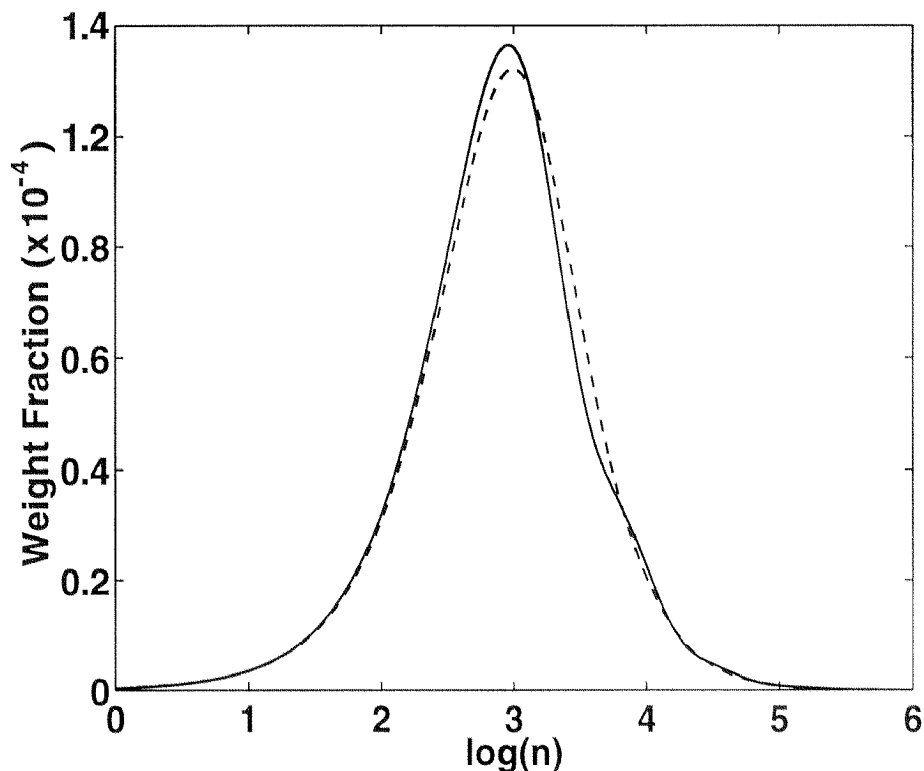


Figure 3.14: Chain length distribution at 50% conversion in the case of termination by combination and high initiator concentration; — : classical NF; --- : reference solution calculated by the detailed method.

of providing a straightforward description of the polymer in terms of branching properties.

3.6 Conclusions

Several numerical methods have been developed in the literature to calculate the MWD in free-radical polymerizations where the occurrence of chain branching leads to rather large polydispersity values and possibly the formation of a gel phase, which implies infinitely large molecules. In this chapter, a detailed numerical method has been developed which, though computationally intensive, allows to calculate the correct MWD. Using this method it was possible to check the reliability of previously proposed approximate techniques which, based on some subdivision of the unknown polymer chain population, provide an estimate of the MWD in reasonable computational times. These techniques are helpful especially when dealing with systems where several internal coordinates appear in the relevant PBEs, e.g. segregated systems. In particular NF was used in the previous Chap. 2 to solve the proposed emulsion polymerization MWD model equations.

The NF method as proposed by Teymour and Campbell [30] was found to constitute a significant improvement compared to the classical method of moments, requiring

an increased but still very limited computational effort (10 generations are usually more than enough to have convergence of the method). However, in some cases it is not able to provide a correct description of the MWD, giving rise to artificial shoulders at high molecular weights. This is due to the nature of the partitioning into generations proposed by Teymour and Campbell, which can lead to the accumulation of chains with a very different number of branches in the first branched generation. This problem is only partially removed by the refined fractionation technique proposed by Arzamendi and Asua [23]. The best solution appears to be to simulate the chains subdividing them according to the number of branches (PANB method), as proposed by Soares and Hamielec [54]. This usually requires integration of a rather large number of ODEs, let's say, ten times as many as classical NF, which implies correspondingly larger computational times, but a very accurate solution is obtained.

It has to be stressed that the geometrical growth mechanism proposed by Teymour and Campbell as a route to gel formation is in any case valuable not only from a physical point of view, but also as a remarkably simple first approximation to a rather difficult problem. Moreover, if average properties of the MWD and not its detailed shape are of interest, which is often the case, NF provides the correct solution (at least if the adopted closure equation is valid) and is not limited to the pre-gel reaction period as the overall method of moments.

If an accurate complete MWD is required, a quick-solution strategy has been indicated: through the classical NF the maximum chain length achieved in the system is first estimated. Then, the number of branches corresponding to this maximum chain length is estimated from the slope of the number of branches vs. chain length relation obtained by the PANB method using a low number of branches. This step requires the number of branches to be a linear function of molecular weight (at least to a fairly good approximation). Note that this requirement was completely fulfilled in all cases examined. Finally, the MWD is computed through the PANB method using the calculated maximum number of branches. This method provides, along with the MWD, the branching distribution function.

Chapter 4

Effects of Compartmentalization on Molecular Weight Distribution and Gel Formation

4.1 Introduction

It was shown in Chap. 2 that large errors are made in the calculation of the instantaneous properties of the MWD of a polymer produced in emulsion if a bulk model, i.e., a model ignoring active chain compartmentalization, is employed. In the literature several models can however be found (e.g. [6, 22, 23]) which involve a greater detail compared to a simple bulk model. These models include the description of the particles in the different states (i.e., containing a different number of radicals) and calculate correctly the rates of reaction in each particle state and the MWD of the active chains. However, they do not include the concept of ‘doubly distinguished particles’, i.e., they do not consider the distribution of the pairs of chains belonging to the same particle. As Lichti et al. [7] showed, the knowledge of the MWD of the active chains is insufficient to the calculation of the distribution of the terminated polymer in the presence of termination by combination, since this reaction mechanism couples the lengths only of those pairs of chains belonging to the same particles, and not of any pair of chains in the system. In this case, the doubly distinguished particles (or an equivalent distribution) are required. The same authors [39] examined a particular case (zero-one-two system controlled by termination by combination) to show that the instantaneous polydispersity would be incorrectly calculated by ignoring this specific requirement of compartmentalization.

In the present chapter an extensive analysis is performed of the role of compartmentalization in determining the MWD characteristics in the presence of termination by combination, both for linear and for branched polymers. Significant information was obtained by analysing the differences between the model developed in this work (‘correct model’)

which accounts for the CLD of the pairs of active chains belonging to the same particle, and another model ('approximate model') which limits itself to the calculation of the CLD of the active chains, as done by the literature models [6, 22, 23]. Such an analysis has been carried out both in terms of instantaneous properties, which can be directly related to the reaction mechanisms active in the system, and of cumulative properties, which are those of interest in applications.

The understanding of the mechanisms through which compartmentalization acts is helpful for the selection of proper conditions for desired molecular weights. Moreover, it permits to develop simplified models which, while accounting correctly for the compartmentalization effects, allow an easier inclusion of secondary effects, such as chain-length dependent reaction rates, non-steady-state conditions, and so on. Taking advantage on the understanding achieved in the first part of the chapter, the bases for the development of such a simplified model ('SDP model') are given in Section 4.6.

4.2 Model Summary

4.2.1 Correct Model

The equations of the correct model, which accounts for the length distribution of the pairs of chains belonging to the same particle (doubly distinguished particle distribution), are those reported in Chap. 2.

4.2.2 Approximate Model

To compare the predictions of the correct model with those of a model neglecting the effect of compartmentalization on the length of the chains terminated by combination, an approximate version of the model is developed in this section ('approximate model'). The equations are written following the formalism used for the correct model (i.e., the distinguished particle approach) to make the comparison between the two models straightforward. Despite the different form, the approximate model is conceptually equivalent to that developed in ref. [6].

The main idea underlying this model is to evaluate the rate of production of chains of length n due to the combination reaction in particles with i radicals by multiplying the rate of combination of chains of length l in particles of the same type by the probability that the coupling chain has a length $n-l$, and summing over all l values from 0 to n . The key assumption is that this probability is independent of the fact that a chain with the length of the first chosen chain is already present in the particle and can be consequently

evaluated from the CLD of the active polymer in state i particles, without introducing a CLD for the pairs of chains. As discussed also in ref. [6], this assumption is certainly valid if each particle contains a statistical number of growing chains; for a smaller number of growing chains per particle (say less than 10), this validity is less obvious. It is actually the validity of this assumption that we are discussing here.

In the approach which exploits the concepts of distinguished particles, this assumption leads to the significant simplification of ignoring the distribution of the doubly distinguished particles. In the case of linear chains, the rate of combination in state i particles of two radicals, one of current lifetime t' and the other of current lifetime t'' , is given by the rate of combination of radicals with lifetime t' , $2c_c(i-1)N_i'(t, t')$, times the probability that the coupling chain has a lifetime t'' , $N_i'(t, t'')/iN_i$ (where this probability is assumed independent of t'). In the case of branched chains, it is enough to introduce the pre-lives of one or both chains.

Accordingly, in comparison to the correct model, the equations for calculating the doubly distinguished particle distributions (eqs (2.8)-(2.11)) are omitted and equations (2.18)-(2.21) are substituted by the following:

$$\frac{d[v_P \bar{S}^C(t_e, t', t'')]}{dt_e} = \left\{ 2c_c \sum_{i=2}^N (i-1) N_i'(t_e - t', t'') \frac{N_i'(t_e - t', t'')}{iN_i} + \right. \\ \left. - (k_{fp} + k_p^* \gamma) (\alpha t' + \alpha t'') \bar{S}^C(t_e, t', t'') \bar{n} \right\} \frac{1}{N_A} \quad (4.1)$$

$$\frac{d[v_P \bar{V}^C(t_e, t', t'', n')]}{dt_e} = \left\{ 2c_c \sum_{i=2}^N (i-1) B_i'(t_e - t', t'', n') \frac{N_i'(t_e - t', t'')}{iN_i} + \right. \\ \left. - (k_{fp} + k_p^* \gamma) (n' + \alpha t' + \alpha t'') \bar{V}^C(t_e, t', t'', n') \bar{n} \right\} \frac{1}{N_A} \quad (4.2)$$

$$\frac{d[v_P \bar{G}^C(t_e, t', t'', n', n'')]}{dt_e} = \left\{ 2c_c \sum_{i=2}^N (i-1) B_i'(t_e - t', t'', n') \frac{B_i'(t_e - t', t'', n'')}{iN_i} + \right. \\ \left. - (k_{fp} + k_p^* \gamma) (n' + n'' + \alpha t' + \alpha t'') \bar{G}^C(t_e, t', t'', n', n'') \bar{n} \right\} \frac{1}{N_A} \quad (4.3)$$

Here, distributions $\bar{S}^C(t_e, t', t'')$, $\bar{V}^C(t_e, t', t'', n')$ and $\bar{G}^C(t_e, t', t'', n', n'')$ are the distributions at time t_e of the dead polymer formed by combination at any reaction time from active chains of given current lifetimes t' and t'' and, in the case, pre-lives n' and n'' . The length of the resulting chain is given by $n = n' + n'' + \alpha(t' + t'')$ (with n' or n'' equal to zero, if the corresponding chain is linear).

Note that, differently from the case of the correct model, three distributions only are required: $\bar{S}^C(t_e, t', t'')$, $\bar{V}^C(t_e, t', t'', n')$ and $\bar{G}^C(t_e, t', t'', n', n'')$. More specifically, distributions $V^C(t_e, t', t'', n')$ and $W^C(t_e, t', t'', n'')$ of the correct model are replaced by a single distribution $\bar{V}^C(t_e, t', t'', n')$. This happens because the approximate model does not take into account which of the two chains of the pair is first born (or re-born) and, accordingly, saying that one of the two chains is branched and the other linear is enough to

distinguish them. This also reflects the reduced level of detail of the approximate model.

In conclusion, the approximate version of the model is constituted by eqs (2.5), (2.6), (2.16), (2.17), (4.1)-(4.3). From the mathematical point of view, the resulting system is closely similar to the one obtained in the case of the correct model. Moreover, the numerical solving procedure adopted is the same (NF and method of moments, see Appendix A) and requires an equivalent computational effort.

4.3 Illustrative Calculations

In the following a comparison between the MWD properties calculated by the two models is performed. In Section 4.3.1 the analysis is performed in terms of instantaneous properties, i.e., those of the infinitesimal amount of dead polymer produced at a particular instant during the polymerization reaction. In this case, only the equations detailed in the previous section are required. Even though the meaning of these quantities becomes less clear when dealing with branching systems, the comparison remains significant and illustrates interesting features of the two approaches.

In Section 4.3.2 an analogous comparison is carried out in terms of MWD properties of the polymer actually produced, i.e., in terms of cumulative molecular weights. In this case, the previous equations have to be coupled to a model able to account for the evolution during the emulsion polymerization of all those quantities which influence the MWD of the product, for instance particle size, monomer concentration in the particles and so on. In particular, the model proposed by Storti et al. [41] has been used; main assumptions are particle size monodispersity and thermodynamic equilibrium conditions for the phase partitioning of the monomer.

4.3.1 Instantaneous Properties

The numerical values of the model parameters used for the calculation of the instantaneous properties are summarized in Table 4.1. Each of these values applies when the corresponding reaction mechanism is considered to be operative; if not, it is set equal to zero.

In all cases the instantaneous polydispersity ratio, P_d^i , is shown as a function of the average number of active chains per particle, \bar{n} . The variation of \bar{n} has been obtained by changing the value of the entry rate of the active radicals from the aqueous phase to the particles, ρ . Note that while low \bar{n} values are typical of emulsion polymerization systems, at increasing values of the number of active chains per particle the behavior of

Parameter	Value
C_m	$5.7 \cdot 10^{-3} \text{ mol cm}^{-3}$
k_d	$1.3 \cdot 10^{-3} \text{ s}^{-1}$
k_{fm}	$10 \text{ cm}^3 \text{ mol}^{-1} \text{ s}^{-1}$
k_{fp}	$10 \text{ cm}^3 \text{ mol}^{-1} \text{ s}^{-1}$
k_p	$2.6 \cdot 10^5 \text{ cm}^3 \text{ mol}^{-1} \text{ s}^{-1}$
k_p^*	$5 \text{ cm}^3 \text{ mol}^{-1} \text{ s}^{-1}$
k_{tc}	$1.16 \cdot 10^9 \text{ cm}^3 \text{ mol}^{-1} \text{ s}^{-1}$
k_{td}	$0 \text{ cm}^3 \text{ mol}^{-1} \text{ s}^{-1}$
v_P	$1.21 \cdot 10^{-15} \text{ cm}^3$
$\sigma^{(0)}$	$2.38 \cdot 10^{-7} \text{ mol cm}^{-3}$
$\sigma^{(1)}$	$3.22 \cdot 10^{-3} \text{ mol cm}^{-3}$
$\sigma^{(2)}$	$105.3 \text{ mol cm}^{-3}$

Table 4.1: Numerical values of the model parameters used for the calculations of instantaneous properties. The moments $\sigma^{(k)}$ of the dead polymer are referred to the particle phase volume.

each particle approaches that of a bulk system and any compartmentalization effect is expected to vanish.

In Figs 4.1 and 4.3 the case of linear chains is examined; thus, k_{fp} and k_p^* are set to zero.

In Fig. 4.1 combination has been considered the only operating termination mechanism, and both chain transfer to monomer and desorption from the particles have been neglected, i.e., $k_{fm} = k_d = 0$.

By inspection of the calculated curves (continuous curve for the correct model and broken curve for the approximate model) it appears that the same number-average degree of polymerization (Fig. 4.1(a)) is predicted, since the two curves are in fact superimposed. However, the different behavior of the polydispersity ratio predicted by the two models (Fig. 4.1(b)) proves the need for taking into account chain compartmentalization through the doubly distinguished particle distributions.

Note that the continuous curve exhibits two physically significant extreme values, i.e., $P_d^i = 2$ at $\bar{n} = 0.5$ and P_d^i approaching 1.5 at large \bar{n} values. At large \bar{n} values, $P_d^i = 1.5$ corresponds to the value for bulk polymerization with dominant bimolecular termination by combination. This result is physically sound since in this situation the particles can be regarded as mini-bulks. At $\bar{n} = 0.5$, instead, the situation is that of chains mainly growing undisturbed in state one particles to very great lengths (see Fig. 4.1(a)). This is due to very low entry frequencies. When a new radical enters the particle, bimolecular termination by combination occurs rapidly ($c \gg \rho$), so that the units added to the two chains between the entry and the termination are negligible compared to the final length of the

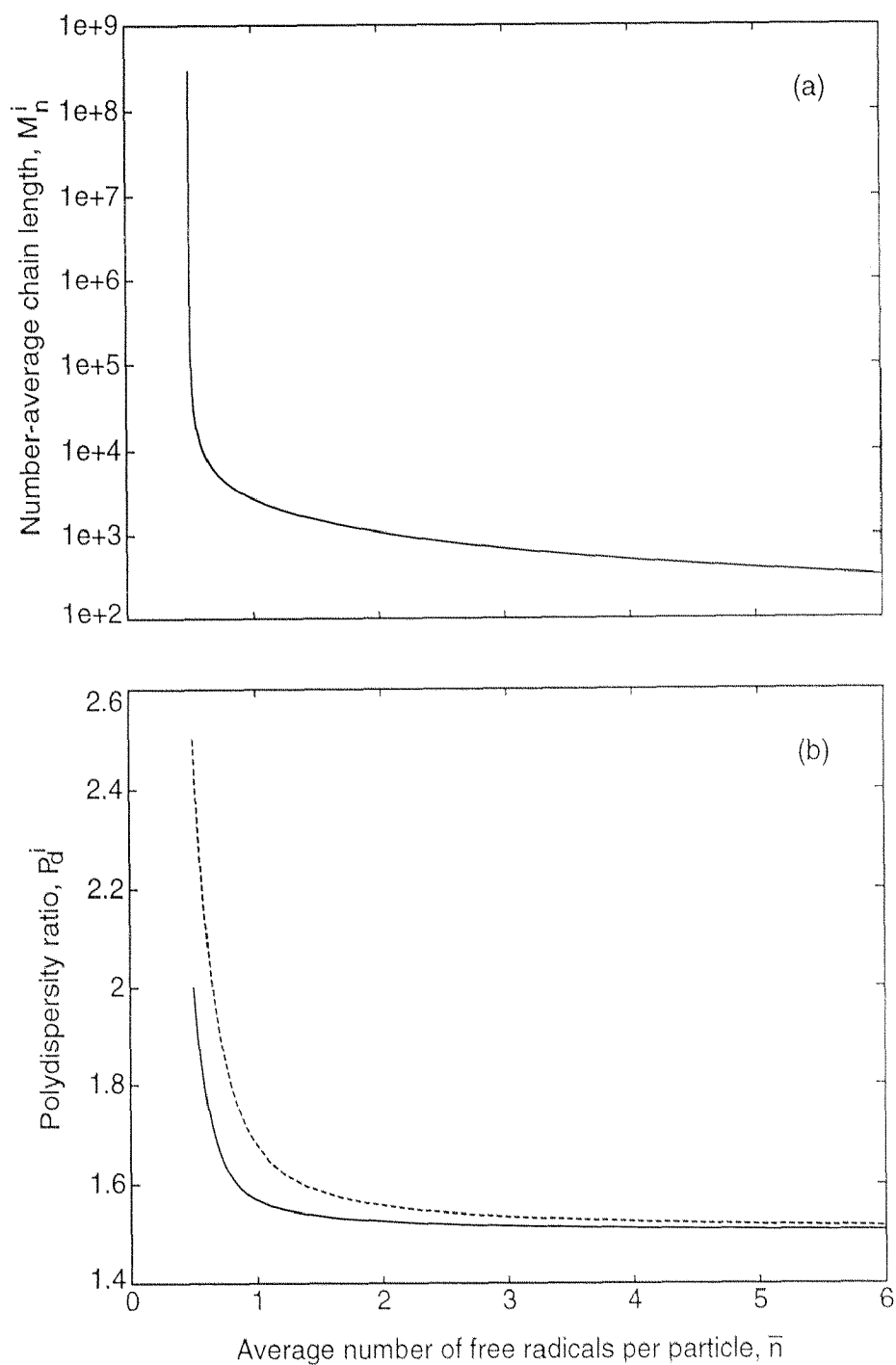


Figure 4.1: (a) Number-average chain length and (b) polydispersity ratio as a function of the average number of active chains per particle, \bar{n} . Parameter values as in Table 4.1 but with $k_d = k_{fm} = k_{fp} = k_p^* = 0$. — : correct model; --- : approximate model.

chain. The termination mechanism can thus be compared to a monomolecular termination mechanism, because it preserves the length of the growing chain. This doesn't necessarily mean that bimolecular termination is 'instantaneous' upon entry, in the sense that it is faster than propagation, but just that the length of the chain is determined by the entry frequency rather than by that of combination. This termination mechanism corresponds to a polydispersity value of 2, which is indeed typical of monomolecular termination.

The situation examined here above at $\bar{n} = 0.5$ ($\rho \ll c$) also provides a good picture for understanding the need for the doubly distinguished particle description. Assuming that in these conditions the particles containing more than two radicals are negligible in number, the situation can be depicted as in Fig. 4.2(a). This figure shows a population of state one particles containing chains growing alone up to high lengths, corresponding to characteristic times τ_ρ given by the inverse of the entry frequency ρ . Upon entry of a second radical, a population of state two particles appears where the first chain is still growing but now a second chain grows along with it. The typical length of this second chain is determined by the bimolecular termination frequency c and corresponds to the characteristic time $\tau_c = 1/2c$. As $\rho \ll c$, $\tau_c \ll \tau_\rho$. Accordingly, two very different chain populations are present in the state two particles. The first chain population has a long characteristic lifetime τ_ρ , while the second has a short characteristic lifetime τ_c . This is illustrated in Fig. 4.2(b), where these two components of the N'_2 distribution (distribution of the active chains in state two particles) are qualitatively shown. In all particles containing two chains, one chain belongs to the distribution with $\tau = \tau_\rho$ (broken curve in Fig. 4.2(b)) and the other to the distribution with $\tau = \tau_c$ (solid curve in Fig. 4.2(b)). It is clear that in a termination by combination event it can never happen that two chains belonging to the same of these distributions couple together. The doubly distinguished particle approach accounts for the presence of these two different chain populations through the idea of first-born and last-born chain. Given the distribution $N'_2(t, t', t'')$, the time t' during which the first-born chain grows alone is related to characteristic time τ_ρ , while the time t'' during which the two chains grow together is related to characteristic time τ_c . If this kind of description is not adopted, as in the approximate model, coupling of two chains belonging to the same component of distribution N'_2 (solid or broken curve in Fig. 4.2(b)) is allowed. Accordingly, a greater amount of short-short and long-long chain combination is admitted in comparison to reality. This explains the larger polydispersity ratio calculated by the approximate model at $\bar{n} = 0.5$, as shown by the broken curve in Fig. 4.1(b). On the other hand, it has been shown in Fig. 4.1(a) that the number-average chain length M_n^i is calculated correctly by the approximate model. This is due to the fact that it is just the

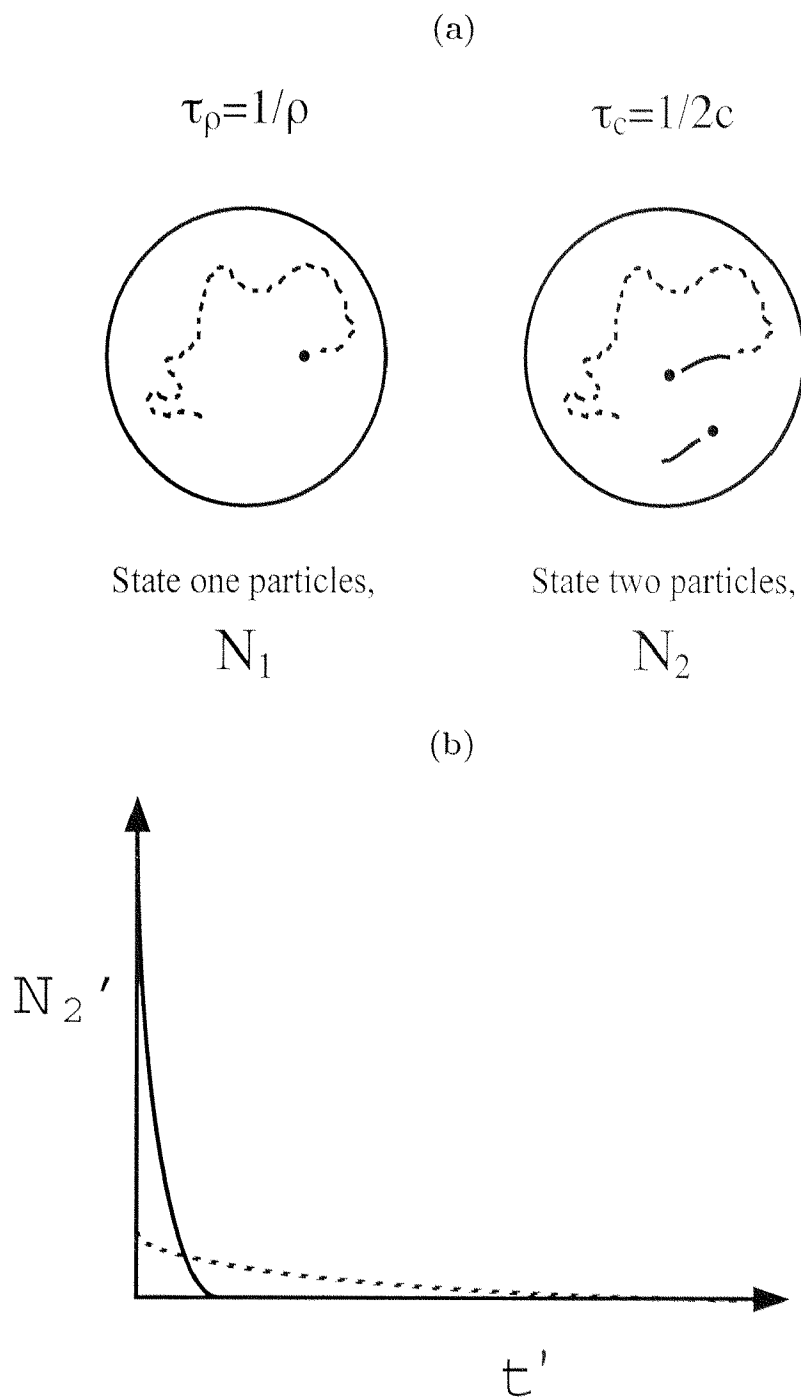


Figure 4.2: (a) Picture of the chain lengths in state 1 and 2 particles at entry frequencies much smaller than the bimolecular termination frequency. (b) Two components of the chain length distribution in state 2 particles, with different characteristic lifetimes. — : $\tau_c = 1/2c$; --- : $\tau_p = 1/\rho$.

way in which the active chains couple which is incorrectly described by this model, while the length of these chains and the number of the coupling events is computed correctly.

The physical considerations above can be confirmed analytically by writing the balance equations for the singly and doubly distinguished particles in the case where the polymer particles containing more than two active chains are negligible in number. The following balances for the singly distinguished particles result:

$$\frac{\partial N_1'(t, t')}{\partial t'} = -\rho N_1'(t, t') \quad (4.4)$$

$$\frac{\partial N_2'(t, t')}{\partial t'} = \rho N_1'(t, t') - (\rho + 2c)N_2'(t, t') \quad (4.5)$$

with initial conditions:

$$N_1'(t, t' = 0) = \rho N_0(t) \quad (4.6)$$

$$N_2'(t, t' = 0) = \rho N_1(t) \quad (4.7)$$

Remember that no desorption is assumed to take place ($k_d = 0$). Solution of system (4.4)-(4.5), accounting for the fact that $\rho \ll c$, yields:

$$N_1'(t, t') = \rho N_0 e^{-\rho t'} \quad (4.8)$$

$$N_2'(t, t') = \frac{\rho^2 N_0}{2c} e^{-\rho t'} + \rho N_1 e^{-2ct'} \quad (4.9)$$

with $N_0 \simeq N_1 \simeq 0.5$. Observing the expression of N_2' , it can be seen that this is constituted by two exponential terms with different characteristic decay times, as depicted in Fig. 4.2(b). However, from expression (4.9) it is still not clear whether two chains belonging to the same particle can contribute to the same exponential term or not.

The rate of production at time t of terminated chains of a given length $\alpha \bar{t}$ is calculated by the approximate model as:

$$\hat{S}^{C,s}(t, \bar{t}) = \frac{1}{2} \int_0^{\bar{t}} 2c N_2'(t, \bar{t} - t') \frac{N_2'(t, t')}{2N_2} dt' \quad (4.10)$$

This implies multiplication of distribution N_2' by itself, with the appearance of terms arising from the multiplication of each exponential contribution $e^{-\rho t'}$ and $e^{-2ct'}$ by itself. These terms physically represent the short-short and long-long chain terminations which are in practice prevented by compartmentalization, and which cause an erroneous increase in the calculated polydispersity. Integral (4.10) can be carried out analytically, using eq. (4.9) for $N_2'(t, t')$. This gives:

$$\hat{S}^{C,s}(t, \bar{t}) = c^2 \left\{ \rho N_1 \bar{t} e^{-2c\bar{t}} + \frac{\rho^3 N_0}{4c^2} \bar{t} e^{-\rho \bar{t}} + \frac{\rho^2 N_0}{2c^2} \left[e^{-\rho \bar{t}} - e^{-2c\bar{t}} \right] \right\} \quad (4.11)$$

What is interesting in this expression is the appearance of the two terms of the form $\bar{t}e^{-a\bar{t}}$, typical of a bimolecular termination by combination mechanism. These terms are precisely those which arise from the combination of chains within each of the two distributions constituting the N_2' distribution, the impossibility of which has been discussed above.

A correct analytical solution can be obtained by use of the doubly distinguished particle distribution. Assuming again a negligible amount of particles containing more than two radicals, the balance for $N_2''(t, t', t'')$ is given by:

$$\frac{\partial N_2''(t, t', t'')}{\partial t''} = -(\rho + 2c)N_2''(t, t', t'') \quad (4.12)$$

with initial conditions:

$$N_2''(t, t', t'' = 0) = \rho N_1'(t, t') \quad (4.13)$$

This yields ($\rho \ll c$):

$$N_2''(t, t', t'') = \rho^2 N_0 e^{\rho t'} e^{-2ct''} \quad (4.14)$$

In a different form, it appears again that the chains belonging to state two particles can be subdivided into two families, the first with characteristic lifetime $\tau_\rho = 1/\rho$ and the second with characteristic lifetime $\tau_c = 1/2c$. However, this time it appears that each one of the chains in a state two particle belongs to a distribution with a different characteristic lifetime.

The correct model calculates the rate of formation at time t of terminated chains of length $\alpha\bar{t}$ as:

$$\hat{S}^{C,d}(t, \bar{t}) = \int_0^{\bar{t}/2} 2cN_2''(t, \bar{t} - 2t'', t'') dt'' \quad (4.15)$$

By substitution of eq. (4.14) in integral (4.15), it appears that only coupling of chains with different characteristic times is admitted. The analytical solution of integral (4.15) yields:

$$\hat{S}^{C,d}(t, \bar{t}) = \rho^2 N_0 \left(e^{-\rho\bar{t}} - e^{-c\bar{t}} \right) \quad (4.16)$$

This time the terms of the form $\bar{t}e^{-a\bar{t}}$ do not appear. The bimolecular nature of the termination event under consideration appears from the fact that $\hat{S}^{C,d}(t, \bar{t} = 0) = 0$. However, at lifetimes $\bar{t} = \tau_c$, i.e., very short compared to those achieved on an average, $\hat{S}^{C,d}(t, \bar{t}) \simeq \rho^2 N_0 e^{-\rho\bar{t}}$, i.e., the distribution has the form of that given by a monomolecular termination mechanism, implying $P_d^i = 2$.

The analysis above shows that situations exist where the lengths of the two colliding chains are correlated, so that the assumption of independence of the two lengths (see Section 4.2.2) fails. In these cases, the approximate model is no longer valid. The nature of this correlation is analysed in detail in Section 4.4 from a statistical point of view.

At increasing \bar{n} values, the broken curve in Fig. 4.1(b) approaches the solid one. One expects this to happen at very high \bar{n} values, in conditions where all particles can be considered as mini-bulks, i.e., they contain a statistical number of chains, which implies no correlation of the chain lengths. This is because all particles contain such a high number of chains that extracting a chain from a particle would cause no significant disturbance to the distribution of the chain lengths in that particle, which is the same as that in all the other particles. It follows that choosing a second chain to couple to the first from the same particle or from a different one is exactly the same. However, observing Fig. 4.1(b), it can be seen that the answers of the two models (correct and approximate) are very close already at \bar{n} values (e.g. $\bar{n} = 3$) which are much smaller than those required for all particles to be considered as mini-bulks. In these conditions, a large fraction of particles containing very few radicals (e.g. one or two) are still present. The analysis previously conducted at $\bar{n} = 0.5$, where the pairwise correlation between the chain lengths was explained on the basis of the fact that $\rho \ll c$, suggests that this correlation disappears when $\rho \gg c$, i.e., much before all particles contain a statistical number of active chains. In Fig. 4.1(b), we have in fact $\rho/c \rightarrow 0$ as $\bar{n} \rightarrow 0.5$, $\rho/c = 1$ at $\bar{n} = 0.9$ and $\rho/c = 16$ at $\bar{n} = 3$. This point will be better clarified in Section 4.4 through statistical arguments.

A similar analysis can be made in the presence of both chain transfer to monomer and desorption, with the results shown in Fig. 4.3. Due to the desorption mechanism, in this case the minimum value of \bar{n} is zero. The value $P_d^i = 2$ calculated at $\bar{n} \rightarrow 0$, corresponds to dominant monomolecular termination. Both models predict this asymptotic value, since in these conditions particles in state two and consequently bimolecular terminations are completely negligible. However, differences arise around $\bar{n} = 0.5$, where the approximate model overestimates again the broadness of the MWD. Instead, the same M_n^i is predicted by the two models at all \bar{n} values.

With reference to branched polymers, the case of chain transfer to polymer has first been considered. All the parameter values reported in Table 4.1 have been used, except for crosslinking which is considered to be absent ($k_p^* = 0$). Fig. 4.4 shows that the two models predict significantly different polydispersity ratios. In particular, the approximate model calculates, as for the case of linear chains, larger P_d^i values than the correct one, especially at \bar{n} values between 0.5 and 1. The error introduced may be significant, more than 15% in the worst case. Again, the same M_n^i is predicted by the two models.

Similar results are obtained in the case of nonlinear chains produced by the crosslinking reaction (see Fig. 4.5). For the calculations reported in this figure the numerical values of Table 4.1 have been used but $k_{fp} = 0$. In this case, the qualitative behavior of the

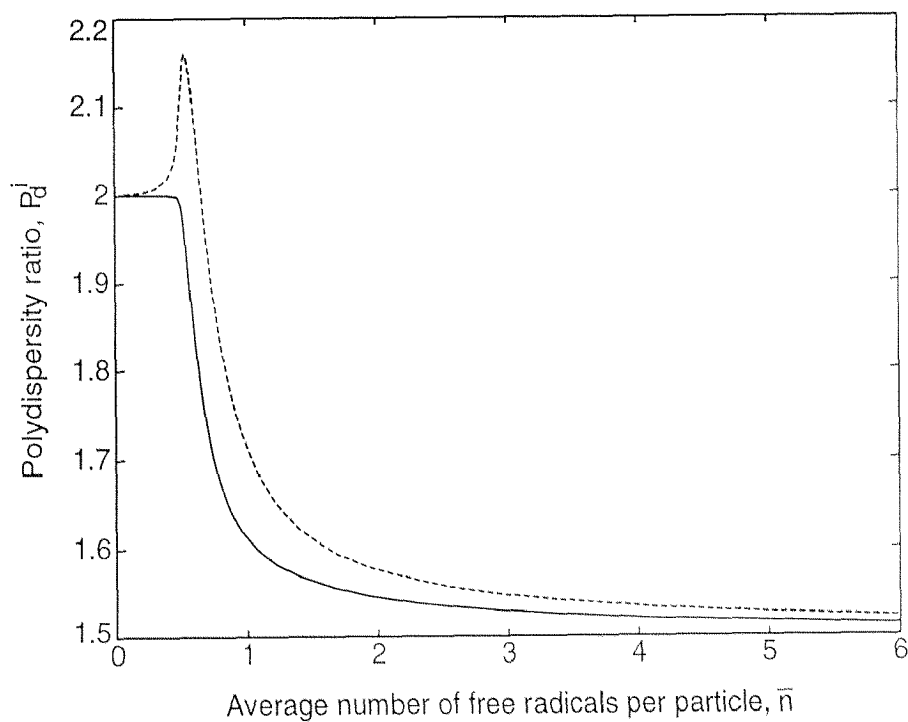


Figure 4.3: Polydispersity ratio as a function of the average number of active chains per particle, \bar{n} . Parameter values as in Table 4.1 but with $k_{fp} = k_p^* = 0$. — : correct model; --- : approximate model.

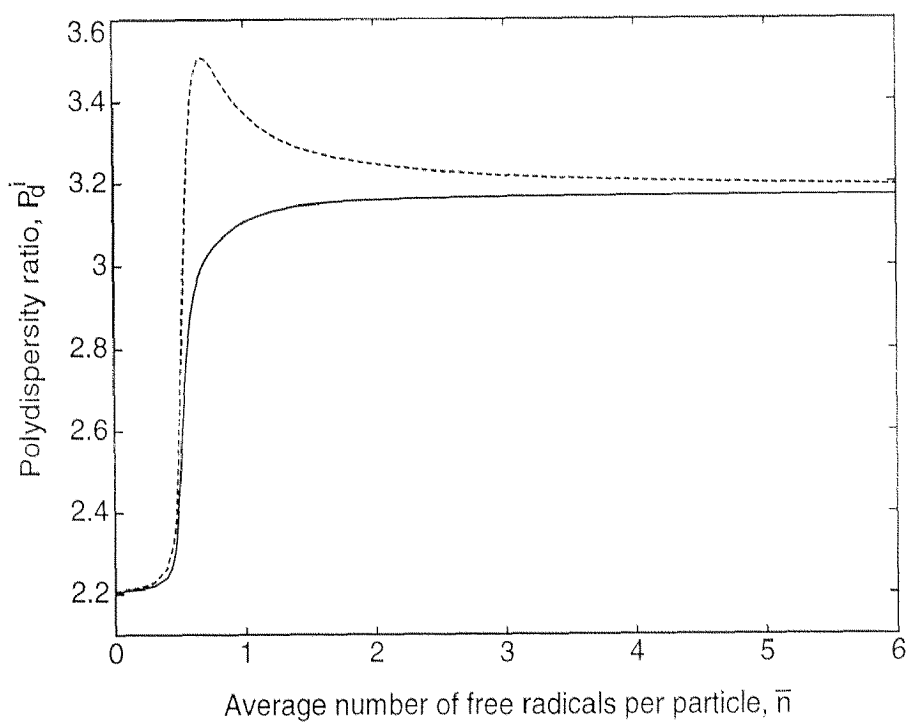


Figure 4.4: Polydispersity ratio as a function of the average number of active chains per particle, \bar{n} . Parameter values as in Table 4.1 but with $k_p^* = 0$. — : correct model; --- : approximate model.

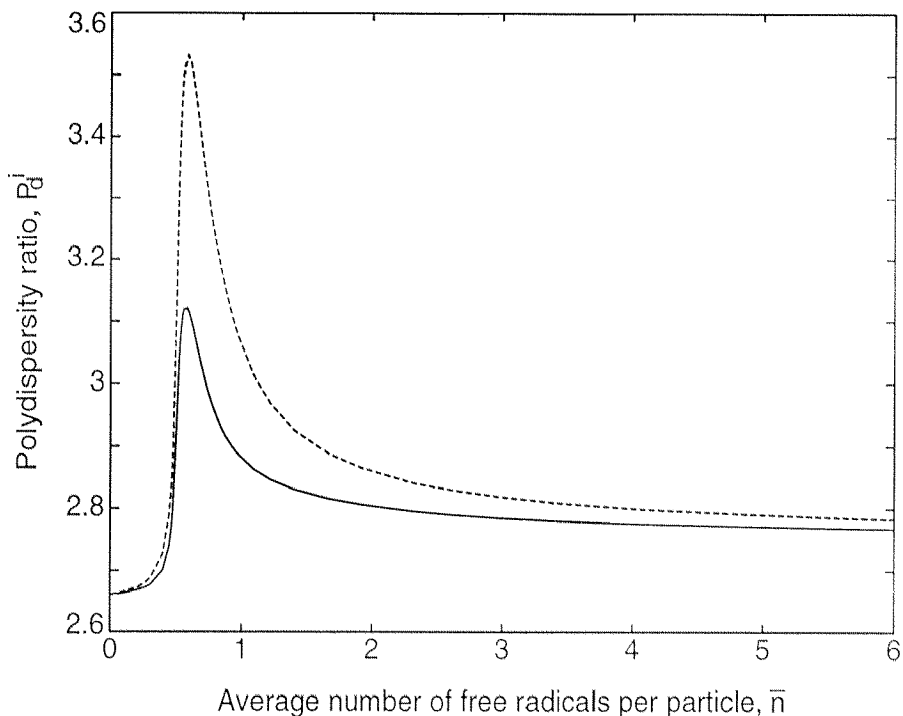


Figure 4.5: Polydispersity ratio as a function of the average number of active chains per particle, \bar{n} . Parameter values as in Table 4.1 but with $k_{fp} = 0$. — : correct model; --- : approximate model.

polydispersity curves predicted by the two models is the same, exhibiting a maximum in both cases. However, significant discrepancies arise around \bar{n} values typical of an emulsion polymerization system.

The analysis carried out in this section in terms of instantaneous MWD properties shows that a model neglecting the concept of doubly distinguished particles is able to predict correct number-average molecular weights but overestimates the values of the polydispersity ratio, especially in the range $0.4 < \bar{n} < 2$, which is typical of many emulsion systems.

However, it may be questioned how significant this error on the instantaneous properties is when they are integrated over the entire process, i.e., when the cumulative properties of the polymer are calculated. Consequently, in the following section a comparison of the two models is carried out in terms of cumulative properties.

4.3.2 Cumulative Properties

To permit the calculation of cumulative quantities, the equations illustrated above for the MWD calculation have been coupled to a model [41] able to account for the evolution during the polymerization process of all those quantities which determine the parameters

Parameter	Value	Meaning
B	0.939	Trommsdorff effect parameter [41]
C	3.875	Trommsdorff effect parameter [41]
$C_{m,w}^*$	$3.68 \cdot 10^{-6}$ mol cm ⁻³	monomer water concentration at saturation
D	-0.494	Trommsdorff effect parameter [41]
k_e	$2 \cdot 10^{-13}$ cm ³ s ⁻¹	entry rate constant
k_{fm}	9.07 cm ³ mol ⁻¹ s ⁻¹	chain transfer to monomer rate constant
k_{fp}	30 cm ³ mol ⁻¹ s ⁻¹	chain transfer to polymer rate constant
k_I	$1.18 \cdot 10^{-6}$ s ⁻¹	initiator decomposition rate constant
k_p	$2.59 \cdot 10^5$ cm ³ mol ⁻¹ s ⁻¹	propagation rate constant
k_p^*	3 cm ³ mol ⁻¹ s ⁻¹	crosslinking rate constant
k_{tc}	$5.97 \cdot 10^9$ cm ³ mol ⁻¹ s ⁻¹	termination by combination rate constant
k_{td}	0 cm ³ mol ⁻¹ s ⁻¹	termination by disproportionation rate constant
$[I]_w^0$	$2.13 \cdot 10^{-6}$ mol cm ⁻³	initial molar concentration of initiator
M_n^{seed}	$1.8 \cdot 10^4$	seed number-average chain length
N_P	$1 \cdot 10^{14}$ cm ⁻³	seed particle concentration
P_d^{seed}	2	seed polydispersity ratio
M_m	104.2 g mol ⁻¹	monomer molecular weight
V_m	113.8 cm ³	total volume of charged monomer
$v_{P,0}$	$5 \cdot 10^{-18}$ cm ³	initial particle volume
V_w	1012.3 cm ³	total volume of charged water
η	1	initiator efficiency
ϕ_m^*	0.68	particle monomer volume fraction at saturation
ρ_m	0.878 g cm ⁻³	monomer density
ρ_p	1.05 g cm ⁻³	polymer density

Table 4.2: Numerical values of the model parameters used for the calculations of cumulative properties.

appearing in the MWD equations.

The simulation results discussed here below refer to seeded batch reactions. The numerical values of the model parameters together with the seed characteristics are summarized in Table 4.2.

The case of linear chains has first been considered ($k_{fp} = k_p^* = 0$). In Fig. 4.6(a) the number- and weight-average chain lengths are reported in logarithmic scale as a function of conversion. The solid line refers to the correct model and the dashed line to the approximate model. As expected, the same number-average chain length M_n is predicted by the two models over the entire conversion range, while the weight-average chain length M_w is overestimated by the approximate model (by about 10%). This is in accordance with the fact that larger instantaneous polydispersities are calculated by the approximate model. The predicted values of the average number of radicals per particle \bar{n} are reported in Fig. 4.6(b) as a function of conversion. They can be seen to range from 0.5 to 1.4, i.e., they lie in a region where compartmentalization is actually expected to play a significant

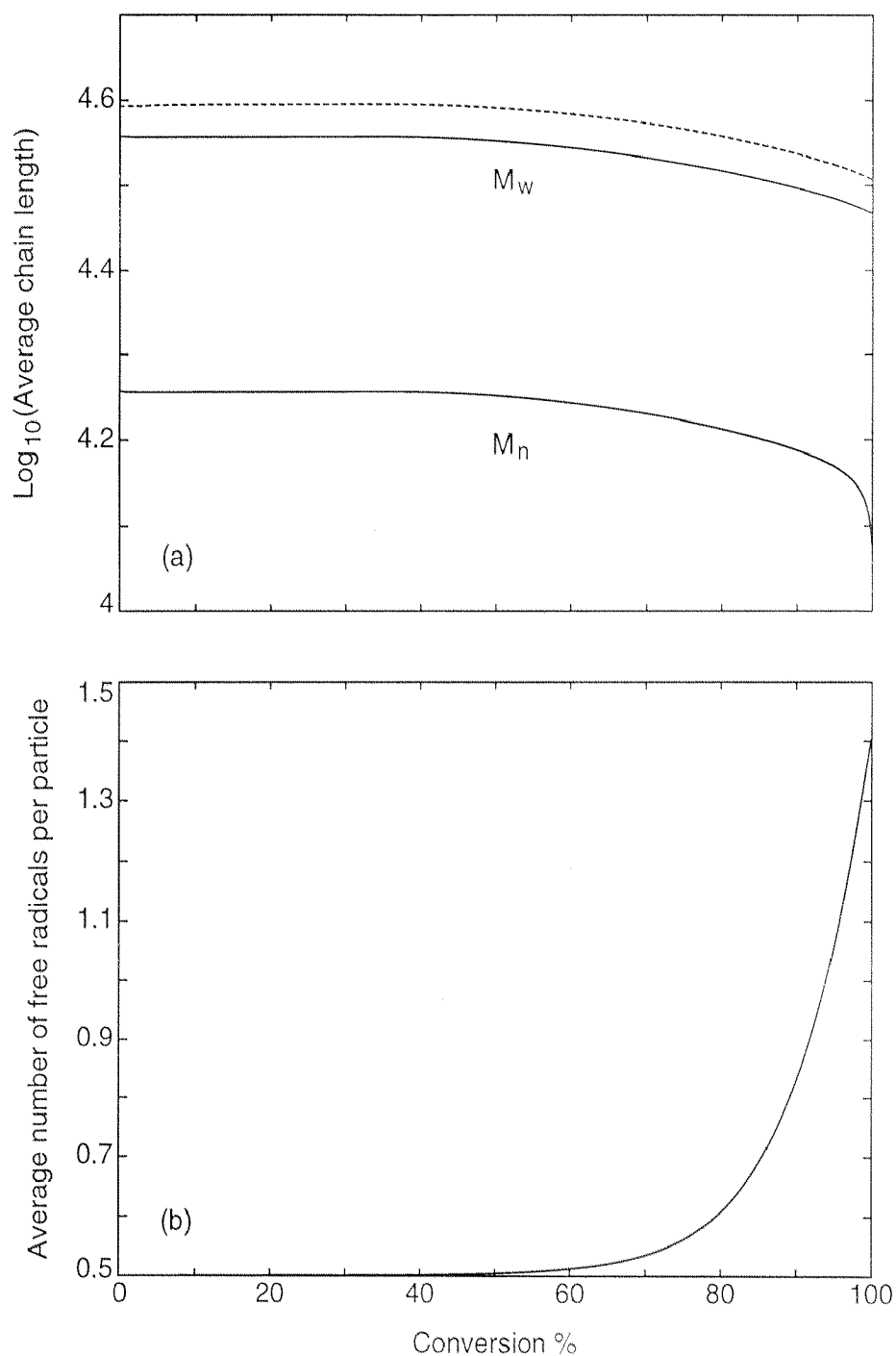


Figure 4.6: (a) Number- and weight-average chain length and (b) average number of active chains per particle as a function of conversion in the case of linear chains. Parameter values as in Table 4.2, but with $k_{fp} = k_p^* = 0$. — : correct model; --- : approximate model.

role (see Section 4.3.1).

When the presence of chain transfer to polymer ($k_{fp}=30 \text{ cm}^3 \text{ mol}^{-1} \text{ s}^{-1}$, $k_p^*=0$) is considered, the results shown in Fig. 4.7 are obtained. In Fig. 4.7(a) the average chain lengths of the sol polymer fraction are plotted as a function of conversion, while in Fig. 4.7(b) the gel weight fraction is reported. It can be seen that the two models yield completely different predictions in terms of weight-average chain length and of gel point. The approximate model results to be absolutely inadequate in this case. The marked difference between the predictions of the two models can be ascribed to the fact that the bimolecular termination mechanism is responsible for gelation in the presence of chain transfer to polymer as the sole branching mechanism. This happens because one of the requirements for the formation of gel is the presence of a mechanism connecting the chains together, and this is provided by the combination reaction in the present case. An incorrect evaluation of the way in which combination joins together the polymer chains, which is reflected by incorrect instantaneous polydispersity values calculated by the approximate model, results in gel formation predicted to occur at much lower conversions. Considering that the \bar{n} vs. conversion profile coincides with that reported for linear chains in Fig. 4.6(b) (all possible influences of the presence of branching on the \bar{n} evolution have been neglected), it is interesting to note that the approximate model predicts gelation in a region where $\bar{n} = 0.5$, i.e., the main mode of termination is combination with very short radicals incoming from the water phase. In these conditions no gelation is obviously possible, since no coupling between branched chains can occur. With respect to this, it is to be excluded that the short incoming radicals transfer their activity to the dead polymer before the combination event, since $c \gg k_{fp}\sigma^{(1)}$ (i.e., the frequency of combination is much greater than that of chain transfer to polymer) up to over 70% conversion. The approximate model permits instead the combination of branched chains (although they belong to different particles) also in these highly compartmentalized conditions because it admits a certain amount of long-long chain coupling, as discussed in detail with regard to Figs 4.1 and 4.2. Therefore, the approximate model is shown to predict gelation in conditions where its occurrence is physically precluded.

Smaller differences between the results of the two models are found when termination by combination is no more an essential requirement for gel formation. This can be seen in Fig. 4.8, where the case of crosslinking as the only source of chain branching is considered ($k_p^*=3 \text{ cm}^3 \text{ mol}^{-1} \text{ s}^{-1}$, $k_{fp}=0$). In this case the mechanism of chain coupling is provided by crosslinking itself, which alone is able to lead to the formation of a gel phase. Accordingly, the wrong evaluation of the combination mechanism through the approximate model does

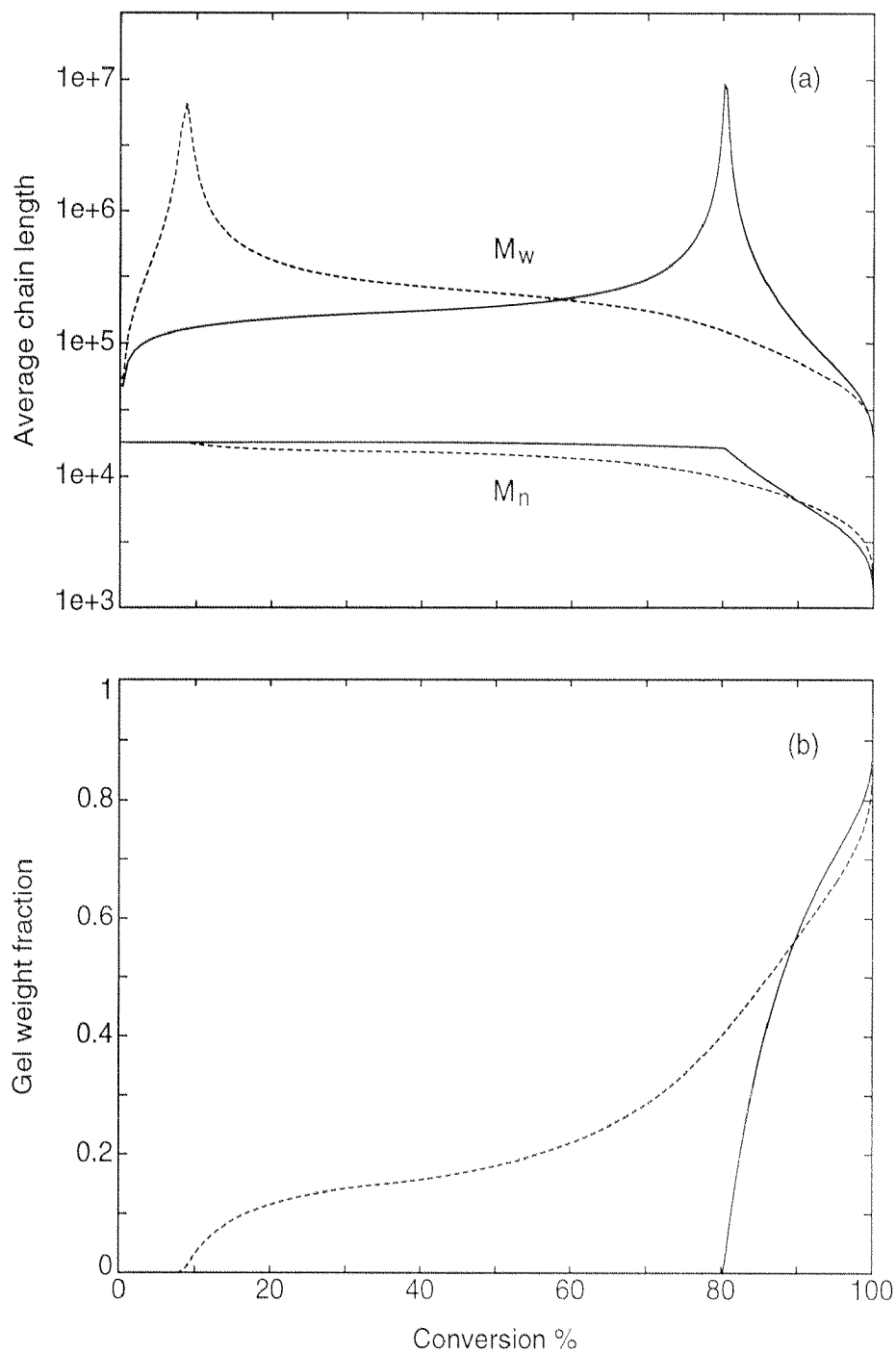


Figure 4.7: (a) Number- and weight-average chain length and (b) gel weight fraction as a function of conversion in the case of chain branching occurring through chain transfer to polymer. Parameter values as in Table 4.2, but with $k_p^* = 0$. — : correct model; --- : approximate model.

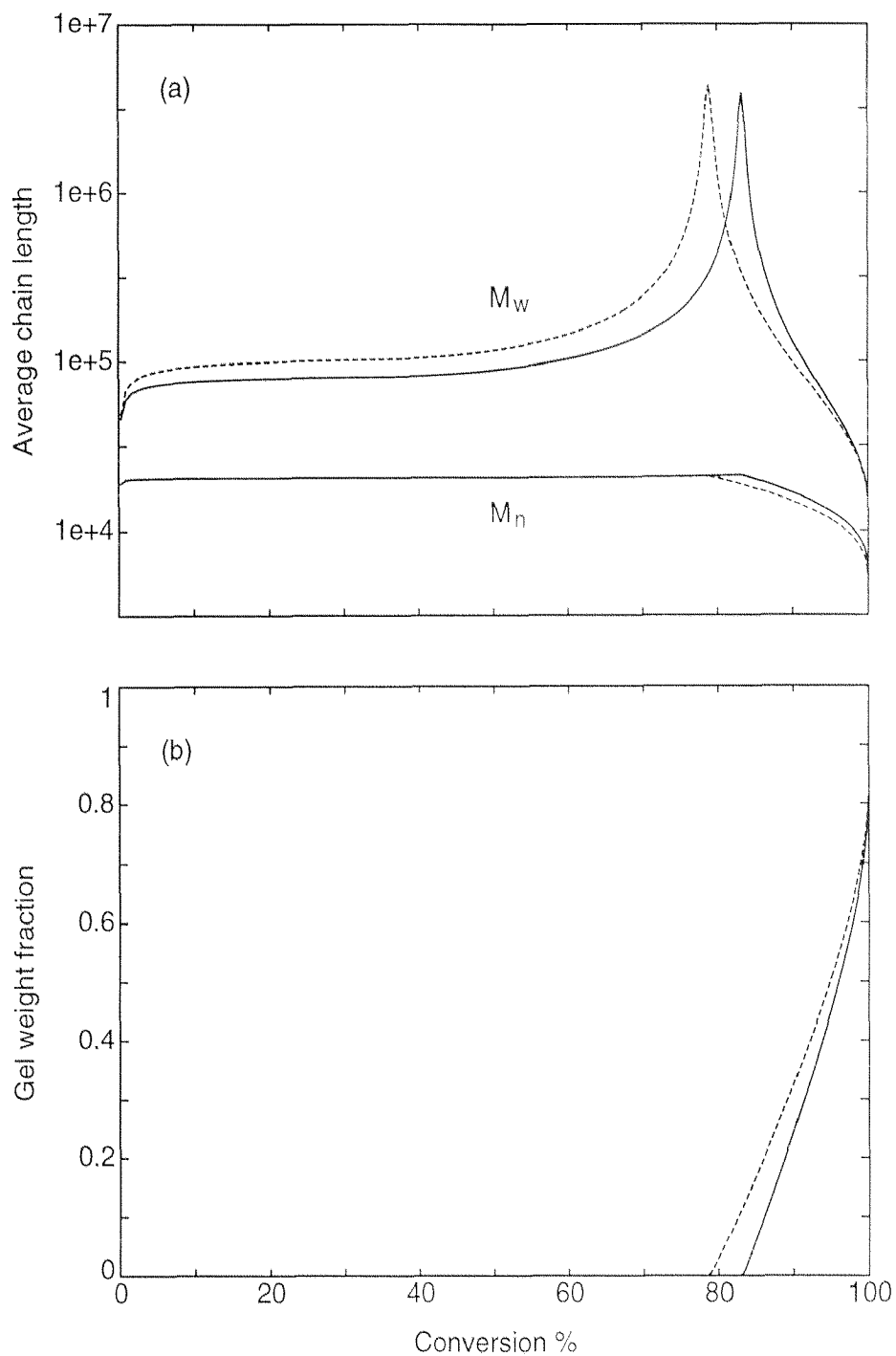


Figure 4.8: (a) Number- and weight-average chain length and (b) gel weight fraction as a function of conversion in the case of chain branching occurring through crosslinking. Parameter values as in Table 4.2, but with $k_{fp} = 0$. — : correct model; --- : approximate model.

not induce huge inaccuracies in the evaluation of the MWD properties and of the gel point.

Finally, note that both in the case of chain transfer to polymer and of crosslinking, the same number-average chain length M_n is predicted by the two models up to the gel point (as predicted by the approximate model). After this point, the curves move apart. This happens because it is the M_n of the sol phase which is being calculated, and this is influenced by the amount of polymer belonging to the gel phase, which is different for the two models.

4.4 Analysis of the Assumption of Independence of the Two Lengths of a Pair of Chains

As already mentioned in Section 4.2.2, in the calculation of the length of a dead chain from a combination reaction, the approach leading to the approximate model considers the length of the two live chains independent one of each other. In other words, given an active chain of current lifetime \bar{t} , the probability that another chain growing in the same particle has lifetime t_L is simply given by the number of chains of lifetime t_L divided by the overall number of chains (in particles of the same type):

$$\mathcal{P}_i^a(t_2 = t_L | t_1 = \bar{t}) = \mathcal{P}_i(t_2 = t_L) = \frac{N'_i(t_e - t_L, t_L)}{iN_i(t_e)} \quad (4.17)$$

where $\mathcal{P}_i^a(t_2 = t_L | t_1 = \bar{t})$ represents the conditional probability (according to the approximate model) of finding a chain of lifetime t_L in a particle of state i conditioned on the fact that a chain of lifetime \bar{t} is growing in the same particle, while $\mathcal{P}_i(t_2 = t_L)$ is the probability of finding a chain of lifetime t_L irrespective of the lifetime of the other chains. Note that here we are referring to linear chains only for simplicity.

The distribution $\mathcal{P}_i^a(t_2 = t_L | t_1 = \bar{t})$ is normalized to one, since integration of the singly distinguished particle distribution over all current lifetimes yields the overall number of active chains in particles of state i :

$$\int_0^\infty N'_i(t_e - t_L, t_L) dt_L = iN_i(t_e) \quad (4.18)$$

Note that the integration can be carried out to infinity, instead of t_e , since the times of decay of distribution N'_i , corresponding to the growth times of polymer chains in the system, are usually much smaller than experimental time t_e . This also admits the approximation $N'_i(t_e - t_L, t_L) \simeq N'_i(t_e, t_L)$ in the solution of integral (4.18) and in the calculation of probability (4.17).

The correctness of eq. (4.17), which contains the assumption of independence of the two chain lengths, can be checked by comparing probability $\mathcal{P}_i^a(t_2 = t_L | t_1 = \bar{t})$ to that

calculated by the correct model, which will be indicated by $\mathcal{P}_i^c(t_2 = t_L | t_1 = \bar{t})$.

This last conditional probability can be calculated through the following statistical relation:

$$\mathcal{P}_i^c(t_1 = \bar{t}, t_2 = t_L) = \mathcal{P}_i(t_1 = \bar{t}) \cdot \mathcal{P}_i^c(t_2 = t_L | t_1 = \bar{t}) \quad (4.19)$$

which states that the probability of extracting a pair of chains from state i particles, the first of which of lifetime \bar{t} and the second of lifetime t_L , is given by the probability of finding a chain of lifetime \bar{t} times the conditional probability of finding a second chain of length t_L .

The probability $\mathcal{P}_i^c(t_1 = \bar{t}, t_2 = t_L)$ can be calculated as the number of pairs of chains of the two given lengths divided by the total number of pairs of chains in state i particles, and again divided by two since the order of extraction of the two chains of each length must be the given one. Accordingly:

$$\mathcal{P}_i^c(t_1 = \bar{t}, t_2 = t_L) = \begin{cases} \frac{N_i''(t_e - \bar{t}, \bar{t} - t_L, t_L)}{i(i-1)N_i(t_e)} & \text{for } t_L < \bar{t} \\ \frac{N_i''(t_e - t_L, t_L - \bar{t}, \bar{t})}{i(i-1)N_i(t_e)} & \text{for } t_L > \bar{t} \end{cases} \quad (4.20)$$

where the former or the latter relation holds according to whether the chain of lifetime \bar{t} is the older or the younger of the pair, respectively.

The probability $\mathcal{P}_i(t_1 = \bar{t})$ is instead simply calculated as the number of chains of lifetime \bar{t} divided by the overall number of chains in particles of type i :

$$\mathcal{P}_i(t_1 = \bar{t}) = \frac{N_i'(t_e - \bar{t}, \bar{t})}{iN_i(t_e)} \quad (4.21)$$

Substituting eqs (4.20) and (4.21) in eq. (4.19) one obtains:

$$\mathcal{P}_i^c(t_2 = t_L | t_1 = \bar{t}) = \begin{cases} \frac{N_i''(t_e - \bar{t}, \bar{t} - t_L, t_L)}{(i-1)N_i'(t_e - \bar{t}, \bar{t})} & \text{for } t_L < \bar{t} \\ \frac{N_i''(t_e - t_L, t_L - \bar{t}, \bar{t})}{(i-1)N_i'(t_e - \bar{t}, \bar{t})} & \text{for } t_L > \bar{t} \end{cases} \quad (4.22)$$

The distribution $\mathcal{P}_i^c(t_2 = t_L | t_1 = \bar{t})$ is normalized to one, since integration over all possible lifetimes t_L of the pairs of chains, one of which of lifetime t_L and the other of lifetime \bar{t} , must result in the total number of chains which make pair with a chain of lifetime \bar{t} :

$$\int_0^{\bar{t}} N_i''(t_e - \bar{t}, \bar{t} - t_L, t_L) dt_L + \int_{\bar{t}}^{\infty} N_i''(t_e - t_L, t_L - \bar{t}, \bar{t}) dt_L = (i-1)N_i'(t_e - \bar{t}, \bar{t}) \quad (4.23)$$

As mentioned above, comparison of probability $\mathcal{P}_i^a(t_2 = t_L | t_1 = \bar{t})$ (which assumes independency of the active chain lengths) to probability $\mathcal{P}_i^c(t_2 = t_L | t_1 = \bar{t})$, gives a good idea about when the assumption of independency is satisfied.

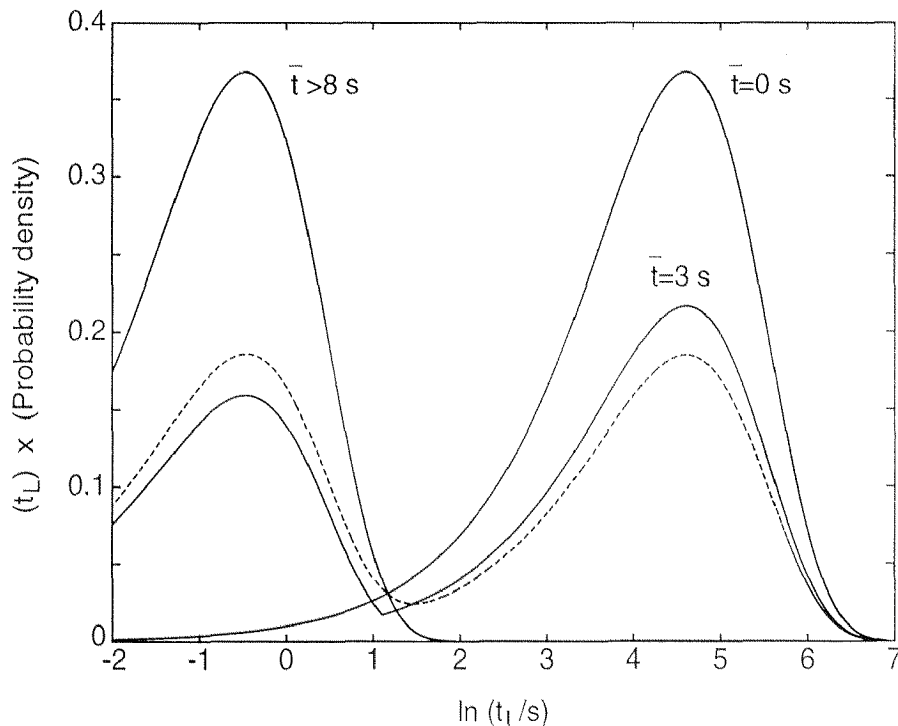


Figure 4.9: Probability of finding a radical of lifetime t_L in a state 2 particle, given another radical of lifetime \bar{t} in the same particle, multiplied by t_L . Bimolecular termination by combination frequency $c = 0.8 \text{ s}^{-1}$ and entry frequency $\rho = 0.01 \text{ s}^{-1}$ ($\bar{n} \rightarrow 0.5$). — : correct model; --- : approximate model.

As an example, let's go back to the case considered in Section 4.3.1 of linear chains in the presence of combination as the sole termination mechanism (cf. Fig. 4.1). The conditional probabilities \mathcal{P}_i^a and \mathcal{P}_i^c can be compared at values of \bar{n} approaching 0.5, where the difference between the approximate and the correct model is most significant in terms of instantaneous polydispersity, and at larger \bar{n} values, where this difference tends to reduce.

Fig. 4.9 shows the quantities $t_L \mathcal{P}_2^a$ and $t_L \mathcal{P}_2^c$ (i.e., in state 2 particles) as a function of t_L in the case of $\bar{n} \rightarrow 0.5$, obtained assuming the frequency of entry of radicals from the water phase $\rho = 0.01 \text{ s}^{-1}$. The other parameters correspond to those used in Fig. 4.1 (which give $c = 0.8 \text{ s}^{-1}$). A logarithmic representation on the t_L -axis has been chosen due to the very different time-scales of the various curves, while multiplication of the probability densities by t_L assures that the normalization of the areas beneath the curves to one is maintained. Note that this kind of representation makes the plots in Fig. 4.9 conceptually equivalent to weight CLDs. The probability \mathcal{P}_2^c depends upon the value of \bar{t} . Accordingly, various curves are reported at different \bar{t} values (solid curves). On the other hand, \mathcal{P}_2^a is independent of \bar{t} and a single curve results (dashed curve).

The probabilities \mathcal{P}_2^a and \mathcal{P}_2^c are calculated by solving analytically systems (2.5) and (2.8) with initial conditions (2.3) and (2.12), respectively. The analytical solution is obtained from the usual eigenvalue method, i.e., given the ordinary differential system

$$\frac{d\underline{\mathbf{y}}(t)}{dt} = \underline{\mathbf{B}} \underline{\mathbf{y}}(t) \quad (4.24)$$

(where $\underline{\mathbf{B}}$ is independent of t) with initial conditions

$$\underline{\mathbf{y}}(t=0) = \underline{\mathbf{y}}_0 \quad (4.25)$$

its analytical solution is given by:

$$\underline{\mathbf{y}}(t) = \sum_j \underline{\mathbf{r}}_j (\underline{\mathbf{l}}_j \cdot \underline{\mathbf{y}}_0) e^{\lambda_j t} \quad (4.26)$$

Here, $\underline{\mathbf{r}}_j$ and $\underline{\mathbf{l}}_j$ are the right and left eigenvectors of the matrix $\underline{\mathbf{B}}$ of system (4.24) corresponding to eigenvalue λ_j .

Going back to Fig. 4.9, the strong dependence of probability \mathcal{P}_2^c on \bar{t} is shown by the marked change of the solid curves at increasing \bar{t} values. An asymptotic curve is reached at high \bar{t} values ($\bar{t} > 8$ in the figure). The evolution of the curves shows that a short chain has a high probability of making pair with a long one, and vice versa. Chains of intermediate lengths (e.g. $\bar{t} = 3$) have instead a substantially equivalent probability of being in the presence of shorter (left-hand side peak) or longer chains (right-hand side peak). The dashed curve, obtained from the approximate model, would incorrectly suggest that chains of any length have the same probability of making pair either with short or with long chains. The two peaks of the dashed curve correspond to the two different contributions to the active chain distribution in state two particles, discussed with reference to Figs 4.1 and 4.2.

A similar analysis can be carried out for the probabilities \mathcal{P}_i^a and \mathcal{P}_i^c in state i particles with $i > 2$. Similar results are obtained, in the sense that \mathcal{P}_i^c is significantly dependent on the value of \bar{t} . This indicates a strong correlation between the lengths of two chains belonging to the same particle.

The same calculations have been repeated at increasing \bar{n} values. In Fig. 4.10, $t_L \mathcal{P}_2^a$ and $t_L \mathcal{P}_2^c$ are reported as a function of $\ln(t_L)$ for a value of $\rho = 5 \text{ s}^{-1}$, corresponding to $\bar{n} = 2$. It can be seen that the dependence of \mathcal{P}_2^c on \bar{t} is much weaker than in the previous case and therefore the assumption of chain length independence is verified with better approximation. The probability of matching with chains of a given length is very similar at all chain lengths, and not far from that calculated by the approximate model (dashed curve). Note that the dashed curve does not present a bimodality as in the previously

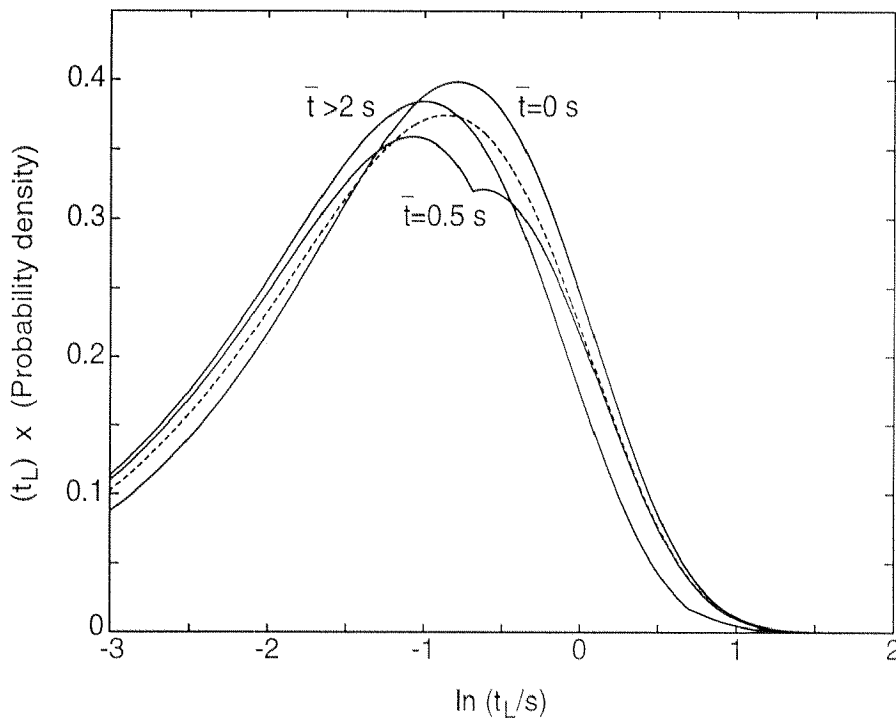


Figure 4.10: Probability of finding a radical of lifetime t_L in a state 2 particle, given another radical of lifetime \bar{t} in the same particle, multiplied by t_L . Bimolecular termination by combination frequency $c = 0.8 \text{ s}^{-1}$ and entry frequency $\rho = 5 \text{ s}^{-1}$ ($\bar{n} = 2$). — : correct model; --- : approximate model.

examined case. This shows that, at increasing values of the entry frequency ρ compared to the combination frequency c , the distribution of the active chains is represented by a single component (differently from the case $\rho \ll c$). All that has been discussed here above for state two particles is true also for particles containing $i > 2$ radicals and is reflected in smaller errors, in comparison to the case of lower \bar{n} values, when the approximate model is used for the calculation of the polydispersity ratio (cf. Fig. 4.1).

The case of a higher \bar{n} value ($\bar{n} = 4$, given by $\rho = 25 \text{ s}^{-1}$), has also been examined. This yields the results presented in Fig. 4.11, which are substantially equivalent to those shown in Fig. 4.10, but still interesting because convergence of the \mathcal{P}_2^c curves (solid curves) to the \mathcal{P}_2^a curve (dashed curve) is seen to be approached, i.e., \mathcal{P}_2^c tends to become independent of the value of \bar{t} and equal to \mathcal{P}_2^a at all t_L values. Again, this holds true also for $i > 2$. The assumption of independence of the chain lengths in a pair is thus verified better and better at increasing \bar{n} values.

What is most interesting is that this independence, being related to the relative value of the entry frequency compared to the bimolecular termination frequency, is achieved not only in particles containing a high number of radicals (which tend to be the most

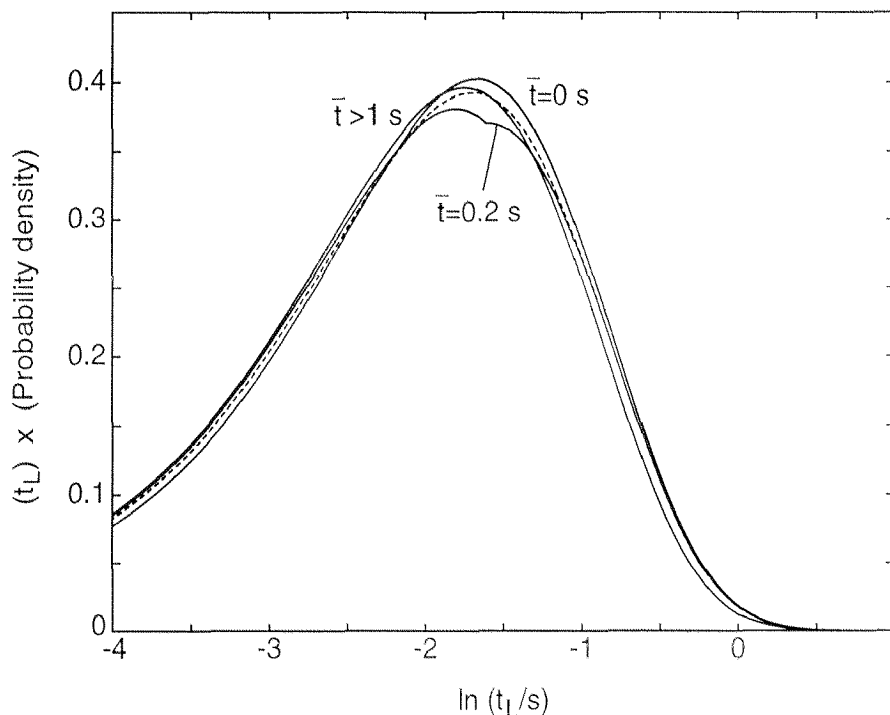


Figure 4.11: Probability of finding a radical of lifetime t_L in a state 2 particle, given another radical of lifetime \bar{t} in the same particle, multiplied by t_L . Bimolecular termination by combination frequency $c = 0.8 \text{ s}^{-1}$ and entry frequency $\rho = 25 \text{ s}^{-1}$ ($\bar{n} = 4$). — : correct model; --- : approximate model.

numerous at high \bar{n} values and thus those mainly contributing to the polymer produced in the whole system) but also in particles containing few radicals, $i = 2$ in the limit. Thus, in these conditions, the properties of the produced polymer are well calculated by use of the approximate model not only as a whole but also when focusing on the polymer produced in particles of a given state, even for low states.

4.5 Case Studies

Three polymerization systems, namely, styrene, methyl methacrylate and vinyl acetate, have been studied at 50°C . The instantaneous MWD averages have been analysed as a function of particle radius to establish the ranges, for certain reaction conditions (temperature, initiator concentration, etc.), where the use of the approximate model is unsatisfactory. Particle radii from 5 nm up to 100 nm have been considered, i.e., from micellar size to typical dimensions of final latexes. The equations and the parameters for the systems examined have been taken from Rawlings and Ray [59, 60], with the exception of the entry constant k_{mp} , which has been assumed $k_{mp} = 6 \cdot 10^{19} \text{ cm}^3/\text{mol}/\text{s}$ for all systems. The radical concentration in the water phase has been taken constant and equal to 10^{-10}

mol cm⁻³. In all cases the polymer particles have been considered monomer saturated (Smith-Ewart intervals I and II). The Trommsdorff effect has been accounted for through the empirical correlations reported by Friis and Hamielec [61].

4.5.1 Styrene

Bimolecular termination has been assumed to occur by combination [36]. The dependence of the average number of radicals per particle \bar{n} on particle radius r_P is shown in Fig. 4.12(a). Due to the low desorption frequencies, the system is bound for a wide range of radius values to $\bar{n} = 0.5$ (Smith-Ewart case 2, dotted line in the figure). In this range the approximate and correct model show the greatest differences in terms of instantaneous polydispersities (Fig. 4.12(b)). This could be predicted after inspection of Fig. 4.3, where the case of a system with moderate desorption and with chain transfer to monomer was examined. In the case of styrene, an error on polydispersity of 15% up to over 20% is made by the approximate model for particle radii ranging from 10 to 60 nm. At particle radii approaching 100 nm, this error tends to disappear, far before reaching ‘pseudo-bulk’ conditions. This is in accordance with the discussion in Sections 4.3 and 4.4.

4.5.2 Methyl Methacrylate

Bimolecular termination has been assumed to occur two thirds by disproportionation and one third by combination [36]. Due to higher desorption rates and a stronger Trommsdorff effect in this case, no 0.5 value plateau is observed for the average number of radicals per particle (Fig. 4.13(a)). Since the amount of combination occurring in this system is limited, the error made by the approximate model in the polydispersity calculation never exceeds 7% for all particle radii (Fig. 4.13(b)). Discrepancies of this magnitude would be hardly detectable by any analytical technique. The polydispersity behavior, exhibiting a maximum, is that typical of systems in which bimolecular termination by disproportionation is important.

4.5.3 Vinyl Acetate

The nature of the bimolecular termination mechanism for this system is still an open question [36]. The gelation technique [62] suggests that combination is the predominant termination mechanism at 25°C. A greater amount of disproportionation may be expected at higher temperatures, for instance at the monomer boiling point where the polymerization is often performed to use the reflux condenser to remove the heat from the reaction system. Here, bimolecular termination has been assumed to occur by combination. In this

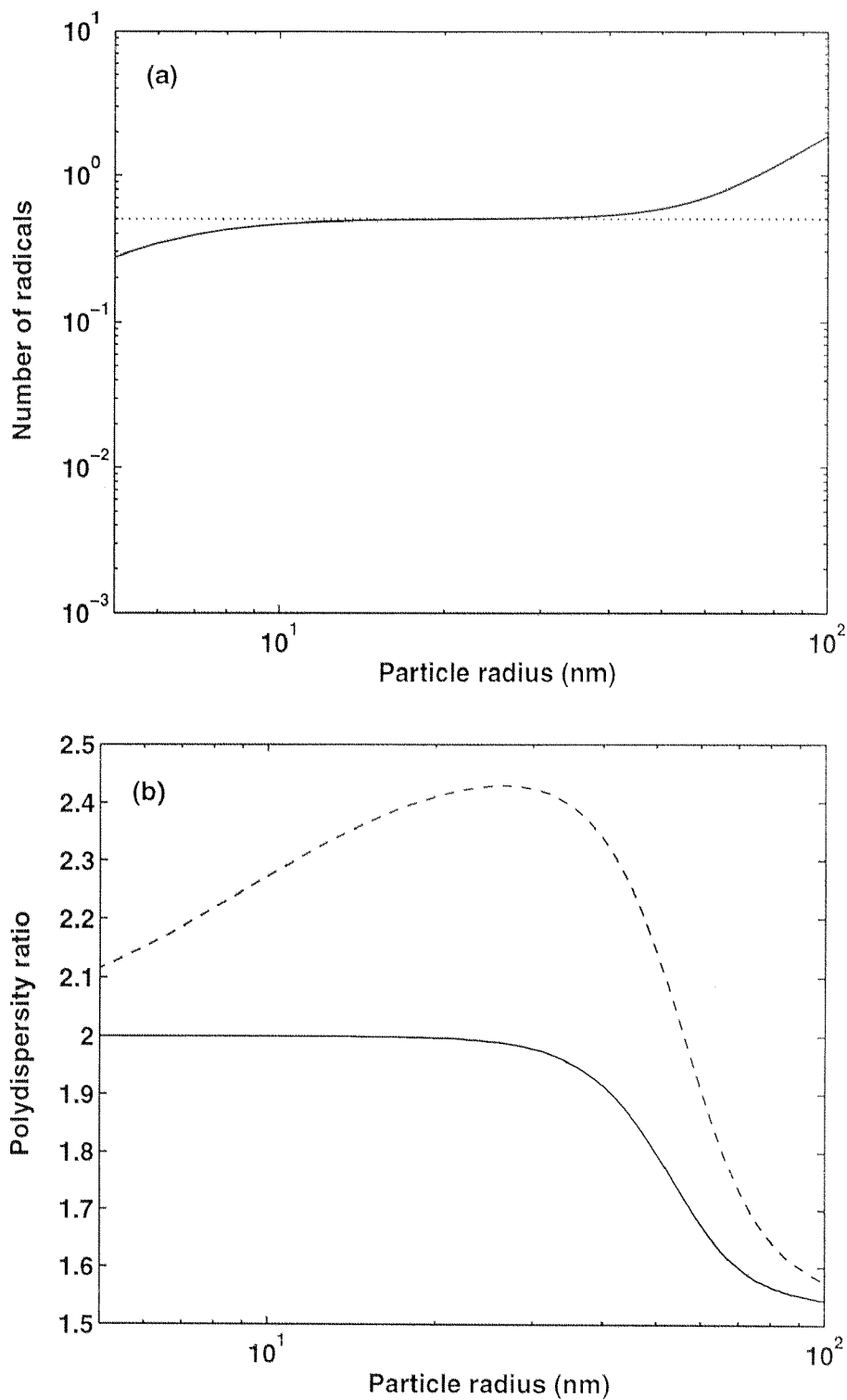


Figure 4.12: (a) Average number of radicals per particle (\cdots : Smith-Ewart case 2, $\bar{n} = 0.5$) and (b) polydispersity ratio as a function of particle radius for styrene polymerization. — : correct model; --- : approximate model.

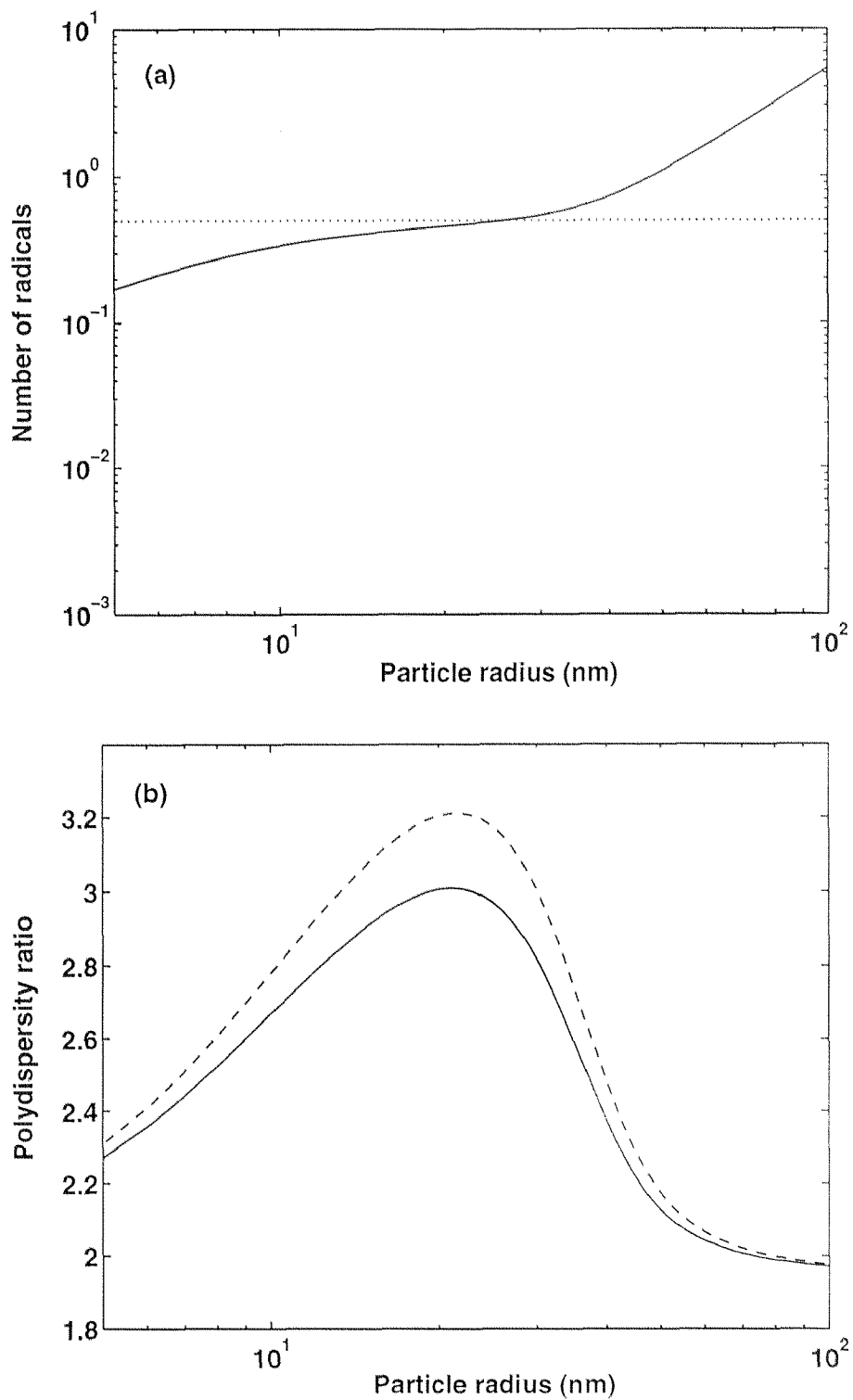


Figure 4.13: (a) Average number of radicals per particle (\cdots : Smith-Ewart case 2, $\bar{n} = 0.5$) and (b) polydispersity ratio as a function of particle radius for methyl methacrylate polymerization. — : correct model; --- : approximate model.

way, the worst possible conditions are chosen in terms of agreement of the approximate model with the correct one. A value of $c_p = k_{fp}/k_p = 3.96 \cdot 10^{-4}$ [63] has been chosen for the chain transfer to polymer reaction. The dead polymer on which this mechanism acts has been assumed to have a number-average chain length $M_n = 10^4$ and a polydispersity $P_d = 4$.

In Fig. 4.14(a), the average number of radicals per particle is reported. Very high desorption frequencies for this system keep the average number of radicals per particle far below 0.5 for low radius values. Thus, only at intermediate r_P values (e.g. 30 nm) the two models start to move significantly apart in terms of polydispersity (Fig. 4.14(b)). At larger particle radii, even though chain transfer to monomer rates are very high, the discrepancy on the calculated polydispersity reaches values of 20%. Moreover, this discrepancy is a function of the polydispersity P_d of the dead polymer upon which the branching mechanism is operative. At increasing P_d values, the two models move more and more apart. Accordingly, limited differences in instantaneous polydispersities initially calculated by the two models may result crucial in cumulative terms. In Section 4.3.2 it has been shown that accounting incorrectly for combination in a system where branching occurs through chain transfer to polymer may lead to very large errors in the weight-average molecular weight calculation. If one assumes combination as the dominant bimolecular termination, this is the case for vinyl acetate.

4.6 Singly Distinguished Particle Approach Adapted to the Features of Radical Compartmentalization

4.6.1 Concepts

As shown in the previous sections, the detailed description of the lengths of the pairs of chains belonging to the same particle is required to evaluate correctly the molecular weight distribution of a polymer produced in typical emulsion reaction conditions when bimolecular termination by combination is active in the system. This is a peculiar feature of compartmentalization which arises (in the absence of other mechanisms) when the entry frequency ρ is much smaller than the bimolecular termination frequency c , so that two types of active chains appear in the system: the first have a characteristic lifetime τ_ρ related to the entry rate ($\tau_\rho = 1/\rho$) and the second a characteristic lifetime τ_c related to the bimolecular termination rate ($\tau_c = 1/2c$). In this case it never happens that two radicals belonging to the same distribution combine, because combination occurs practically exclusively in particles with two radicals, one of which is always of 'type ρ ' and

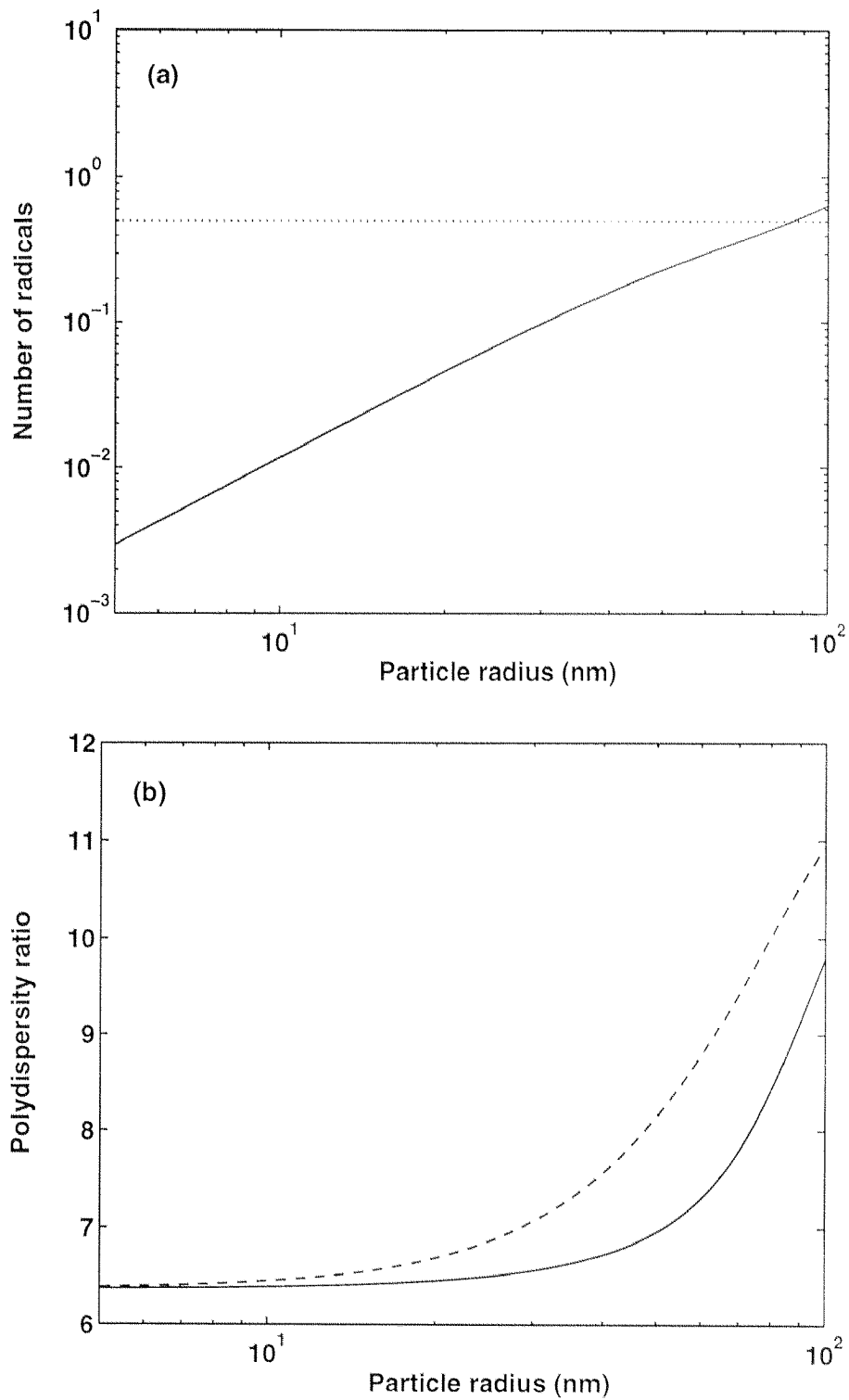


Figure 4.14: (a) Average number of radicals per particle (\cdots : Smith-Ewart case 2, $\bar{n} = 0.5$) and (b) polydispersity ratio as a function of particle radius for vinyl acetate polymerization. — : correct model; --- : approximate model.

the other of 'type c'.

In the presence of other termination mechanisms the situation here referred to may differ. For instance, if a chain transfer reaction is present (e.g. to monomer or chain transfer agent), the frequency of which is much greater than the bimolecular termination frequency, a single distribution of active chains is present and compartmentalization plays no role. It is evident that when the chains die monomolecularly, the fact that they grow segregated one from the other has no influence at all.

However, in an intermediate situation, i.e., when the frequency of transfer lies between those of entry and of bimolecular termination, two kinds of active chains can still be detected within particles containing more than one radical: the first kind, the lifetime of which is determined by the transfer reaction, is given by chains which have been growing alone in a particle until another radical has entered the particle; the second kind is given by the new entered radicals, and their lifetime is determined by the frequency of bimolecular termination.

To account for these different kinds of chain and for the fact that not any combination between them is allowed, it is necessary, as already often noted, to describe the length distribution of the pairs of active chains belonging to the same particle. In the distinguished particle approach this is given by the doubly distinguished particle distribution. This distribution corresponds to the distribution of the particles containing a given number of chains, two of which of specified length. The number of active chains in a particle is usually quite low, but chain lengths can reach values up to several tens of thousands. Accordingly, the use of a detailed technique for the solution of the equations governing the behavior of the distribution of the pairs of chains would require covering a bidimensional domain in terms of chain lengths, which would result very heavy from the point of view of computational times. On the other hand, it is of interest to reduce the problem to a form which can be treated by use of commercial calculation codes for polyreaction distributions, e.g. the code PREDICI[®]. Accordingly, it is of interest to look for a formulation of the problem of the description of the compartmentalized pairs of chains in terms of a certain number of distributions with a single chain length as internal coordinate, rather than in terms of a single two-dimensional chain length distribution.

To develop such a model (the case of linear chains is treated to provide a starting point), a suggestion comes from the existence of two different active CLDs within the particles in certain reaction conditions, which was identified as a distinguishing feature of compartmentalization. What we are referring to is of course the existence of chains the length of which is determined by entry rather than by termination in the case where the

former of these mechanisms is much slower than the latter. The model which develops, however, should be flexible enough to consider the two different CLDs to become a single one when the reaction conditions are such that compartmentalization does not play a role (e.g. in the presence of high chain transfer to monomer or when entry dominates over bimolecular termination).

Starting from the ideas above, and considering the case in which the compartmentalization effects are most evident ($\rho \ll c$ and no chain transfer reactions), it is possible to distinguish between chains which are growing or have been growing alone in a particle (which we will call ' ρ -chains' due to the fact that their length is related to the frequency of entry) and all other chains (which we will call ' c -chains' since their length is related to the frequency of bimolecular termination).

Once this distinction has been made, to properly consider the combination events between active chains it must be imposed that two ρ -chains never combine, since it never happens that two ρ -chains coexist in the same particle, while combination is admitted between the ρ -chain and other c -chains which make pair with it. Combinations among the c -chains belonging to a same particle (there can in fact be more than one c -chain in a particle) are of course allowed.

To develop proper equations for the calculation of the ρ - and c -chain distributions, the events creating a ρ - and c -chain, respectively, of a given length, must be considered.

With respect to the desorption (exit) reaction, the classical assumption is here made that the only radical species able to desorb are the short (monomeric) radicals created by chain transfer to monomer or chain transfer agent (CTA). Accordingly, the succession of the two mechanisms chain transfer followed by exit of the produced radical will be referred to as a transfer-desorption event.

The entry reaction is instead considered to involve radicals so short that they can be considered to have length zero.

4.6.2 Equation Development

In the distinguished particle approach, we can define the ρ -chain distribution by introducing distribution $N_i^{(\rho)}(t, t')$. Quantity $N_i^{(\rho)}(t, t')dt'$ represents the fraction of particles in state i (i.e., containing i chains), one of which (distinguishing chain) is of type ρ , was born at time t and is still growing at a time between $t + t'$ and $t + t' + dt'$. A similar distribution can be defined for the c -chains: distribution $N_i^{(c)}(t, t')$ is equivalent to distribution $N_i^{(\rho)}(t, t')$, except that the distinguishing chain is a c -chain.

We now consider the events creating a ρ -chain of a given lifetime.

Since when a chain remains alone in a particle it becomes by definition a ρ -chain, the case of state 1 particles represents a special case and must be considered separately.

A $N_1^{(\rho)}(t, t')$ particle

- appears:

- 1) with $t' = 0$ (initial condition):

- a) entry in an empty particle;

- b) transfer to monomer or CTA (not resulting in desorption) in a state one particle;

- 2) with $t' > 0$:

- a) transfer-desorption of the non-distinguishing chain from a $N_2^{(\rho)}(t, t')$ particle;

- b) transfer-desorption of the non-distinguishing chain from a $N_2^{(c)}(t, t')$ particle;

- c) bimolecular termination of the two non-distinguishing chains in a $N_3^{(\rho)}(t, t')$ particle;

- d) bimolecular termination of the two non-distinguishing chains in a $N_3^{(c)}(t, t')$ particle;

- disappears:

- 3)
 - a) entry in the distinguished particle under consideration;

- b) transfer to monomer or CTA of the distinguished chain.

Note that terms 1a) and 1b) appear only for $i = 1$, since entry in a particle which is not empty or chain transfer in a particle containing more than one radical yields a new chain which is of type c , not of type ρ .

Moreover, terms 2b) and 2d) appear because when a c -chain remains alone in a particle it becomes by definition of type ρ . This terms relates the $N_1^{(\rho)}(t, t')$ distribution to the $N_i^{(c)}(t, t')$ distribution and does not appear for $i > 1$.

According to the scheme described here above, the balance for the $N_1^{(\rho)}(t, t')$ distribution can be written as:

$$\begin{aligned} \frac{\partial N_1^{(\rho)}(t, t')}{\partial t'} = & -[\rho + f + k_d]N_1^{(\rho)}(t, t') + k_d N_2^{(\rho)}(t, t') + k_d N_2^{(c)}(t, t') \\ & + 2cN_3^{(\rho)}(t, t') + 2cN_3^{(c)}(t, t') \end{aligned} \quad (4.27)$$

with initial condition:

$$N_1^{(\rho)}(t, t' = 0) = \rho N_0(t) + f N_1(t)$$

Here above, $N_i(t)$ is the fraction of particles containing i radicals (given by the Smith-Ewart equations), and parameter f is defined as:

$$f = k_{fm}C_m + k_{ft}C_t - k_d$$

and takes account of all transfer to small molecule events, save those which result in chain desorption.

To write the balance for $N_i^{(\rho)}(t, t')$ with $i > 1$, the events causing the appearance and the disappearance of a ρ -chain of a given lifetime in a particle containing $i > 1$ radicals must be considered.

A $N_i^{(\rho)}(t, t')$ particle ($i > 1$)

- appears:

- 1) with $t' = 0$ (initial condition):

- a) never;

- 2) with $t' > 0$:

- a) entry in a $N_{i-1}^{(\rho)}(t, t')$ particle;

- b) transfer-desorption of a non-distinguishing chain from a $N_{i+1}^{(\rho)}(t, t')$ particle;

- c) bimolecular termination of two non-distinguishing chains in a $N_{i+2}^{(\rho)}(t, t')$ particle;

- disappears:

- 3)
 - a) entry in the distinguished particle under consideration;

- b) transfer to monomer or CTA of the distinguished chain;

- c) transfer-desorption of a non-distinguishing chain from the particle under consideration;

- d) bimolecular termination between any two chains in the particle under consideration.

Considering the scheme above, the following equation and initial conditions are derived for distribution $N_i^{(\rho)}(t, t')$ ($i > 1$):

$$\begin{aligned} \frac{\partial N_i^{(\rho)}(t, t')}{\partial t'} &= \rho N_{i-1}^{(\rho)}(t, t') - [\rho + f + ik_d + i(i-1)c]N_i^{(\rho)}(t, t') \\ &\quad + ik_d N_{i+1}^{(\rho)}(t, t') + i(i+1)cN_{i+2}^{(\rho)}(t, t') \end{aligned} \quad (4.28)$$

$$N_i^{(\rho)}(t, t' = 0) = 0$$

Passing to the balance for the c -chains, a $N_i^{(c)}(t, t')$ particle (with $i > 1$, $N_1^{(c)}(t, t') = 0$ by definition)

- appears:

1) with $t' = 0$ (initial condition):

- a) entry in a particle containing $i - 1$ radicals;
- b) transfer to monomer or CTA (not resulting in desorption) in a particle in state i ;

2) with $t' > 0$:

- a) entry in a $N_{i-1}^{(c)}(t, t')$ particle;
- b) transfer-desorption of a non-distinguishing chain from a $N_{i+1}^{(c)}(t, t')$ particle;
- c) bimolecular termination of two non-distinguishing chains in a $N_{i+2}^{(c)}(t, t')$ particle;

- disappears:

- a) entry in the distinguished particle under consideration;
- b) transfer to monomer or CTA of the distinguished chain;
- c) transfer-desorption of a non-distinguishing chain from the particle under consideration;
- d) bimolecular termination between any two chains in the particle under consideration.

The equation and initial conditions for distribution $N_i^{(\rho)}(t, t')$ corresponding to the scheme above are ($i > 1$):

$$\begin{aligned} \frac{\partial N_i^{(c)}(t, t')}{\partial t'} &= \rho N_{i-1}^{(c)}(t, t') - [\rho + f + ik_d + i(i-1)c]N_i^{(c)}(t, t') \\ &\quad + ik_d N_{i+1}^{(c)}(t, t') + i(i+1)cN_{i+2}^{(c)}(t, t') \end{aligned} \quad (4.29)$$

$$N_i^{(\rho)}(t, t' = 0) = \rho N_{i-1}(t) + f N_i(t)$$

The system constituted by eqs (4.27),(4.28) and (4.29) can be truncated as usual at a sufficiently high particle state value ($i = N$) by imposing that entry in a state N particle results in immediate termination between the new entered radical and a pre-existing radical, which gives a state $N - 1$ particle.

Note that summation of the equations and initial conditions for the ρ - and the c -chains yields the classical singly distinguished particle equations. It must of course be so, since $N_i^{(\rho)}(t, t') + N_i^{(c)}(t, t') = N_i'(t, t')$.

Moreover, it is worth noting that the portion of the system given by eqs (4.29) with $i = 2, N$ can be solved independently of the portion constituted by eqs (4.27)-(4.28). Therefore, the system can be split up in two subsystems, one homogeneous [eqs (4.29)] and the other [eqs (4.27)-(4.28)] with a non-homogeneous part given by the solution of the previous system (4.29) [terms relating the ρ -chain to the c -chain distribution in eq. (4.27)]. Thus, the two subsystems can be solved in sequence.

For simplicity we will rewrite them in matrix form:

$$\frac{\partial \underline{\mathbf{N}}^{(\rho)}(t, t')}{\partial t'} = \underline{\mathbf{R}}(t)\underline{\mathbf{N}}^{(\rho)}(t, t') + \underline{\mathbf{c}}(t, t') \quad (4.30)$$

and

$$\frac{\partial \underline{\mathbf{N}}^{(c)}(t, t')}{\partial t'} = \underline{\mathbf{C}}(t)\underline{\mathbf{N}}^{(c)}(t, t') \quad (4.31)$$

where $\underline{\mathbf{R}}(t)$ and $\underline{\mathbf{C}}(t)$ are the matrices of the coefficients of the homogeneous parts of systems (4.27)-(4.28) for the ρ -chains and (4.29) for the c -chains, respectively, while $\underline{\mathbf{c}}(t, t')$ represents the non-homogeneous part of system (4.27)-(4.28). Matrix $\underline{\mathbf{R}}$ has dimensions $N \times N$ while matrix $\underline{\mathbf{C}}$ has dimensions $(N - 1) \times (N - 1)$.

In order to calculate the CLD of the terminated chains, one must distinguish between the chains which died 'monomolecularly' (or better by any mechanism which preserves the length of the chain upon termination) and by combination.

The contribution of the chains which died monomolecularly can be calculated through the classical distinguished particle approach, without making difference between the ρ -

and the c -chains. As noted above, distribution $N_i'(t, t')$ can be calculated by summing up $N_i^{(\rho)}(t, t')$ and $N_i^{(c)}(t, t')$, without solving a further system.

However, here it is the contribution of combination which is of interest. Therefore, the possible combinations between active chains must be properly taken into account. In a particle containing one ρ -type active chain (note that it can never be more than one), combination can occur either between this chain and a c -chain or between two c -chains (when $i > 2$). Instead, in a particle containing no ρ -type active chains, combination can occur exclusively between two c -chains. The contributions of these two different situations must be considered and then summed up according to how many particles contain a ρ -chain and how many do not. Therefore, we must subdivide the N_i particles calculated through the Smith-Ewart equations into $N_i^{(\rho)}$ and $N_i^{(c)}$. The former, $N_i^{(\rho)}$, represents the fraction of particles containing i radicals, one of which of type ρ . The latter, $N_i^{(c)}$, is instead the fraction of particles containing i radicals none of which of type ρ .

In the first kind of particles, combination occurs between a ρ -chain and a c -chain with frequency $2c_c(i-1)$ (in a state i particle) while it occurs between two c -chains with frequency $c_c(i-1)(i-2)$, where c_c is the contribution of combination to c . In the $N_i^{(c)}$ particles, combination occurs between two c -chains with frequency $c_c i(i-1)$.

Given a certain particle state i , the probability that at a given reaction time t_e the ρ -chain involved in the combination event is of a given lifetime \bar{t}' , is calculated as the ratio between the ρ -chains of a given length in the particle state considered and all the ρ -chains in the same kind of particle:

$$\mathcal{P}_i^{(\rho)}(t' = \bar{t}') = \frac{N_i^{(\rho)}(t_e - \bar{t}', \bar{t}')}{\int_0^\infty N_i^{(\rho)}(t_e - t', t') dt'}$$

Similarly for the c -chains:

$$\mathcal{P}_i^{(c)}(t' = \bar{t}') = \frac{N_i^{(c)}(t_e - \bar{t}', \bar{t}')}{\int_0^\infty N_i^{(c)}(t_e - t', t') dt'}$$

Combining the frequencies of combination between the different kinds of pairs of chains in different kinds of particles, the probabilities that the particles considered are of a given kind and the probabilities that the two chains involved are of two given lengths (consideration of the ρ - and c -chain distributions permits to consider the latter probabilities independent), one can finally write the equation for the polymer terminated by combination:

$$\frac{d[v_P \bar{S}^C(t_e, t', t'')]}{dt_e} = \sum_{i=2}^N \left[2c_c(i-1) \mathcal{P}_i^{(\rho)}(t') \mathcal{P}_i^{(c)}(t'') N_i^{(\rho)} \right]$$

$$\begin{aligned}
& +c_c(i-1)(i-2)\mathcal{P}_i^{(c)}(t')\mathcal{P}_i^{(c)}(t'')N_i^{(\rho)} \\
& +c_c i(i-1)\mathcal{P}_i^{(c)}(t')\mathcal{P}_i^{(c)}(t'')N_i^{(c)}] \frac{1}{N_A}
\end{aligned} \tag{4.32}$$

where distribution $\bar{S}^C(t_e, t', t'')$ is the distribution at time t_e of the terminated polymer formed at any reaction time from the combination of two active chains of lifetimes t' and t'' (length of the resulting terminated chain $n = \alpha(t' + t'')$).

Besides the knowledge of the ρ - and c -chain distributions, eq. (4.32) requires the calculation of the fractions of particles $N_i^{(\rho)}$ and $N_i^{(c)}$ containing and not containing, respectively, a chain of type ρ . These quantities are straightforward to calculate, since every $N_i^{(\rho)}$ particle contains one ρ -type chain. Accordingly:

$$N_i^{(\rho)} = \int_0^\infty N_i^{(\rho)}(t_e - t', t') dt' \tag{4.33}$$

$N_i^{(c)}$ can be calculated by difference as $N_i - N_i^{(\rho)}$.

4.6.3 Equation Solution in Terms of Moments

The equations for the ρ - and c -chain distributions and for the terminated polymer distribution can be solved in terms of moments to evaluate the averages of these distributions.

The following moments are defined:

$$\lambda_{i,k}^{(\rho)} = \int_0^\infty (\alpha t')^k N_i^{(\rho)}(t_e - t', t') dt' \tag{4.34}$$

$$\lambda_{i,k}^{(c)} = \int_0^\infty (\alpha t')^k N_i^{(c)}(t_e - t', t') dt' \tag{4.35}$$

$$\mu_k^C = \int_0^\infty \int_0^\infty [\alpha(t' + t'')]^k \bar{S}^C(t_e, t', t'') dt' dt'' \tag{4.36}$$

Parameter $\alpha = k_p C_m$ is the frequency of propagation, so that by multiplying by the lifetime, one obtains the chain length.

Applying the moment operator to systems (4.30) and (4.31), one obtains, after integration by parts of the left-hand side, the following linear systems for the moments of the ρ - and c -chain distributions:

ρ -chains

- $k = 0$

$$\underline{\underline{\mathbf{R}}} \lambda_0^{(\rho)} = -\underline{\underline{\mathbf{N}}}^{(\rho)}(t_e, t' = 0) - \int_0^\infty \underline{\underline{\mathbf{c}}}(t_e, t') dt' \tag{4.37}$$

- $k \geq 1$

$$\underline{\underline{\mathbf{R}}} \lambda_k^{(\rho)} = -\alpha k \lambda_{k-1}^{(\rho)} - \int_0^\infty (\alpha t')^k \underline{\underline{\mathbf{c}}}(t_e, t') dt' \tag{4.38}$$

with

$$N_i^{(\rho)}(t_e, t' = 0) = \begin{cases} \rho N_0(t_e) + f N_1(t_e) & \text{for } i = 1 \\ 0 & \text{for } i \geq 2 \end{cases} \quad (4.39)$$

and

$$\int_0^\infty (\alpha t')^k c_i(t_e, t') dt' = \begin{cases} k_d \lambda_{2,k}^{(c)} + 2c \lambda_{3,k}^{(c)} & \text{for } i = 1 \\ 0 & \text{for } i \geq 2 \end{cases} \quad (4.40)$$

c-chains

- $k = 0$

$$\underline{\underline{C}} \lambda_0^{(c)} = -\underline{\underline{N}}^{(c)}(t_e, t' = 0) \quad (4.41)$$

- $k \geq 1$

$$\underline{\underline{C}} \lambda_k^{(c)} = -\alpha k \lambda_{k-1}^{(c)} \quad (4.42)$$

with

$$N_i^{(c)}(t_e, t' = 0) = \rho N_{i-1}(t_e) + f N_i(t_e) \quad (i \geq 2) \quad (4.43)$$

Passing to the terminated polymer distribution, application of the moment operator to equation (4.32) yields, after algebraic manipulation (and remembering that $N_i^{(\rho)} = \lambda_{i,0}^{(\rho)}$ and that $N_i^{(c)} = N_i - N_i^{(\rho)}$), the following differential equation:

$$\begin{aligned} \frac{d[v_P \mu_k^C]}{dt_e} &= c_c \sum_{i=2}^N \left[\frac{2(i-1)}{\lambda_{i,0}^{(c)}} \sum_{j=0}^k \binom{k}{j} \lambda_{i,k-j}^{(\rho)} \lambda_{i,j}^{(c)} \right. \\ &\quad + \frac{(i-1)(i-2) \lambda_{i,0}^{(\rho)}}{[\lambda_{i,0}^{(c)}]^2} \sum_{j=0}^k \binom{k}{j} \lambda_{i,k-j}^{(c)} \lambda_{i,j}^{(c)} \\ &\quad \left. + \frac{i(i-1)(N_i - \lambda_{i,0}^{(\rho)})}{[\lambda_{i,0}^{(c)}]^2} \sum_{j=0}^k \binom{k}{j} \lambda_{i,k-j}^{(c)} \lambda_{i,j}^{(c)} \right] \frac{1}{N_A} \end{aligned} \quad (4.44)$$

4.6.4 Results

In order to check the results of the ‘singly distinguished particle’ (SDP) model here developed, the instantaneous averages (polydispersity and number-average chain length) are calculated and compared to those predicted by the correct model (doubly distinguished particle model). Moreover, the values predicted by the approximate model considered in the first part of this chapter are reported, in order to show the improvements given by the present model.

The analysis is first made in the case of a real system (styrene) and the average chain length values are calculated as a function of particle radius. The parameters and equations used for the calculation of entry, exit and combination are the same used for styrene in Section 4.5, i.e., they are taken from refs [59] and [60]. As in Section 4.5, the radical concentration in the aqueous phase is considered constant (equal to 10^{-10} mol cm $^{-3}$) and the particles are considered at saturation. The radius is varied from 5 nm to 200 nm (i.e., from the dimensions of a micelle to those of a large latex particle).

The evolution of the average number of free-radicals per particle \bar{n} with particle radius r_P is of course independent of the molecular weight model selected (\bar{n} is calculated from the Smith-Ewart equations) and is the same as that shown in Fig. 4.12(a).

In Fig. 4.15(a) the number-average chain length calculated as a function of particle radius by the three models (correct, approximate and SDP model) is reported. The three models give the same answer and a single curve results.

In Fig. 4.15(b) the polydispersity is represented as a function of particle radius. The solid line is predicted by the correct model and is thus the reference solution. The dashed line is given by the SDP model while the dotted line is the result of the approximate model. The SDP model is seen to represent a significant improvement with respect to the approximate model. Especially, the correct limiting polydispersity values (1.5 and 2) are calculated at high and low radius values and the discrepancy from the correct model is small and limited to a narrow interval of radius values.

The same conclusions can be drawn by observation of Fig. 4.16, where the polydispersity is reported as a function of the average number of free-radicals per particle. It is interesting to observe that, at high values of the average number of radicals per particle, the dashed curve (SDP model) moves to the limiting value of 1.5 with a behavior which superimposes to that of the approximate model. This is because in these conditions the contribution of the ρ -chains vanishes and the model reduces to a singly distinguished particle model involving a single active chain distribution, just as in the approximate model. The polydispersity is seen to be slightly underestimated by the SDP model around $\bar{n} = 1$.

The same calculations are repeated for an imaginary system by imposing $k_{fm} = 0$ (which also implies $k_d = 0$). This is done to show the behavior of the model in the simplest case possible, when no monomolecular reaction superimposes to the reactions which are determining the effects of compartmentalization (entry and bimolecular termination). Here in fact, at $\bar{n} \rightarrow 0.5$ (limiting \bar{n} value) the system is in the situation where it contains truly ρ -chains (the length of which is determined purely by entry) and c -chains (length determined by bimolecular termination).

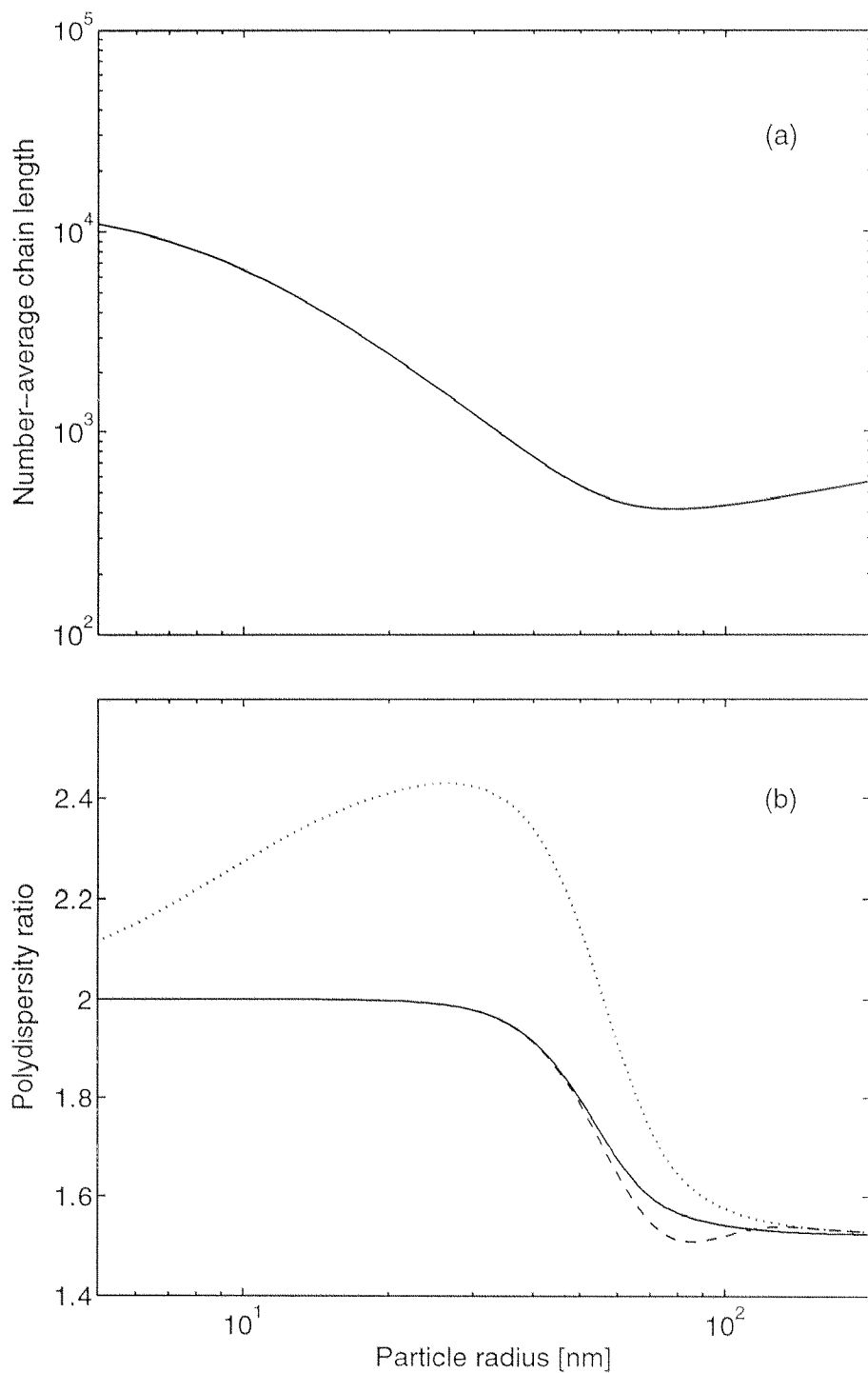


Figure 4.15: (a) Number-average chain length and (b) polydispersity ratio as a function of particle radius for styrene polymerization. — : correct model; --- : SDP model; \cdots : approximate model.

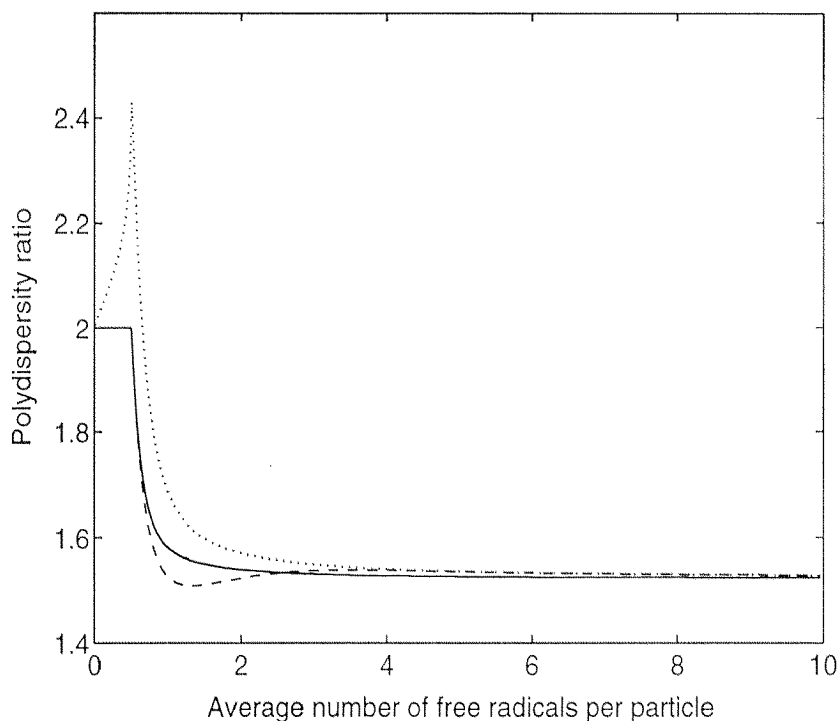


Figure 4.16: Polydispersity ratio as a function of the average number of radicals per particle for styrene polymerization. — : correct model; --- : SDP model; ... : approximate model.

The results are reported in Figs 4.17 and 4.18 in analogy to Figs 4.15 and 4.16. The same comments apply. It is worth noting that the SDP model provides the correct polydispersity value of 2 at $\bar{n} \rightarrow 0.5$ (small r_P values) in opposition to the value 2.5 given by the approximate model.

The results shown in Figs 4.15-4.18 show that the model for linear chains developed in this section (SDP model), based on the subdivision of the active chains into two subpopulations, the ρ -chains and the c -chains, is able to account properly for the features of radical compartmentalization. Therefore, it constitutes a valid basis for the application of detailed techniques for solving the MWD calculation problem in emulsion polymerization, which might be useful, for instance, when chain-length dependent rate coefficients must be included. The SDP model only slightly underestimates the polydispersity at \bar{n} values around 1 and it predicts the correct polydispersity values at the two limits of high \bar{n} and $\bar{n} \rightarrow 0$ ($\rightarrow 0.5$ in the absence of desorption). The SDP model constitutes a big improvement with respect to the approximate model presented in the first part of this chapter, which coincides with several literature models.

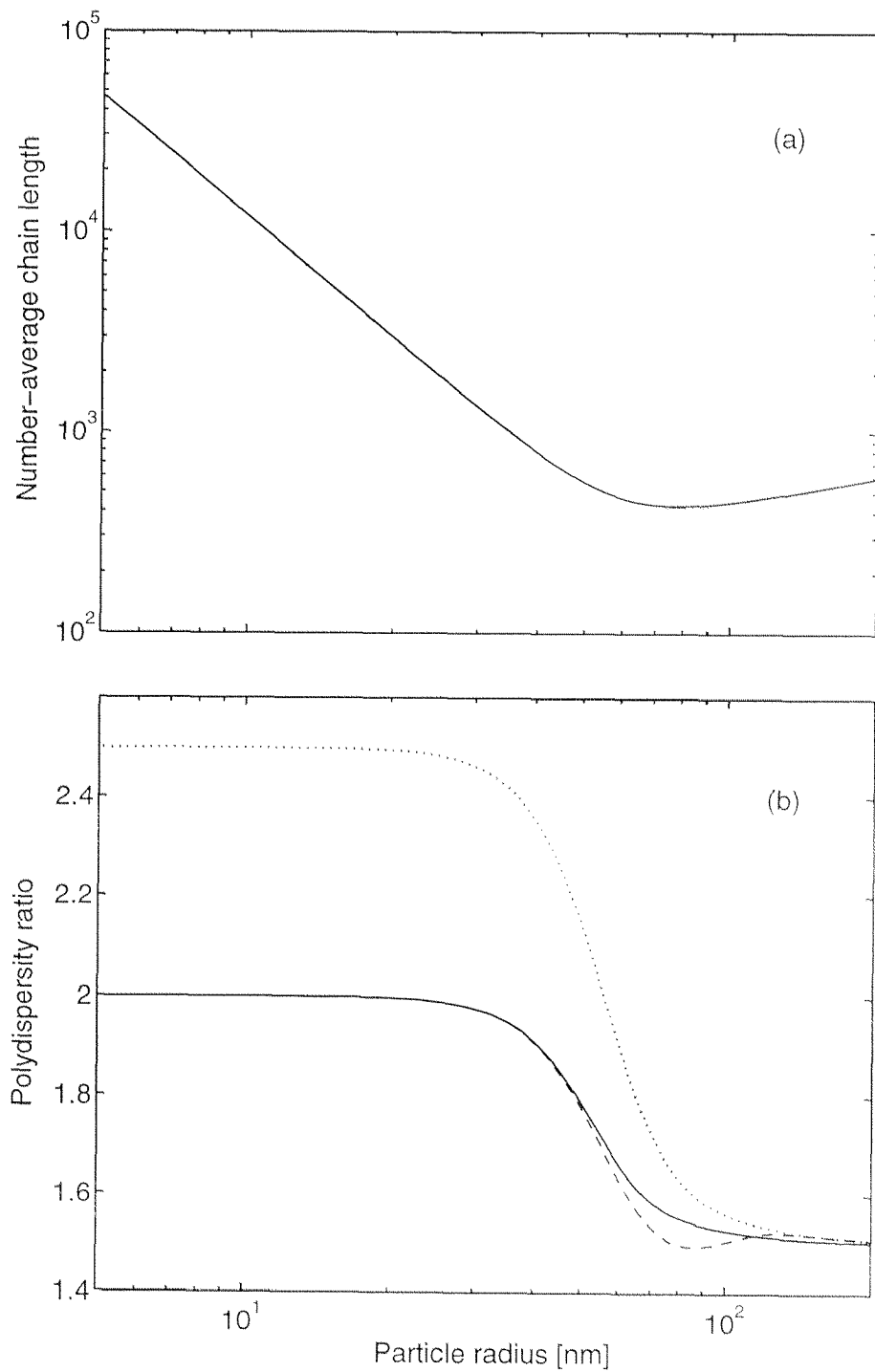


Figure 4.17: (a) Number-average chain length and (b) polydispersity ratio as a function of particle radius for an imaginary system with entry and combination only. — : correct model; --- : SDP model; \cdots : approximate model.

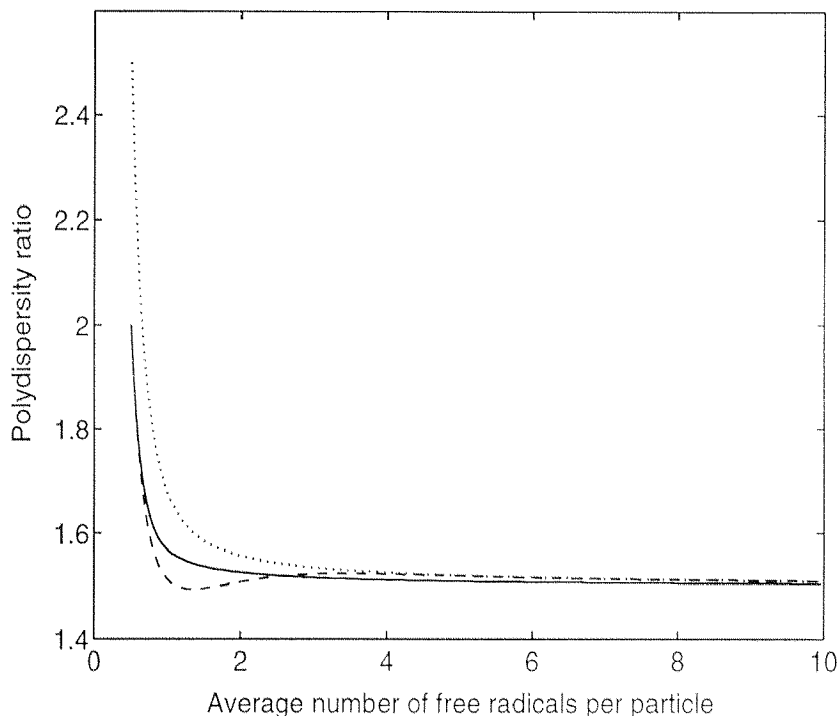


Figure 4.18: Polydispersity ratio as a function of the average number of radicals per particle for an imaginary system with entry and combination only. — : correct model; --- : SDP model; \cdots : approximate model.

4.7 Conclusions

Through a comparison between two models having a different level of detail, it has been shown that significant errors can be introduced in the calculation of the polydispersity ratio of a polymer produced in emulsion in the presence of termination by combination if the distribution of the lengths of the pairs of chains belonging to the same particle is not taken into consideration. This distribution is accounted for through the concept of ‘doubly distinguished particles’ in the correct model.

An analysis of the instantaneous MWD properties as a function of the average number of free radicals per particle \bar{n} has shown that these errors are greater in an interval of \bar{n} values, typical of emulsion polymerization, ranging from 0.4 to about 2. At high \bar{n} values, instead, when the entry frequency becomes much greater than the bimolecular termination frequency, the effects of compartmentalization tend to vanish and the two models give the same results. No difference is observed in the number-average chain length on the entire range of \bar{n} values.

An analysis of the cumulative properties shows similar inaccuracies when neglecting the doubly distinguished particle distributions. In particular, very large errors are made

when the termination by combination mechanism is responsible for gelation, such as in the case of branching occurring through chain transfer to polymer. In this case, the use of a model accounting for the compartmentalization effects in an approximate manner is absolutely unsatisfactory.

Three case studies of practical importance were analysed in order to establish the ranges of polymer particle size (at least under fixed reaction conditions) where the use of the correct model is necessary. For styrene, this is true for an intermediate range of radius values (from $r_P = 10$ nm to $r_P = 60$ nm in the conditions studied). At lower values, chain transfer to monomer is important, while at higher values the system becomes dominated by bimolecular termination. In both cases, compartmentalization effects vanish. In the case of methyl methacrylate, limited differences are found at all r_P values, due to the small combination/disproportionation ratio. For vinyl acetate, where the desorption rates are very large, significant differences arise only in the higher r_P range ($r_P > 30$ nm). The presence of a branching reaction in this case makes even limited differences in the instantaneous polydispersity values important on a cumulative scale.

By understanding the mechanisms through which compartmentalization acts on molecular weights, it was possible to develop a simplified model (SDP model) which, while accounting correctly for the compartmentalization effects, does not involve distributions with two chain lengths as internal coordinates (such as the doubly distinguished particles), thus permitting the easier application of detailed techniques for the equation solution. This can be particularly useful when secondary effects, such as chain-length dependent reaction rates, non-steady-state conditions, and so on, need to be included.

Chapter 5

Model Application to Experimental Systems - Vinyl Chloride and Vinyl Acetate

5.1 Introduction

In this chapter the model is applied to describe literature molecular weight data from vinyl chloride (VC) and vinyl acetate (VAc) emulsion polymerizations. In the case of VC, branching was found to be of limited significance. On the other hand, it has a great influence on the molecular weight development in the case of VAc. In both cases, application of the model to the data provides a great insight into the mechanisms underlying the process and how they affect the final polymer.

To apply the model for the molecular weight calculation, it is necessary to provide expressions for the evaluation at all reaction times of all the parameters and quantities appearing in the molecular weight equations (Chap. 2). These are primarily the entry, desorption and termination rate coefficients, the distribution of radicals in the particles, the average number of radicals per particle and the monomer concentration in the particles. These quantities are also those which determine the kinetic behavior and will be calculated, for the theoretical description of the experimental systems considered, by the general equations given in Section 5.2 of the present chapter. If some specific expression is required for some other parameter applying to a specific monomer, this will be given in the section dealing with that monomer.

5.2 Model for the Kinetics

5.2.1 Entry, Desorption and Bimolecular Termination Frequencies. Distribution of Radicals in the Particles

Several models have been proposed for the evaluation of the entry rate. According to the conceptual model selected (diffusion control, surfactant displacement, colloidal entry or aqueous-phase growth control model [64]), a different equation results for the frequency of entry ρ . Here, a simple empirical law is used, stating that the rate of entry r_e (mol $\text{cm}^{-3} \text{s}^{-1}$) is proportional through a constant k_e to the radical concentration R_w^\bullet and the particle density N_P :

$$r_e = k_e R_w^\bullet N_P$$

The frequency of entry of radicals in a polymer particle is therefore given by:

$$\rho = r_e N_A / N_P = k_e N_A R_w^\bullet \quad (5.1)$$

where N_A is Avogadro's number.

Desorption from the particles is described according to the model proposed by Asua et al. [28]. In agreement with many other models (e.g. [26, 27, 29]), this model considers the desorbing species to be the monomeric radicals produced by chain transfer to monomer (and to other small molecules subject to transfer if present). The desorption of chains longer than one unit is considered to be negligible, due to the decrease in diffusivity and solubility of these species compared to the monomeric radical [29]. Once the desorbed radical is in the water phase, it can either react (by propagation or termination) or re-enter a particle as a monomeric radical, i.e., as a species capable of desorption. Considering the previous mechanisms, the following expression for the desorption coefficient k_d is derived [28] (where $k_d \bar{n} N_P / N_A$ is the rate of desorption from all particles in $\text{mol cm}^{-3} \text{s}^{-1}$):

$$k_d = k_{fm} C_m \frac{k_o}{\beta k_o + k_p C_m} \quad (5.2)$$

with k_o the rate of diffusion of the monomeric radical out of a particle and β its probability of reacting in the water phase. Coefficient k_o was calculated by Nomura as [27]:

$$k_o = \frac{3D_{eff}}{r_P^2} \quad (5.3)$$

where r_P is the swollen particle radius and D_{eff} is an effective diffusion coefficient defined as:

$$D_{eff} = \frac{D_p D_w}{m_d D_p + 2D_w} \quad (5.4)$$

with D_p and D_w monomer diffusion coefficients in the particles and in water, respectively, and m_d an equilibrium constant defining the partitioning of the monomer between particle and aqueous phase ($m_d = (C_m/C_{m,w})_{eq}$). Probability β is given by [28]:

$$\beta = \frac{k_{t,w}R_w^\bullet + k_{p,w}C_{m,w}}{k_{t,w}R_w^\bullet + k_{p,w}C_{m,w} + k_{re}N_P} \quad (5.5)$$

where $k_{t,w}$ and $k_{p,w}$ are the bimolecular termination and propagation rate constants in the aqueous phase, R_w^\bullet and $C_{m,w}$ the concentrations of radicals and of monomer in the same phase, and k_{re} is the rate constant for the re-entry of monomeric radicals into polymer particles.

Finally, the bimolecular termination frequency is related to the bimolecular termination rate constant k_t by:

$$c = \frac{k_t}{2N_A v_P} \quad (5.6)$$

(where k_t is defined so that the rate of termination in a bulk is given by $r_t = k_t R^{\bullet 2}$, with R^\bullet overall radical concentration).

To calculate the entry and desorption frequencies, the radical concentration in the water phase R_w^\bullet is required. This can be calculated from the following material balance:

$$\frac{dR_w^\bullet}{dt} = 0 = 2k_I\eta[I]_w - k_{t,w}R_w^{\bullet 2} - k_e N_P R_w^\bullet + \frac{k_d \bar{n} N_P}{N_A} \quad (5.7)$$

where the equality to zero comes from the application of the QSSA to the radical species. The first term on the right-hand side represents the generation of radicals in the aqueous phase due to initiator decomposition and the second term the consumption due to bimolecular termination, while the third and fourth terms account for the disappearance and appearance of radicals in the water phase due to transport to and from the particles (entry and desorption, respectively). Accordingly, k_I is the initiator decomposition rate constant, η an efficiency parameter and $[I]_w$ the concentration of initiator in the water phase.

The average number of radicals per particle \bar{n} appearing in eq. (5.7) can be calculated by solving the classical Smith-Ewart equations [37] in the steady state:

$$\frac{dN_i}{dt} = 0 = \rho N_{i-1} - [\rho + k_d i + c i(i-1)]N_i + k_d(i+1)N_{i+1} + c(i+2)(i+1)N_{i+2} \quad (5.8)$$

where N_i represents the fraction of particles containing i radicals. Note that this quantity appears in the initial conditions (2.3) and (2.4) for the singly distinguished particles, and is therefore required for the molecular weight calculation. Eqs (5.8) (for $i = 0, 1, \dots$) can be easily solved numerically by imposing a maximum number of radicals per particle N

[40]. The average number of radicals per particle \bar{n} is then given by:

$$\bar{n} = \sum_{i=0}^N iN_i \quad (5.9)$$

Note that eqs (5.7) and (5.8) are coupled, since the frequencies of entry and desorption in eq. (5.8) depend on R_w^\bullet (see eqs (5.1) and (5.5), respectively), while the overall desorption rate in eq. (5.7) depends on \bar{n} . Accordingly, these equations must be solved simultaneously. This can be done by assigning a first-guess value to \bar{n} and iterating until convergence on this quantity is achieved. Since \bar{n} varies with continuity during the reaction, its value at the previous integration step (when considering the whole reaction) is a very good initial guess and convergence is reached rapidly.

Summarizing, eqs (5.1)-(5.9) permit to calculate the entry, desorption and bimolecular termination frequencies, ρ , k_d and c , respectively, the radical distribution in the particles N_i and the average number of radicals per particle \bar{n} . The latter quantity is directly involved in determining the rate of reaction, according to eq. (5.14). All the other quantities appear in the molecular weight equations which were presented in Chap. 2.

5.2.2 Monomer Concentration in the Particle Phase

A further quantity which both determines the rate of reaction (see eq. (5.14)) and appears in the molecular weight equations (Chap. 2) is the concentration of monomer in the particles C_m .

To calculate this quantity, the monomer is considered to be partitioned among the different phases of the system according to thermodynamic equilibrium. Therefore, the transport of monomer from the droplets to the polymer particles which occurs through the water phase during the first two stages of an emulsion polymerization [37] is considered not to be rate determining.

The monomer is present in three phases: the water, the particles and the droplets (when existing). The following relevant material balances and partition equations can be written:

$$\frac{dn_m}{dt} = - \left[(k_p + k_{fm}) C_m \frac{\bar{n} N_P V_w}{N_A} + (k_{p,w} + k_{fm,w}) C_{m,w} R_w^\bullet V_w \right] \quad (5.10)$$

$$n_m = V_w C_{m,w} + \frac{n_p M_m}{(1 - \phi_m) \rho_p} C_m + \frac{V_d}{V_m} \quad (5.11)$$

$$C_{m,w} / C_{m,w}^* = \phi_m / \phi_m^* \quad (5.12)$$

The first eq. (5.10) calculates the rate of consumption of the overall moles of monomer in the system n_m , due to propagation and chain transfer reactions both in the particle and

in the water phase. Polymerization in the droplets is neglected. This equation requires the knowledge of \bar{n} and of R_w^\bullet , the equations for which are given in the previous Section 5.2.1. V_w represents the volume of the water phase.

The second eq. (5.11) simply states that the overall moles of monomer n_m are partitioned between the different phases, in the order, water, particles and droplets. Here, n_p represents the total moles of polymerized monomer in the system, M_m the molecular weight of the monomer, ϕ_m the volume fraction of monomer in the particles, ρ_p the density of the pure polymer, V_d the volume of the droplet phase and \tilde{V}_m the molar volume of the pure liquid monomer. Quantity n_p can be expressed as $n_m^0 - n_m$, where n_m^0 are the moles of monomer initially charged.

Eq. (5.12) is a linear equation for the partition of the monomer between the water and particle phases. It is a simple empirical law which has however proved efficient for several systems, in particular for monomers with low water solubility [65, 66]. In this relation, $C_{m,w}^*$ and ϕ_m^* are the values of $C_{m,w}$ and ϕ_m at saturation. During the first reaction period, the so-called Smith-Ewart's intervals I and II, both the left-hand side and the right-hand side of eq. (5.12) are equal to unity, due to the presence of monomer droplets.

Assuming that the radical concentrations are known, system (5.10)-(5.12) can be solved in Smith-Ewart's intervals I and II of the polymerization to obtain V_d . In this interval, concentration C_m is simply given by its saturation value:

$$C_m = C_m^* = \frac{\phi_m^* \rho_m}{M_m} \quad (5.13)$$

where ρ_m is the density of the pure monomer. In interval III, $V_d = 0$ (the particles are depleted) and the monomer concentrations (including C_m) are obtained from (5.10)-(5.12).

5.2.3 Rate of Reaction

The rate of the polymerization reaction, defined as the time derivative of the monomer conversion χ , can be calculated from:

$$\frac{d\chi}{dt} = \frac{k_p C_m \bar{n} N_P V_w}{n_m^0 N_A} \quad (5.14)$$

where n_m^0 are the initial moles of monomer in the reactor. The calculation of the quantities \bar{n} and C_m is described in the previous Sections 5.2.1 and 5.2.2. The number of particles N_P is constant in a seeded reaction where no secondary nucleation occurs. For an ab initio reaction, proper equations must be developed to describe the variation of particle number during the nucleation stage (interval I).

Parameter	Value	Reference
c_{fp}	$5 \cdot 10^{-5}$	[69]
$C_{m,w}^*$	$1.9 \cdot 10^{-4} \text{ mol cm}^{-3}$	[72]
D_p	$1 \cdot 10^{-6} \text{ cm}^2 \text{ s}^{-1}$	[69]
D_w	$1 \cdot 10^{-5} \text{ cm}^2 \text{ s}^{-1}$	[73]
k_{fm}	$1.1 \cdot 10^4 \text{ cm}^3 \text{ mol}^{-1} \text{ s}^{-1}$	[70]
k_I	$1.7 \cdot 10^{-6} \text{ s}^{-1}$	[71]
k_p	$1 \cdot 10^7 \text{ cm}^3 \text{ mol}^{-1} \text{ s}^{-1}$	[69]
k_{td}	$3 \cdot 10^{10} \text{ cm}^3 \text{ mol}^{-1} \text{ s}^{-1}$	[69]
ϕ_m^*	0.4	[69]
ρ_m	0.85 g cm^{-3}	[69]
ρ_p	1.40 g cm^{-3}	[69]

Table 5.1: Parameters for VC emulsion polymerization at 50°C.

5.3 Vinyl Chloride Polymerization

5.3.1 Parameters

The model (including the equations for the kinetics detailed here above and those for molecular weight described in Chap. 2) was applied to represent reaction rate and molecular weight data of VC emulsion polymerization. Data from the literature were considered [67, 68]. All parameter values except for the entry parameter k_e were taken from the literature and are listed in Table 5.1. The parameter for re-entry k_{re} in eq. (5.5) was considered equal to k_e and the rate constants for the aqueous phase reactions were assumed equal to those for the particle phase. In Table 5.1, c_{fp} is the ratio between the chain transfer to polymer and the propagation rate constants.

5.3.2 Results

In Fig. 5.1 experimental reaction rate data at different initiator concentrations and a constant particle number are shown to fit well to the model with $k_e = 1.4 \cdot 10^{-13} \text{ cm}^3 \text{ s}^{-1}$. The model predicts correctly the concave shape of the rate of reaction and the quantitative effect of increasing initiator concentrations.

In Fig. 5.2 the molecular weight distribution of PVC produced at 55°C is reported for two different conversions and compared to the prediction of the model. A rescaled Γ -distribution was used to reconstruct the distribution from its moments [45]. For each conversion, two theoretical curves are reported, one obtained assuming no chain branching, and the other assuming a value of $5 \cdot 10^{-5}$ [69] for the chain transfer to polymer parameter c_{fp} . In the case of $c_{fp} \neq 0$, numerical fractionation was used adopting a rescaled Γ -distribution for each generation. In the representation chosen, where the molecular weight

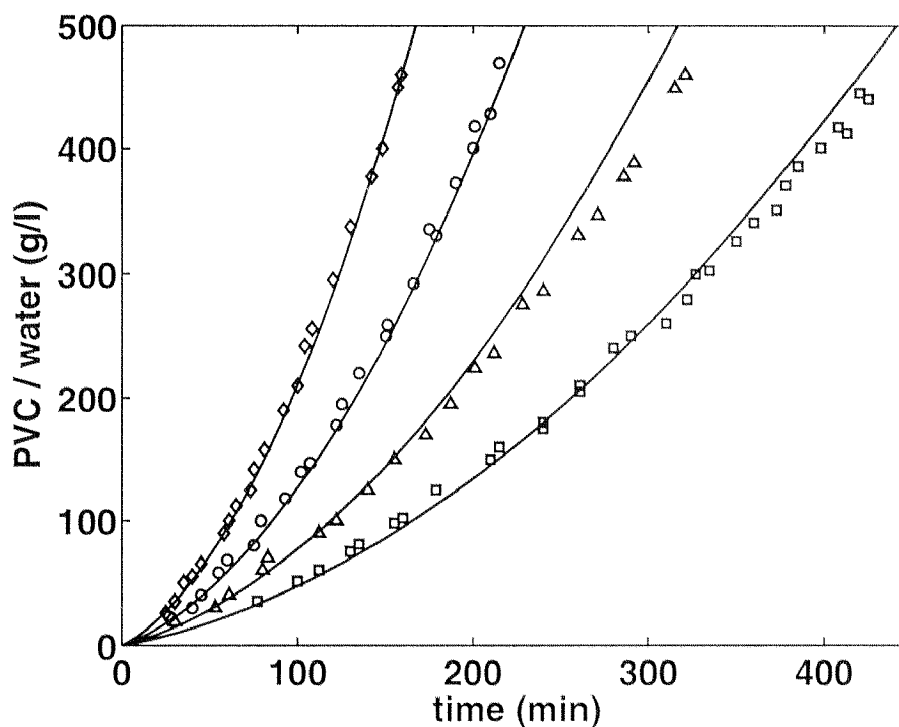


Figure 5.1: Conversion histories of VC polymerization at 50°C for different initiator concentrations $[I]$ and a constant particle number $N_P = 2.5 \cdot 10^{19} \text{ m}^{-3}$. — : model; experimental: \square : $[I]=1.7 \text{ mol m}^{-3}$, Δ : $[I]=3.4 \text{ mol m}^{-3}$, \circ : $[I]=6.8 \text{ mol m}^{-3}$ and \diamond : $[I]=13.6 \text{ mol m}^{-3}$. The experimental data are taken from ref. [67].

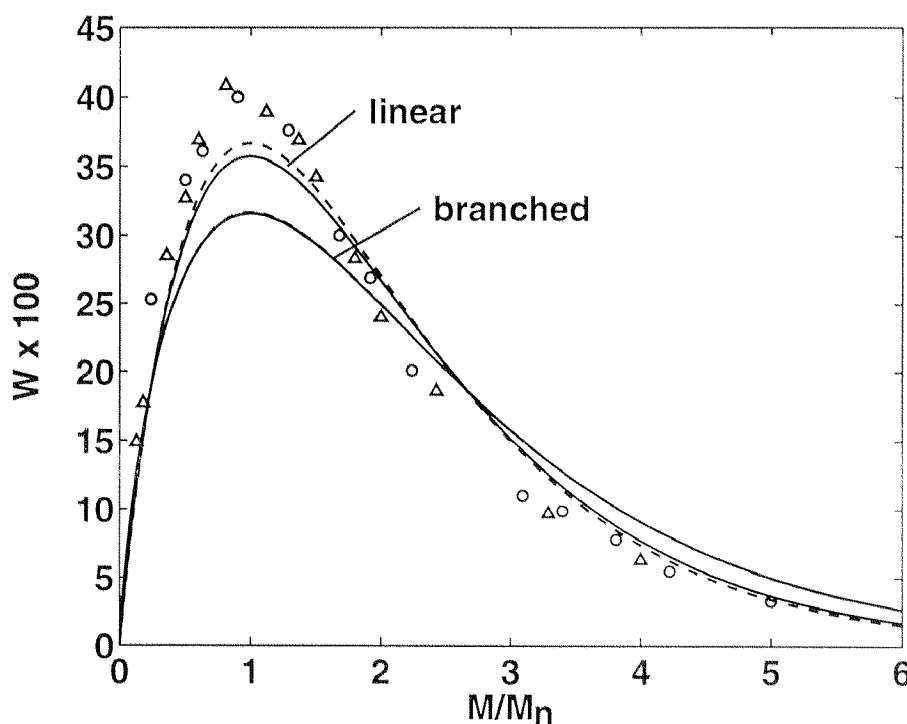


Figure 5.2: MWD of PVC produced at 55°C for two different conversions. Model: — : 5.7 % conversion and - - - : 92.5 % conversion; experimental: \circ : 5.7 % conversion and Δ : 92.5 % conversion. The experimental data are taken from ref. [68].

Parameter	Value	Reference
D_p	$1 \cdot 10^{-6} \text{ cm}^2 \text{ s}^{-1}$	[75]
D_w	$1.86 \cdot 10^{-5} \text{ cm}^2 \text{ s}^{-1}$	[76]
c_{fm}	$2.5 \cdot 10^{-4}$	[77]
c_{fp}	$3.96 \cdot 10^{-4}$	[63]
C_m^*	$8.95 \cdot 10^{-3} \text{ mol cm}^{-3}$	[76]
$C_{m,w}^*$	$0.33 \cdot 10^{-3} \text{ mol cm}^{-3}$	[76]
k_I	$1.7 \cdot 10^{-6} \text{ s}^{-1}$	[71]
k_p	$6.68 \cdot 10^6 \text{ cm}^3 \text{ mol}^{-1} \text{ s}^{-1}$	[78]
k_t	$9.37 \cdot 10^{10} \text{ cm}^3 \text{ mol}^{-1} \text{ s}^{-1}$	[75]

Table 5.2: Parameters for VAc emulsion polymerization at 50°C

is scaled according to its number-average, both experimental and theoretical distributions do not change significantly with conversion. This is especially true in the branched case, where the two curves at different conversions are almost completely superimposed. However, the curves with no branching are in better agreement with experiment, which would indicate that $c_{fp} < 5 \cdot 10^{-5}$, i.e., that branching has little or no importance in VC emulsion polymerization.

5.4 Vinyl Acetate Polymerization

5.4.1 Parameters

In the free radical polymerization of VAc, chain branching is usually considered to occur both by chain transfer to polymer and by TDB propagation [63, 74].

The values of the parameters used in the model are reported in Table 5.2 together with their source. The dimensionless parameters c_{fm} and c_{fp} represent the ratios between the rate constants for chain transfer to monomer (k_{fm}) and chain transfer to polymer (k_{fp}), respectively, and the rate constant for propagation (k_p). A correction factor was applied to the diffusivity of the monomer in the particles D_p to account for the viscosity change in the particles with conversion, according to Friis and Nyhagen [75]. The parameters α and β appearing in the equation by these authors were chosen as $\alpha = 0.60$ and $\beta = 4.68$. The bimolecular termination rate constant k_t used also accounts for the viscosity change ('gel' effect) in the particles according to the equation and parameter values given by the same authors [75].

With respect to bimolecular termination, whether it occurs by combination or by disproportionation at 50°C is still an open question. While early reports have suggested that termination during VAc polymerization involved predominantly disproportionation, it is thought [36] that these investigations did not adequately allow for the occurrence of

transfer events, which are extremely important in VAc polymerization. These problems were addressed by Bamford et al. [62] who used the gelation technique to show that the predominant radical-radical termination mechanism is combination at 25°C. The contribution of disproportionation at higher temperatures can however be significant. In any case, the emulsion polymerization of VAc exhibits very low average number of radicals per particle, so that the nature of the bimolecular termination mechanisms has no influence on the resulting polymer produced, as will be discussed in the next Section 5.4.2.

In order to account for the effect of the viscosity change in the particles on the TDB propagation rate constant k_p^* [63], the following relation was used

$$k_p^* = k_p[A_1 + A_2(\chi_p - \chi_p^*) + A_3(\chi_p - \chi_p^*)^2 + A_4(\chi_p - \chi_p^*)^3] \quad (5.15)$$

where $A_1 = 0.566$, $A_2 = -0.0595$, $A_3 = -0.504$ and $A_4 = -0.420$, χ_p is the apparent fractional conversion in the particles and $\chi_p^* = 0.208$ is the value of χ_p when the system is saturated in monomer, i.e., in intervals I and II.

The value of the entry rate constant k_e in eq. (5.1) was chosen as $k_e = 1.2 \cdot 10^{-14} \text{ cm}^3 \text{ s}^{-1}$. The same value was taken for the re-entry parameter k_{re} in eq. (5.5).

Finally, the rate constants for the aqueous phase reactions were assumed equal to those for the particle phase.

5.4.2 Results

The model has first been used to describe conversion vs. time data of VAc emulsion polymerizations taken from ref. [69]. The parameters which vary from one reaction to the other are the initiator concentration and the latex particle number, while the temperature is the same for all runs (50°C). In Fig. 5.3 the calculated conversion curves are shown together with the experimental data. The results of the model, which does not include the description of the nucleation stage, are shown from 5% conversion on, where the system reaches experimentally a constant number of particles [69] and can therefore be considered as a seeded system. The model describes fairly well the effect of initiator concentration and particle number on reaction rate.

Molecular weight data from VAc emulsion polymerizations carried out at 50°C have also been described by the model. The experimental data have been taken from ref. [63] and are shown in Fig. 5.4 together with the theoretical results. The data were obtained from reactions at different initiator concentrations and particle numbers and can be seen to be insensitive to these variables. This is also predicted by the model, since a single curve results in all cases. This insensitivity can be explained by the fact that the system is at

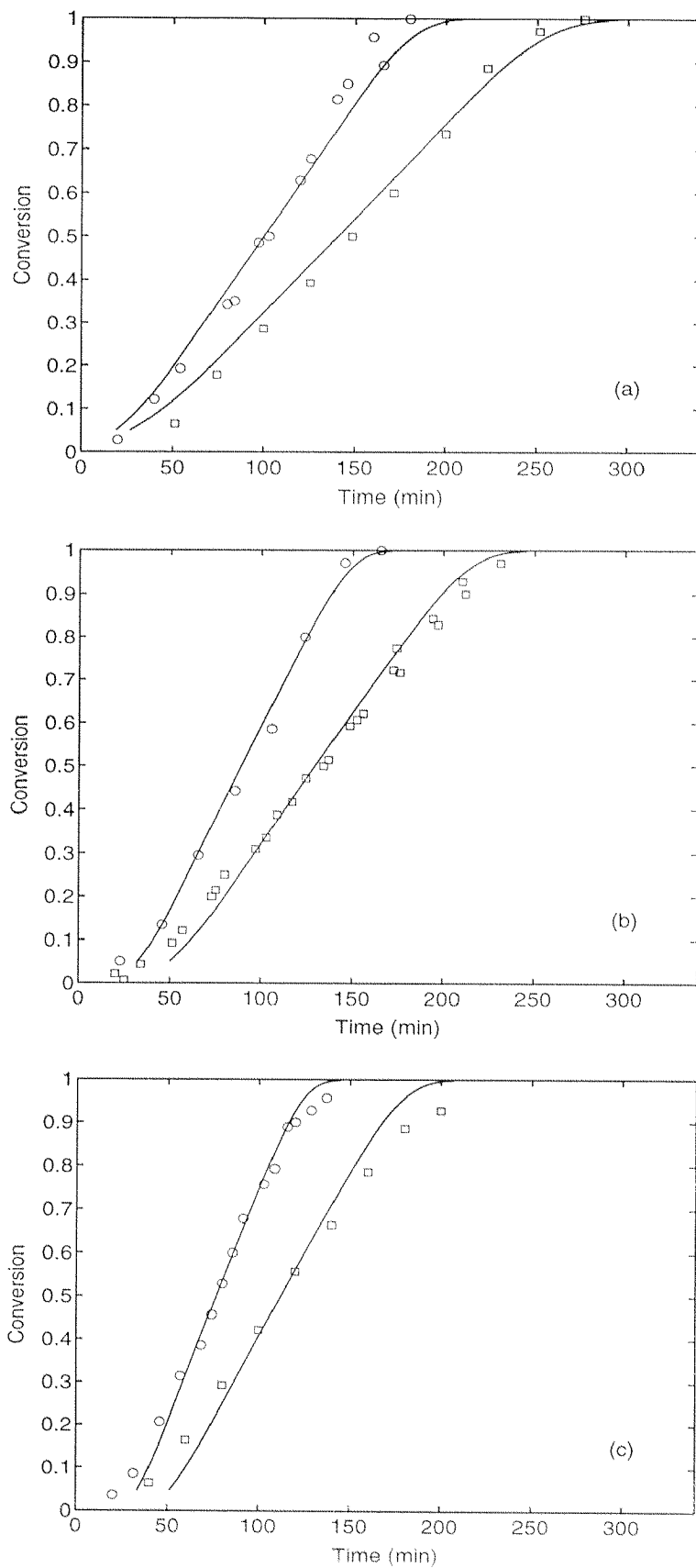


Figure 5.3: Conversion histories of VAc emulsion polymerization at 50°C for different initiator concentrations $[I]$ and different particle numbers N_P : (a) $N_P = 4 \cdot 10^{14} \text{ cm}^{-3}$, (b) $N_P = 8.6 \cdot 10^{14} \text{ cm}^{-3}$ and (c) $N_P = 15 \cdot 10^{14} \text{ cm}^{-3}$. — : theoretical; experimental: \square : $[I]=1.9 \cdot 10^{-4} \text{ g cm}^{-3}$ and \circ : $[I]=3.8 \cdot 10^{-4} \text{ g cm}^{-3}$. The experimental data are taken from ref. [69].

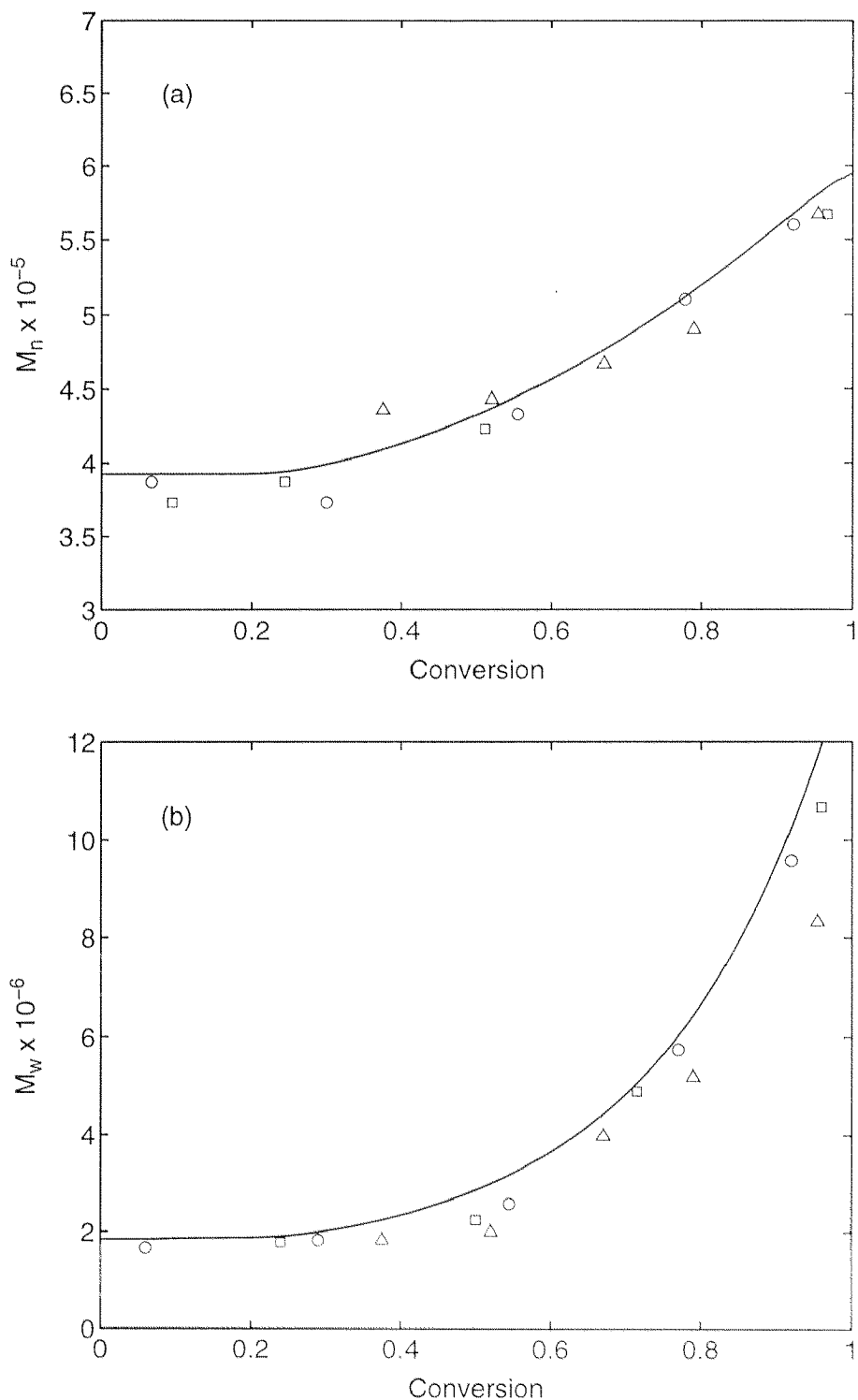


Figure 5.4: Molecular weights from VAc emulsion polymerization at 50°C for different initiator concentrations $[I]$ and different particle numbers N_P . (a) Number-average molecular weight and (b) weight-average molecular weight. — : theoretical; experimental: □ : $[I]=2.7 \cdot 10^{-4} \text{ g cm}^{-3}$ and $N_P = 8.6 \cdot 10^{14} \text{ cm}^{-3}$, ○ : $[I]=2.7 \cdot 10^{-4} \text{ g cm}^{-3}$ and $N_P = 15 \cdot 10^{14} \text{ cm}^{-3}$, △ : $[I]=5.4 \cdot 10^{-4} \text{ g cm}^{-3}$ and $N_P = 15 \cdot 10^{14} \text{ cm}^{-3}$. The experimental data are taken from ref. [63].

very low average number of radicals per particle (calculated always in the range 0.002-0.15, below 0.02 up to at least 70% conversion in all cases) and is characterized by high chain transfer to monomer rates, so that the contribution of bimolecular termination reactions to molecular weight development is negligible [63]. The system is characterized by increasing molecular weights (both number- and weight-averages) and increasing polydispersities with conversion, which can be ascribed to the presence of branching mechanisms.

In order to point out the effect of the two different branching mechanisms (chain transfer to polymer and TDB propagation) the molecular weight vs. conversion curves were re-calculated assuming only TDB propagation ($k_{fp} = 0$), only chain transfer to polymer ($k_p^* = 0$) and no branching ($k_{fp} = k_p^* = 0$), respectively. The results are reported in Fig. 5.5, where the solid curve refers to the case of both branching mechanisms present (real case), the dashed curve to the case of chain transfer to polymer only, the dotted curve to the case of TDB propagation only and the dashed-dotted curve to the case of no branching (linear chains). In Fig. 5.5(a), which shows the number-average molecular weight, the dotted curve is superimposed on the solid curve, while the dashed curve is superimposed on the dashed-dotted curve (linear case). This means that the increase in number-average molecular weight is due exclusively to the TDB propagation. This is easily understood, since the chain transfer to polymer mechanism changes neither the amount of polymerized monomer nor the number of terminated chains, thus having no influence on the ratio between these two quantities, which gives the number-average molecular weight. On the other hand, TDB propagation joins the chains together, thus decreasing their number and increasing the number-average molecular weight compared to linear chains.

The contribution of each mechanism to the increase in weight-average molecular weight cannot be separated as simply. This is apparent when Fig. 5.5(b) is observed. While the increase in weight-average molecular weight (both with conversion and compared to linear chains) is moderate when either of the two branching mechanisms is operative alone, it is very strong when the two mechanisms are present together, much greater than simply the sum of the increases due to each of the two branching reactions. In other words, the two branching mechanisms interact synergically to produce the marked increase in weight-average molecular weight observed experimentally.

The same remarks can be made observing the evolution of the polydispersity index shown in Fig. 5.5(c). While the increase of the polydispersity index due to each of the two mechanisms alone is quite moderate, it is very strong when the two mechanisms are present together. This is understood by considering that the TDB propagation connects together branched polymer chains, where the branches are mainly produced by the chain transfer

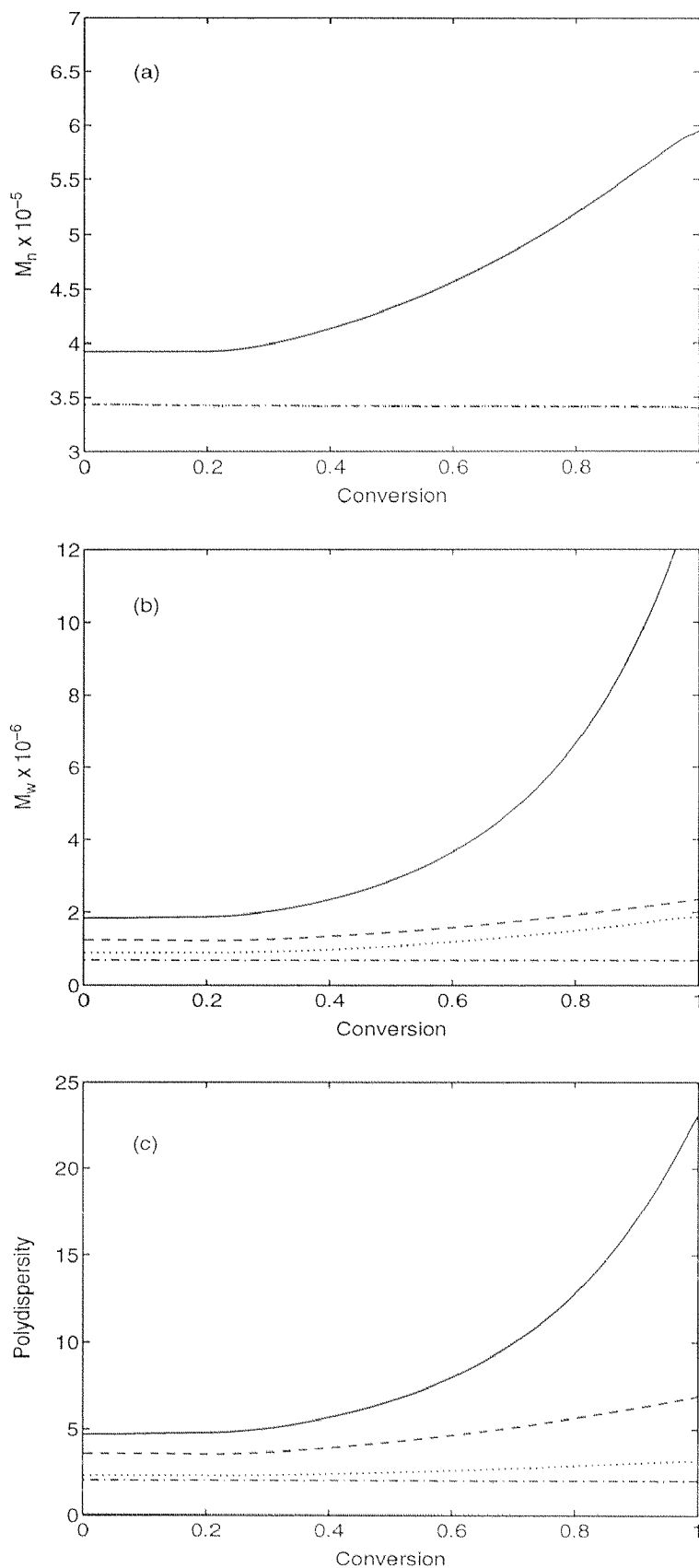


Figure 5.5: Predicted molecular weights for VAc emulsion polymerization at 50°C. (a) Number-average molecular weight, (b) weight-average molecular weight and (c) polydispersity ratio. Solid curve: real case; dashed curve: only chain transfer to polymer ($k_p^* = 0$); dotted curve: only TDB propagation ($k_{fp} = 0$); dashed-dotted curve: no branching ($k_{fp} = k_p^* = 0$). In (a) the dotted curve is superimposed on the solid one, while the dashed curve is superimposed on the dashed-dotted one.

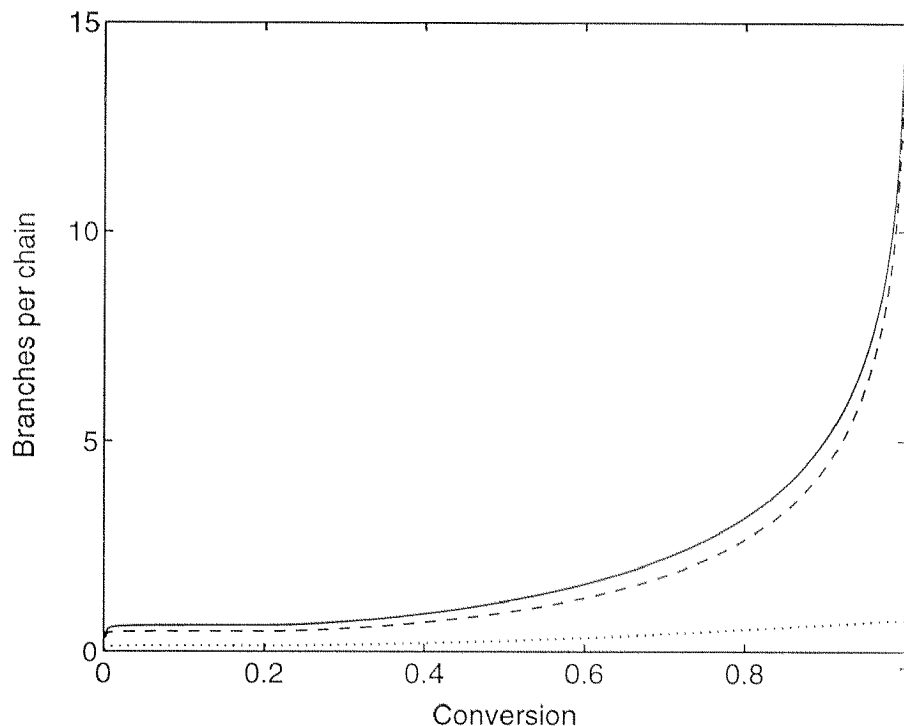


Figure 5.6: Predicted evolution of the average number of branches per chain for VAc emulsion polymerization at 50°C. Solid curve: overall number of branches; dashed curve: branches produced by chain transfer to polymer; dotted curve: branches produced by TDB propagation.

to polymer reaction, as can be deduced by observing Fig. 5.6, where the contribution of each of the two branching mechanisms to the average number of branches per molecule is shown. Chain transfer to polymer plays therefore a major role in producing large branched molecules (it must be recalled that it acts on a mass basis, thus increasing the branch number of the chains which are larger already), while the TDB propagation has the effect of connecting these chains together. With respect to this, it must be noted that bimolecular termination by combination (even when it is assumed significant at 50°C compared to disproportionation) cannot play a role in connecting the chains, since the high segregation of the radicals in the polymer particles prevents this mechanism from taking place and causes it to be of no importance. Thus, one of the two steps leading to the buildup of the very large branched chains which increase polydispersity to such a great extent as observed experimentally would be missing if either of the two branching reactions was not present.

A further proof of the negligible role of the bimolecular termination reactions, besides the insensitivity of the molecular weights to initiator concentration and particle number, is obtained by comparing the molecular weights calculated by the model assuming bimolecu-

lar termination to occur by combination or by disproportionation, respectively. The result is shown in Fig. 5.7, where it is seen that the differences are very small, which would not be the case if bimolecular termination played a major role. The very limited effect of the bimolecular termination reactions is thus confirmed. Fig. 5.7 shows also that the knowledge of the mechanism through which bimolecular termination actually occurs (which is not well established, see Section 5.4.1) is not crucial for a correct molecular weight prediction of poly(VAc) produced in emulsion (at least in the range of conditions considered).

Finally, the slight differences in weight-average molecular weights at high conversions in Fig. 5.7(b) shows that the role of termination, though small, is not completely negligible at these conversions. This suggests that some differences might be found between the predictions of the correct and approximate models illustrated in Chap. 4 when trying to calculate the molecular weight data under examination. However, if this kind of analysis is made, it is found that the predictions of the two models coincide, even supposing bimolecular termination by combination. This is not surprising if the frequencies of the various reactions are observed (Fig. 5.8). It is seen that at the conversion values at which combination starts playing a role (i.e., at which differences can be seen supposing either combination or disproportionation), the chain transfer to polymer frequency is high compared to the combination frequency. This implies that, when a radical enters a particle where another radical is present, it transfers to polymer rather than combining. This transfer event causes the two active chains to lose any correlation in length, which makes the approximate model equivalent to the correct one.

5.5 Conclusions

In the case of the emulsion polymerization of VC, application of the model to describe the MWD has shown that the role of chain transfer to polymer is negligible. On the other hand, branching plays a major role in the emulsion polymerization of VAc. In this system, while the increase in number-average molecular weight with conversion is due exclusively to the TDB propagation reaction, the very strong increase of the polydispersity index can be ascribed to the interaction of this mechanism with chain transfer to polymer. While the latter has the effect of producing highly branched molecules and of reactivating the larger terminated chains, TDB propagation permits the connection between these chains, thus providing a path to the formation of the very large molecules which are responsible for the high weight-average molecular weights (and polydispersities). From the viewpoint of the numerical fractionation technique, TDB propagation allows the passage of chains

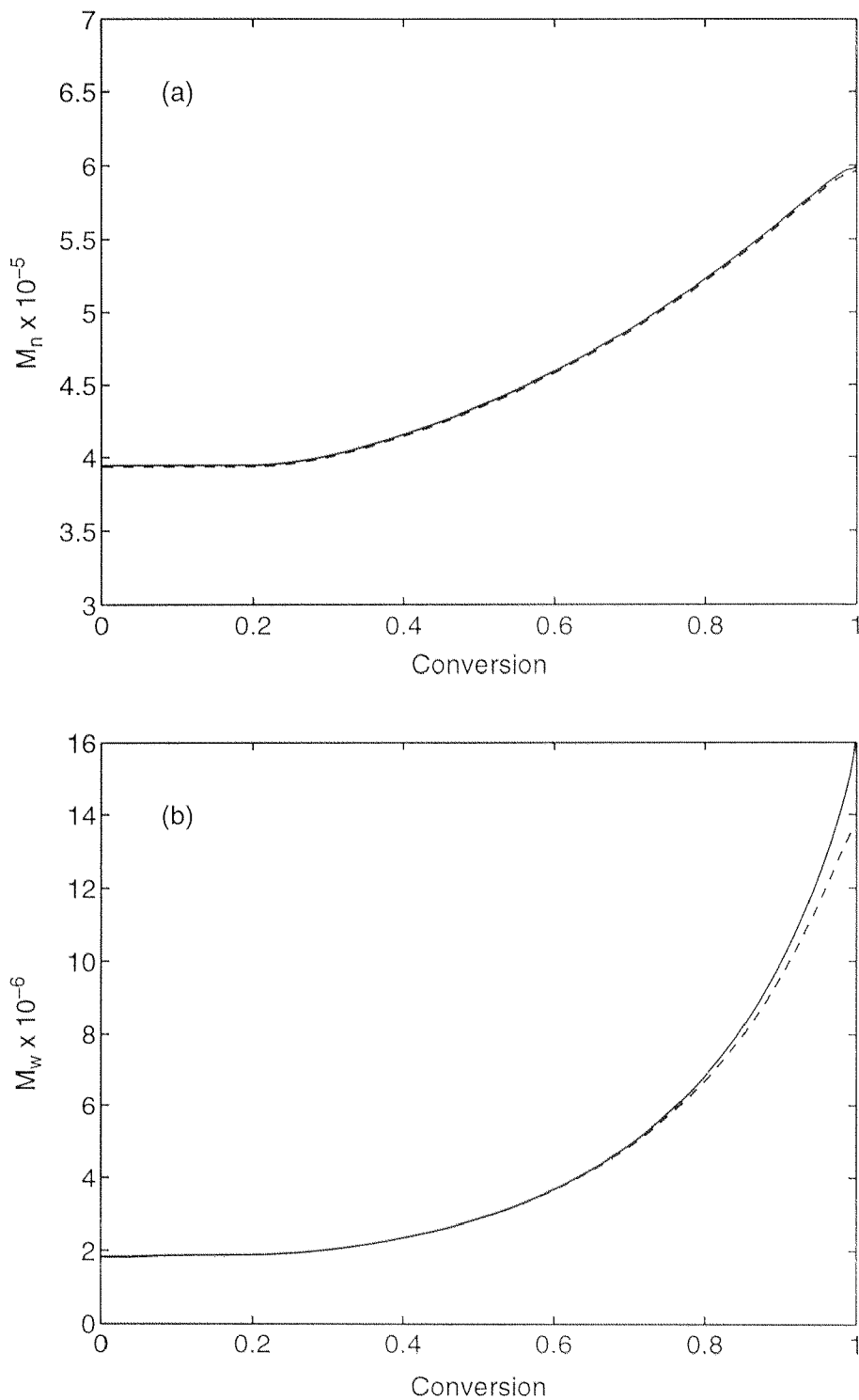


Figure 5.7: Predicted molecular weights for VAc emulsion polymerization at 50°C. (a) Number-average molecular weight and (b) weight-average molecular weight. Solid curve: bimolecular termination by combination; dashed curve: bimolecular termination by disproportionation.

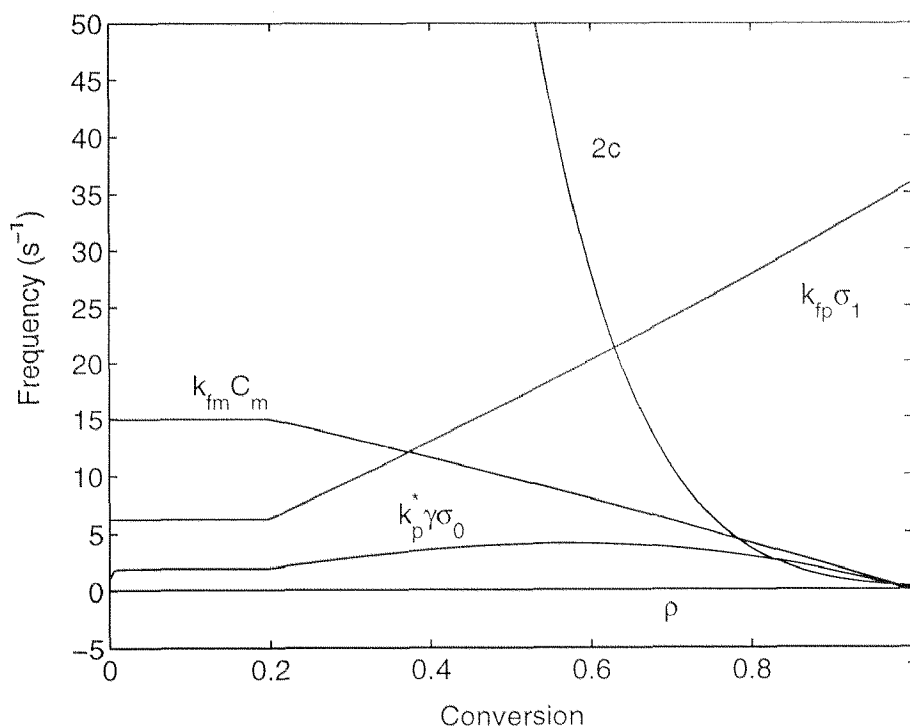


Figure 5.8: Frequencies of various mechanisms for VAc emulsion polymerization. Frequency of bimolecular termination: $2c$; of chain transfer to polymer: $k_{fp}\sigma_1$; of chain transfer to monomer: $k_{fm}C_m$; of TDB propagation: $k_p^*\gamma\sigma_0$; of entry: ρ .

from one branched generation to the following. Due to the very low average numbers of radicals per particle, bimolecular terminations have a negligible effect on the molecular weights produced. This is proved by the insensitivity, both theoretical and experimental, of the molecular weights to particle numbers and initiator concentrations, and by the fact that changing the nature of the bimolecular termination reaction (combination rather than disproportionation) in the simulations does not alter significantly the predictions of the model. Bimolecular termination by combination is therefore not to be considered responsible, together with chain transfer to polymer, for the marked increase in polydispersity, as it is often the case for bulk polymerization systems or emulsion systems at a higher average number of radicals per particle.

Seite Leer /
Blank leaf

Chapter 6

Model Application to an Experimental System - Butyl Acrylate

6.1 Introduction

In the previous Chap. 5, kinetic and molecular weight data of vinyl chloride and vinyl acetate polymerizations taken from the literature were analysed using the model for molecular weight calculation developed in Chap. 2 and the model for the kinetics described in Chap. 5. While in vinyl chloride branching was shown to be of scarce significance, in vinyl acetate polymerization the system exhibits high chain transfer to monomer rates which, combined with a relatively high water solubility of the monomer, result in so low numbers of radicals per particle that bimolecular termination is practically not taking place in the system. These two monomers are therefore not adequate to highlight experimentally the effect of compartmentalization in a system with branching occurring through chain transfer to polymer and with dominant (or at least significant) ‘instantaneous’ combination, where the differences in terms of molecular weight evolution and gel point prediction between a correct and an approximate model are shown to be the greatest (Chap. 4, see Fig. 4.7 and discussion). The selection of such a system needs several requirements to be satisfied: (a) branching must occur through chain transfer to polymer (b) combination must be the operative bimolecular termination (i.e., it must be important compared to disproportionation) (c) radicals must not desorb to too great an extent (so that a radical entering a particle has a certain probability of finding a second radical for combination) (d) the system must be away from pseudo-bulk conditions (where any compartmentalization effect vanishes). Conditions (c) and (d) imply the average number of radicals per particle to have values around 0.5. Condition (c) implies the system to exhibit low chain transfer to monomer rates and/or low solubility of the monomer in water.

The previous requirements should be met by alkyl acrylates, which are monomers with low solubility in water (at a high enough length of the alkyl group) and which give termination by combination and extensive chain transfer to polymer [36]. In particular, butyl acrylate (BA) has a solubility which is comparable to that of styrene (i.e., 'low'). Moreover, a considerable amount of work on the polymerization of this monomer is reported in the literature, so that reliable values of the parameters required for a kinetic description of this system can be found. Finally, gel formation has been reported for BA polymerization (e.g. [79]). It is therefore expected that this system shows the typical delay in the gel point due to compartmentalization which was discussed in Chap. 4 (see Fig. 4.7(b)).

In this chapter experimental data of BA emulsion polymerization at 50° are presented. The kinetic behavior of the system was monitored by reaction calorimetry, which gives very detailed information (it gives the rate of reaction, from which conversion is obtained by integration, while other techniques providing directly conversion may lead to misinterpretation of the kinetic behavior [80]). The gel content of the polymer was determined by ultracentrifugation [3]. It must be noted that when talking about 'gel' in emulsion polymerization, we are actually referring to huge chains (compared to ordinary soluble chains produced in emulsion), but not 'infinite' in size, since the chains are growing inside the latex particles and cannot reach sizes greater than that of the particles. These very large chains of colloidal size are better referred to as 'microgel' rather than 'gel'. As a matter of fact, all techniques appropriate for 'macrogel' characterization [3] which were attempted on the BA emulsion polymerizations presented in this work failed to give a measurement of the gel content. These techniques were filtering, soxhlet extraction and extraction in a glass vessel with periodic renewal of the solvent.

Many examples can be found in the literature of microgel weight fraction characterization of emulsion produced polymers. A very exhaustive paper reviewing work up to 1993 was written by Lee [3]. Several techniques have been employed for microgel content analysis, including ultrafiltration, ultracentrifugation, size exclusion chromatography, static light scattering, field flow fractionation (all reviewed in [3]) and analytical ultracentrifugation [81, 82]. All works focus on the analysis of final crosslinked polymer samples, except for one [83] which examines through size exclusion chromatography the evolution of the microgel content with conversion in copolymerizations involving acrylonitrile as comonomer. The quantitative determination of microgel is however discredited by the fact that poly(acrylonitrile) is insoluble in the mobile phase used (acetonitrile) and acrylonitrile rich polymer may therefore be included in the insoluble polymer identified as graft polymer (microgel).

In this chapter, data on the microgel content evolution with conversion are reported for the BA experiments performed. As mentioned above, these data were obtained by ultracentrifugation. Significant fractions of gel were measured only at high conversions (above 70%). On the other hand, insoluble polymer has been reported for low conversion samples in BA bulk polymerization at 50° [79]. This agrees with the theoretical results presented in Chap. 4 which indicate the gel point to be delayed in emulsion polymerization (for a system giving gel formation through chain transfer to polymer and combination) by the compartmentalization of the branched radicals in the polymer particles.

6.2 The RC1 Reaction Calorimeter

6.2.1 The Instrument

The Mettler RC1 reaction calorimeter is a commercial laboratory scale calorimeter, the working principles of which have been described in the literature [84, 85, 80]. The instrument permits to run experiments in one of the following four operating modes: (1) reactor temperature (T_r) mode, where the temperature of the reactor contents T_r is controlled, (2) jacket temperature (T_j) mode, where the temperature of the jacket fluid T_j is controlled, (3) distillation mode, where the temperature difference $T_j - T_r$ between the jacket and the reactor is controlled and (4) adiabatic mode, where the temperature difference $T_j - T_r$ between the jacket and the reactor is controlled and kept equal to zero. Note that the adiabatic mode is a special case of the distillation mode with $T_j - T_r = 0$. These different possible operating modes permit to run experiments in any of the three classical methods used for polymerization reaction calorimetry [86]: (1) isothermal, where T_r is kept at a constant value and there is no heat accumulation in the reactor, (2) isoperibolic, where T_j is kept at a constant value and the reaction temperature follows the reaction profile, (3) adiabatic, where $T_j - T_r$ is kept equal to zero so as not to have any heat flux across the reactor wall, and the reactor behaves as an isolated vessel.

The complete RC1 system is comprised of the actual RC1 Reaction Calorimeter (with thermostat, stirrer motor and cabinet for the electronic control and monitoring system), a chemical reactor (glass or metal, ambient or high pressure) and a personal computer. Up to three controllers (RD10) can be added to the system for acquisition of additional measured values and for pump and valve control. The computer serves as an interface between the user and the reaction calorimeter, since it displays and stores the data acquired by the RC1 and RD10 during the experiments and it transfers the set points and the safety and control parameters to the RC1 and RD10 units.

The thermostat unit pumps the heat transfer fluid (silicon oil) through the jacket of the reactor from a closed system. This system is made up of two subsystems connected by a stepper-motor regulated valve: the heated circulation system (which includes the jacket) with electrical heating and the cooled circulation system, cooled by heat exchange through a coil with an external cooling medium. By regulating the electrical heating and the valve opening, the temperature of the heated circulation system, and thus of the jacket, is controlled.

The values of the variables (e.g. T_r , T_j , stirred speed, etc.) are acquired every two seconds and stored by the computer with the desired frequency. These values are used to calculate other quantities, such as the heat of reaction \dot{Q}_r , the time derivative of the reactor temperature dT_r/dt , etc., which are also displayed and stored.

A schematic diagram of the RC1 system is given in Fig. 6.1.

6.2.2 The Energy Balance

To evaluate the heat released by a chemical or physical process occurring in the reactor, an energy balance around the reactor has to be considered (Fig. 6.2). Neglecting the kinetic and potential terms, the energy balance can be written as:

$$\dot{Q}_r + \dot{Q}_c + \dot{Q}_{stir} = \dot{Q}_f + \dot{Q}_a + \dot{Q}_i + \dot{Q}_{dos} + \dot{Q}_{loss} + \dot{Q}_{cond} \quad (6.1)$$

where

\dot{Q}_r :	heat generation of the chemical or physical process
\dot{Q}_c :	power from the calibration heater
\dot{Q}_{stir} :	power dissipated from the stirring
\dot{Q}_f :	heat flow through the reactor wall to the jacket
\dot{Q}_a :	heat accumulation in the reaction mass
\dot{Q}_i :	heat accumulation in the reactor inserts
\dot{Q}_{dos} :	heat input due to dosing of process components
\dot{Q}_{loss} :	heat flow through the reactor head assembly
\dot{Q}_{cond} :	heat flow through the condenser wall

An estimation of all heat flow terms (or their constancy, which permits them to be included in the baseline) allows the evaluation of the heat generation \dot{Q}_r . In the case of a homopolymerization, i.e., of a single chemical reaction, \dot{Q}_r is related to the rate of reaction r_p by:

$$\dot{Q}_r = (-\Delta H_P)r_p V_{TOT} \quad (6.2)$$

where ΔH_P is the molar reaction heat and V_{TOT} the overall volume of the phase where the reaction takes place.

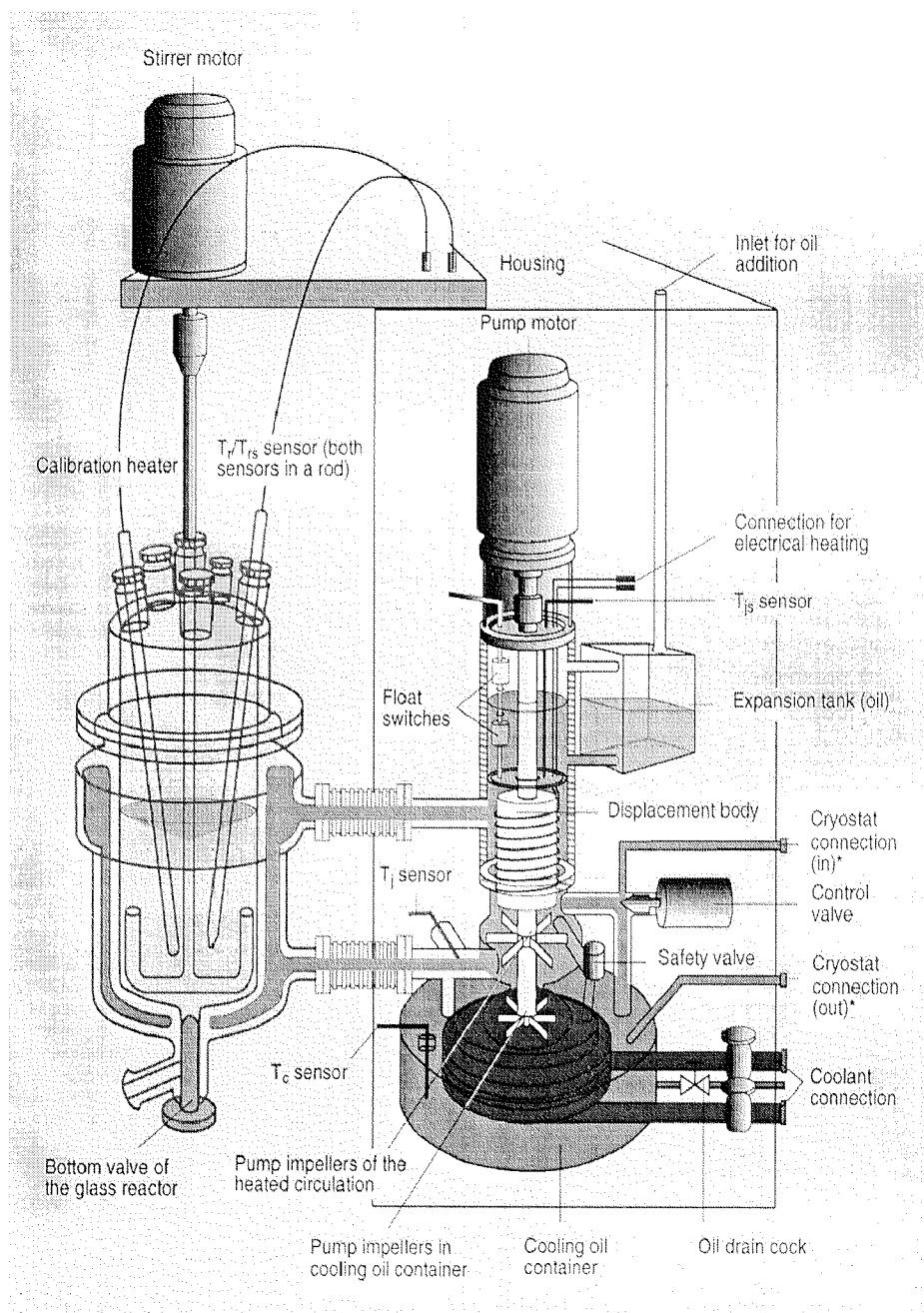


Figure 6.1: Schematic functional diagram of the RC1 thermostat and reactor.

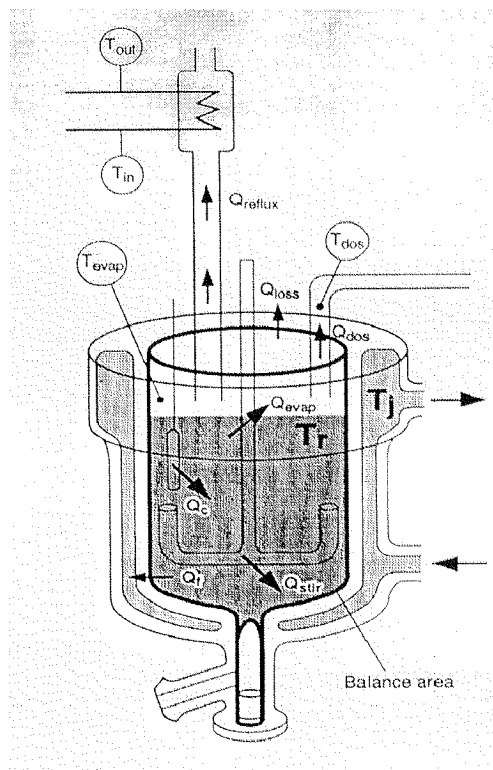


Figure 6.2: Heat flow balance around the reactor.

The most relevant terms in the energy balance (6.1) in ordinary emulsion polymerization conditions are \dot{Q}_r , \dot{Q}_f and, if the reaction is very exothermic so that the system cannot be maintained in isothermal conditions, \dot{Q}_a .

The heat flow to the jacket \dot{Q}_f is estimated as

$$\dot{Q}_f = UA(T_r - T_j) \quad (6.3)$$

where U is a heat exchange coefficient and A is the heat exchange area. A correction for T_j is implemented in the RC1 software to account for non-stationary conditions. The heat exchange coefficient U is measured through a calibration procedure which is detailed below.

The heat accumulation in the reaction mass \dot{Q}_a is calculated as:

$$\dot{Q}_a = mc_p \frac{dT_r}{dt} \quad (6.4)$$

where m is the reaction mass, c_p the specific heat of the reactor contents and dT_r/dt the rate of change of the reactor temperature. The heat capacity c_p can be either assigned or calculated from a temperature ramp, as explained below.

The accumulation term \dot{Q}_i can be calculated similarly to \dot{Q}_a if the heat capacity of the reactor inserts $C_{p,i}$ at a given immersion depth is known:

$$\dot{Q}_i = C_{p,i} \frac{dT_r}{dt} \quad (6.5)$$

The term \dot{Q}_{dos} related to the dosing of components to the reactor can be calculated as the heat required to heat up (or cool down) the dosed mass to the reactor temperature:

$$\dot{Q}_{dos} = \dot{m}_{dos} c_{p,dos} (T_r - T_{dos}) \quad (6.6)$$

where \dot{m}_{dos} is the instantaneously dosed mass, $c_{p,dos}$ its specific heat and T_{dos} its temperature. If the component is added at the temperature of the reactor this term is zero.

The loss term \dot{Q}_{loss} can be calculated by assuming it proportional to the difference in temperature between the reactor and the ambient (or the temperature of the thermostating fluid if the head of the reactor is thermostated). In both cases a heat exchange coefficient is required. However, if the loss term can be confidently considered constant throughout the reaction (which may be true especially if operating isothermally), it may be neglected in the energy balance and included in the baseline.

The heat \dot{Q}_{cond} given out through the condenser can be calculated if the instantaneous mass (mass per unit time) and the condensation heat of the condensing vapours are known. This requires the composition and the amount of the condensed liquid to be measured with time. A simpler way to calculate this term is to measure the difference in temperature of the cooling fluid at the inlet and outlet of the condenser and its flowrate. The heat term \dot{Q}_{cond} is then given by:

$$\dot{Q}_{cond} = \dot{m}_c c_{p,c} (T_{out} - T_{in}) \quad (6.7)$$

where \dot{m}_c is the flowrate of the cooling medium, $c_{p,c}$ its specific heat, and T_{out} and T_{in} the temperatures at the outlet and at the inlet, respectively.

The heat term \dot{Q}_c is the power given in to the system through an electrical heater for calibration purposes (see below) and can be calculated from current and voltage (it is displayed as known in the RC1 software).

Finally, the heat input \dot{Q}_{stir} by the stirrer can in principle be calculated from an equation relating dissipated power to stirrer speed and size. However, if the stirrer is kept at a constant speed and the viscosity of the reactor contents does not change significantly, this heat term can be considered constant and included in the baseline.

Calibration (U determination)

In order to determine the heat exchange coefficient U , a calibration is performed. This operation consists in activating an electrical heater which is placed in the reactor while holding constant the reaction temperature. The energy balance (6.1) reduces to:

$$\dot{Q}_c = \dot{Q}_f \quad (6.8)$$

where \dot{Q}_{stir} , \dot{Q}_{loss} and \dot{Q}_{cond} are considered constant over the calibration time and are included in the baseline, while all other heat flow terms are zero. Recalling expression (6.3) for \dot{Q}_f one obtains:

$$\dot{Q}_c = UA(T_r - T_j) \quad (6.9)$$

Since \dot{Q}_c is given and $(T_r - T_j)$ is measured, the product UA is obtained. By calculating A from the reaction volume (which can be read on the graduated reactor wall), the heat exchange coefficient through the reactor wall U is finally obtained.

Temperature ramp (c_p determination)

In order to determine the specific heat coefficient c_p of the reactor contents, a temperature ramp is performed. This is done by requiring the reactor temperature to move between two temperatures in a long enough time, so that a constant derivative dT_r/dt can be maintained. During such a ramp, the energy balance (6.1) reduces to:

$$0 = \dot{Q}_f + \dot{Q}_a + \dot{Q}_i \quad (6.10)$$

which, by recalling the expression for the various heat terms, can be rearranged as:

$$c_p = \frac{UA(T_j - T_r) - C_{p,i} \frac{dT_r}{dt}}{m \frac{dT_r}{dt}} \quad (6.11)$$

This equation permits to evaluate c_p at the beginning and at the end of a temperature ramp if the U coefficients at the beginning and at the end of the ramp are known (i.e., measured by two calibrations). An accurate value of the c_p at the reaction temperature is essential for the evaluation of \dot{Q}_r only if the reaction proceeds in non-isothermal conditions.

6.3 Experimental

Ab initio and seeded batch emulsion polymerizations of BA were carried out in the Mettler RC1 reaction calorimeter in the isothermal mode at 50°C and ambient pressure

For the ab initio reactions the recipes reported in Table 6.1 were used. Reactions BA2, BA3 and BA6 involve three different initiator levels, reaction BA5 a different monomer to water ratio and BA4 is identical to reaction BA3 but for a reduced amount of all components.

The seeded reactions were performed using the recipes reported in Table 6.2. The seed was constituted by a latex with 9.5% solids content and particles 121 nm in diameter (measured by photon correlation spectroscopy, PCS). This corresponds to a particle concentration of $1 \cdot 10^{14} \text{ cm}^{-3}$ (referred to the water phase). Seed preparation is described

Reaction	Monomer (g)	Water (g)	Emulsifier (g)	Initiator (g)
BA2	300	1000	5.0	1.1
BA3	300	1000	5.0	0.9
BA4	200	667	3.3	0.6
BA5	200	1100	5.0	0.9
BA6	300	1000	5.0	0.7

Table 6.1: Recipes for the ab initio BA emulsion polymerizations (50°C). Emulsifier: SLS, initiator: KPS

Reaction	Seed latex (g)	Monomer (g)	Water (g)	Emulsifier (g)	Initiator (g)
BAs1	109.5	31.9	900	0.22	1.297
BAs2	711.9	205.5	-	1.42	0.505
BAs3	711.9	203.7	-	1.42	0.181
BAs4	711.8	203.3	-	1.42	0.065
BAs5	109.6	31.3	900	0.22	3.602
BAs6	109.5	31.3	900	0.22	3.602
BAs7	109.5	31.3	900	0.22	0.278
BAs8	109.5	31.3	900	0.22	10.028
BAs9	109.5	75.5	900	0.22	0.278

Table 6.2: Recipes for the seeded BA emulsion polymerizations (50°C). Seed latex: 9.5% solids content and $N_P = 1 \cdot 10^{14} \text{ cm}^{-3}$. Emulsifier: SLS, initiator: KPS

below. The recipes in Table 6.2 involve two different initial particle concentrations and several initial initiator concentrations. These are reported in Table 6.3. Note that the monomer to seed polymer ratio was virtually the same (3.3 w/w) for all reactions except for reaction BAs9, where it is higher (7.9 w/w).

For all reactions (ab initio and seeded) the monomer (Fluka >99%) was purified from the stabilizer (hydroquinone monomethyl ether) by adsorption on a column packed with inhibitor removal material (Aldrich). Distilled-deionized (DDI) water was used. The remaining materials were used as received. Sodium lauryl sulfate (SLS, Fluka >99%) was used as emulsifier and potassium persulfate (KPS, Fluka >99%) as initiator.

A 2 liter glass reactor (AP01) with a four pitched-blade (45°) upflow action propeller stirrer was used. The stirrer speed was 600 rpm for all ab initio runs and 400 rpm for all seeded runs. Baffles were introduced in the reactor to avoid vortex forming.

The following procedure was adopted for all experiments. The DDI water and the emulsifier were charged to the reactor and the stirring started. A small amount of water, depending on the amount of initiator to be charged, was spared for preparing the initiator solution. After the SLS had dissolved, the monomer was charged. At this point the seed latex was added in the case of the seeded reactions and the particles were allowed to swell

Reaction	Particle concentration $\times 10^{-13}$ (cm $^{-3}$)	Initiator concentration $\times 10^3$ (g cm $^{-3}$)
BAs1	1	1.297
BAs2	10	0.775
BAs3	10	0.278
BAs4	10	0.100
BAs5	1	3.602
BAs6	1	3.602
BAs7	1	0.278
BAs8	1	10.028
BAs9	1	0.278

Table 6.3: Initial particle and initiator concentrations for the seeded BA emulsion polymerizations. Both concentrations are referred to the volume of water.

for about four hours at ambient temperature. This step is of course skipped in the ab initio reactions. The emulsion was then stripped with a lively nitrogen flow for one hour, during which the temperature was gradually raised to 45°C. The nitrogen flow was passed through a condenser before discharge to minimize reactant losses. When the temperature reached 45°C, the stripping was stopped, but a slight nitrogen overpressure was kept inside the reactor throughout the whole experiment to avoid the inflow of oxygen, which acts as reaction inhibitor.

A 10 min calibration (for the calculation of the heat exchange coefficient U across the reactor wall) was made, then the reactor temperature was brought to 50°C in 10 min, and a second calibration was performed. Before and after each calibration and the temperature ramp, all measured quantities were allowed to settle for at least 10 minutes, in order to obtain stable baselines. During the last settling period, the initiator solution was prepared and heated to the reaction temperature (50°C). It was then dosed to the reactor to start the polymerization.

During the reaction samples were taken periodically for the ab initio reactions. In the case of the seeded reactions, samples were taken only before charging the initiator and after the end of the reaction. With respect to sampling, note that calorimetric monitoring of the reaction is a useful tool, since it shows clearly when the reaction has started (in the case there is any inhibition period), how the reaction evolves and when it is over. Every emulsion sample was subdivided in two (seeded runs) or three (ab initio runs) parts: (a) a few drops of emulsion were diluted in a water solution of SLS and inhibitor (hydroquinone) for particle size determination, (b) about 2 ml of emulsion were put in tared glass vessels with a known amount of inhibitor solution for conversion determination by gravimetry, (c) from 3 to 10 ml about (larger amounts at lower conversions) of emulsion were put in

glass vessels containing inhibitor solution for microgel weight fraction determination (ab initio runs only).

After some time the reaction heat curve had settled to its final baseline value, a 10 min calibration was performed, then the reactor temperature was taken to 55°C in 10 min and a final calibration was made.

Seed preparation

The PBA seed was prepared in the 2 l calorimeter reactor at 50°C, though the large quantity of monomer charged and the very high reaction rate did not allow temperature control and almost 80°C were reached during the reaction. The recipe was the following: 630 g monomer, 1260 g water, 19 g emulsifier and 2.6 g initiator. The reaction was over in about 16 min. The temperature was then raised to 85°C and kept at this value for over 20 h, in order to have total depletion of the KPS. Some coagulum formed in this stage was separated by centrifugation. The latex was then stripped with nitrogen to remove possible residual monomer. A PCS analysis revealed the average diameter of the formed particles to be 121 nm. By addition of DDI water the seed latex was diluted to 9.5% solids content, corresponding to a particle concentration of $1 \cdot 10^{14} \text{ cm}^{-3}$ (referred to the water phase). This seed latex was used without further treatment for the seeded runs BA1 to BA9.

Particle size measurement

The emulsion samples for particle size measurement were diluted and then stripped from the monomer by using a stream of nitrogen, in order to measure the size of unswollen (dry) particles. An average particle diameter was measured by PCS at a 90° angle in a Malvern Zetasizer 5000 instrument. Transmission electron microscopy (TEM) images were also taken of some of the final samples to check qualitatively for the dispersion of particle sizes.

Gravimetric determination of conversion

Samples for gravimetric determination of conversion were dried in a vacuum oven at 90°C for at least 24 h until a constant weight was reached.

Microgel weight fraction determination

Samples for gel fraction determination were precipitated by freezing and thawing the emulsion. The resulting precipitate was repeatedly washed in water and then cut into small pieces before drying under vacuum at ambient temperature. About 0.2 g of the

dry samples were dissolved in 40 ml acetone stirring for 48 h. The 40 ml solutions were ultracentrifuged for one hour at 20,000 rpm in tared steel tubes in a Kontron Hermle Centricon H-401 ultracentrifuge. The supernatant solution was carefully poured in tared glass vessels, while the gel precipitate was left in the ultracentrifuge tube. Both the solute and the microgel precipitate were dried in a vacuum oven at 90°C for at least 24 h until a constant weight was reached. The microgel content was then determined both directly from the precipitate to sample weight ratio and indirectly from the solute to sample weight ratio.

6.4 Data Evaluation

6.4.1 Conversion by Calorimetry

In a batch polymerization reactor, the material balance for the total moles of monomer, n_m , present in the system is:

$$\frac{dn_m}{dt} = -r_p V_{TOT} \quad (6.12)$$

where r_p is the polymerization rate and V_{TOT} is the overall volume of the phase where the reaction takes place.

Defining the conversion χ as

$$\chi = 1 - \frac{n_m}{n_m^0} \quad (6.13)$$

where n_m^0 are the initial moles of monomer, the material balance (6.12) can be rewritten as:

$$n_m^0 \frac{d\chi}{dt} = r_p V_{TOT} \quad (6.14)$$

Since the rate of reaction can be related to the heat released by eq. (6.2), eq. (6.14) becomes:

$$\frac{d\chi}{dt} = \frac{\dot{Q}_r}{(-\Delta H_P)n_m^0} \quad (6.15)$$

If the reaction is isothermal, ΔH_P is constant in time. Thus, integration of eq. (6.15) gives:

$$\chi(t) = \frac{Q_r(t)}{(-\Delta H_P)n_m^0} \quad (6.16)$$

where $Q_r(t) = \int_0^t \dot{Q}_r(t) dt$ is the heat released by the reaction from its start to time t . Since the dependence of ΔH_P from temperature is generally not too strong, relation (6.16) is approximately valid also in non-isothermal conditions, provided that the change in temperature is not too relevant. Eq. (6.16) is the equation required for the calorimetric evaluation of the conversion vs. time profile.

The evaluation of the heat released by the reaction \dot{Q}_r was performed by considering only the flux and accumulation terms in eq. (6.1):

$$\dot{Q}_r = \dot{Q}_f + \dot{Q}_a + \dot{Q}_i \quad (6.17)$$

The terms \dot{Q}_{stir} and \dot{Q}_{loss} were considered constant and included in the baseline, while the term \dot{Q}_{dos} is zero because the initiator solution was pre-heated to the reaction temperature before dosing to the reactor ($T_{dos} = T_r$). Finally, the term \dot{Q}_{cond} was checked to be absolutely negligible in the experimental conditions adopted. Its evaluation was performed through eq. (6.7), where the temperature difference ($T_{out} - T_{in}$) was determined by a differential temperature measurement and \dot{m}_c regulated by a flow controller.

For the calculation of the flow and accumulation term, the heat exchange coefficient U and the specific heat c_p were considered to vary linearly during the reaction (i.e., between the values determined just before and just after the reaction).

6.4.2 Conversion by Gravimetry

The conversion of monomer into polymer was determined by taking samples from the reaction mixture and analysing their solid content. While in a (non-seeded) bulk system the solid weight fraction coincides with the fractional conversion (if the concentration of the initiator and of other additives can be neglected), in an emulsion the presence at least of the water phase must be accounted for. This requires the initial recipe to be known. The conversion was obtained from gravimetric measurements through the following equation:

$$\chi(t) = \frac{1}{M^0} \left[(W + M^0 + E + I + V + S) \frac{\omega_d}{\omega_s} - (E + I + S) \right] \quad (6.18)$$

where

M^0 = mass of charged monomer

W = mass of charged water

E = mass of charged emulsifier

I = mass of charged initiator

V = mass of charged volatile additive

S = mass of charged non-volatile additive (including an eventual polymer seed)

ω_s = weight of the sample withdrawn at time t

ω_d = weight of the dried sample

Eq. (6.18) can be easily understood by considering that for the solid weight fraction ω_d/ω_s the following equality holds:

$$\frac{\omega_d}{\omega_s} = \frac{P + E + I + S}{W + M + P + E + I + V + S} = \frac{M^0 - M + E + I + S}{W + M^0 + E + I + V + S} \quad (6.19)$$

where M and P are the masses of monomer and of polymer (excluding the seed if present), respectively, in the reactor at the instant of sampling. Note that if the volatile additive is included into the polymer during the reaction, it will not evaporate in the drying and it will contribute to the solids. Therefore, its conversion needs to be known. However, compounds of this kind (e.g., volatile chain transfer agents) are usually used in such small amounts that the quantity V in eq. (6.18) can be safely neglected. In the present polymerization reactions no volatile additives were used, so V is rigorously zero.

The amount of solid inhibitor used in each glass vessel to stop the reaction after sampling was so small that it could be safely neglected when weighing the dry sample.

6.4.3 Polymer Particle Concentration

From polymer particle size and monomer conversion the polymer particle concentration was determined as:

$$N_P = \frac{M^0 \chi}{\rho_p v_{P,d} V_w} \quad (6.20)$$

where M^0 is the mass of charged monomer, $v_{P,d}$ the dry (unswollen) volume of one particle (calculated from the average diameter $d_{P,d}$ measured by PCS), ρ_p the polymer density and V_w the volume of water in the reactor. Eq. (6.20) assumes the particles to be monodisperse in size. This assumption needs to be checked.

6.4.4 Average Number of Free Radicals per Particle

The overall volume of the particle phase, i.e., the phase where the polymerization reaction takes place, is given by:

$$V_{TOT} = v_P N_P V_w \quad (6.21)$$

while the rate of reaction can be expressed in terms of the average number of radicals per polymer particle \bar{n} as:

$$r_p = k_p C_m \left(\frac{\bar{n}}{N_A v_P} \right) \quad (6.22)$$

where k_p is the propagation rate constant, C_m the monomer concentration in the particles and N_A Avogadro's number. Note that the term between brackets corresponds to

the average radical concentration in the particle phase. Substituting the previous expressions (6.21) and (6.22) in eq. (6.2) and rearranging, one obtains:

$$\bar{n} = \frac{\dot{Q}_r N_A}{k_p C_m N_P V_w (-\Delta H_P)} \quad (6.23)$$

which is the equation used to determine the average number of radicals per particle from the measured heat \dot{Q}_r and from the particle concentration N_P given by eq. (6.20).

Monomer concentration in the particles

To obtain values for \bar{n} from eq. (6.23), the monomer concentration in the particles C_m must be known. It is usually assumed that the monomer transport from the droplets to the particles is not rate-determining, i.e., the monomer concentration in the different phases is at thermodynamic equilibrium. According to this assumption, the monomer concentration C_m in the particles depends upon whether the reaction is in intervals I-II (the system is monomer saturated) or in interval III.

In intervals I and II the monomer concentration in the particle is fixed and given by:

$$C_m = \frac{\rho_m \phi_m}{M_m} \quad (6.24)$$

where ρ_m is the monomer density, $\phi_m = \phi_m^*$ is the volume fraction of monomer in the particles at saturation and M_m is the monomer molecular weight.

In interval III, C_m is still given by relation (6.24), but the volume fraction of monomer in the particles ϕ_m is no more at its saturation value ϕ_m^* . Instead, if the monomer is scarcely water soluble so that the amount in the aqueous phase can be neglected, it is given by:

$$\phi_m = \frac{\rho_p(1 - \chi)}{\rho_m \chi + \rho_p(1 - \chi)} \quad (6.25)$$

where ρ_p is the polymer density.

The conversion $\chi_{II \rightarrow III}$ at which interval II is over is obtained by imposing $\phi_m = \phi_m^*$ in eq. (6.25) (i.e., all of the monomer is in the particles - neglecting that in the aqueous phase - but the system is still monomer saturated). Solving for $\chi_{II \rightarrow III}$ gives:

$$\chi_{II \rightarrow III} = \frac{(1 - \phi_m^*) \rho_p}{\phi_m^* \rho_m + (1 - \phi_m^*) \rho_p} \quad (6.26)$$

Summarizing, eqs (6.24)-(6.26) permit to calculate C_m at all conversions if the system can be assumed at thermodynamic equilibrium with respect to monomer partitioning. Given a conversion value χ , this conversion is compared to $\chi_{II \rightarrow III}$ to establish whether

Parameter	Value	Reference
k_p	$2.7 \cdot 10^7 \text{ cm}^3 \text{ mol}^{-1} \text{ s}^{-1}$	[87]
M_m	128.2 g mol ⁻¹	
ΔH_P	18.6 kcal mol ⁻¹	[88, 89]
ϕ_m^*	0.66	[90]
ρ_m	0.87 g cm ⁻³	[91]
ρ_p	1.03 g cm ⁻³	[91]

Table 6.4: Parameters for the evaluation of experimental data of BA emulsion polymerization at 50°C.

the reaction is in intervals I-II or in interval III. In the former case, eq. (6.24) is used with $\phi_m = \phi_m^*$, else ϕ_m is given by eq. (6.25).

6.4.5 Parameters

The values of the parameters required for the experimental evaluation of monomer conversion, latex particle concentration and average number of radicals per particle according to the equations reported in Sections 6.4.1-6.4.4 are reported in Table 6.4 together with their literature source.

6.5 Results and Discussion

6.5.1 Ab Initio Reactions - Kinetics

The conversion versus time curves obtained by calorimetry for the five reactions whose recipes are reported in Table 6.1 are shown in Figs 6.3-6.7 together with the gravimetric conversion data. For reaction BA4 only a final gravimetric point is available because no intermediate sampling was performed in order to have a calorimetric signal as undisturbed as possible. For all reactions three final gravimetries were performed at the same reaction time to check the accuracy of the gravimetric measurement, at least at high conversion. It can be seen that the accuracy is excellent.

Comparing the calorimetric and gravimetric techniques, these are always in good agreement, which confirms that the approximations involved in the calorimetric evaluation of conversion (terms neglected or assumed constant in the heat flow balance, U and c_p coefficients assumed to vary linearly during the reaction) introduce negligible errors. With respect to the assumption of U and c_p coefficients varying linearly in time, the error introduced is small independently of the correctness of this assumption because the U coefficient varied in practice very little from beginning to end (never more than 5%) and because, being the temperature control fairly good (the maximum offset was 3°C) and

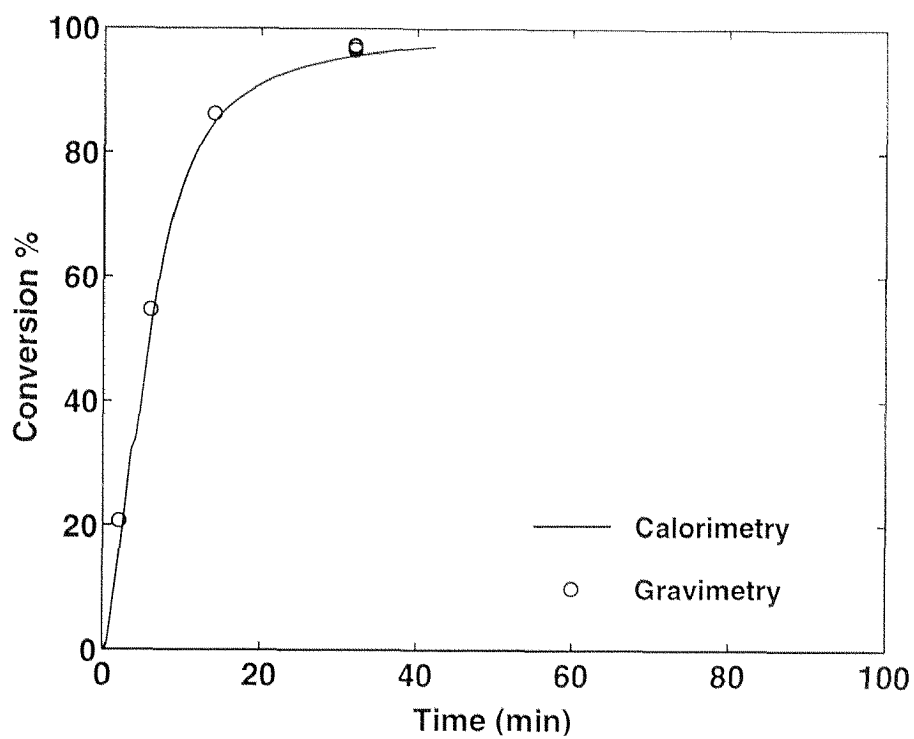


Figure 6.3: Conversion history for reaction BA2.

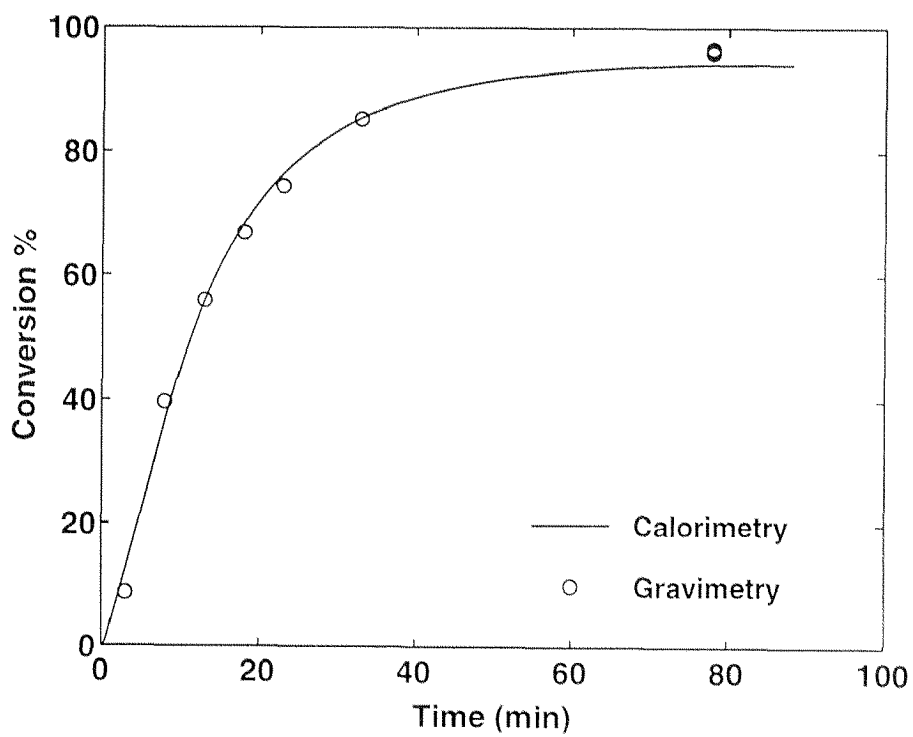


Figure 6.4: Conversion history for reaction BA3.

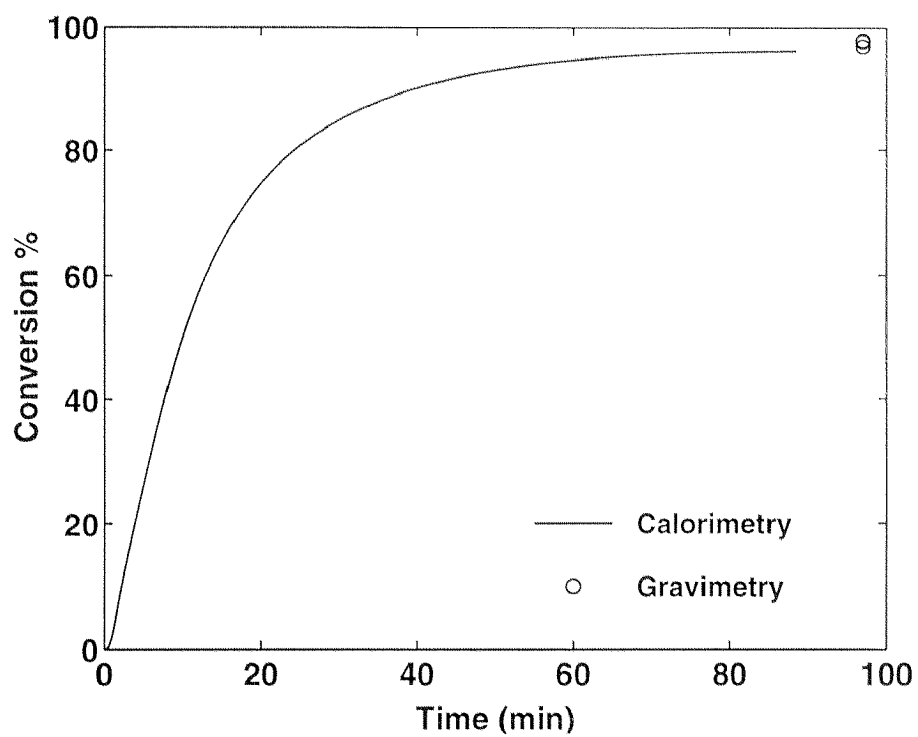


Figure 6.5: Conversion history for reaction BA4.

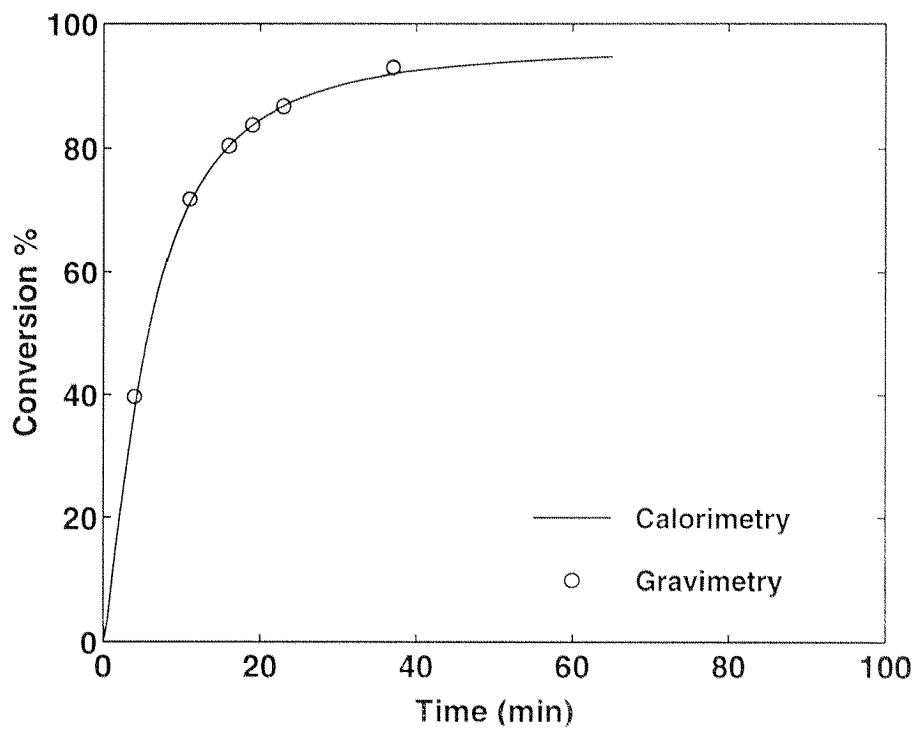


Figure 6.6: Conversion history for reaction BA5.

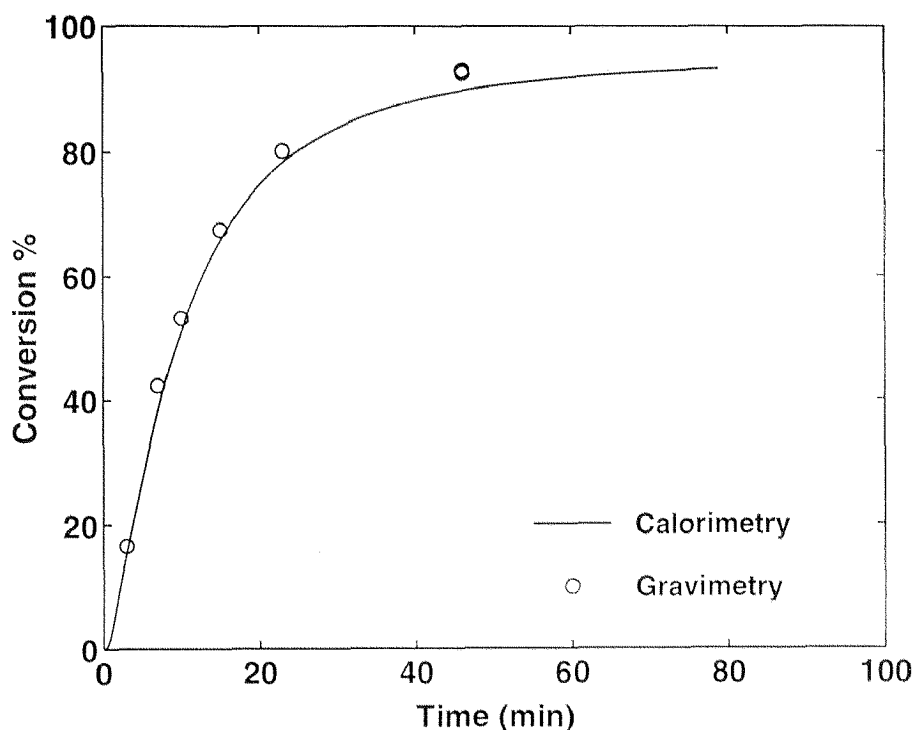


Figure 6.7: Conversion history for reaction BA6.

the c_p coefficient almost constant (it never varied more than 8% across the reaction), the accumulation term resulted small in all cases (always less than 0.5% of the flow term). While the gravimetric technique does not involve such assumptions and it requires a very simple instrumentation, it yields far less detailed information compared to calorimetry. In fact, calorimetry, besides giving a virtually continuous measurement, does not provide the conversion versus time curve but rather its derivative (cf. eq. (6.15)), from which a much deeper and unequivocal understanding of the kinetics of the system can be extracted. It has been shown for instance [80] that, while a constant rate of reaction period (identified with Smith-Ewart's interval II) would be inferred from discrete conversion versus time data in emulsion polymerizations of styrene, this constant rate period is not seen if the rate of reaction is observed directly through calorimetry. This clearly makes a great difference in the interpretation of the kinetics of the system. In the case of the BA emulsion polymerizations here examined, the situation is exactly the same. From the examination of the conversion versus time curves, one would deduce a constant rate up to about 40% conversion at least, which does not instead appear from a direct observation of the heat of reaction curves. These are reported in Fig. 6.8 as a function of conversion for reactions BA3-BA6. The signal from reaction BA2 was very disturbed by the sampling and is not reported. All reactions exhibit a sharp peak at the beginning. This peak may be due

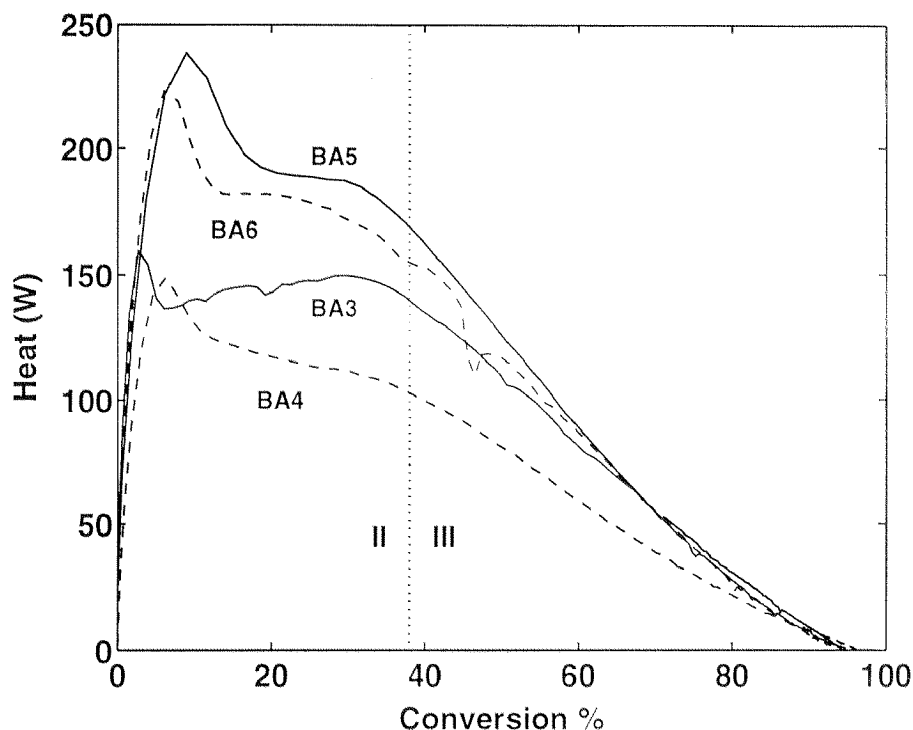


Figure 6.8: Reaction heat as a function of conversion for reactions BA3-BA6.

to the fast coagulation of nuclei which have formed extremely rapidly at the start of the reaction (as is proved by the very rapid start of the polymerization). The coagulation of nuclei quickly reduces the particle number and consequently the reaction rate. The behavior of the heat curves after the peak is not the same for all reactions. In two cases (BA5 and BA6) a constant rate is achieved, in another case (BA3) the rate increases and, finally, in the last case (BA4) it decreases. In all cases, however, a point is reached where the released heat begins to decrease or to decrease more rapidly (BA4). This happens always before (but not too far from) the conversion at which the transition from interval II to interval III theoretically occurs (see eq. (6.26)), represented in Fig. 6.8 by the vertical dotted line.

The evolution of particle concentration for reactions BA2, BA3, BA5 and BA6 as given by eq. (6.20) is shown in Fig 6.9 as a function of conversion (determined by gravimetry). All reactions exhibit a growing particle concentration in the first reaction period, after which the concentration increases so slightly that it can be considered practically constant. No monotonic relation is found in reactions BA2, BA3 and BA6 between initiator and final particle concentration, which indicates that the change in initiator concentration is too small among these three reactions to overcome experimental error.

The evolution of the average number of radicals per particle \bar{n} as a function of conver-

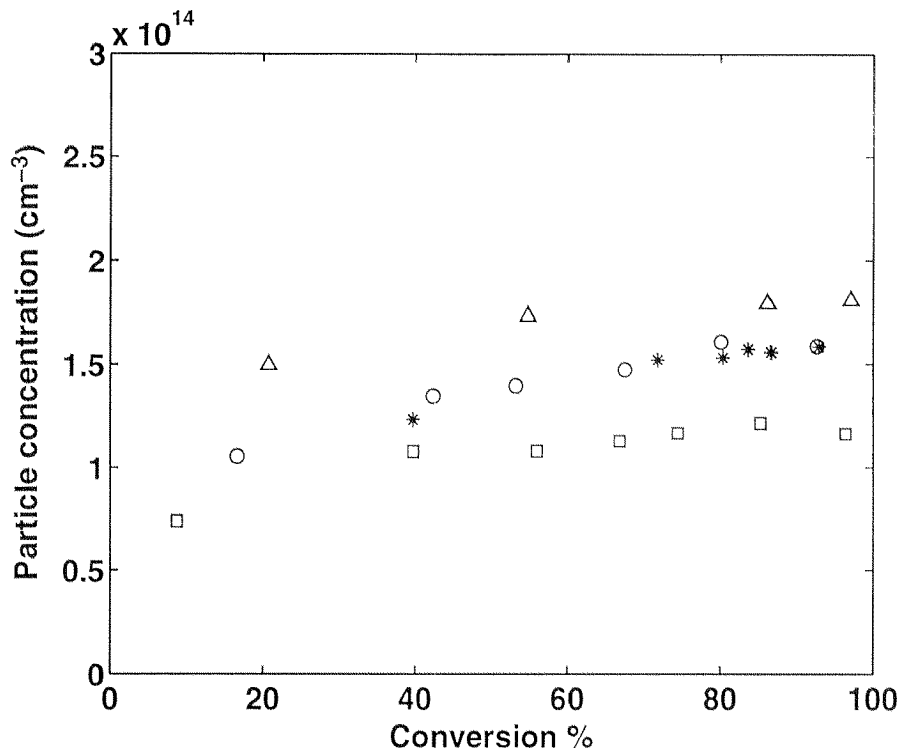


Figure 6.9: Particle concentration as a function of conversion; Δ : BA2, \square : BA3, * : BA5 and \circ : BA6.

sion is reported in Fig 6.10 for reactions BA3, BA5 and BA6 as calculated from eq. (6.23), assuming the system to be at thermodynamic equilibrium with respect to monomer partitioning (eqs (6.24)-(6.26)). The minor deviation from the set temperature of 50°C was taken in account in the calculation of the propagation constant k_p according to the Arrhenius equation given in ref. [87]. The calorimetric signal of reaction BA2 was far too disturbed by the sampling to extract from it reliable information on the evolution of \bar{n} . In all cases, very small values of the average number of radicals per particle are obtained (always smaller than 0.13), which implies a significant role of the desorption mechanism, and \bar{n} decreases almost linearly (especially for reactions BA5 and BA6) with conversion. The reasons for such small values of \bar{n} and its decrease with conversion are not obvious. With respect to the small values, BA is a poorly water-soluble monomer (comparable, for instance, to styrene [1]) and therefore expected not to give significant desorption. With respect to the decrease with conversion, increasing particle volume (up to the end of interval II, in interval III the volume undergoes a slight contraction) and increasing intraparticle viscosity (in interval III), imply decreasing bimolecular termination and desorption frequencies. This would let one expect increasing values of \bar{n} with conversion. Other effects must therefore be invoked to explain the decreasing behavior. The use of a mathematical

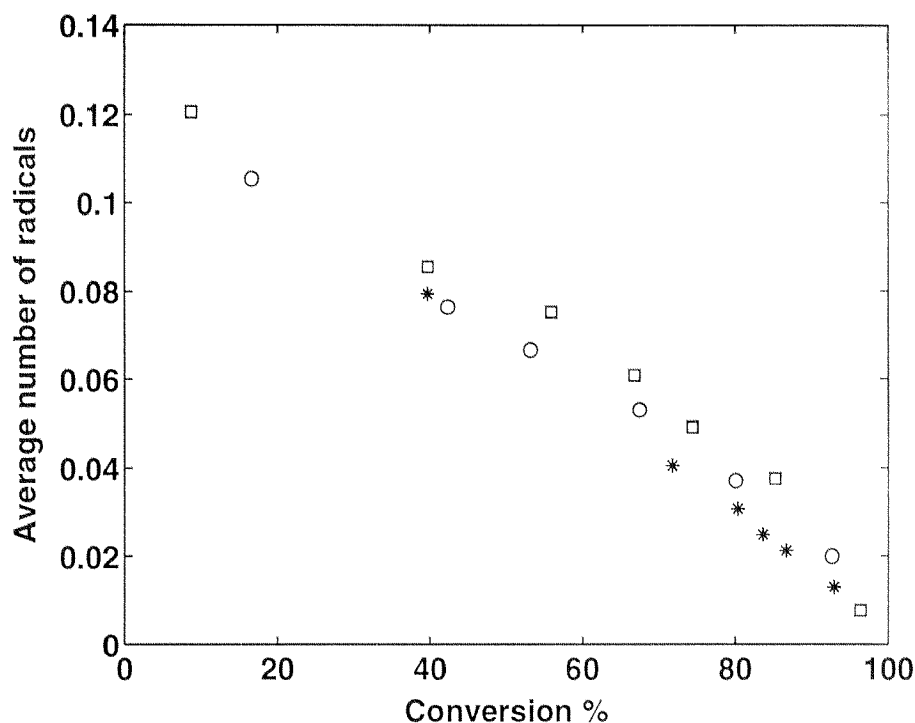


Figure 6.10: Average number of free radicals per particle as a function of conversion; □ : BA3, * : BA5 and ○ : BA6.

model is helpful in interpreting these unexpected results and is considered in Section 6.6.

6.5.2 Ab Initio Reactions - Gel Formation

The microgel weight fraction separated by ultracentrifugation is reported for reactions BA2, BA3, BA5 and BA6 in Figs 6.11-6.14. Both the direct and indirect measurements (i.e., obtained by weighing the dry precipitate or the dry solute, respectively) are reported. The agreement is very good at all conversions. The measurement was repeated for two samples (at 85% conversion in reaction BA3 and at 93% conversion in reaction BA5) and shows good reproducibility. For all reactions a significant amount of gel is never measured before 70% conversion. All measurements at lower conversions give a small amount of gel (up to maximum 3%) but this is most probably due to a small amount of solute which remained on the walls of the centrifuge tube. Actually, not even a very small amount of gel precipitate could be distinguished for these samples, while at higher gel fractions a precipitate of gelatinous consistency could be clearly seen at the bottom of the tube. Therefore, the small values of gel fraction which are obtained at lower conversions have to be most probably interpreted as zero gel. The formation and fast growth of significant amounts of gel apparently occurs after 70% conversion, so that the 'gel point' can be defined to occur between 70% and 80% conversion (actually, before 75% for reaction BA3

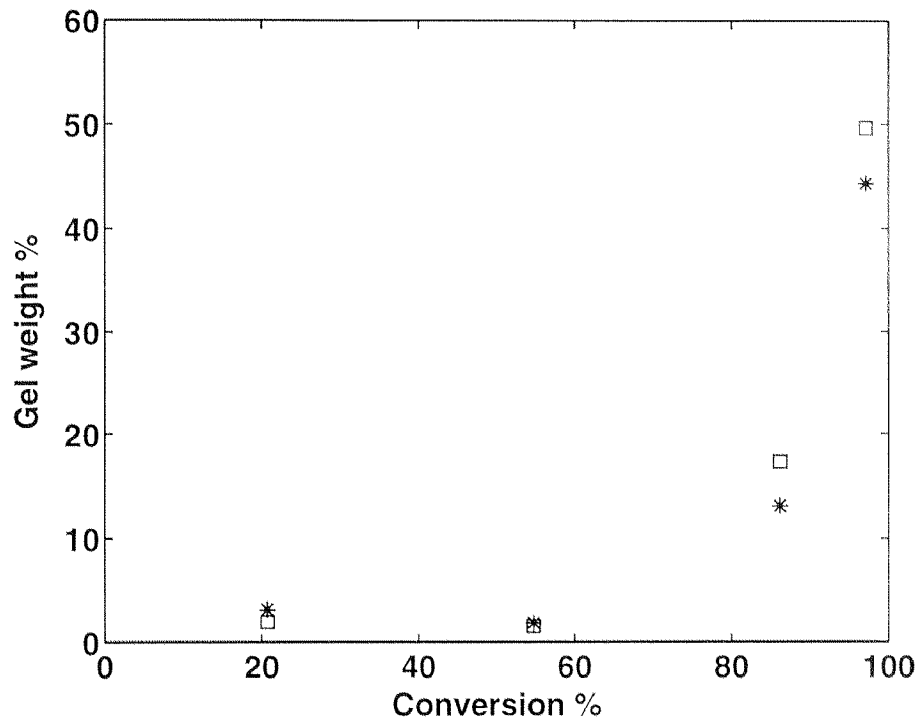


Figure 6.11: Gel weight percentage as a function of conversion for reaction BA2; □ : direct method, * : indirect method.

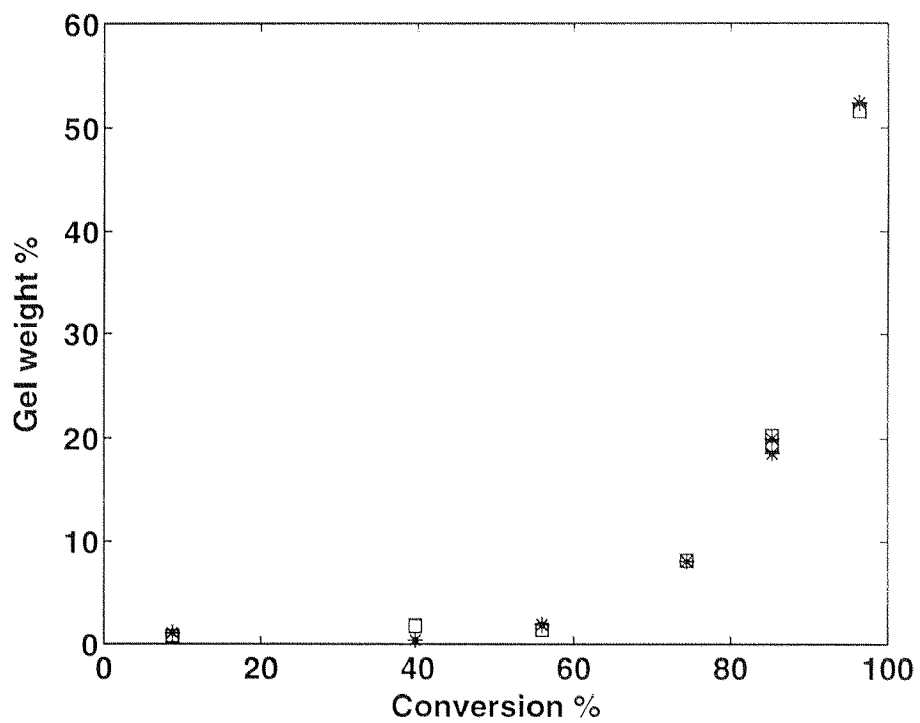


Figure 6.12: Gel weight percentage as a function of conversion for reaction BA3; □ : direct method, * : indirect method.

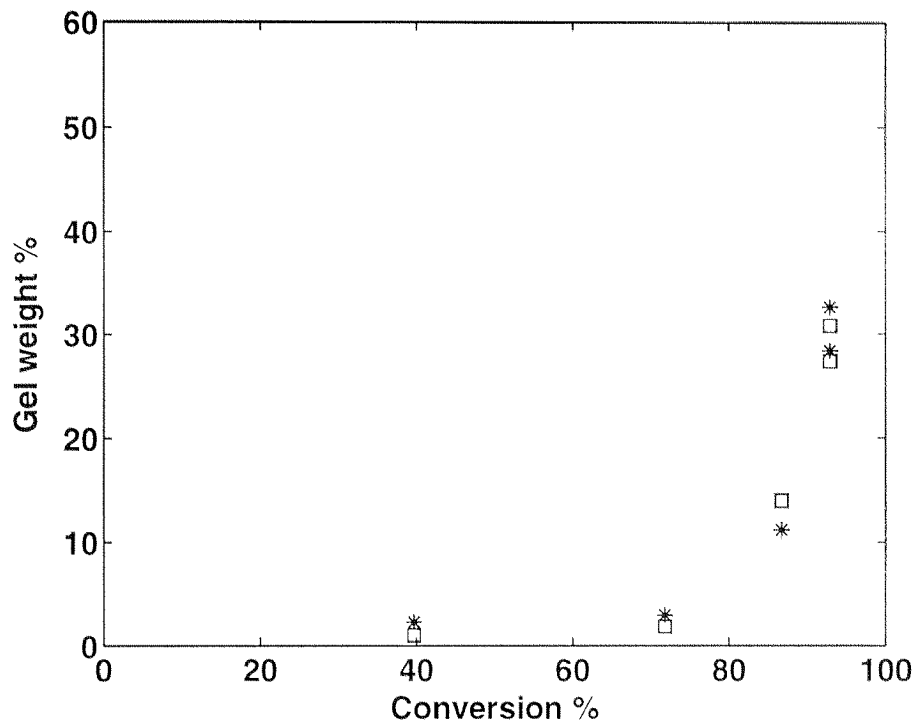


Figure 6.13: Gel weight percentage as a function of conversion for reaction BA5; □ : direct method, * : indirect method.

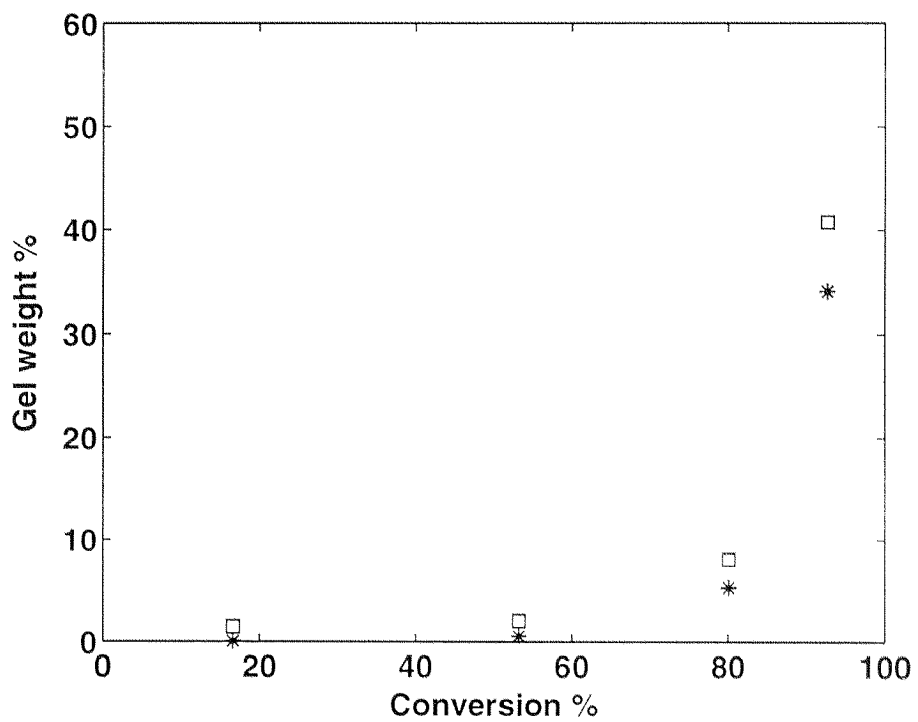


Figure 6.14: Gel weight percentage as a function of conversion for reaction BA6; □ : direct method, * : indirect method.

and after 70% for reaction BA5, in all cases certainly after 55%).

6.5.3 Seeded Reactions - Kinetics

The conversion vs. time curves for two seeded reactions (BA5 and BA9) is shown in Figs 6.15 and 6.16. Samples for gravimetric determination of conversion were taken only at the beginning and at the end of the reaction, to check for initial and final conversion. Two samples were taken at the end and the accuracy of the measurement is seen to be very good. Moreover, the final conversion measured by gravimetry is in good agreement with the calorimetric value. Compared to the ab initio reactions, the temperature control was even better (maximum offset 1.5°C) and the variation of the U coefficient during the reaction smaller (never more than 2.5%). Therefore, the assumptions involved in the evaluation of the heat data should be even better satisfied.

The conversion history is apparently similar in behavior to the ab initio reactions. However, if the heat of reaction is observed, instead of its integral, it is clear that the kinetic behavior is not the same. In Fig. 6.17 the heat of reaction is reported as a function of conversion for reactions BA1, BA6, BA7 and BA8 (reactions at lower particle concentration). In Fig. 6.18 the same quantity is shown for reactions BA2, BA3 and BA4 (reactions at higher particle concentration). The typical peak in the reaction rate detected at the beginning of the ab initio reactions is never observed in the seeded runs. This is in agreement with the explanation proposed for the peaks, involving the formation of instable nuclei. In the presence of the seed, the radicals formed from the initiator are captured from the start of the reaction by the polymer particles and the formation of such nuclei is prevented. The reactions at lower particle concentration (Fig. 6.17) show a quite extended region where the rate is next to being constant, though never rigorously constant. At the higher reaction rates (BA6 and BA8) the rate keeps slightly increasing up to 10-15% conversion beyond the conversion at which the passage from interval II to III should theoretically occur (vertical dotted line). This could be explained by some secondary nucleation occurring at higher initiator concentrations. Observing the TEM graphs of the final samples, a high polydispersity of the particle diameters is actually found, which could include the effect of secondary nucleation. However, the presence of two distinct populations is not detected, so that the amount of (eventual) secondary nucleation is not straightforward to calculate. To have an estimate of the increase in number of the particles during the reaction, the particle concentration in the final latex was calculated from the final diameter measured by PCS and the final conversion, assuming all the particles to be the same in size (eq. (6.20) corrected for a non-zero initial particle volume). The increase

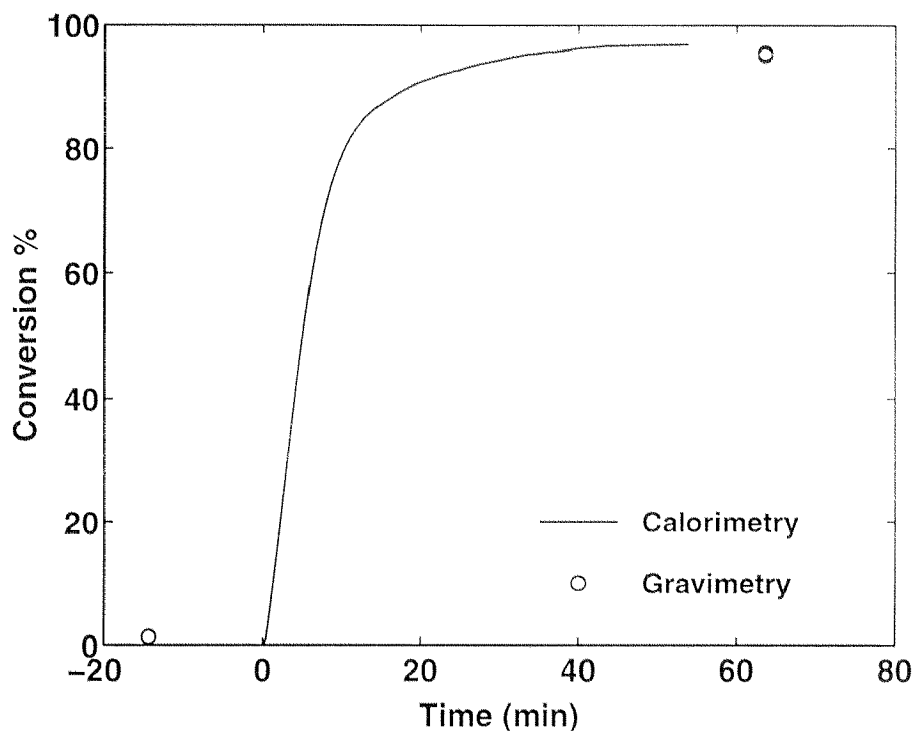


Figure 6.15: Conversion history for reaction BA6.

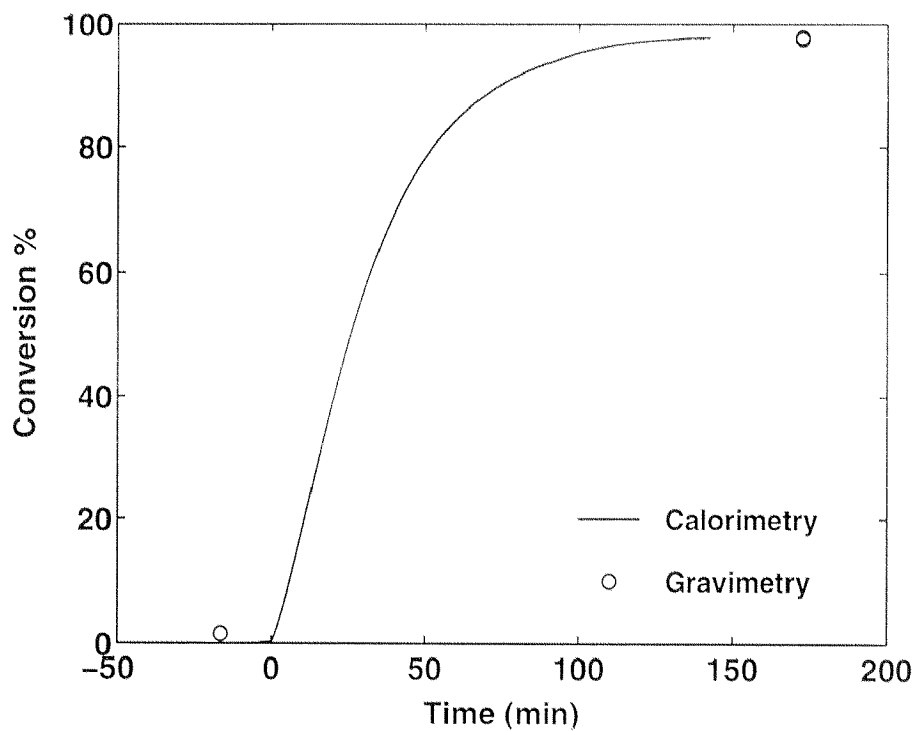


Figure 6.16: Conversion history for reaction BA9.

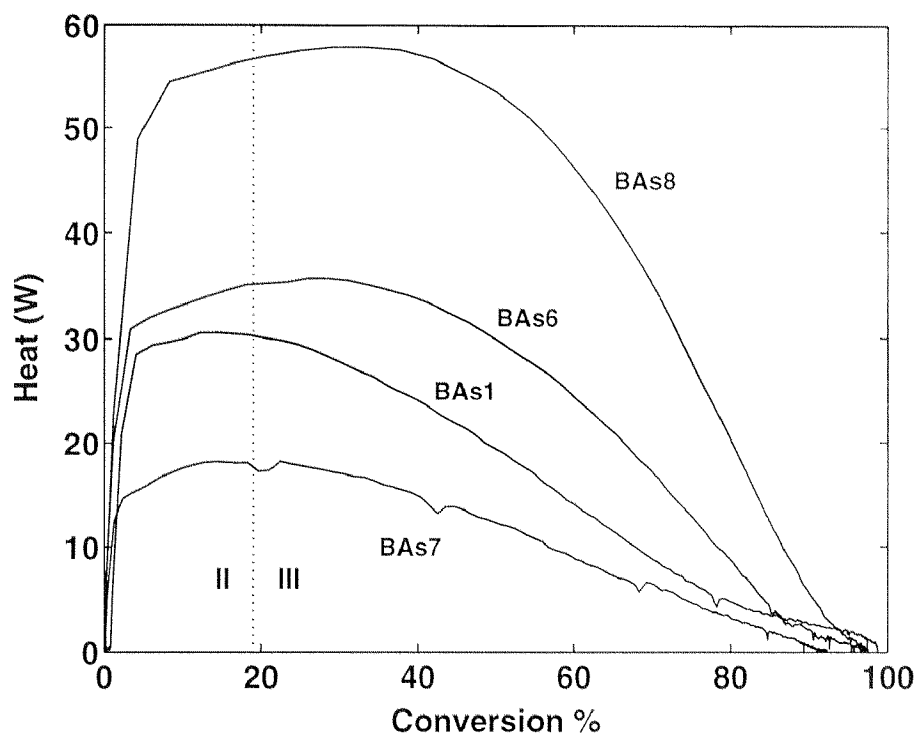


Figure 6.17: Reaction heat as a function of conversion for reactions at $N_P \cdot 10^{13} \text{ cm}^{-3}$ and different initiator concentrations.

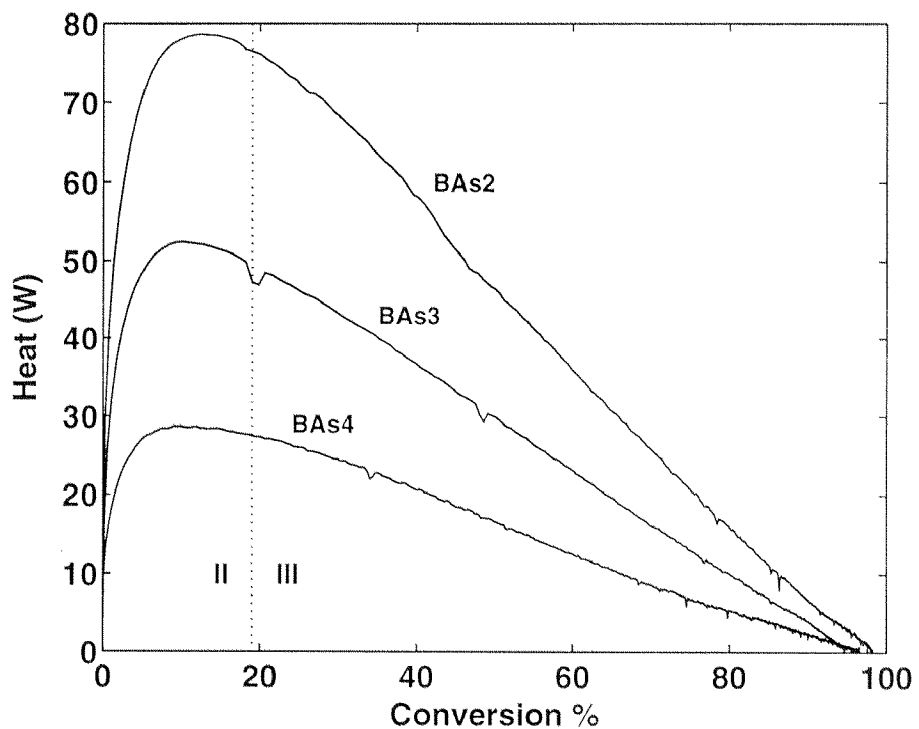


Figure 6.18: Reaction heat as a function of conversion for reactions at $N_P \cdot 10^{14} \text{ cm}^{-3}$ and different initiator concentrations.

Reaction	Concentration increase (%)
BAs1	25.0
BAs2	19.1
BAs3	8.7
BAs4	8.9
BAs5	8.6
BAs6	23.2
BAs7	27.2
BAs8	27.2
BAs9	29.4

Table 6.5: Increase per cent in particle concentration for the seeded reactions.

per cent of the particle concentration calculated in this way is reported in Table 6.5 for all reactions. This is never more than 30%, which implies, since no small particles are detected by TEM, that secondary nucleation is not very significant. No monotonic relation is observed between particle or initiator concentration and increase in particle number.

Another hypothesis which can be put forth to justify the shift in maximum reaction rate in Fig. 6.17, is that the reaction is limited in rate by the diffusion of the monomer from the droplets to the particles. If this is true, the conversion at which the monomer droplets disappear is delayed at increasing initiator concentrations, and this could result in a delay of the point where the reaction rate starts to decrease. However, the calculations reported in Appendix F show that monomer diffusion limitations do not explain the presence a maximum. Rather, transfer limitations would cause the reaction rate to decrease continuously with conversion.

Reaction BAs9 was performed with a larger amount of monomer to have a higher theoretical conversion at which the droplets disappear ($\chi_{II \rightarrow III} = 30\%$), and therefore a more extended region where the particles are saturated with monomer. The initiator and particle concentration were the same as in reaction BAs7. It can be seen in Fig. 6.19 that a constant rate of reaction is actually achieved for a 10% conversion interval, and that the rate starts to decrease at $\chi_{II \rightarrow III} = 30\%$ (vertical dotted line in the figure). It is interesting to note that the reaction heat at the plateau is virtually equal to the heat at the maximum in reaction BAs7 (approx. 18 W), even though the monomer charged is different in amount. This is a consequence of the mechanism of emulsion polymerization, where the reaction heat is determined not by the overall amount of monomer, but by the saturation concentration (if the monomer is enough to saturate the particles), besides initiator concentration and particle number.

The reaction rate at the maximum for each reaction was taken as representative of

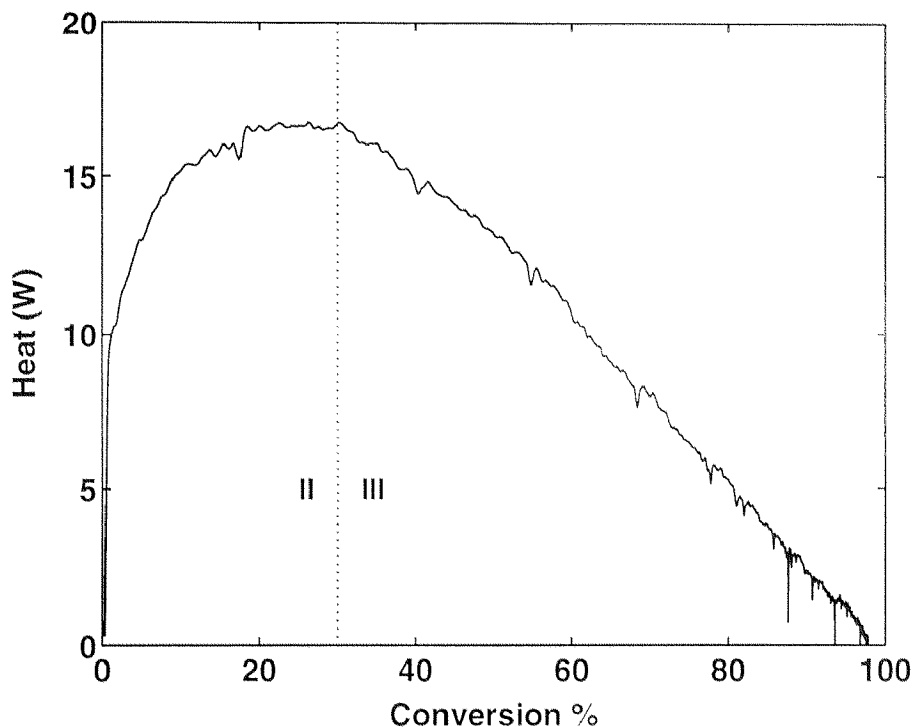


Figure 6.19: Reaction heat as a function of conversion for reaction BAs9.

the reaction rate at monomer saturation conditions to estimate the average number of radicals per particle. To this purpose eq. (6.23) was used. The particle concentrations are given in Table 6.3, and the other parameters in Table 6.4. A significant way of representing average number of radicals per particle data in reactions at different initiator and particle concentrations is according to the approach proposed by Ugelstad et al. [92]. Following these authors, \bar{n} is represented as a function of three dimensionless parameters, $\bar{n} = \bar{n}(\alpha_I, m, Y)$, with:

$$\alpha_I = \frac{\mathcal{R}_I N_A}{N_P c} \quad (6.27)$$

$$m = \frac{k_d}{c} \quad (6.28)$$

$$Y = \frac{k_{t,w} c}{k_e^2 N_P N_A} \quad (6.29)$$

Parameter α_I is the ratio between the rate of radical generation in the water phase (per particle) and the frequency of bimolecular termination, while m is the ratio between the desorption and bimolecular termination frequencies. Parameter Y accounts for the importance of water phase termination. It is zero if $k_{t,w} = 0$. Note that expression (6.29) for Y results only if the entry rate ρ is given by eq. (5.1). More generally:

$$Y = \frac{k_{t,w} c R_w^\bullet N_A}{\rho^2 N_P} \quad (6.30)$$

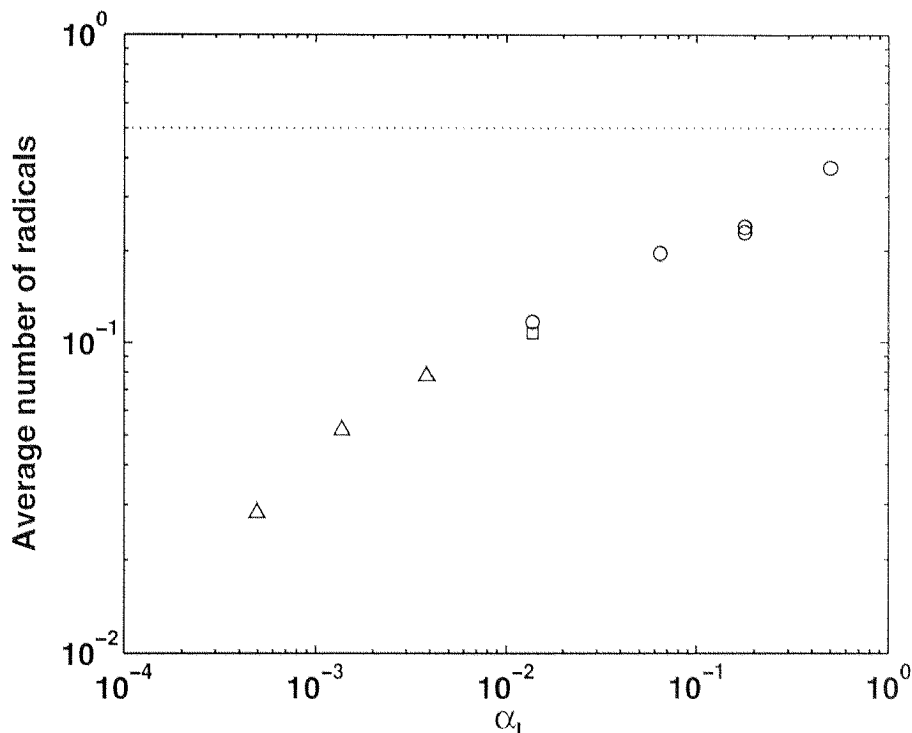


Figure 6.20: Average number of free radicals per particle as a function of the dimensionless parameter α_I for the seeded reactions. Δ : reactions at high N_P , \circ : reactions at low N_P , \square : reaction BAs9. Dotted line: Smith-Ewart case 2 ($\bar{n} = 0.5$).

The average number of radicals per particle \bar{n} can be represented as a function of α_I , considering m and Y as parameters. In this case, logarithmic diagrams are obtained where \bar{n} increases with α_I . Depending on the values of m and Y , a plateau may appear. This plateau reduces to an inflection point and eventually disappears at increasing values of the desorption parameter m . What is most relevant is that, if a plateau or an inflection point are observed, these correspond always to $\bar{n} = 0.5$.

If the \bar{n} values calculated using the maximum reaction rate are plotted as a function of α_I for all seeded reactions, the diagram reported in Fig. 6.20 is obtained. In this diagram an inflection point can be observed which is however below $\bar{n} = 0.5$. The data can be considered to be at a virtually constant value of m , since the particle dimension is the same at the beginning for all reactions, and a rate very near to that measured at the maximum is reached at very early conversions in all cases. Moreover, it has been shown [93] that \bar{n} is independent of Y (which is a function of particle concentration) on the left of the plateau or of the inflection point, if this is present. The data, the reproducibility of which is quite good, suggest therefore that the values of \bar{n} obtained experimentally are systematically underestimated. This must be due to the incorrect value of one or more quantities appearing in eq. (6.23). The discussion about the reliability of each of these

Parameter	Value	Reference
c_{fm}	$5.6 \cdot 10^{-5}$	[94]
$C_{m,w}^*$	$6 \cdot 10^{-6} \text{ mol cm}^{-3}$	[91]
D_p	$5.2 \cdot 10^{-6} \text{ cm}^2 \text{ s}^{-1}$	[94]
D_w	$7.5 \cdot 10^{-6} \text{ cm}^2 \text{ s}^{-1}$	[73]
k_I	$1.7 \cdot 10^{-6} \text{ s}^{-1}$	[71]
k_p	$2.7 \cdot 10^7 \text{ cm}^3 \text{ mol}^{-1} \text{ s}^{-1}$	[87]
$k_{t,w}$	$3.7 \cdot 10^{12} \text{ cm}^3 \text{ mol}^{-1} \text{ s}^{-1}$	[64]
M_m	128.2 g mol^{-1}	
ϕ_m^*	0.66	[90]
ρ_m	0.87 g cm^{-3}	[91]
ρ_p	1.03 g cm^{-3}	[91]

Table 6.6: Parameters for BA emulsion polymerization at 50°C.

quantities is reported in Section 6.6.2, where a quantitative analysis of the \bar{n} values is reported.

6.6 Model Interpretation

6.6.1 Parameters

The parameters used in the kinetic model (Chap. 2 and Section 5.2) were taken from the literature and are listed in Table 6.6 together with their source. Some remarks ought to be made about the values of these parameters.

Considering reaction rate coefficients, the chain transfer constant c_{fm} (ratio between the chain transfer to monomer rate constant k_{fm} and the propagation rate constant k_p) reported in Table 6.6 was measured by Maeder and Gilbert [94] from the slope of the logarithmic plot of the MWD of PBA produced in a “hetero-seeded” emulsion polymerization carried out in zero-one conditions with slow entry. A polystyrene seed was used to avoid having chain transfer to polymer. The value reported by these authors seems to be more reliable than those reported by Beuermann et al. [95] and by Devon and Rudin [96]. Beuermann et al. report a value $c_{fm} = 1.3 \cdot 10^{-4}$. However, these authors observe no temperature dependence of the c_{fm} constant, i.e., same activation energies for transfer and propagation, which seems unlikely from consideration of the transition states involved in the two reactions. The value $c_{fm} = 2.5 \cdot 10^{-4}$ at 60°C reported by Devon and Rudin, which differs significantly from $c_{fm} = 7 \cdot 10^{-5}$ reported by Maeder and Gilbert at the same temperature, was inferred by modeling copolymerization reactions with styrene where the highest mole fraction of BA was $x_{BA} = 0.65$ and neglecting branching in the data analysis. A value $c_{fm} = 5.4 \cdot 10^{-5}$, very similar to that reported by Maeder and Gilbert for BA,

was previously reported for butyl methacrylate [97].

While the propagation rate constant was once thought to have a value of the order of $5 \cdot 10^5 \text{ cm}^3 \text{ mol}^{-1} \text{ s}^{-1}$ [91], recent advances in the measurement of propagation rate constants in free radical polymerization (by pulsed laser techniques) show that BA is much more reactive than formerly believed. The value of k_p reported in Table 6.6 results from Arrhenius constants obtained by pulsed laser polymerization reactions carried out between -7°C and -45°C [87]. Data obtained between 5°C and 30°C through the same technique yield a value $k_p = 2.1 \cdot 10^7 \text{ cm}^3 \text{ mol}^{-1} \text{ s}^{-1}$ at 50°C [95], while the combined use of the two sets of data in the different temperature ranges yields a value $k_p = 2.8 \cdot 10^7 \text{ cm}^3 \text{ mol}^{-1} \text{ s}^{-1}$ at 50°C [95], which is very near to the value given in [87].

In the absence of specific data, the propagation rate constant in the water phase $k_{p,w}$ has been assumed to be the same as that in the particle phase k_p .

Considering monomer concentrations, a value of the concentration of monomer in water at saturation $C_{m,w}^* = 6.4 \cdot 10^{-6} \text{ mol cm}^{-3}$, i.e., very similar to that reported in Table 6.6, is reported by Capek et al. [90].

Several values can be found in the literature for the concentration of monomer in the particles at saturation. These lie in the range $3 \div 5 \cdot 10^{-3} \text{ mol cm}^{-3}$ [1, 90, 91, 97]. The value of the monomer volume fraction in the particles at saturation $\phi_m^* = 0.66$ given in Table 6.6 corresponds to a value $C_m^* = 4.5 \cdot 10^{-3} \text{ mol cm}^{-3}$ taken from [90].

Considering diffusion coefficients, the value of the diffusion coefficient for a monomeric species in the particle phase D_p given in Table 6.6 was calculated as in [94] from the experimentally determined relationship for butyl methacrylate oligomers as a function of polymer weight fraction:

$$D_i(w_p)/\text{cm}^2\text{s}^{-1} = \frac{1.69 \cdot 10^{-5} - 4.5 \cdot 10^{-5}w_p + 3.72 \cdot 10^{-5}w_p^2}{i^{(0.664+2.02w_p)}} \quad (6.31)$$

where i are the units in the oligomer and w_p is the polymer weight fraction. The value $D_p = 5.2 \cdot 10^{-6} \text{ cm}^2 \text{ s}^{-1}$ in the table corresponds to $i = 1$ and $w_p = 0.38$, i.e., the polymer weight fraction in the particles at saturation (calculated from the ϕ_m^* , ρ_m and ρ_p values given in Table 6.6).

The diffusion coefficient for a monomeric species in water D_w in Table 6.6 was calculated from the Wilke and Chang equation [73] for liquid in liquid diffusion, rather than taking the value reported for styrene ($D_w = 10^{-6} \text{ cm}^2 \text{ s}^{-1}$) as it was done elsewhere [91, 97].

To calculate the ratio c_t between the bimolecular termination rate coefficient k_t and the propagation rate coefficient k_p , the relation given by Buback and Degener [98] was

used:

$$c_t = k_t/k_p = c_{RD}(1 - w_p) \quad (6.32)$$

with $c_{RD} = 1500 \pm 300$ and w_p polymer weight fraction in the reaction locus (conversion in a bulk). Note that k_t in eq. (6.32) is defined so that the rate of termination in a bulk is $r_t = 2k_t R^{\bullet 2}$. Therefore, $c = k_t/N_A v_P$. Relation (6.32) was obtained from data from laser-induced polymerization experiments performed in bulk over wide ranges of temperatures and pressures and is valid above $w_p = 0.1$. Data up to $w_p = 0.8$ were available. The linear dependence of c_t on conversion in eq. (6.32) follows from the fact that the termination reaction is reaction (propagation) diffusion controlled already above 10% conversion [98]. It has of course to be considered whether the use of relation 6.32, obtained in a bulk system, can be extended to emulsion polymerization. It may in fact be expected that the bimolecular termination in emulsion polymerization involves newly entered short (i.e., rapidly diffusing) radicals and that the determining mechanism is different, giving faster termination rates. As a matter of fact, calculations by Maeder and Gilbert [94] have shown that at unswollen particle diameters larger than 60 nm already the probability of an incoming radical of propagating significantly (e.g. to 50 units) rather than terminating with a pre-existing radical is very high. As the length of the radical grows, its diffusivity decreases and the termination reaction becomes reaction diffusion controlled, i.e., eq. (6.32) must be valid. The length of a radical at which a diffusion controlled law for radical termination yields the same value of the termination constant as given by eq. (6.32) (i.e., above which diffusion can be considered not to be rate determining) can be estimated at the different polymer weight fractions. For instance, at $w_p = 0.38$ (saturation conditions), eq. (6.32) yields $k_t = 2.5 \cdot 10^{10} \text{ cm}^3 \text{ mol}^{-1} \text{ s}^{-1}$. The same value is obtained from a diffusion-controlled (Smoluchowski) expression for k_t [94]:

$$k_t^i = 4\pi D_i \sigma N_A p \quad (6.33)$$

when $D_i = 1.9 \cdot 10^{-8} \text{ cm}^2 \text{ s}^{-1}$. In eq. (6.33), i is the length of the oligomer (the mate radical is assumed 'long'), and it has been taken $\sigma = 7 \text{ nm}$ and $p = 0.25$ [94]. From eq. (6.31) with $w_p = 0.38$, a length $i = 50$ is estimated corresponding to this D_i value. Since the probability of propagating to this length is very high already at small particle sizes, the use of eq. (6.32) even at low conversions is justified (consider for instance that an unswollen particle diameter $d_{P,d} = 87 \text{ nm}$ was measured in reaction BA3 at 9% conversion).

While the propagation rate constant in the aqueous phase has been assumed to be the same as in the particle phase, this would not be correct for the bimolecular termination rate constant. In fact, it has been shown that the aqueous phase termination of oligomeric

radicals in the water phase is diffusion limited [1]. Therefore, the diffusion-controlled value $k_{t,w} = 3.7 \cdot 10^{12} \text{ cm}^3 \text{ mol}^{-1} \text{ s}^{-1}$ [64] has been taken.

With respect to the mechanism of bimolecular termination, it is believed that PBA, like other poly(alkyl acrylates), terminates predominantly by combination [36]. This is also supported by the ease with which a gel phase is formed in this polymerization system [79].

The value of the chain transfer to polymer rate constant is not available in the literature for PBA. Branching density data obtained by NMR spectroscopy have been presented by Lovell et al. for PBA produced both in emulsion [99] and solution [100]. Ref [100] contains extensive branching data at different conversions and initial monomer concentrations in solution which can be used for estimating the chain transfer constant. This is however complicated by the very important role of the backbiting reaction, which is proved by the high branching densities at low conversion for reactions with low initial monomer concentrations [100].

6.6.2 Model Results

The model was first applied to describe the kinetic behavior of the system. Rather than trying to describe the cumulative history represented by the conversion profiles, it was checked whether the model is able to describe the measured instantaneous rates of reaction, given the measured particle number. In other words, the description of the evolution of particle number was at first skipped and it was checked whether the use of the equations for the calculation of the average number of radicals per particle \bar{n} (Section 5.2) could describe the experimental values at different conversions (Fig 6.10), given conversion and particle number. In Fig. 6.21 the comparison between theoretical and experimental points is shown for reaction BA6. A value of the entry parameter $k_e = 4 \cdot 10^{-15} \text{ cm}^3 \text{ s}^{-1}$ in eq. (5.1) was taken. The same value was taken for the re-entry parameter k_{re} in eq. (5.5). No effect of the enhancement of viscosity at increasing polymer fractions in the particles was included in the description of the desorption mechanism, i.e., a constant $D_p = 5.2 \cdot 10^{-6} \text{ cm}^2 \text{ s}^{-1}$ was considered. The slight decrease of initiator concentration with time was included, and the effect of the moderate deviation from the set point of 50°C on k_p was verified to be negligible. Though the k_e value was appropriately chosen to have quantitative agreement at intermediate conversions, it is clear that the predicted behavior of \bar{n} is not in agreement with the experimental one. Neglecting the discrepancy for the point at the lowest conversion (which might be attributed to the presence of nucleation in the real system, see Fig. 6.9, and not in the model), the slight decrease of the calculated values

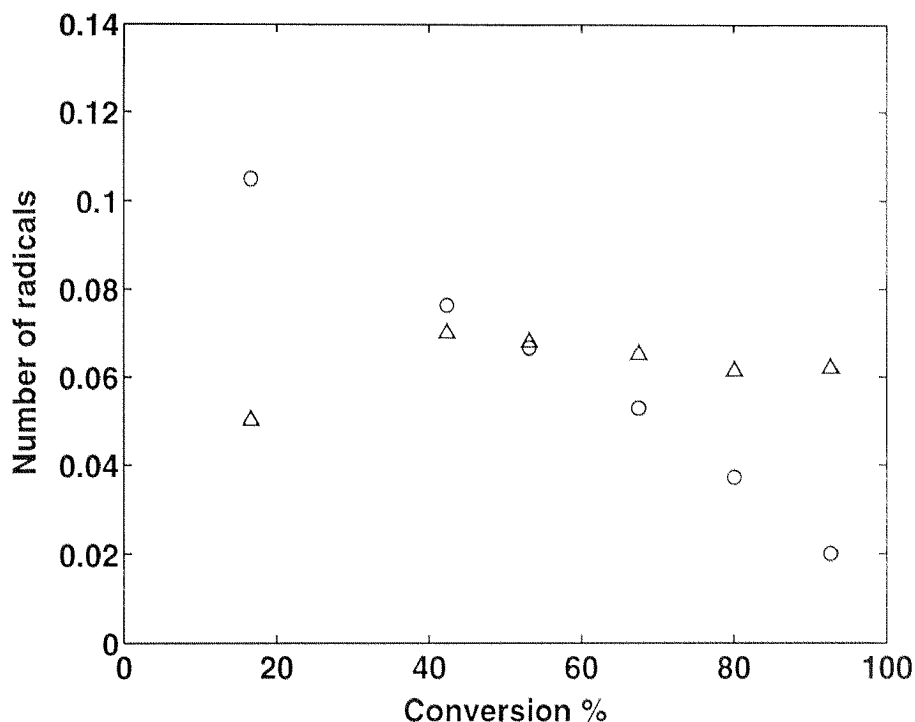


Figure 6.21: Average number of radicals as function of conversion for reaction BA6; \circ : experimental, \triangle : model. Parameters in Table 6.6 and $k_e = k_{re} = 4 \cdot 10^{-15} \text{ cm}^3 \text{ s}^{-1}$

due mainly to the contraction of particle volume in interval III is far from describing the strong decrease observed experimentally. Therefore, since the very slight decrease in particle size in interval III cannot justify marked increases in the frequency of desorption k_d or of termination c , the reason for the decreasing behavior of \bar{n} has to be sought in a decrease of the entry rate with conversion. Effects changing desorption and termination rates, such as intraparticle viscosity changes, diminish k_d and c at increasing conversions and worsen the agreement between model and experiment.

A possible mechanism to explain entry rates decreasing with conversion, is to assume that the process of entry is rate limited by propagation in the aqueous phase [64]. Namely, it is assumed that a radical produced from the water-soluble initiator, ionic in nature, must add a few monomer units in the aqueous phase before its entry in the particle phase is favored. This propagation step is considered to be rate determining for the process. At increasing conversions (if in interval III) the monomer concentration in the water phase, as well as in the particle phase, is decreasing. Thus, the propagation in the water phase gets slower. This results in a higher probability for termination of the oligomers in the water phase (compared to propagation and subsequent entry) and in lower entry rates. A quantitative treatment of this effect can be made considering the equation given by

Maxwell et al. [64] for propagation limited entry:

$$\rho_I = 2k_I[I]_w \frac{N_A}{N_P} \left(\frac{k_{t,w}R_w^\bullet}{k_{p,w}C_{m,w}} + 1 \right)^{1-z} \quad (6.34)$$

where ρ_I is the portion of entry related to initiator-derived radicals and z is the critical length for entry. Eq. (6.34) was obtained assuming that initiator-derived radicals of length below z are not capable of irreversible entry, while those of critical length z give irreversible entry faster than any other reaction. Though this is of course a simplified picture, it supposes propagation in the water phase to be rate determining. Moreover, eq. (6.34) was found to be in accord with entry data for styrene at 50°C.

In the frame of this model, the overall entry frequency ρ is obtained adding to the entry ρ_I of initiator-derived radicals the entry ρ_D of desorbed non-ionic radicals. This is simply obtained by multiplying the rate of desorption by the probability of re-entry (compared to that of termination in the water phase):

$$\rho_D = k_d \bar{n} (1 - P_R) \quad (6.35)$$

where

$$P_R = \frac{k_{t,w}R_w^\bullet}{k_{t,w}R_w^\bullet + k_{re}N_P} \quad (6.36)$$

is the probability of termination in the water phase. If the re-entry of the non-ionic desorbed radicals is considered diffusion limited, k_{re} is given by

$$k_{re} = 4\pi D_w r_P \quad (6.37)$$

where r_P is particle radius.

The results obtained assuming the entry rate to be determined by aqueous phase propagation, i.e., using eqs (6.34)-(6.37), is reported in Fig. 6.22 for reaction BA6 for two values of the critical length for entry z ($z = 3$ and $z = 6$). Note that a value of 2-3 for z is estimated by Gilbert [1] for BA. The model overestimates the \bar{n} values by a factor 4 at the lowest conversion and by a factor 18 (for $z = 3$) at the highest. Higher values of z improve the quantitative agreement at high conversion (which is however still poor) but not the agreement in terms of behavior. Therefore, the model is in accord with the data neither on a quantitative nor on a qualitative basis.

A large quantitative disagreement between model predictions and experimental \bar{n} values for BA has already been reported by Maeder and Gilbert [94]. These authors performed seeded BA emulsion polymerizations with a small-sized polystyrene seed (30 nm unswollen diameter). The comparison was made for only one value of \bar{n} , which was the steady state

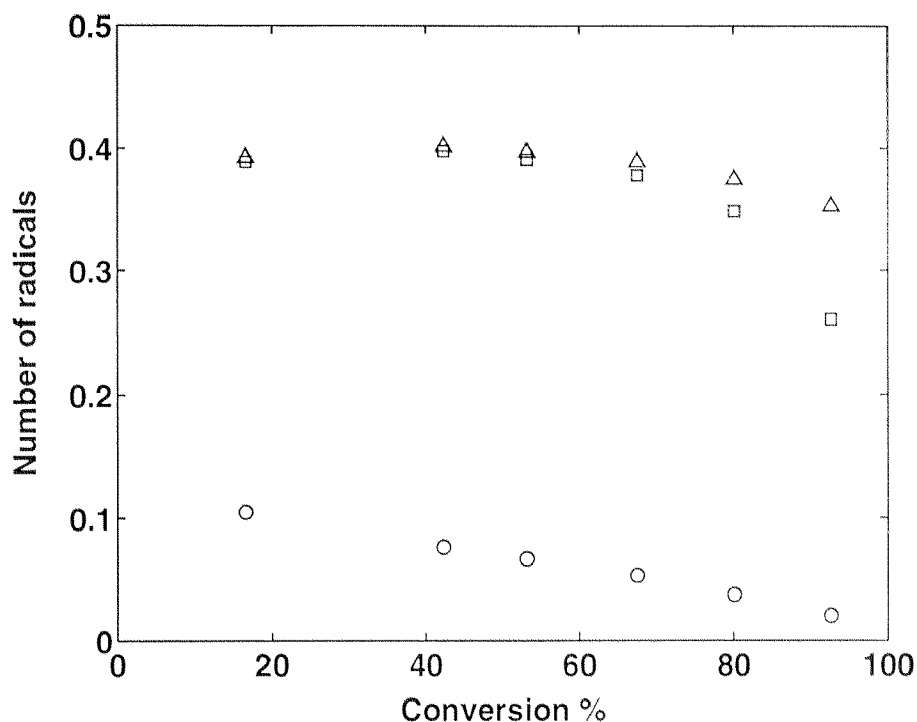


Figure 6.22: Average number of radicals as function of conversion for reaction BA6; ○ : experimental, △ : model with $z = 3$, □ : model with $z = 6$. Parameters in Table 6.6 and ρ from eqs (6.34)-(6.37).

value of one reaction. The experimental value was $\bar{n} = 0.0012$ while the calculated value was $\bar{n} = 0.033$, i.e., 28 times as large. A zero-one model was employed (after checking the zero-one assumption) using established values of the model parameters. Several explanations were attempted to explain the discrepancy between model and experiment. The disagreement could not be ascribed to uncertainties in the model parameters. A second explanation was looked for based on the fact that the used seed was not really monodisperse (it showed a mean radius of 15 nm and a standard deviation of 6 nm). Taking this in account, a theoretical value $\bar{n} = 0.016$ was calculated, which is still 13 times as large as the experimental value. Finally, it was assumed that a pseudo-bulk kinetics might prevail in the larger particles of the polydisperse seed, yielding a lower value of the calculated \bar{n} due to the presence of bimolecular terminations. No quantitative check of the results obtained under this hypothesis was however performed. With respect to this, it should be noted that supposing pseudo-bulk kinetics in particles of radii just a few nm larger than those where the zero-one assumption was shown to be valid, holds only on a qualitative basis. A more complete model, including intermediate kinetic situations, should be employed.

Though the parameters in Table 6.6 are thought to be reliable, it has been checked whether different values could explain the experimentally observed \bar{n} values and behavior.

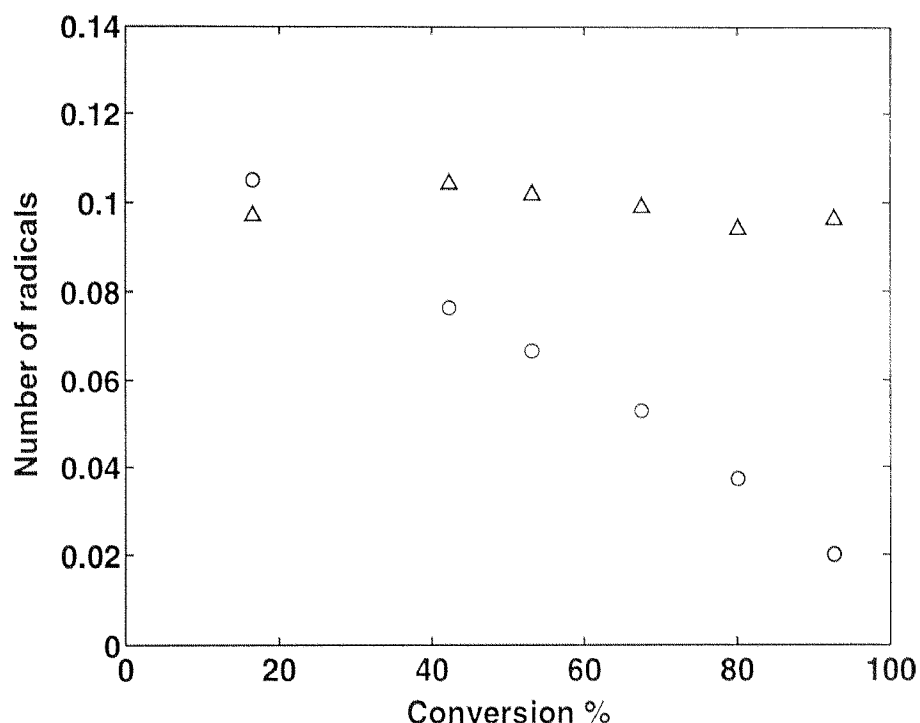


Figure 6.23: Average number of radicals as function of conversion for reaction BA6; ○ : experimental, △ : model. Parameters as in Table 6.6 except for $D_w = D_p = 10^{-5} \text{ cm}^2 \text{ s}^{-1}$ and $c_{fm} = 2.8 \cdot 10^{-3}$. Critical length for entry $z = 3$.

The calculated \bar{n} can of course be lowered by enhancing the desorption rate. Assuming $D_w = D_p = 10^{-5} \text{ cm}^2 \text{ s}^{-1}$ (which is a reasonable upper bound value for liquid in liquid diffusion) and c_{fm} 50 times as large as the literature value reported in Table 6.6, the result reported in Fig. 6.23 is obtained. Even using such an unreasonable value of the chain transfer to monomer parameter the agreement is very poor, and the \bar{n} are still overestimated at high conversions.

The effect of varying the propagation rate constant k_p is more significant, especially because the experimental \bar{n} values are inversely proportional to k_p (see eq. (6.23)). Moreover, since the propagation rate constant in the water phase $k_{p,w}$ is assumed to be the same as k_p , a decrease in its value increases the effect of the monomer depletion in the water phase on the entry rate. The results obtained using $k_p = k_{p,w} = 7.3 \cdot 10^6 \text{ cm}^3 \text{ mol}^{-1} \text{ s}^{-1}$ (which is almost 4 times as small as the literature value) are shown in Fig. 6.24 for $z = 3$ and $z = 5$. It is seen that for $z = 3$ the values from the model are not too far from the experimental ones, but the behavior is clearly different, the theoretical values showing concavity downwards. For $z = 5$ the agreement is much better above 40% conversion, since the effect of the monomer depletion is strong from the beginning of interval III. However, the theoretical values are still concave downwards more markedly than the

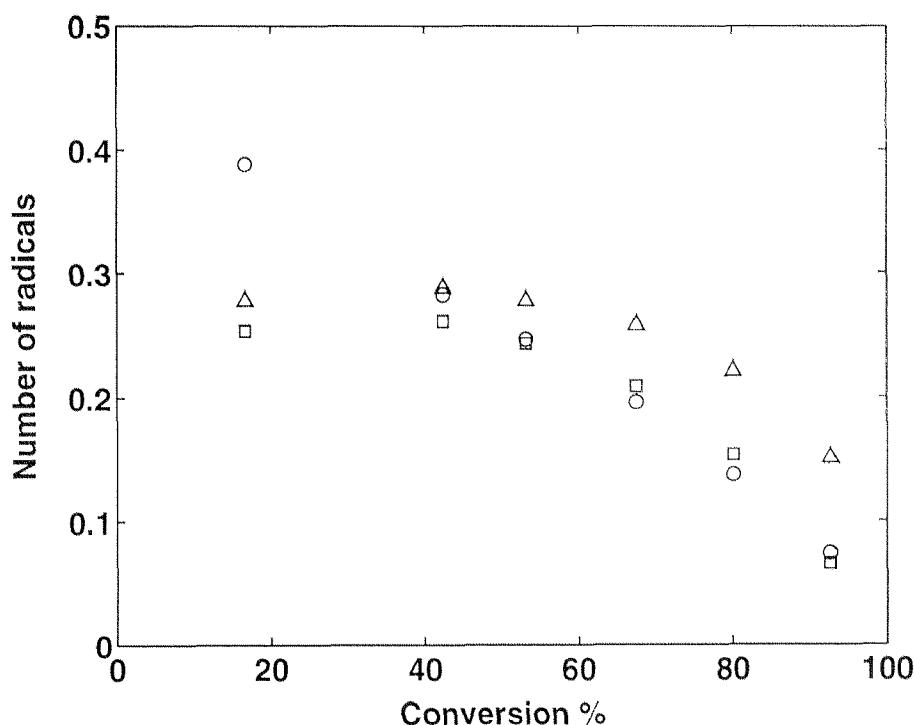


Figure 6.24: Average number of radicals as function of conversion for reaction BA6; ○ : experimental, △ : model with $z = 3$, □ : model with $z = 5$. Parameters as in Table 6.6 except for $k_p = k_{p,w} = 7.3 \cdot 10^6 \text{ cm}^3 \text{ mol}^{-1} \text{ s}^{-1}$.

experimental values. With respect to this, note from Fig. 6.10 that the experimental behavior is not completely clear. Reaction BA5 shows a virtually linear behavior with conversion, reaction BA6 exhibits a slight concavity downwards, which gets more marked for reaction BA3. No justification for these different behaviors can be given on the base of the reaction recipes reported in Table 6.1. Going back to Fig. 6.24, it must be noted that if the agreement reached between model and experimental data (for $z = 5$) may be judged satisfactory above 40% conversion, this is not true at lower conversion (interval II). It must therefore be concluded that even using a modified k_p value (far outside the confidence limits reported in [95]) and a high critical length z the model is unable to describe the experimental data.

The effect of modifying other parameters in the model (also outside reasonable ranges) was checked in a similar way, but no satisfactory agreement was found between model and experiment, the best fit obtained being that reported in Fig. 6.24 for $z = 5$.

Since the qualitative behavior of the experimental \bar{n} data is in contrast not only with the model predictions but also with the basic physical intuition regarding the processes regulating this quantity, and since the values are far too low compared to what would be expected for a scarcely water soluble monomer such as BA, it is reasonable to make some

hypotheses about possible mechanisms which could lead to underestimated experimental \bar{n} values (i.e., calculated through eq. (6.23)). Values of \bar{n} greater than those reported in Fig. 6.10 are supported by the large amount of gel which is measured at high conversion (see Figs 6.11-6.14). The formation of such a gel phase presumably occurs through significant bimolecular termination by combination between the branched chains created by chain transfer to polymer, which would require the system to move away from the very low \bar{n} values reported (where the bimolecular termination rates are negligible). An alternative explanation could be that the branched chains are joined by a terminal double bond propagation reaction to form a gel phase. In this case low \bar{n} values could be admitted and the presence of a gel is therefore not conclusive.

Since the heat of reaction \dot{Q}_r and the particle density N_P can be measured with a certain reliability, and since the molar heat of polymerization ΔH_P taken from the literature is proved to be correct by the agreement between the conversion curves obtained calorimetrically and gravimetrically (Figs 6.3-6.7), to justify an error in the experimental evaluation of \bar{n} through eq. (6.23) it is reasonable to turn the attention to the two remaining variables: the concentration of monomer in the particles C_m and the propagation rate constant k_p . With respect to N_P , it is worth saying that a virtually constant number of particles was measured after the first reaction period (see Fig. 6.9), which is expected according to the classical theory of emulsion polymerization [37], and the decreasing behavior of \bar{n} cannot therefore be ascribed to a wrong measurement of this quantity.

As reported above, several values can be found in the literature for the concentration of the monomer in the particles at saturation C_m^* , lying in the range $3 \div 5 \cdot 10^{-3}$ mol cm^{-3} [1, 90, 91, 97]. These values were obtained from equilibrium swelling or kinetic measurements. The uncertainty on this variable is not such to justify large changes in the experimental \bar{n} values. Moreover, different C_m^* values imply different monomer concentrations in the particles at saturation conditions and different conversion degrees at which the droplets disappear, but not different monomer concentrations after this instant, which occurs between 30% and 60% conversion (corresponding to the C_m^* range reported, see eq. (6.26)). Therefore, all the \bar{n} data above this conversion are left unchanged by considering different monomer concentration saturation values.

Another effect which could have an influence on the monomer concentration and thus on the experimentally calculated \bar{n} values is diffusion limitation during the transport of the monomer from the droplet to the particle phase. This limitation would invalidate the assumption of equilibrium conditions which has been considered to hold up to this point. Such a diffusion control of the monomer concentration would of course give lower

concentrations in the reaction locus, and correspondingly higher \bar{n} values. However, this would be true only until the droplets are present, thus giving an even more marked decrease moving to high conversions and the same \bar{n} values at the end of the reaction. It might as well be supposed that diffusion limitations are so strong that the droplets are present up to the very end of the reaction, in which case the effect would be present at all times. To clear this point, a quantitative analysis of the role of monomer mass transfer in the system has been performed. From this analysis, which is reported in Appendix F, it may be concluded that monomer transfer limitations play an important role in the experimental conditions investigated. However, it is also shown that the rates of reaction and the monomer concentrations in the particle phase approach at high conversions the values obtained in equilibrium conditions (see Fig. F.1, curve labelled h_d). Therefore, values of \bar{n} similar to those shown in Fig. 6.10 are calculated at high conversion also including mass transfer effects. Moreover, the monomer concentrations during the whole reaction are not so far from the equilibrium values as to justify the discrepancy between experimental and calculated \bar{n} values also at lower conversions. Therefore, the inclusion in the model of equations for the description of mass transfer does not improve the overall agreement between model results and experimental data, though mass transfer is recognized as an important rate determining factor.

Turning the attention to the other variable which has a strong influence on the experimental value of \bar{n} , namely k_p , some suppositions can be put forth about mechanisms which can make k_p different from the value measured under pulsed laser polymerization conditions (i.e., in pure monomer) [87] and decreasing with conversion (in order to have a non-decreasing \bar{n}). Glass transition effects are to be excluded due to the very low glass transition temperature of the polymer. A possible explanation could be that the branching mechanisms, including chain transfer to polymer and back-biting [100], become important at increasing polymer and decreasing monomer concentrations, creating tertiary radicals which are less reactive, thus decreasing the rate of the propagation process. Admitting this mechanisms, the effective k_p is given by:

$$k_p = k_{pp} \frac{k_{pt} C_m}{k_{bb} + k_{fp} \sigma_1 + k_{pt} C_m} + k_{pt} \frac{k_{bb} + k_{fp} \sigma_1}{k_{bb} + k_{fp} \sigma_1 + k_{pt} C_m} \quad (6.38)$$

where k_{pp} and k_{pt} are the propagation rate constants for primary and tertiary radicals, respectively, k_{bb} is the frequency of back-biting and σ_1 the polymer concentration. The two ratios appearing on the right-hand side represent the fraction of radicals in the primary and in the tertiary state, respectively. The back-biting mechanism was already investigated to explain orders of reaction greater than one with respect to monomer concentration in the

solution polymerization of BA [101]. The explanation involving stable tertiary radicals is however doubtful for two main reasons. First, so high rates of the branching reactions should be admitted in order to get k_p values decreasing significantly not only at very high conversions, that the branching densities would be overestimated by far compared to experimental data available [100]. Secondly, it has been shown in laser initiated bulk polymerization of BA that the k_p is constant up to 80% conversion [98], which should reasonably hold also for the chemically initiated radicals within the polymer particles. Moreover, the backbiting mechanism was also shown to be unable to justify the high monomer reaction orders in BA solution polymerizations [101].

Another possible explanation for the decrease in k_p with monomer conversion is that propagation occurs not only to the monomer but also to a dimer which could be formed by association of acrylate monomer pairs [101]. Again, this possibility was investigated to explain monomer orders greater than one in the solution polymerization of BA [101]. In this case, the effective k_p would be a linear function of monomer concentration:

$$k_p = k_{pm} + 2k_{pd}K_dC_m \quad (6.39)$$

where k_{pm} and k_{pd} are the propagation rate constants to the monomer and to the dimer, respectively, and K_d the equilibrium constant for monomer pair association. Besides the fact that monomer association should be important (which seems not to be the case from NMR measurements [101]) or propagation to the dimer very much faster than that to the monomer to have a significant contribution of dimer addition, this explanation is again in contrast with the constant k_p value measured experimentally by Buback and Degener [98], and seems therefore rather doubtful.

6.7 Conclusions

In this chapter the gel formation in the emulsion polymerization of BA was investigated experimentally. This system was selected as it gives significant chain transfer to polymer and termination by combination, which easily leads to gel formation in a bulk. Therefore, it was thought to be a good system to test experimentally the theoretical findings on the delay in gel formation which is caused by the compartmentalization of branched radicals, as shown in Chap. 4. Indeed, for all reactions considered, significant fractions of gel were found only at very high conversion, which gives a strong qualitative support to the theoretical description. However, a quantitative prediction of the molecular weight and gel fraction evolution was not performed due to the fact that it was not possible to describe appropriately the kinetics of the system. Namely, very low values (< 0.13) and

a decreasing behavior with conversion of the average number of radicals per particle \bar{n} were found experimentally, which could not be explained by any mechanism, employing reasonable values of the model parameters. In particular, decreasing entry rates due to a mechanism which assumes propagation in the water phase to be rate determining for the entry of initiator-derived radicals could not justify the decreasing behavior even on a qualitative basis.

Besides a very low water solubility of the monomer, support for the hypothesis that the experimental \bar{n} values are underestimated is given by a kinetic analysis performed through seeded runs at different initiator and particle concentrations, and by the fact that a gel phase is formed.

The parameters which determine the experimentally obtained value of \bar{n} were therefore taken in exam, with particular attention to the monomer concentration in the particles C_m and the propagation rate constant k_p . Several suppositions were made to account for possible effects which might modify the value of these quantities compared to the values obtained in the conditions considered in the literature works from which they were taken. Considering monomer concentration, the uncertainty in the value of the saturation value and the role of monomer mass transfer limitations were examined. With respect to the propagation rate constant k_p , branching reactions and propagation to the dimer were considered as possible effects which decrease the k_p at low monomer concentrations. None of these mechanisms was able to explain the low \bar{n} values measured experimentally and their decrease with conversion.

Seite Leer /
Blank leaf

Conclusions

In this work a kinetic model for the molecular weight calculation of polymers produced in emulsion is developed. Compared to other models previously proposed in the literature, the main achievement of the present model is the correct description of active chain compartmentalization while taking into account also all branching mechanisms. Models accounting correctly for active chain compartmentalization existed for linear chains, and many models describing the formation of branched chains during polymerization were also available, but these two features were never present together in the same model.

In the molecular weight model here presented, active chain compartmentalization is accounted for by taking advantage of the 'doubly distinguished particle' distribution, which is conceptually equivalent to the length distribution of the pairs of chains belonging to the same particles. The branching mechanisms are instead accounted for through the concept of 'pre-life', which represents the length of an active chain due to the monomer units which were added by propagation during previous growth periods. The pre-life concept had already been previously used for the description of chain transfer to polymer, but it is here extended to describe the very different step-growth mechanism related to crosslinking and TDB propagation reactions. The dimensionality of the problem is therefore not enhanced.

The PBEs which result from the description of the molecular weight distribution were solved by means of the numerical fractionation (NF) technique and the method of moments. The combination of the two permits the passage from integro-differential PBEs to sets of algebraic linear systems for the moments of the active chains and ODEs for the moments of the terminated chains. The major problem is shown to consist in the reconstruction of the overall MWD from the moments. An analysis of the performances of NF was carried out by comparison with the results of a detailed model. It is shown that in some cases NF predicts the appearance of fictitious shoulders in the high molecular weight tail of the MWD. In these cases, which sometimes occur when chain transfer to polymer is present as a branching mechanism, partitioning the polymer according to the number of branches gives very accurate solutions with limited numerical effort. A fast procedure is proposed to determine the number of branches to be used.

The compartmentalized model was used to investigate the nature of radical compartmentalization and its effects on the MWD. It is shown that compartmentalization results in pairwise correlation of the lengths of the active chains belonging to the same particle for average number of radicals per particle typical of emulsion polymerization. This correlation depends on the relative value of the entry and combination frequencies and not on whether a statistical number of radicals exists in the particles. Of course, in the latter case (pseudo-bulk conditions) any compartmentalization effect vanishes.

It is shown that pairwise correlation of the chain lengths needs to be accounted for in molecular weight modeling when combination is present. Approximate models neglecting this peculiar feature of compartmentalization lead to errors in the prediction of the polymer weight average molecular weight and polydispersity. These errors may be very large in the presence of branching, especially when combination represents a route to the formation of large branched chains (and eventually to gel). For instance, gel points occurring as early as 10% conversion are calculated by an approximate model in cases where the gel is predicted to form around 80% conversion by the model here presented, which correctly accounts for radical compartmentalization. This delay in gel formation is actually shown to be a direct effect of compartmentalization, due to the fact that branched radicals are segregated in the particles and can therefore not combine to form gel molecules.

The model was applied to describe literature molecular weight data from vinyl chloride and vinyl acetate emulsion polymerizations. In the case of vinyl chloride, it is shown that branching plays a minor role. In the case of vinyl acetate, instead, the strong increase of weight average molecular weight and of polydispersity with conversion is explained as a result of the synergic interaction between the two branching mechanisms present, namely, chain transfer to polymer and TDB propagation. In this system, bimolecular termination is completely prevented by high compartmentalization, i.e., extremely low values of the average number of radicals per particle. Therefore, even a model not correctly accounting for pairwise chain length correlation in the calculation of combination provides correct results.

Finally, butyl acrylate emulsion polymerizations experiments are reported. This monomer system is known to easily give gel formation in bulk polymerization by chain transfer to polymer and bimolecular combination. The aim of performing such experiments was to provide experimental support to the theoretical finding that gel formation is delayed by active chain compartmentalization. Indeed, gel was measured only at high conversions, typically above 70-80% conversion, while polymer produced in bulk often results to be insoluble at conversions even lower than 10%. This provides a strong qualitative validation

of the model. However, difficulties to achieve a quantitative validation resulted from the impossibility to model the kinetic behavior of the system. More specifically, unexpectedly low values of the average number of radicals per particle were measured which could neither be explained theoretically, nor proven false by analysing the parameters which appear in the experimental measurement of this quantity.

Bibliography

- [1] R.G.Gilbert, Emulsion Polymerization. A Mechanistic Approach, Academic Press: London, 1995
- [2] W.Funke, O.Okay, B.Joos-Müller, Microgels - Intramolecularly Crosslinked Macromolecules with a Globular Structure, *Adv. Polym. Sci.*, **136**, 139-234 (1998)
- [3] S.Lee, Determination of Gel Content in Polymers, *Trends Polym. Sci.*, **1**, 303-309 (1993)
- [4] J.L.Gardon, Emulsion Polymerization. I. Recalculation and Extension of the Smith-Ewart Theory, *J. Polym. Sci.: Part A-1*, **6**, 623-641 (1968)
- [5] S.Katz, R.Shinnar, G.M.Saidel, Molecular Weight Distribution for Polymerization in Two-Phase Systems, *Adv. Chem. Ser.*, **91**, 145-157 (1969)
- [6] K.W.Min, W.H.Ray, On the Mathematical Modeling of Emulsion Polymerization Reactors, *J. Macromol. Sci. Rev. Macromol. Chem.*, **C11**, 177-255 (1974)
- [7] G.Lichti, R.G.Gilbert, D.H.Napper, Molecular Weight Distributions in Emulsion Polymerizations, *J. Polym. Sci., Polym. Chem. Ed.*, **18**, 1297-1323 (1980)
- [8] G.Storti, G.Polotti, M.Cociani, M.Morbidelli, Molecular Weight Distribution in Emulsion Polymerization. I. The Homopolymer Case, *J. Polym. Sci.: Part A: Polym. Chem.*, **30**, 731-750 (1992)
- [9] P.A.Clay, R.G.Gilbert, Molecular Weight Distributions in Free-Radical Polymerizations. 1. Model Development and Implications for Data Interpretation, *Macromolecules*, **28**, 552-569 (1995)
- [10] P.J.Flory, Molecular Size Distribution in Three Dimensional Polymers. I. Gelation, *J. Am. Chem. Soc.*, **63**, 3083-3090 (1941)
- [11] P.J.Flory, Molecular Size Distribution in Three Dimensional Polymers. II. Trifunctional Branching Units, *J. Am. Chem. Soc.*, **63**, 3091-3096 (1941)

- [12] P.J.Flory, Molecular Size Distribution in Three Dimensional Polymers. III. Tetra-functional Branching Units, *J. Am. Chem. Soc.*, **63**, 3096-3100 (1941)
- [13] W.H.Stockmayer, Theory of Molecular Size Distribution and Gel Formation in Branched-Chain Polymers, *J. Chem. Phys.*, **11**, 45-55 (1943)
- [14] W.H.Stockmayer, Theory of Molecular Size Distribution and Gel Formation in Branched Polymers. II. General Cross Linking, *J. Chem. Phys.*, **12**, 125-131 (1944)
- [15] T.Y.Xie, A.E.Hamielec, Modelling free-radical copolymerization kinetics - evaluation of the pseudo-kinetic rate constant method, 1. Molecular weight calculations for linear copolymers, *Makromol. Chem., Theory. Simul.*, **2**, 421-454 (1993)
- [16] T.Y.Xie, A.E.Hamielec, Modelling free-radical copolymerization kinetics - evaluation of the pseudo-kinetic rate constant method, 2. Molecular weight calculations for copolymers with long chain branching, *Makromol. Chem., Theory. Simul.*, **2**, 455-483 (1993)
- [17] T.Y.Xie, A.E.Hamielec, Modelling free-radical copolymerization kinetics, 3. Molecular weight calculations for copolymers with crosslinking, *Makromol. Chem., Theory. Simul.*, **2**, 777-803 (1993)
- [18] S.Zhu, A.E.Hamielec, Gel Formation in Free Radical Polymerization via Chain Transfer and Terminal Branching, *J. Polym. Sci.: Part B: Polym. Phys.*, **32**, 929-943 (1994)
- [19] H.Tobita, Kinetics of Long-Chain Branching via Chain Transfer to Polymer: 1. Branched Structure *Polym. React. Eng.*, **1**, 357-378 (1992-93)
- [20] H.Tobita, Kinetics of long-chain branching in emulsion polymerization: 1. Chain transfer to polymer, *Polymer*, **35**, 3023-3038 (1994)
- [21] D.Charmot, J.Guillot, Kinetic modelling of network formation in styrene-butadiene emulsion copolymers: a comparative study with the generalized form of Flory's theory of gelation, *Polymer*, **33**, 352-360 (1992)
- [22] G.Arzamendi, J.Forcada, J.M.Asua, Kinetics of Long-Chain Branching in Emulsion Polymerization, *Macromolecules*, **27**, 6068-6079 (1994)
- [23] G.Arzamendi, J.M.Asua, Modeling Gelation and Sol Molecular Weight Distribution in Emulsion Polymerization, *Macromolecules*, **28**, 7479-7490 (1995)

- [24] A.Ghielmi, S.Fiorentino, G.Storti, M.Mazzotti, M.Morbidelli, Long Chain Branching in Emulsion Polymerization, *J. Polym. Sci.: Part A: Polym. Chem.*, **35**, 827-858 (1997)
- [25] H.Tobita, Y.Takada, M.Nomura, Simulation Model for the Molecular Weight Distribution in Emulsion Polymerization, *J. Polym. Sci.: Part A: Polym. Chem.*, **33**, 441-453 (1995)
- [26] J.Ugelstad, F.K.Hansen, Kinetics and Mechanism of Emulsion Polymerization, *Rubber Chem. Technol.*, **49**, 536-609 (1976)
- [27] M.Nomura, Desorption and Reabsorption of Free Radicals in Emulsion Polymerization, in *Emulsion Polymerization*, Piirma, I., Ed., Academic Press: New York, 1982; p. 191
- [28] J.M.Asua, E.D.Sudol, M.S.El-Aasser, Radical Desorption in Emulsion Polymerization, *J. Polym. Sci. A: Polym. Chem.*, **27**, 3903-3913 (1989)
- [29] B.S.Casey, B.R.Morrison, I.A.Maxwell, R.G.Gilbert, D.H.Napper, Free Radical Exit in Emulsion Polymerization. I. Theoretical Model, *J. Polym. Sci. A: Polym. Chem.*, **32**, 605-630 (1994)
- [30] F.Teymour, J.D.Campbell, Analysis of the Dynamics of Gelation in Polymerization Reactors Using the "Numerical Fractionation" Technique, *Macromolecules*, **27**, 2460-2469 (1994)
- [31] M.Nomura, J.Ikoma, K.Fujita, Kinetics and Mechanisms of Particle Formation and Growth in the Emulsion Polymerization Initiated by the Oil-Soluble Initiator 2,2'-Azobisisobutyronitrile, *ACS Symp. Ser.*, **492**, 55-71 (1992)
- [32] W.D.Harkins, A General Theory of the Mechanism of Emulsion Polymerization, *J. Am. Chem. Soc.*, **69**, 1428-1444 (1947)
- [33] H.Tobita, Cross-Linking Kinetics in Emulsion Copolymerization, *Macromolecules*, **25**, 2671-2678 (1992)
- [34] M.Apostolo, V.Arcella, G.Storti, M.Morbidelli, Kinetics of the emulsion polymerization of vinylidene fluoride and hexafluoropropylene, *Macromolecules*, **32**, 989-1003 (1999)

- [35] P.J.Flory, Principles of Polymer Chemistry, Cornell University Press: Ithaca, NY, 1953; chap. 9
- [36] G.Moad, D.H.Solomon, The chemistry of free radical polymerization, Pergamon Press: Oxford, U.K., 1995; chap. 5
- [37] W.V.Smith, R.M.Ewart, Kinetics of Emulsion Polymerization, *J. Chem. Phys.*, **16**, 592-599 (1948)
- [38] M.C.Grady, Studying Radical Exit in Emulsion Polymerization, *6th International Workshop on Polymer Reaction Engineering, DECHEMA Monographs*, **134**, 313-326 (1998)
- [39] G.Lichti, R.G.Gilbert, D.H.Napper, Theoretical Predictions of the Particle Size and Molecular Weight Distributions in Emulsion Polymerizations, in *Emulsion Polymerization*; Piirma, I., Ed., Academic Press: New York, 1982; p. 93
- [40] M.Ballard, R.G.Gilbert, D.H.Napper, Improved Methods for Solving the Smith-Ewart Equations in the Steady State, *J. Polym. Sci., Polym. Lett. Ed.*, **19**, 533-537 (1981)
- [41] G.Storti, G.Polotti, S.Carrá, M.Morbidelli, Modelling of Molecular Weight Distribution in Semi-Batch Emulsion Polymerization Reactors, Application to the Case of Polystyrene, *4th International Workshop on Polymer Reaction Engineering, DECHEMA Monographs*, **127**, 407-415 (1992)
- [42] F.W.Billmeyer, Textbook of Polymer Science, Wiley-Interscience: New York, 1962
- [43] M.Mazzotti, S.Fiorentino, A.Ghielmi, M.Morbidelli, G.Storti, Kinetics of Long-Chain Branching in Emulsion Polymerization, *Macromol. Symp.*, **111**, 183-193 (1996)
- [44] P.J.Flory, Effects of Cross-Linking and Branching on the Molecular Constitution of Diene Polymers, *J. Am. Chem. Soc.*, **69**, 2893-2899 (1947)
- [45] H.M.Hulburt, S.Katz, Some Problems in Particle Technology. A Statistical Mechanical Formulation. *Chem. Eng. Sci.*, **19**, 555-574 (1964)
- [46] H.Tobita, A.E.Hamielec, Modeling of Network Formation in Free-Radical Polymerization, *Macromolecules*, **22**, 3098-3105 (1989)

- [47] A.M.Basedow, K.H.Ebert, H.J.Ederer, Kinetic Studies of the Acid Hydrolysis of Dextran, *Macromolecules*, **11**, 774-781 (1978)
- [48] S.Katz, G.M.Seidel, Moments of the Size Distribution in Radical Polymerization, *AIChE J.*, **13**, 319-326 (1967)
- [49] C.H.Bamford, H.Tompa, On the Calculation of Molecular Weight Distributions from Kinetic Schemes, *J. Polym. Sci.*, **10**, 345-350 (1953)
- [50] M.Wulkow, Adaptive Treatment of Polyreactions in Weighted Sequence Spaces, *Impact Comput. Sci. Eng.*, **4**, 153-193 (1992)
- [51] P.Canu, W.H.Ray, Discrete Weighted Residual Methods Applied to Polymerization Reactions *Comput. Chem. Eng.*, **15**, 549-564 (1991)
- [52] G.G.Lowry, Ed., Markov Chains and Monte Carlo Calculations in Polymer Science, Dekker: New York, 1970
- [53] M.Wulkow, The simulation of molecular weight distributions in polyreaction kinetics by discrete Galerkin methods, *Macromol. Theory Simul.*, **5**, 393-416 (1996)
- [54] J.B.P.Souares, A.E.Hamielec, Bivariate chain length and long chain branching distribution for copolymerization of olefins and polyolefin chains containing terminal double-bonds, *Macromol. Theory Simul.*, **5**, 547-572 (1996)
- [55] H.Tobita, Molecular weight distribution in random branching of polymer chains, *Macromol. Theory Simul.*, **5**, 129-144 (1996)
- [56] H.Tobita, Random sampling technique to predict the molecular weight distribution in nonlinear polymerization, *Macromol. Theory Simul.*, **5**, 1167-1194 (1996)
- [57] O.Saito, K.Nagasubramanian, W.W.Graessley, Molecular Weight Distribution in Branched Polymers, *J. Polym. Sci., Part A-2*, **7**, 1937-1954 (1969)
- [58] H.Tobita, K.Ito, On the calculation of molecular weight distribution from the moments using Laguerre polynomials, *Polym. React. Eng.*, **1**, 407-425 (1992-1993)
- [59] J.B.Rawlings, W.H.Ray, The Modeling of Batch and Continuous Emulsion Polymerization Reactors. Part I: Model Formulation and Sensitivity to Parameters, *Polym. Eng. Sci.*, **28**, 237-256 (1988)

- [60] J.B.Rawlings, W.H.Ray, The Modeling of Batch and Continuous Emulsion Polymerization Reactors. Part II: Comparison with Experimental Data from Continuous Stirred Tank Reactors, *Polym. Eng. Sci.*, **28**, 257-274 (1988)
- [61] N.Friis, A.E.Hamielec, Gel-Effect in Emulsion Polymerization of Vinyl Monomers, *ACS Symp. Ser.*, **24**, 82-91 (1976)
- [62] C.H.Bamford, R.W.Dyson, G.C.Eastmond, Network Formation IV. The Nature of the Termination Reaction in Free-Radical Polymerization, *Polymer*, **10**, 885-899 (1969)
- [63] N.Friis, D.Goosney, J.D.Wright, A.E.Hamielec, Molecular Weight and Branching Development in Vinyl Acetate Emulsion Polymerization, *J. Appl. Polym. Sci.*, **18**, 1247-1259 (1974)
- [64] I.A.Maxwell, B.R.Morrison, D.H.Napper, R.G.Gilbert, Entry of Free Radicals into Latex Particles in Emulsion Polymerization, *Macromolecules*, **24**, 1629-1640 (1991)
- [65] I.A.Maxwell, J.Kurja, G.H.J.Van Doremaele, A.L.German, B.R.Morrison, Partial Swelling of Latex Particles with Monomers, *Makromol. Chem.*, **193**, 2049-2063 (1992)
- [66] I.A.Maxwell, J.Kurja, G.H.J.Van Doremaele, A.L.German, Thermodynamics of Swelling of Latex Particles with Two Monomers, *Makromol. Chem.*, **193**, 2065-2080 (1992)
- [67] J.Ugelstad, P.C.Mørk, P.Dahl, P.Ragnes, A Kinetic Investigation of the Emulsion Polymerization of Vinyl Chloride, *J. Polym. Sci. C*, **27**, 49-68 (1969)
- [68] J.Lyngaae-Jørgensen, Molecular Weight Distribution of Poly(Vinyl Chloride), *J. Polym. Sci. C*, **33**, 39-54 (1971)
- [69] N.Friis, A.E.Hamielec, Kinetics of Vinyl Chloride and Vinyl Acetate Emulsion Polymerization, *J. Appl. Polym. Sci.*, **19**, 97-113 (1975)
- [70] G.Vidotto, A.Crosato-Arnaldi, G.Talamini, Determination of Transfer to Monomer in the Vinyl Chloride Polymerization, *Makromol. Chem.*, **114**, 217-225 (1968)
- [71] I.M.Kolthoff, I.K.Miller, The Chemistry of Persulfate. I. The Kinetics and Mechanism of the Decomposition of the Persulfate Ion in Aqueous Medium, *J. Am. Chem. Soc.*, **73**, 3055-3059 (1951)

- [72] K.Tauer, G.Reinisch, H.Gajewski, I.Müller, Modeling of Emulsion Polymerization of Vinyl-Chloride, *J. Macromol. Sci.-Chem.*, **A28 (3-4)**, 431-460 (1991)
- [73] C.R.Wilke, P.C.Chang, Correlation of Diffusion Coefficients in Dilute Solutions, *AIChE J.*, **1**, 264-270 (1955)
- [74] W.W.Graessley, R.D.Hartung, W.C.Uy, Studies of Branching in Polyvinyl Acetate, *J. Polym. Sci. A-2*, **7**, 1919-1935 (1969)
- [75] N.Friis, L.Nyhagen, A Kinetic Study of the Emulsion Polymerization of Vinyl Acetate, *J. Appl. Polym. Sci.*, **17**, 2311-2327 (1973)
- [76] M.Nomura, M.Harada, W.Eguchi, S.Nagata, Kinetics and Mechanism of the Emulsion Polymerization of Vinyl Acetate, *ACS Symp. Ser.*, **24**, 102-121 (1976)
- [77] P.Harriott, Kinetics of Vinyl Acetate Emulsion Polymerization, *J. Polym. Sci. A-1*, **9**, 1153-1163 (1971)
- [78] R.A.Hutchinson, D.A.Paquet, Jr., J.H.McMinn, S.Beuermann, The Application of Pulsed-Laser Methods for the Determination of Free-Radical Polymerization Coefficients, *5th International Workshop on Polymer Reaction Engineering, DECHEMA Monographs*, **131**, 467-492 (1995)
- [79] M.A.Dubé, K.Rilling, A.Penlidis, A Kinetic Investigation of Butyl Acrylate Polymerization, *J. Appl. Polym. Sci.*, **43**, 2137-2145 (1991)
- [80] L.Varela de la Rosa, E.D.Sudol, M.S.El-Aasser, A Klein, Details of the Emulsion Polymerization of Styrene Using a Reaction Calorimeter, *J. Polym. Sci.: Part A: Polym. Chem.*, **34**, 461-473 (1996)
- [81] V.E.Shashoua, R.G.Beamon, Microgel: An Idealized Polymer Molecule, *J. Polym. Sci.*, **33**, 101-117 (1958)
- [82] H.G.Müller, A.Schmidt, D.Kranz, Determination of the degree of swelling and crosslinking of latex particles by analytical ultracentrifugation, *Progr. Colloid Polym. Sci.*, **86**, 70-75 (1991)
- [83] T.J.Williamson, V.F.Gaylor, I.Piirma, Exclusion Chromatography Analysis of Latex Solutions for Monitoring Nitrile Resin Polymerizations, *ACS Symp. Ser.*, **138**, 77-91 (1980)

- [84] B.Grob, R.Riesen, K.Vogel, Reaction Calorimetry for the Development of Chemical-Reactions, *Thermochim. Acta*, **114**, 83-90 (1987)
- [85] R.Riesen, Balance-Based Reaction-Calorimetry, *Thermochim. Acta*, **119**, 219-222 (1987)
- [86] H.-U.Moritz, Polymerization Calorimetry - A Powerful Tool for Reactor Control, in *Polymer Reaction Engineering*, K.H.Reichert and W.Geiseler, Eds, VCH Verlag: Weinheim, Germany, 1989; p. 248
- [87] R.A.Lyons, J.Hutovic, M.C.Piton, D.I.Christie, P.A.Clay, B.G.Manders, S.H.Kable, R.G.Gilbert, Pulsed-Laser Polymerization Measurements of the Propagation Rate Coefficient for Butyl Acrylate, *Macromolecules*, **29**, 1918-1927 (1996)
- [88] J.Brandup, E.H.Immergut, Eds, Polymer Handbook, 3rd edition, Wiley-Interscience: New York, 1989; p. 298
- [89] H.F.Mark, N.M.Bikales, C.G.Overberger, G.Menges, Eds, Encyclopedia of Polymer Science and Engineering, 2nd edition, Vol. 1, Wiley-Interscience: New York, 1989; p. 236
- [90] I.Capek, J.Barton, E.Orolinova, Emulsion Polymerization of Butyl Acrylate, *Chem. Zvesti*, **38**, 803-822 (1984)
- [91] I.A.Maxwell, D.H.Napper, R.G.Gilbert, Emulsion Polymerization of Butyl Acrylate, *J. Chem. Soc., Faraday Trans. 1*, **83**, 1449-1467 (1987)
- [92] J.Ugelstad, P.C.Mork, J.O.Aasen, Kinetics of Emulsion Polymerization, *J. Polym. Sci.: Part A-1*, **5**, 2281-2288 (1967)
- [93] D.M.Lange, G.W.Poehlein, S.Hayashi, A.Komatsu, T.Hirai, Kinetic Analysis of Seeded Emulsion Polymerization of Vinyl Acetate, *J. Polym. Sci.: Part A: Polym. Chem.*, **29**, 785-792 (1991)
- [94] S.Maeder, R.G.Gilbert, Measurement of Transfer Constant for Butyl Acrylate Free-Radical Polymerization, *Macromolecules*, **31**, 4410-4418 (1998)
- [95] S.Beuermann, D.A.Paquet, Jr., J.H.McMinn, R.A.Hutchinson, Determination of Free-Radical Propagation Rate Coefficients of Butyl, 2-Ethylhexyl, and Dodecyl Acrylates by Pulsed-Laser Polymerization, *Macromolecules*, **29**, 4206-4215 (1996)

- [96] M.J.Devon, A.Rudin, Monomer Chain Transfer in the Copolymerization of Styrene and Butyl Acrylate, *J. Polym. Sci.: Part A: Polym. Chem.*, **24**, 2191-2198 (1986)
- [97] P.Mallya, S.S.Plamthottam, Termination rate constant in butyl acrylate batch emulsion polymerization, *Polym. Bull.*, **21**, 497-504 (1989)
- [98] M.Buback, B.Degener, Rate coefficients for free-radical polymerization of butyl acrylate to high conversion, *Makromol. Chem.*, **194**, 2875-2883 (1993)
- [99] P.A.Lovell, T.H.Shah, F.Heatley, Correlation of the Extent of Chain Transfer to Polymer with Reaction Conditions for Emulsion Polymerization of *n*-Butyl Acrylate, *ACS Symp. Ser.*, **492**, 188-202 (1992)
- [100] N.M.Ahmad, F.Heatley, P.A.Lovell, Chain Transfer to Polymer in Free-Radical Solution Polymerization of *n*-Butyl Acrylate Studied by NMR Spectroscopy, *Macromolecules*, **31**, 2822-2827 (1998)
- [101] G.E.Scott, E.Senogles, Polymerization Kinetics of *n*-Alkyl Acrylates, *J. Macromol. Sci.-Chem.*, **A8**, 753-773 (1974)
- [102] G.S.Laddha, T.E.Degaleesan, Transport Phenomena in Liquid Extraction, McGraw-Hill: New Delhi, 1976
- [103] W.E.Ranz, W.R.Marshall, Jr., Evaporation from Droplets, *Chem. Eng. Prog.*, **48**, 141-146 (1952)
- [104] V.G.Levich, Physicochemical Hydrodynamics, Prentice-Hall: Englewood Cliffs, N.J., 1962
- [105] H.T.Chen, S.Middleman, Drop Size Distribution in Agitated Liquid-Liquid Systems, *AIChE J.*, **13**, 989-995 (1967)

Seite Leer /
Blank leaf

Notation

$\underline{\underline{\mathbf{A}}}$	matrix of the coefficients for the singly distinguished particles
B'_i	distribution of the singly distinguished particles, branched
$\underline{\mathbf{B}}'$	column vector for the B'_i distribution
B''_i	distribution of the doubly distinguished particles, branched
$\underline{\mathbf{B}}''$	column vector for the B''_i distribution
$B'_{i,g'}$	fractionated distribution of the singly distinguished particles
$\underline{\mathbf{B}}'_{g'}$	column vector for the $B'_{i,g'}$ distribution
$B''_{i,g',g''}$	fractionated distribution of the doubly distinguished particles
$\underline{\mathbf{B}}''_{g',g''}$	column vector for the $B''_{i,g',g''}$ distribution
b	number of branches in a chain
b_M	total number of branches used in the PANB method
\bar{b}_n	average number of branches in chains of length n
c	$= (c_c + c_d)$, overall bimolecular termination frequency
c_c	termination by combination frequency
c_d	termination by disproportionation frequency
c_{fm}	ratio between chain transfer to monomer and propagation rate constants
c_{fp}	ratio between chain transfer to polymer and propagation rate constants
C_m	monomer concentration in the particles
C_m^*	monomer concentration in the particles at saturation
$C_{m,w}$	monomer concentration in the water phase
$C_{m,w}^*$	monomer concentration in the water phase at saturation
c_p	specific heat of the reaction mass
$\underline{\underline{\mathbf{D}}}$	matrix of the coefficients for the doubly distinguished particles

D	CLD of the dead polymer
D_B	total moles of internal double bonds in the system
D_g	CLD of the dead polymer of generation g
d_P	swollen particle diameter
$d_{P,d}$	unswollen (dry) particle diameter
f	pseudo-first-order rate constant for the transfer events which do not result in desorption
f_u	functionality of the monomer
g'	generation of the older distinguishing chain
g''	generation of the younger distinguishing chain
G^C	distribution of the polymer terminated by combination coming from a pair of distinguishing chains, both branched
\bar{G}^C	distribution of the polymer terminated by combination coming from a pair of distinguishing chains, both branched, as calculated by the approximate model
$G_{g',g''}^C$	fractionated distribution of the polymer terminated by combination
G^M	distribution of the polymer terminated by monomolecular mechanisms, branched
$G_{g'}^M$	fractionated distribution of the polymer terminated by monomolecular mechanisms
i	number of radicals in a particle
I	(concentration of) initiator molecules
$[I]_w$	concentration of initiator in the water phase
$\underline{\mathbf{I}}$	identity matrix
k	moment order
k_d	radical desorption frequency
k_e	rate constant for radical entry

k_{fm}	rate constant for chain transfer to monomer
$k_{fm,w}$	rate constant for chain transfer to monomer in water
k_{fp}	rate constant for chain transfer to polymer
k_{ft}	rate constant for chain transfer to CTA
k_I	rate constant for initiator decomposition
k_{max}	maximum moment order in the method of moments
k_p	rate constant for chain propagation
$k_{p,w}$	rate constant for chain propagation in water
k_p^*	rate constant for crosslinking
$k_p^{*(TDB)}$	rate constant for propagation to TDB
k_{re}	rate constant for monomeric radical re-entry
k_t	rate constant for bimolecular termination
k_{tc}	rate constant for termination by combination
k_{td}	rate constant for termination by disproportionation
$k_{t,w}$	rate constant for bimolecular termination in water
M	(concentration of) monomer molecules
M_m	monomer molecular weight
M_n	number-average chain length
M_n^i	instantaneous number-average chain length
M_w	weight-average chain length
M_w^i	instantaneous weight-average chain length
n	chain length
n'	pre-life of the older distinguishing chain
n''	pre-life of the younger distinguishing chain

\bar{n}	average number of free radicals per particle
N	maximum number of free radicals in a particle
N_A	Avogadro's number
n_b	number of branched generations whose index coincides with the number of chain branches in the refined NF technique
n_g, NG	total number of branched generations used in NF
N_i	distribution of the particles containing i radicals
N'_i	distribution of the singly distinguished particles, linear
\underline{N}'	column vector for the N'_i distribution
N''_i	distribution of the doubly distinguished particles, linear
\underline{N}''	column vector for the N''_i distribution
n_m	overall moles of monomer in the reactor
n_m^0	initial moles of monomer charged
n_M	maximum chain length in the detailed solution method for the bulk
N_P	water phase concentration of the polymer particles
n_T	total moles of polymer chains in the system
O''_i	distribution of the doubly distinguished particles with the older distinguishing chain branched
\underline{O}''	column vector for the O''_i distribution
P_d	polydispersity ratio
P_d^i	instantaneous polydispersity ratio
P_i	probability of desorption from a particle in state i
P_n	(concentration of) terminated chains of length n
$P_n^{(g)}$	(concentration of) terminated chains of length n belonging to generation g

$P_n(TDB)$	dead polymer chain of length n , bearing a TDB
$P_{n,b}$	(concentration of) terminated chains of length n with b branches
q	ratio between chain transfer to polymer and bimolecular termination frequency
q^*	ratio between crosslinking and bimolecular termination frequency
$q^{*(TDB)}$	ratio between TDB propagation and bimolecular termination frequency
\dot{Q}_r	instantaneous heat of reaction
$\mathcal{P}(x_1 = \bar{x}_1)$	probability of occurrence of event \bar{x}_1
$\mathcal{P}(x_1 = \bar{x}_1, x_2 = \bar{x}_2)$	probability of occurrence of event \bar{x}_1 followed by event \bar{x}_2
$\mathcal{P}(x_2 = \bar{x}_2 x_1 = \bar{x}_1)$	probability of occurrence of event \bar{x}_2 conditioned on event \bar{x}_1
\mathcal{R}_I	rate of initiation
r_P	swollen particle radius
R_n^\bullet	(concentration of) active chains of length n
$R_n^{\bullet(g)}$	(concentration of) active chains of length n belonging to generation g
$R_{n,b}^\bullet$	(concentration of) active chains of length n with b branches
R_w^\bullet	(concentration of) radicals in the water phase
S^C	distribution of the linear polymer terminated by combination
\bar{S}^C	distribution of the linear polymer terminated by combination, as calculated by the approximate model
S^M	distribution of the polymer terminated by monomolecular mechanisms, linear
t	birth time of the (older) distinguishing chain
t'	current lifetime
t''	current lifetime of the younger distinguishing chain of a pair
T	(concentration of) chain transfer agent molecules

t_e	experimental time
T_{DB}	total moles of TDBs in the system
T_j	jacket temperature
T_r	reactor temperature
U	heat exchange coefficient through the reactor wall
V^C	distribution of the polymer terminated by combination coming from a pair of distinguishing chains, the older of which branched and the younger linear
\bar{V}^C	distribution of the polymer terminated by combination coming from a pair of distinguishing chains, one of which branched and the other linear, as calculated by the approximate model
v_P	swollen particle volume
$v_{P,d}$	unswollen (dry) particle volume
V_d	volume of the droplet phase
\tilde{V}_m	molar volume of pure monomer
V_w	volume of the water phase
W^C	distribution of the polymer terminated by combination coming from a pair of distinguishing chains, the older of which linear and the younger branched
Y_i''	distribution of the doubly distinguished particles with the younger distinguishing chain branched
\underline{Y}''	column vector for the Y_i'' distribution
z	critical length for entry

Greek letters

α	propagation frequency
β	probability of reaction by propagation or termination in the water phase for a desorbed monomeric radical

γ	ratio between internal double bonds and polymerized monomer units in a chain
$\gamma^{(TDB)}$	average number of TDBs per chain
ν	total moles of crosslinked monomer units in the system
ρ	frequency of radical entry
ρ_D	frequency of re-entry of desorbed radicals
$\rho_{i,g'}^{(k)}$	k^{th} -order moment of distribution $B'_{i,g'}$
$\rho_{i,g',g''}^{(k)}$	k^{th} -order moment of distribution $B''_{i,g',g''}$
ρ_m	pure monomer density
ρ_p	pure polymer density
ρ_{re}	frequency of re-entry of desorbed monomeric radicals
ϕ_m	monomer volume fraction in the particles
ϕ_m^*	monomer volume fraction in the particles at saturation
$\sigma^{(k)}$	k^{th} -order moment of the CLD of the dead polymer
$\sigma_g^{(k)}$	k^{th} -order moment of the CLD of the dead polymer belonging to generation g
$\sigma_{M,g}^{(k)}$	k^{th} -order moment of the CLD of the polymer formed by monomolecular termination, belonging to generation g
$\sigma_{C,g}^{(k)}$	k^{th} -order moment of the CLD of the polymer formed by combination, belonging to generation g
$\bar{\sigma}_{C,g',g''}^{(k)}$	k^{th} -order moment of distribution $G_{g',g''}^C$
θ	total moles of polymerized monomer units in the system
$\delta_{i,j}$	Kronecker's index
η	initiation efficiency
λ_k	k^{th} -order moment of the CLD of the active polymer (bulk)

μ_k	k^{th} -order moment of the CLD of the terminated polymer (bulk)
$\mu_{k,b}$	k^{th} -order moment of the CLD of the terminated polymer with b branches (bulk)
$\mu_k^{(g)}$	k^{th} -order moment of the CLD of the terminated polymer of generation g (bulk)
τ_c	characteristic time for combination
τ_ρ	characteristic time for entry
χ	fractional conversion
ΔH_P	molar heat of polymerization

Abbreviations

BA	Butyl acrylate
CLD	Chain length distribution
KPS	Potassium persulfate
MWD	Molecular weight distribution
NF	Numerical fractionation
PANB	Partitioning according to the number of branches
PBA	Poly(butyl acrylate)
PBE	Population balance equation
PCS	Photon correlation spectroscopy
PVAc	Poly(vinyl acetate)
PVC	Poly(vinyl chloride)
QSSA	Quasi-steady-state assumption
SLS	Sodium lauryl sulfate
TDB	Terminal double bond
TEM	Transmission electron microscopy
VAc	Vinyl acetate
VC	Vinyl chloride

Seite Leer /
Blank leaf

Appendix A

Model Solution

A.1 Numerical Fractionation

The numerical procedure adopted for the solution of the model is based on the fractionation technique developed by Teymour and Campbell [30] in the context of bulk polymerization. According to this procedure, the polymer chain population is subdivided into a finite number $NG + 2$ of generations, each consisting of individuals similar in length and degree of branching. The first generation is constituted of linear chains, the following NG include the branched chains belonging to the sol polymer fraction and the last one is the polymer gel. The definition of the rules governing the passage from one generation to another permits to derive the balance equations for the chain populations of each generation. As a general rule, the coupling of two chains belonging to the same generation, which may occur through termination by combination, crosslinking or propagation to TDB, yields a chain of the subsequent generation. Hence, the passage from one generation to another occurs when there is a scale transition in the dimensions of the chain, i.e., a geometric growth of the chain size. The coupling between two chains belonging to different generations yields a chain of the higher generation of the two. All mechanisms not involving chain coupling (monomolecular terminations, termination by disproportionation, chain transfer to polymer) do not cause generation transitions. An exception is represented by linear chains, which pass to the first branched generation when they undergo chain transfer to polymer. Moreover, the bimolecular combination of two linear chains produces a chain which is still linear, and no generation transition occurs in this case.

When a chain is sufficiently large and branched, i.e., it belongs to a generation higher than the highest sol generation NG , it is considered to be part of the gel. However, no arbitrary condition on the value of NG must be introduced. This has simply to be taken large enough, so that a further increase would not affect the results of the model, i.e., convergence has been achieved (see for instance Fig. 2.7). The amount of gel formed is

calculated as the difference between the total formed polymer, obtained from an overall balance, and that present in the $NG + 1$ sol generations.

A.2 Fractionated Population Balance Equations

In the following the PBEs for each generation of polymer chains are derived. These result from the application of the NF technique to the case of emulsion polymerization. In order to identify the generation which the chain belongs to, a subscript g' is added to the distributions of the singly distinguished particles and of the polymer terminated by monomolecular combination. When the chains under examination are two, i.e., in the case of doubly distinguished particles and chains terminated by combination, two indices g' and g'' are needed. Index $g = 0$ implies that the chain is linear; in this case, the distribution does not depend on pre-life.

Singly Distinguished Particles

The fractionated equations for the singly distinguished particles can be written in analogy with eqs (2.5) and (2.6), which refer to the overall distributions. Considering that a live chain of generation g' is formed when a crosslinking reaction occurs between two chains both of generation $g' - 1$ or one of generation g' and the other of a lower generation, the following equations can be derived:

• $g' = 0$

$$\frac{\partial \underline{\mathbf{B}}'_0(t, t')}{\partial t'} = \underline{\mathbf{A}}(t) \underline{\mathbf{B}}'_0(t, t') \quad (\text{A.1})$$

• $g' = 1$

$$\begin{aligned} \frac{\partial \underline{\mathbf{B}}'_1(t, t', n')}{\partial t'} &= \underline{\mathbf{A}}(t) \underline{\mathbf{B}}'_1(t, t', n') + \int_0^{n'} k_p^* \gamma \underline{\mathbf{B}}'_1(t, t', n' - m) m^l D_0(t, m) dm \\ &\quad + k_p^* \gamma \underline{\mathbf{B}}'_0(t, t') n'^l [D_0(t, n') + D_1(t, n')] \end{aligned} \quad (\text{A.2})$$

• $g' \geq 2$

$$\begin{aligned} \frac{\partial \underline{\mathbf{B}}'_{g'}(t, t', n')}{\partial t'} &= \underline{\mathbf{A}}(t) \underline{\mathbf{B}}'_{g'}(t, t', n') + \int_0^{n'} k_p^* \gamma \underline{\mathbf{B}}'_{g'-1}(t, t', n' - m) m^l D_{g'-1}(t, m) dm \\ &\quad + \sum_{r=0}^{g'-1} \left(\int_0^{n'} k_p^* \gamma \underline{\mathbf{B}}'_{g'}(t, t', n' - m) m^l D_r(t, m) dm \right) \\ &\quad + \sum_{r=1}^{g'-1} \left(\int_0^{n'} k_p^* \gamma \underline{\mathbf{B}}'_r(t, t', n' - m) m^l D_{g'}(t, m) dm \right) \end{aligned} \quad (\text{A.3})$$

$$+k_p^* \gamma \underline{\mathbf{B}}'_0(t, t') n^l D_{g'}(t, n')$$

where $D_{g'}(t, n')$ is the CLD of the dead polymer of generation g' and $\underline{\mathbf{A}}$ is the same band matrix used in eq. (2.5). Note that the distribution vector $\underline{\mathbf{B}}'_0(t, t')$ coincides with $\underline{\mathbf{N}}'(t, t')$ appearing in eq. (2.5). In matrix $\underline{\mathbf{A}}$, the moment $\sigma^{(l)}$ appearing in the diagonal terms must account for the overall dead polymer, i.e., both sol and gel fractions if gelation occurred, since an active chain can react by chain transfer or crosslinking with any dead chain. Moreover, it is worth recalling that $l = 1$ for the crosslinking reaction and $l = 0$ for the propagation to TDB reaction.

According to the fact that chain transfer to polymer causes a generation transition only when involving a linear dead chain, the following initial conditions hold for eqs (A.1) to (A.3):

$$\bullet g' = 0 \quad B'_{i,0}(t, t' = 0) = \rho N_{i-1}(t) + k_{fm} C_m i N_i(t) \quad (\text{A.4})$$

$$\bullet g' = 1 \quad B'_{i,1}(t, t' = 0, n') = k_{fp} i N_i(t) n' [D_1(t, n') + D_0(t, n')] \quad (\text{A.5})$$

$$\bullet g' \geq 2 \quad B'_{i,g'}(t, t' = 0, n') = k_{fp} i N_i(t) n' D_{g'}(t, n') \quad (\text{A.6})$$

where $1 \leq i \leq N$.

Doubly Distinguished Particles

As for the singly distinguished particles, by applying the rules which govern the transitions between generations caused by the crosslinking reaction, the PBEs for the fractionated doubly distinguished particle distributions can be obtained as follows:

- *both chains linear*

$$\frac{\partial \underline{\mathbf{B}}''_{0,0}(t, t', t'')}{\partial t''} = \underline{\mathbf{D}}(t) \underline{\mathbf{B}}''_{0,0}(t, t', t'') \quad (\text{A.7})$$

where $\underline{\mathbf{D}}$ is the same band matrix used in eq. (2.8) and $\underline{\mathbf{B}}''_{0,0}(t, t', t'')$ coincides with $\underline{\mathbf{N}}''(t, t', t'')$ in the same equation.

- *older chain branched*

$$\frac{\partial \underline{\mathbf{B}}''_{g',0}(t, t', t'', n')}{\partial t''} = \underline{\mathbf{D}}(t) \underline{\mathbf{B}}''_{g',0}(t, t', t'', n')$$

$$\begin{aligned}
& +k_p^*\gamma \left[\int_0^{n'} \underline{\mathbf{B}}''_{g'-1,0}(t, t', t'', n' - m)m^l D_{g'-1}(t, m)dm \right. \\
& + \sum_{r=0}^{g'-1} \int_0^{n'} \underline{\mathbf{B}}''_{g',0}(t, t', t'', n' - m)m^l D_r(t, m)dm \\
& \left. + \sum_{r=1}^{g'-1} \int_0^{n'} \underline{\mathbf{B}}''_{r,0}(t, t', t'', n' - m)m^l D_{g'}(t, m)dm + \underline{\mathbf{B}}''_{0,0}(t, t', t'')n^l D_{g'}(t, n') \right] \quad (\text{A.8})
\end{aligned}$$

Note that this equation is formally correct only when $g' \geq 2$. When $g' = 1$, the first integral term on the right-hand side must be replaced by the term $\underline{\mathbf{B}}''_{0,0}(t, t', t'')n^l D_0(t, n')$, since the linear active chain yielding the chain of the first generation has no pre-life. Accordingly, the length of the dead chain undergoing the crosslinking reaction is fixed to n' and no integration is required.

- *younger chain branched*

$$\begin{aligned}
\frac{\partial \underline{\mathbf{B}}''_{0,g''}(t, t', t'', n'')}{\partial t''} & = \underline{\mathbf{D}}(t)\underline{\mathbf{B}}''_{0,g''}(t, t', t'', n'') \\
& +k_p^*\gamma \left[\int_0^{n''} \underline{\mathbf{B}}''_{0,g''-1}(t, t', t'', n'' - m)m^l D_{g''-1}(t, m)dm \right. \\
& + \sum_{r=0}^{g''-1} \int_0^{n''} \underline{\mathbf{B}}''_{0,g''}(t, t', t'', n'' - m)m^l D_r(t, m)dm \\
& \left. + \sum_{r=1}^{g''-1} \int_0^{n''} \underline{\mathbf{B}}''_{0,r}(t, t', t'', n'' - m)m^l D_{g''}(t, m)dm + \underline{\mathbf{B}}''_{0,0}(t, t', t'')n^{ll} D_{g''}(t, n'') \right] \quad (\text{A.9})
\end{aligned}$$

As for eq. (A.8), this equation is correct when $g'' \geq 2$. When $g'' = 1$, the first integral term on the right-hand side must be replaced by the term $\underline{\mathbf{B}}''_{0,0}(t, t', t'')n^{ll} D_0(t, n'')$.

- *both chains branched*

$$\begin{aligned}
\frac{\partial \underline{\mathbf{B}}''_{g',g''}(t, t', t'', n', n'')}{\partial t''} & = \underline{\mathbf{D}}(t)\underline{\mathbf{B}}''_{g',g''}(t, t', t'', n', n'') \\
& +k_p^*\gamma \left[\int_0^{n'} \underline{\mathbf{B}}''_{g'-1,g''}(t, t', t'', n' - m, n'')m^l D_{g'-1}(t, m)dm \right. \\
& + \int_0^{n''} \underline{\mathbf{B}}''_{g',g''-1}(t, t', t'', n', n'' - m)m^l D_{g''-1}(t, m)dm + \\
& \sum_{r=0}^{g'-1} \int_0^{n'} \underline{\mathbf{B}}''_{g',g''}(t, t', t'', n' - m, n'')m^l D_r(t, m)dm \\
& \left. + \sum_{r=0}^{g''-1} \int_0^{n''} \underline{\mathbf{B}}''_{g',g''}(t, t', t'', n', n'' - m)m^l D_r(t, m)dm \right] \quad (\text{A.10})
\end{aligned}$$

$$\begin{aligned}
& \sum_{r=1}^{g'-1} \int_0^{n'} \underline{\mathbf{B}}''_{r,g''}(t, t', t'', n' - m, n'') m^l D_{g'}(t, m) dm \\
& + \sum_{r=1}^{g''-1} \int_0^{n''} \underline{\mathbf{B}}''_{g',r}(t, t', t'', n', n'' - m) m^l D_{g''}(t, m) dm + \\
& \left[\underline{\mathbf{B}}''_{0,g''}(t, t', t'', n'') n''^l D_{g''}(t, n'') + \underline{\mathbf{B}}''_{g',0}(t, t', t'', n') n'^l D_{g'}(t, n') \right]
\end{aligned}$$

This equation is correct when both $g' \geq 2$ and $g'' \geq 2$. When $g' = 1$ or $g'' = 1$, some integral terms must be modified, similarly to what shown for eqs (A.8) and (A.9).

The form of the initial conditions depends upon the value of the generation index g'' :

$$\begin{aligned}
\bullet g'' = 0 \quad B''_{i,g',0}(t, t', t'' = 0, n') &= \rho B'_{i-1,g'}(t, t', n') \\
&+ k_{fm} C_m (i-1) B'_{i,g'}(t, t', n') \quad (A.11)
\end{aligned}$$

$$\begin{aligned}
\bullet g'' = 1 \quad B''_{i,g',1}(t, t', t'' = 0, n', n'') &= k_{fp} (i-1) B'_{i,g'}(t, t', n') n'' \cdot \\
&[D_0(t, n'') + D_1(t, n'')] \quad (A.12)
\end{aligned}$$

$$\begin{aligned}
\bullet g'' \geq 2 \quad B''_{i,g',g''}(t, t', t'' = 0, n', n'') &= k_{fp} (i-1) B'_{i,g'}(t, t', n') n'' \cdot \\
&D_{g''}(t, n'') \quad (A.13)
\end{aligned}$$

where $2 \leq i \leq N$ and $0 \leq g' \leq NG$ (with $n' = 0$ when $g' = 0$).

Polymer Formed by Monomolecular Termination

The structure of the equations describing the distributions $G_{g'}^M$ of the polymer belonging to generation g' which has formed by monomolecular termination does not depend on index g' and coincides with that of eq. (2.17) for the corresponding overall distribution. This is because monomolecular terminations never lead to a generation transfer of the active chains. Thus, for $0 \leq g' \leq NG$:

$$\begin{aligned}
\frac{d[v_P G_{g'}^M(t_e, t', n')]}{dt_e} &= \left[(k + k_{fm} C_m + k_{fp} \sigma^{(1)}) \sum_{i=1}^N B'_{i,g'}(t_e - t', t', n') \right. \\
&+ \frac{\rho}{N} B'_{N,g'}(t_e - t', t', n') + 2c_d \sum_{i=2}^N (i-1) B'_{i,g'}(t_e - t', t', n') \\
&\left. - (k_{fp} n + k_p^* \gamma n^l) G_{g'}^M(t_e, t', n') \bar{n} \right] \frac{1}{N_A} \quad (A.14)
\end{aligned}$$

where n is the length of the dead chain, given by $n = n' + \alpha t'$ in the case where $g' \geq 1$. When $g' = 0$, the pre-life of the active chain producing the dead polymer chain is zero. Accordingly, the dependence on n' must be eliminated in eq. (A.14) ($G_0^M = G_0^M(t_e, t')$) and the chain length is $n = \alpha t'$.

Polymer Formed by Combination

As for the case of the polymer formed by monomolecular termination, also the equation describing the time evolution of distribution $G_{g',g''}^C$ of the polymer terminated by combination is identical in structure to that corresponding to the overall distribution, given by eq. (2.21):

$$\begin{aligned} \frac{d[v_P G_{g',g''}^C(t_e, t', t'', n', n'')]}{dt_e} = & [2c_c \sum_{i=2}^N B_{i,g',g''}''(t_e - t' - t'', t', t'', n', n'') \\ & - (k_{fp}n + k_p^* \gamma n^l) G_{g',g''}^C(t_e, t', t'', n', n'') \bar{n}] \frac{1}{N_A} \end{aligned} \quad (\text{A.15})$$

Here n is the length of the dead chain, calculated as $n = n' + n'' + \alpha(t' + 2t'')$. Eq. (A.15) holds for $0 \leq g', g'' \leq NG$. However, when $g' = 0$ or $g'' = 0$, the dependence on n' or n'' , respectively, drops out.

A.3 Fractionated Moment Equations

Equations (A.14) and (A.15) for the dead polymer chain distributions can be solved by using the method of moments. The moments are obtained by multiplying each distribution by an integer power of the corresponding chain length, and integrating over all possible current lifetimes and pre-lives [24].

The equations for the moments of the polymer formed by monomolecular termination and by combination, $\sigma_{M,g'}^{(k)}$ and $\bar{\sigma}_{C,g',g''}^{(k)}$ respectively, can be obtained from eqs (A.14) and (A.15) by applying the moment definition to both sides. It must be observed that moment $\bar{\sigma}_{C,g',g''}^{(k)}$ accounts for both generations of the active chains which produced the dead chain. The moment $\sigma_{C,g}^{(k)}$ of the polymer of generation g terminated by combination are obtained from the quantities $\bar{\sigma}_{C,g',g''}^{(k)}$ by properly applying the rules which govern the transitions between generations caused by termination by combination:

$$\bullet g = 0 \quad \sigma_{C,0}^{(k)} = \bar{\sigma}_{C,0,0}^{(k)} \quad (\text{A.16})$$

$$\bullet g = 1 \quad \sigma_{C,1}^{(k)} = \bar{\sigma}_{C,1,0}^{(k)} + \bar{\sigma}_{C,0,1}^{(k)} \quad (\text{A.17})$$

$$\bullet g \geq 2 \quad \sigma_{C,g}^{(k)} = \sum_{r=0}^{g-1} \left(\bar{\sigma}_{C,r,g}^{(k)} + \bar{\sigma}_{C,g,r}^{(k)} \right) + \bar{\sigma}_{C,g-1,g-1}^{(k)} \quad (\text{A.18})$$

The equations for the moments of the dead polymer of generation g formed through any termination mechanism, $\sigma_g^{(k)}$, are obtained by summing up the moment equations of the polymer formed by monomolecular termination and by combination. The resulting equations are reported in Table A.1, and include the quantities $\rho_{i,g'}^{(k)}$ and $\rho_{i,g',g''}^{(k)}$, which represent the k th order moments of the singly and doubly distinguished particle distributions, respectively.

In Table A.1 a closure equation is also given. This is required by the chain transfer to polymer and the crosslinking reactions (not the propagation to TDB), which imply that each dead polymer moment depends on the next higher. The reported equation results from the model distribution selected for the reconstruction of the CLDs and is reliable when three moments are sufficient for an accurate description of the CLD of each generation [45]. If this is not the case, the same procedure can be adopted, but using a larger number of moments for the description of each generation.

The moments of the singly and doubly distinguished particles are evaluated by applying the moment operator to both sides of the relevant PBEs (i.e., eqs (A.1)-(A.3) for the singly and eqs (A.7)-(A.10) for the doubly distinguished particles) and integrating by parts, as shown in detail in ref. [24]. The additional integral terms due to crosslinking can be handled using the following general formula:

$$\int_0^\infty dn \int_0^n F(\tau)G(n-\tau)d\tau = \int_0^\infty F(n)dn \int_0^\infty G(n)dn \quad (\text{A.19})$$

Integration of the PBEs and subsequent rearrangement of the terms leads to equations for the k^{th} -order moments of the singly and doubly distinguished particles constituted by linear algebraic systems with right-hand sides depending on the initial conditions, on the dead polymer moments and on the live polymer moments of lower order or generation index. The presence of crosslinking causes also the matrices of the coefficients to depend on the moments of the dead polymer, but this does not alter the linearity of the systems. The relevant equations are summarized in Tables A.2, A.3 and A.4. In these equations the sums with negative step, i.e., having the upper limit smaller than the lower one, are defined as equal to zero.

moments of the dead polymer
$\boxed{g = 0}$ $\frac{d[v_P \sigma_0^{(k)}]}{dt_e} = [(k + k_{fm} C_m + k_{fp} \sigma^{(1)}) \sum_{i=1}^N \rho'_{i,0}{}^{(k)} + \frac{\rho}{N} \rho'_{N,0}{}^{(k)} + 2c_d \sum_{i=2}^N (i-1) \rho'_{i,0}{}^{(k)} + 2c_c \sum_{i=2}^N \rho''_{i,0,0}{}^{(k)} - (k_{fp} \sigma_0^{(k+1)} + k_p^* \gamma \sigma_0^{(k+l)}) \bar{n}] \frac{1}{N_A}$
$\boxed{g = 1}$ $\frac{d[v_P \sigma_1^{(k)}]}{dt_e} = [(k + k_{fm} C_m + k_{fp} \sigma^{(1)}) \sum_{i=1}^N \rho'_{i,1}{}^{(k)} + \frac{\rho}{N} \rho'_{N,1}{}^{(k)} + 2c_d \sum_{i=2}^N (i-1) \rho'_{i,1}{}^{(k)} + 2c_c \sum_{i=2}^N (\rho''_{i,1,0}{}^{(k)} + \rho''_{i,0,1}{}^{(k)}) - (k_{fp} \sigma_1^{(k+1)} + k_p^* \gamma \sigma_1^{(k+l)}) \bar{n}] \frac{1}{N_A}$
$\boxed{g \geq 2}$ $\frac{d[v_P \sigma_g^{(k)}]}{dt_e} = [(k + k_{fm} C_m + k_{fp} \sigma^{(1)}) \sum_{i=1}^N \rho'_{i,g}{}^{(k)} + \frac{\rho}{N} \rho'_{N,g}{}^{(k)} + 2c_d \sum_{i=2}^N (i-1) \rho'_{i,g}{}^{(k)} + 2c_c \sum_{i=2}^N \left(\sum_{r=0}^{g-1} (\rho''_{i,r,g}{}^{(k)} + \rho''_{i,g,r}{}^{(k)}) + \rho''_{i,g-1,g-1}{}^{(k)} \right) - (k_{fp} \sigma_g^{(k+1)} + k_p^* \gamma \sigma_g^{(k+l)}) \bar{n}] \frac{1}{N_A}$
closure equation
$\sigma_g^{(3)} = 2 \frac{(\sigma_g^{(2)})^2}{\sigma_g^{(1)}} - \frac{\sigma_g^{(2)} \sigma_g^{(1)}}{\sigma_g^{(0)}}$

Table A.1: Fractionated moment equations of the dead polymer. $l = 1$ for the crosslinking reaction and $l = 0$ for the propagation to TDB reaction.

moments of the singly distinguished particles	
$g' = 0$	
• $k = 0$	$\underline{\underline{\mathbf{A}}}\underline{\underline{\rho}}_0^{(0)} = -\underline{\underline{\mathbf{B}}}'_0(t, t' = 0)$
• $k \geq 1$	$\underline{\underline{\mathbf{A}}}\underline{\underline{\rho}}_0^{(k)} = -\alpha k \underline{\underline{\rho}}_0^{(k-1)}$
$g' \geq 1$	
$(\underline{\underline{\mathbf{A}}} + k_p^* \gamma \sum_{r=0}^{g'-1} \sigma_r^{(l)} \underline{\underline{\mathbf{I}}}) \underline{\underline{\rho}}_{g'}^{(k)} = - \int_0^\infty (n')^k \underline{\underline{\mathbf{B}}}'_{g'}(t, t' = 0, n') dn' - \alpha k \underline{\underline{\rho}}_{g'}^{(k-1)}$ $- k_p^* \gamma \left[\sum_{j=0}^k \binom{k}{j} \underline{\underline{\rho}}_{g'-1}^{(k-j)} \sigma_{g'-1}^{(j+l)} + \sum_{r=0}^{g'-1} \sum_{j=1}^k \binom{k}{j} \underline{\underline{\rho}}_{g'}^{(k-j)} \sigma_r^{(j+l)} \right.$ $\left. + \sum_{r=0}^{g'-1} \sum_{j=0}^k \binom{k}{j} \underline{\underline{\rho}}_r^{(k-j)} \sigma_{g'}^{(j+l)} \right]$	
where ($i = 1, \dots, N$):	
• $g' = 1$	$\int_0^\infty (n')^k B'_{i,1}(t, t' = 0, n') dn' = k_{fp} i N_i [\sigma_0^{(k+1)} + \sigma_1^{(k+1)}]$
• $g' \geq 2$	$\int_0^\infty (n')^k B'_{i,g'}(t, t' = 0, n') dn' = k_{fp} i N_i \sigma_{g'}^{(k+1)}$

Table A.2: Fractionated moment equations of the singly distinguished particle distributions. $l = 1$ for the crosslinking reaction and $l = 0$ for the propagation to TDB reaction.

moments of the doubly distinguished particles

$$\boxed{g' = 0, g'' = 0}$$

$$\underline{\underline{\mathbf{D}}}\rho_{0,0}^{(k)} = -2\alpha k \rho_{0,0}^{(k-1)} - \int_0^\infty (\alpha t')^k \underline{\underline{\mathbf{B}}}_{0,0}''(t, t', t'' = 0) dt'$$

where ($i = 2, \dots, N$):

$$\int_0^\infty (\alpha t')^k \underline{\underline{\mathbf{B}}}_{i,0}''(t, t', t'' = 0) dt' = \rho \rho_{i-1,0}^{(k)} + k_{fm} C_m (i-1) \rho_{i,0}^{(k)}$$

$$\boxed{g' \geq 1, g'' = 0}$$

$$\begin{aligned} \left(\underline{\underline{\mathbf{D}}} + k_p^* \gamma \sum_{r=0}^{g'-1} \sigma_r^{(l)} \underline{\underline{\mathbf{I}}} \right) \underline{\underline{\rho}}_{g',0}^{(k)} &= -2\alpha k \underline{\underline{\rho}}_{g',0}^{(k-1)} - \int_0^\infty \int_0^\infty (n' + \alpha t')^k \underline{\underline{\mathbf{B}}}_{g',0}''(t, t', t'' = 0, n') dt' dn' \\ &\quad - k_p^* \gamma \left[\sum_{j=0}^k \binom{k}{j} \underline{\underline{\rho}}_{g'-1,0}^{(k-j)} \sigma_{g'-1}^{(j+l)} + \sum_{r=0}^{g'-1} \sum_{j=1}^k \binom{k}{j} \underline{\underline{\rho}}_{g',0}^{(k-j)} \sigma_r^{(j+l)} \right. \\ &\quad \left. + \sum_{r=0}^{g'-1} \sum_{j=0}^k \binom{k}{j} \underline{\underline{\rho}}_{r,0}^{(k-j)} \sigma_{g'}^{(j+l)} \right] \end{aligned}$$

where ($i = 2, \dots, N$):

$$\int_0^\infty \int_0^\infty (n' + \alpha t')^k \underline{\underline{\mathbf{B}}}_{i,g',0}''(t, t', t'' = 0, n') dt' dn' = \rho \rho_{i-1,g'}^{(k)} + k_{fm} C_m (i-1) \rho_{i,g'}^{(k)}$$

$$\boxed{g' = 0, g'' \geq 1}$$

$$\begin{aligned} \left(\underline{\underline{\mathbf{D}}} + k_p^* \gamma \sum_{r=0}^{g''-1} \sigma_r^{(l)} \underline{\underline{\mathbf{I}}} \right) \underline{\underline{\rho}}_{0,g''}^{(k)} &= -2\alpha k \underline{\underline{\rho}}_{0,g''}^{(k-1)} - \int_0^\infty \int_0^\infty (n'' + \alpha t')^k \underline{\underline{\mathbf{B}}}_{0,g''}''(t, t', t'' = 0, n'') dt' dn'' \\ &\quad - k_p^* \gamma \left[\sum_{j=0}^k \binom{k}{j} \underline{\underline{\rho}}_{0,g''-1}^{(k-j)} \sigma_{g''-1}^{(j+l)} + \sum_{r=0}^{g''-1} \sum_{j=1}^k \binom{k}{j} \underline{\underline{\rho}}_{0,g''}^{(k-j)} \sigma_r^{(j+l)} \right. \\ &\quad \left. + \sum_{r=0}^{g''-1} \sum_{j=0}^k \binom{k}{j} \underline{\underline{\rho}}_{0,r}^{(k-j)} \sigma_{g''}^{(j+l)} \right] \end{aligned}$$

where ($i = 2, \dots, N$):

$$\bullet g'' = 1 \quad \int_0^\infty \int_0^\infty (n'' + \alpha t')^k \underline{\underline{\mathbf{B}}}_{i,0,1}''(t, t', t'' = 0, n'') dt' dn''$$

$$= k_{fp} (i-1) \sum_{j=0}^k \binom{k}{j} \rho_{i,0}^{(k-j)} [\sigma_0^{(j+1)} + \sigma_1^{(j+1)}]$$

$$\bullet g'' \geq 2 \quad \int_0^\infty \int_0^\infty (n'' + \alpha t')^k \underline{\underline{\mathbf{B}}}_{i,0,g''}''(t, t', t'' = 0, n'') dt' dn''$$

$$= k_{fp} (i-1) \sum_{j=0}^k \binom{k}{j} \rho_{i,0}^{(k-j)} \sigma_{g''}^{(j+1)}$$

Table A.3: Fractionated moment equations of the doubly distinguished particle distributions. $l = 1$ for the crosslinking reaction and $l = 0$ for the propagation to TDB reaction.

moments of the doubly distinguished particles

$$\boxed{g' \geq 1, g'' \geq 1}$$

$$\begin{aligned} & \left[\underline{\underline{\mathbf{D}}} + k_p^* \gamma \left(\sum_{r=0}^{g'-1} \sigma_r^{(l)} + \sum_{r=0}^{g''-1} \sigma_r^{(l)} \right) \underline{\underline{\mathbf{I}}} \right] \underline{\underline{\rho}}_{g',g''}^{n(k)} = -2\alpha k \underline{\underline{\rho}}_{g',g''}^{n(k-1)} \\ & - \int_0^\infty \int_0^\infty \int_0^\infty (n' + n'' + \alpha t')^k \underline{\underline{\mathbf{B}}}_{g',g''}''(t, t', t'' = 0, n', n'') dt' dn' dn'' \\ & - k_p^* \gamma \left[\sum_{j=0}^k \binom{k}{j} \underline{\underline{\rho}}_{g'-1, g''}^{n(k-j)} \sigma_{g'-1}^{(j+1)} + \sum_{j=0}^k \binom{k}{j} \underline{\underline{\rho}}_{g', g''-1}^{n(k-j)} \sigma_{g''-1}^{(j+1)} \right. \\ & + \sum_{r=0}^{g'-1} \sum_{j=1}^k \binom{k}{j} \underline{\underline{\rho}}_{g', g''}^{n(k-j)} \sigma_r^{(j+1)} + \sum_{r=0}^{g''-1} \sum_{j=1}^k \binom{k}{j} \underline{\underline{\rho}}_{g', g''}^{n(k-j)} \sigma_r^{(j+1)} \\ & \left. + \sum_{r=0}^{g'-1} \sum_{j=0}^k \binom{k}{j} \underline{\underline{\rho}}_{r, g''}^{n(k-j)} \sigma_{g'}^{(j+1)} + \sum_{r=0}^{g''-1} \sum_{j=0}^k \binom{k}{j} \underline{\underline{\rho}}_{g', r}^{n(k-j)} \sigma_{g''}^{(j+1)} \right] \end{aligned}$$

where $(i = 2, \dots, N)$:

$$\begin{aligned} \bullet g'' = 1 & \quad \int_0^\infty \int_0^\infty \int_0^\infty (n' + n'' + \alpha t')^k B_{i, g', 1}''(t, t', t'' = 0, n', n'') dt' dn' dn'' \\ & = k_{fp}(i-1) \sum_{j=0}^k \binom{k}{j} \rho_{i, g'}^{n(k-j)} [\sigma_0^{(j+1)} + \sigma_1^{(j+1)}] \\ \bullet g'' \geq 2 & \quad \int_0^\infty \int_0^\infty \int_0^\infty (n' + n'' + \alpha t')^k B_{i, g', g''}''(t, t', t'' = 0, n', n'') dt' dn' dn'' \\ & = k_{fp}(i-1) \sum_{j=0}^k \binom{k}{j} \rho_{i, g'}^{n(k-j)} \sigma_{g''}^{(j+1)} \end{aligned}$$

Table A.4: Fractionated moment equations of the doubly distinguished particle distributions, with $g', g'' \geq 1$. $l = 1$ for the crosslinking reaction and $l = 0$ for the propagation to TDB reaction.

Seite Leer /
Blank leaf

Appendix B

Relation Between Cumulated and Instantaneous Properties

In this Appendix the relations between the cumulated and the instantaneous average chain length properties are derived.

Number-average chain length

The cumulated number-average chain length is defined as:

$$M_n = \frac{\sigma^{(1)}}{\sigma^{(0)}} \quad (\text{B.1})$$

where $\sigma^{(l)}$ is the l^{th} -order moment of the polymer CLD, expressed as moles per particle volume. Derivation of eq. (B.1) with respect to experimental time yields:

$$\begin{aligned} \frac{dM_n}{dt_e} &= \frac{1}{v_P \sigma^{(0)}} \cdot \frac{d(v_P \sigma^{(1)})}{dt_e} - \frac{v_P \sigma^{(1)}}{(v_P \sigma^{(0)})^2} \cdot \frac{d(v_P \sigma^{(0)})}{dt_e} \\ &= \frac{1}{v_P \sigma^{(0)}} \cdot \frac{d(v_P \sigma^{(0)})}{dt_e} \left[\frac{d(v_P \sigma^{(1)})}{d(v_P \sigma^{(0)})} - \frac{\sigma^{(1)}}{\sigma^{(0)}} \right] \end{aligned}$$

which, using the definition of the instantaneous number average chain length (2.46), reduces to:

$$\frac{dM_n}{dt_e} = \frac{1}{v_P \sigma^{(0)}} \cdot \frac{d(v_P \sigma^{(0)})}{dt_e} [M_n^i - M_n] \quad (\text{B.2})$$

Weight-average chain length

The cumulated weight-average chain length is defined as:

$$M_w = \frac{\sigma^{(2)}}{\sigma^{(1)}} \quad (\text{B.3})$$

Derivation with respect to experimental time yields:

$$\frac{dM_w}{dt_e} = \frac{1}{v_P\sigma^{(1)}} \cdot \frac{d(v_P\sigma^{(1)})}{dt_e} \left[\frac{d(v_P\sigma^{(2)})}{d(v_P\sigma^{(1)})} - \frac{\sigma^{(2)}}{\sigma^{(1)}} \right]$$

which, using the definition of the instantaneous weight average chain length (2.47), reduces to:

$$\frac{dM_w}{dt_e} = \frac{1}{v_P\sigma^{(1)}} \cdot \frac{d(v_P\sigma^{(1)})}{dt_e} [M_w^i - M_w] \quad (\text{B.4})$$

Polydispersity ratio

The cumulated polydispersity is defined as:

$$P_d = \frac{M_w}{M_n} = \frac{\sigma^{(2)}\sigma^{(0)}}{[\sigma^{(1)}]^2} \quad (\text{B.5})$$

Derivation with respect to experimental time yields:

$$\begin{aligned} \frac{dP_d}{dt_e} &= \frac{v_P\sigma^{(0)}}{(v_P\sigma^{(1)})^2} \cdot \frac{d(v_P\sigma^{(2)})}{dt_e} + \frac{v_P\sigma^{(2)}}{(v_P\sigma^{(1)})^2} \cdot \frac{d(v_P\sigma^{(0)})}{dt_e} \\ &\quad - 2 \frac{(v_P\sigma^{(2)})(v_P\sigma^{(0)})}{(v_P\sigma^{(1)})^3} \cdot \frac{d(v_P\sigma^{(1)})}{dt_e} = \\ &\quad \frac{1}{v_P\sigma^{(1)}} \cdot \frac{d(v_P\sigma^{(1)})}{dt_e} \left[\frac{\sigma^{(0)}}{\sigma^{(1)}} \cdot \frac{d(v_P\sigma^{(2)})d(v_P\sigma^{(0)})}{d(v_P\sigma^{(1)})^2} \cdot \frac{d(v_P\sigma^{(1)})}{d(v_P\sigma^{(0)})} \right. \\ &\quad \left. + \frac{\sigma^{(2)}\sigma^{(0)}}{[\sigma^{(1)}]^2} \cdot \frac{\sigma^{(1)}}{\sigma^{(0)}} \cdot \frac{d(v_P\sigma^{(0)})}{d(v_P\sigma^{(1)})} - 2 \frac{\sigma^{(2)}\sigma^{(0)}}{[\sigma^{(1)}]^2} \right] \end{aligned} \quad (\text{B.6})$$

which, by use of the definitions (2.46)-(2.48) of the instantaneous molecular weights and polydispersity, leads to:

$$\frac{dP_d}{dt_e} = \frac{1}{v_P\sigma^{(1)}} \cdot \frac{d(v_P\sigma^{(1)})}{dt_e} \left[\frac{M_n^i}{M_n} P_d^i + P_d \frac{M_n}{M_n^i} - 2P_d \right] \quad (\text{B.7})$$

Appendix C

Non-compartmentalized Model

In order to highlight the importance of a correct description of active chain compartmentalization, in section 2.5 the instantaneous molecular weight properties calculated by the model developed in this work have been compared to those calculated by a model which neglects radical segregation in the polymer particles (non-compartmentalized model). In the non-compartmentalized case, the radical concentration R^\bullet has been imposed the same as in the compartmentalized one through the relation $R^\bullet = \bar{n}/N_A v_P$, where \bar{n} is obtained from the Smith-Ewart equations. The equations of the non-compartmentalized model are the following:

$$\begin{aligned} \rho^{(1)} &= \frac{[1 + \tau + \beta + c_p^{*(TDB)} \sigma^{(1)} + (c_p + c_p^*) \sigma^{(2)}]}{[\tau + \beta + c_p \sigma^{(1)}]} \rho^{(0)} \\ \frac{d[v_P \sigma^{(0)}]}{dt} &= k_p C_m \rho^{(0)} \left(\tau + \frac{\beta}{2} - c_p^{*(TDB)} \sigma^{(0)} - c_p^* \sigma^{(1)} \right) v_P \\ \frac{d[v_P \sigma^{(1)}]}{dt} &= k_p C_m \rho^{(0)} (1 + \tau + \beta) v_P \\ \frac{d[v_P \sigma^{(2)}]}{dt} &= k_p C_m \rho^{(0)} \left[1 + \tau + \beta + 2(1 + c_p^{*(TDB)} \sigma^{(1)} + c_p^* \sigma^{(2)}) \frac{\rho^{(1)}}{\rho^{(0)}} + \beta \left(\frac{\rho^{(1)}}{\rho^{(0)}} \right)^2 \right] v_P \end{aligned} \quad (\text{C.1})$$

where $\sigma^{(j)}$ and $\rho^{(j)}$ are the j^{th} -order moments of the dead and active polymer respectively (note that $\rho^{(0)} = R^\bullet$). The parameter $c_p^* = k_p^* \gamma / (k_p C_m)$ accounts for the crosslinking reaction, $c_p^{*(TDB)} = k_p^{*(TDB)} \gamma^{(TDB)} / (k_p C_m)$ for propagation to TDB and $c_p = k_{fp} / (k_p C_m)$ for chain transfer to polymer. Parameters τ and β account for monomolecular and bimolecular termination, respectively. In particular, τ accounts also for radical desorption and entry, which are peculiar of emulsion polymerization:

$$\tau = \frac{k_{fm}C_m + k_{td}\rho^{(0)} + k + \rho N_N/\bar{n}}{k_p C_m}$$

$$\beta = \frac{k_{tc}\rho^{(0)}}{k_p C_m}$$

Appendix D

Derivation of the Overall Moment Equations for a Bulk System

Applying the moment operator $\sum_{n=0}^{\infty} n^k$ to equations (3.1)-(3.2) and recalling the definition of the k^{th} -order moment of the active and terminated chains (i.e., $\lambda_k = \sum_{n=0}^{\infty} n^k R_n^\bullet$ and $\mu_k = \sum_{n=0}^{\infty} n^k P_n$), we obtain ($k \geq 1$):

$$\begin{aligned} \frac{d\lambda_k}{dt} = & k_p M \sum_{n=1}^{\infty} n^k R_{n-1}^\bullet - [k_p M + k_{fm} M + k_{ft} T + (k_{tc} + k_{td}) \lambda_0 + k_{fp} \mu_1] \sum_{n=0}^{\infty} n^k R_n^\bullet \\ & + k_{fp} \lambda_0 \sum_{n=0}^{\infty} n^{k+1} P_n \end{aligned} \quad (\text{D.1})$$

$$\begin{aligned} \frac{d\mu_k}{dt} = & (k_{fm} M + k_{ft} T + k_{td} \lambda_0 + k_{fp} \mu_1) \sum_{n=0}^{\infty} n^k R_n^\bullet + \frac{1}{2} k_{tc} \sum_{n=0}^{\infty} \sum_{m=0}^n n^k R_m^\bullet R_{n-m}^\bullet \\ & - k_{fp} \lambda_0 \sum_{n=0}^{\infty} n^{k+1} P_n \end{aligned} \quad (\text{D.2})$$

In the previous equations some summations can be recognized to be the definitions of λ_k and μ_{k+1} . The remaining summations (first summation in equation (D.1) and the double summation in equation (D.2)) can be calculated through the two following general formulae:

$$(a + b)^k = \sum_{j=0}^k \binom{k}{j} a^j b^{k-j} \quad (\text{D.3})$$

$$\sum_{n=0}^{\infty} \sum_{m=0}^n a_m b_{n-m} = \sum_{n=0}^{\infty} a_n \sum_{m=0}^{\infty} b_m \quad (\text{D.4})$$

Accordingly, the first summation in equation (D.1) leads to (setting $n = m + 1$):

$$\sum_{m=0}^{\infty} (m+1)^k R_m^\bullet = \sum_{j=0}^k \binom{k}{j} \sum_{m=0}^{\infty} m^j R_m^\bullet = \sum_{j=0}^k \binom{k}{j} \lambda_j \quad (\text{D.5})$$

while the double summation in equation (D.2) is given by:

$$\begin{aligned} \sum_{n=0}^{\infty} \sum_{m=0}^n [m + (n - m)]^k R_m^{\bullet} R_{n-m}^{\bullet} &= \sum_{j=0}^k \binom{k}{j} \sum_{n=0}^{\infty} \sum_{m=0}^n (m^j R_m^{\bullet}) [(n - m)^{k-j} R_{n-m}^{\bullet}] = \\ &= \sum_{j=0}^k \binom{k}{j} \sum_{n=0}^{\infty} n^j R_n^{\bullet} \sum_{m=0}^{\infty} m^{k-j} R_m^{\bullet} = \sum_{j=0}^k \binom{k}{j} \lambda_j \lambda_{k-j} \end{aligned} \quad (\text{D.6})$$

Substituting expressions (D.5) and (D.6) in equations (D.1) and (D.2), respectively, we obtain:

$$\begin{aligned} \frac{d\lambda_k}{dt} &= k_p M \sum_{j=0}^k \binom{k}{j} \lambda_j - [k_p M + k_{fm} M + k_{ft} T + (k_{tc} + k_{td}) \lambda_0 + k_{fp} \mu_1] \lambda_k \\ &\quad + k_{fp} \lambda_0 \mu_{k+1} \end{aligned} \quad (\text{D.7})$$

$$\begin{aligned} \frac{d\mu_k}{dt} &= (k_{fm} M + k_{ft} T + k_{td} \lambda_0 + k_{fp} \mu_1) \lambda_k + \frac{1}{2} k_{tc} \sum_{j=0}^k \binom{k}{j} \lambda_j \lambda_{k-j} \\ &\quad - k_{fp} \lambda_0 \mu_{k+1} \end{aligned} \quad (\text{D.8})$$

Finally, applying the QSSA to equation (D.7), expression (3.7) is obtained for λ_k . By substituting this expression in equation (D.8), equation (3.8) is obtained for μ_k .

The derivation of equations (3.5) and (3.6) for the zeroth-order moments requires similar but simpler algebraic handling of equations (3.1)-(3.2) after application of the moment operator with $k = 0$.

Appendix E

Fractionated CLD Equations for a Bulk System

Considering the kinetic scheme reported in section 3.2 and applying the generation transfer rules summarized in Tab. 1, the following fractionated PBEs for the calculation of the polymer CLD result:

- $0 \leq g \leq n_b$

$$\begin{aligned} \frac{dR_n^{\bullet(g)}}{dt} &= k_p M R_{n-1}^{\bullet(g)} - [k_p M + k_{fm} M + k_{ft} T + (k_{tc} + k_{td}) \lambda_0 + k_{fp} \mu_1] R_n^{\bullet(g)} \\ &\quad + k_{fp} \lambda_0 n P_n^{(g-1)} + \delta_{n,0} \delta_{g,0} [(k_{fm} M + k_{ft} T) \lambda_0 + \mathcal{R}_I] \end{aligned} \quad (\text{E.1})$$

$$\begin{aligned} \frac{dP_n^{(g)}}{dt} &= (k_{fm} M + k_{ft} T) R_n^{\bullet(g)} + \frac{1}{2} k_{tc} \sum_{h=0}^g \sum_{m=0}^n R_m^{\bullet(h)} R_{n-m}^{\bullet(g-h)} + k_{td} \lambda_0 R_n^{\bullet(g)} \\ &\quad + k_{fp} \mu_1 R_n^{\bullet(g)} - k_{fp} \lambda_0 n P_n^{(g)} \end{aligned} \quad (\text{E.2})$$

- $g = n_b + 1$

$$\begin{aligned} \frac{dR_n^{\bullet(g)}}{dt} &= k_p M R_{n-1}^{\bullet(g)} - [k_p M + k_{fm} M + k_{ft} T + (k_{tc} + k_{td}) \lambda_0 + k_{fp} \mu_1] R_n^{\bullet(g)} \\ &\quad + k_{fp} \lambda_0 n [P_n^{(g-1)} + P_n^{(g)}] \end{aligned} \quad (\text{E.3})$$

$$\begin{aligned} \frac{dP_n^{(g)}}{dt} &= (k_{fm} M + k_{ft} T) R_n^{\bullet(g)} + \frac{1}{2} k_{tc} \sum_{h=1}^{n_b} \sum_{i=n_b+1-h}^{n_b} \sum_{m=0}^n R_m^{\bullet(h)} R_{n-m}^{\bullet(i)} \\ &\quad + k_{tc} \sum_{h=0}^{n_b} \sum_{m=0}^n R_m^{\bullet(h)} R_{n-m}^{\bullet(g)} + k_{td} \lambda_0 R_n^{\bullet(g)} + k_{fp} \mu_1 R_n^{\bullet(g)} - k_{fp} \lambda_0 n P_n^{(g)} \end{aligned} \quad (\text{E.4})$$

- $n_b + 1 < g \leq n_g$

$$\begin{aligned} \frac{dR_n^{\bullet(g)}}{dt} &= k_p M R_{n-1}^{\bullet(g)} - [k_p M + k_{fm} M + k_{ft} T + (k_{tc} + k_{td}) \lambda_0 + k_{fp} \mu_1] R_n^{\bullet(g)} \\ &\quad + k_{fp} \lambda_0 n P_n^{(g)} \end{aligned} \quad (\text{E.5})$$

$$\begin{aligned} \frac{dP_n^{(g)}}{dt} &= (k_{fm} M + k_{ft} T) R_n^{\bullet(g)} + \frac{1}{2} k_{tc} \sum_{m=0}^n R_m^{\bullet(g-1)} R_{n-m}^{\bullet(g-1)} + k_{tc} \sum_{h=0}^{g-1} \sum_{m=0}^n R_m^{\bullet(h)} R_{n-m}^{\bullet(g)} \\ &\quad + k_{td} \lambda_0 R_n^{\bullet(g)} + k_{fp} \mu_1 R_n^{\bullet(g)} - k_{fp} \lambda_0 n P_n^{(g)} \end{aligned} \quad (\text{E.6})$$

Note that moments λ_0 and μ_1 appearing in the previous equations are moments of the whole polymer CLD, including both the sol and the gel phase. They can be calculated by means of the overall moment equations reported in section 3.3.2.

Appendix F

Monomer Diffusion Limitations in Butyl Acrylate Emulsion Polymerization

In order to describe the mass transport of monomer from the droplets to the particles through the water phase, the boundary layer theory [102] is applied. According to this theory, the resistances to mass transport are concentrated within thin layers in the proximity of the droplet-water and particle-water interface. Moreover, the concentrations at the interface of two faces are assumed to be at thermodynamic equilibrium. The total molar monomer flux J_{md} from the droplet to the particle phase can thus be expressed as:

$$J_{md} = K_{dw} A_d \left(\frac{C_{m,d}}{m} - C_{m,w} \right) \quad (\text{F.1})$$

where K_{dw} is the overall interphase transport coefficient, A_d the total area between the two phases, $C_{m,d}$ the monomer concentration in the bulk of the droplets, $C_{m,w}$ the monomer concentration in the bulk of the water phase and m an equilibrium coefficient which defines the ratio between $C_{m,d}$ and $C_{m,w}$ at equilibrium: $m = (C_{m,d}/C_{m,w})_{eq}$. The coefficient K_{dw} is related to the layer mass transport coefficients for the layer inside (k_{di}) and outside (k_{do}) the droplets by:

$$\frac{1}{K_{dw}} = \frac{1}{k_{di}m} + \frac{1}{k_{do}} \quad (\text{F.2})$$

Analogously, the total molar monomer flux J_{mp} from the water to the particle phase is given by:

$$J_{mp} = K_{pw} A_p \left(C_{m,w} - \frac{C_m}{m'} \right) \quad (\text{F.3})$$

where A_p is the total area between the two phases, C_m the monomer concentration in the bulk of the particles and $m' = (C_m/C_{m,w})_{eq}$. The coefficient K_{pw} is related to the layer mass transport coefficients for the layer inside (k_{pi}) and outside (k_{po}) the particles by:

$$\frac{1}{K_{pw}} = \frac{1}{k_{pi}m'} + \frac{1}{k_{po}} \quad (\text{F.4})$$

Assuming negligible the accumulation and the consumption of monomer in the water phase, which is justified by its low water solubility, one can write:

$$J_{md} = J_{mp} = J_m \quad (\text{F.5})$$

Therefore, considering the expressions (F.1) and (F.3) for J_{md} and J_{mp} :

$$J_m = K_{dw}A_d \left(\frac{C_{m,d}}{m} - C_{m,w} \right) = K_{pw}A_p \left(C_{m,w} - \frac{C_m}{m'} \right) \quad (\text{F.6})$$

Expressing $C_{m,w}$ from the equality above as a function of $C_{m,d}$ and C_m and substituting in any of the two expressions for J_m gives:

$$J_m = \frac{h_d h_p}{h_d + h_p} \frac{1}{m'} \left(\frac{m'}{m} C_{m,d} - C_m \right) \quad (\text{F.7})$$

with

$$h_d = K_{dw}A_d \quad (\text{F.8})$$

and

$$h_p = K_{pw}A_p \quad (\text{F.9})$$

Considering the meaning of m and m' , m'/m defines the ratio between C_m and $C_{m,d}$ at equilibrium. Therefore:

$$\frac{m'}{m} C_{m,d} = C_m^* \quad (\text{F.10})$$

and

$$J_m = \frac{h_d h_p}{h_d + h_p} \frac{1}{m'} (C_m^* - C_m) \quad (\text{F.11})$$

where C_m^* is the concentration of monomer in the particles at equilibrium with the monomer in the droplet phase. Relation (F.11) expresses the flux of monomer in terms of the difference between the actual concentration of monomer and its saturation value in the particles. For the calculation of J_m according to eq. (F.11), quantities h_d and h_p must be evaluated. These involve the calculation of the transport coefficients K_{dw} and K_{pw} and of the areas A_d and A_p .

Transport coefficients

Since it reasonable to assume that the layer mass transport coefficients k_{di} , k_{do} and k_{pi} , k_{po} are of the same order of magnitude, and since the monomer has a low water solubility ($m, m' \gg 1$), eqs (F.2) and (F.4) reduce to:

$$K_{dw} \approx k_{do} \quad (\text{F.12})$$

$$K_{pw} \approx k_{po} \quad (\text{F.13})$$

The layer mass transport coefficients k_{do} and k_{po} can be estimated by taking advantage of the Ranz-Marshall equation [103], which holds for a sphere of radius r moving with a relative velocity u . The Ranz-Marshall equation is written here referring to a droplet:

$$Sh = \frac{2k_{do}r_d}{D_w} = 2 + 0.6 Sc^{1/3} Re^{1/2} \quad (\text{F.14})$$

with

$$\begin{aligned} Sh &: \text{Sherwood number} \\ r_d &: \text{droplet radius} \\ Sc &: \text{Schmidt number} = \mu_w / \rho_w D_w \\ Re &: \text{Reynolds number} = 2\rho_w u r_d / \mu_w \\ \mu_w &: \text{viscosity of water} \\ \rho_w &: \text{density of water} \end{aligned}$$

The same equation can be written for a particle. The analysis is carried on here referring to the droplets, but it can be extended in a straightforward manner to the polymer particles. Eq. (F.14) requires the knowledge of droplet velocity and radius.

To calculate the velocity of droplets relative to the water phase, the Ryhczynski-Hadamart [104] formula was considered:

$$u = \frac{2(\rho_d - \rho_w)gr_d^2}{3\mu_w} \frac{\mu_w + \mu_d}{2\mu_w + 3\mu_d} \quad (\text{F.15})$$

where

$$\begin{aligned} \rho_d, \rho_w &: \text{density of droplet and water, respectively} \\ g &: \text{gravity acceleration} \\ \mu_d, \mu_w &: \text{viscosity of droplet and water, respectively} \end{aligned}$$

It should be noted that the adsorption of emulsifier on the droplet surface causes a retardation of the motion of the droplet, and a correction factor must be applied to eq. (F.15) [104]. However, if it is proved that the effect of motion is negligible on the Sherwood number given by eq. (F.14) when velocity u is calculated by eq. (F.15), this will be even more true including the retardation due to the emulsifier.

To evaluate the droplet radius, which is required both by eq. (F.14) and (F.15), the empirical relation given by Chen [105] was used:

$$r_d = 0.053 \frac{d}{2} \left(\frac{d^3 n^2 \rho_E}{\sigma} \right)^{-0.6} \quad (\text{F.16})$$

with

$$\rho_E = 0.6\rho_d + 0.4\rho_w \quad (\text{F.17})$$

where

$$\begin{aligned} r_d &: \text{average droplet radius (cm)} \\ d &: \text{diameter of the impeller blades (cm)} \\ n &: \text{impeller speed (rps)} \\ \sigma &: \text{interfacial tension (dyne cm}^{-1}\text{)} \\ \rho_d &: \text{density of the droplet (g cm}^{-3}\text{)} \\ \rho_w &: \text{density of water (g cm}^{-3}\text{)} \end{aligned}$$

The validity of this equation is limited to diluted system, i.e., to the situation where the volume fraction of the droplet phase is less than 0.5 (which is verified for all BA reactions performed).

All equations reported above for the monomer droplets can be applied also to polymer particles, except for eq. (F.16), since the phenomena determining the size of droplets are different from those determining the size of particles (e.g. particles are not subject to rupture).

If the conditions at which the BA reactions are carried out are considered, the equations reported here above permit to conclude that the Reynolds number appearing in eq. (F.14) is $\ll 1$, and that the term related to motion is negligible in the calculation of the Sherwood number. This is true for droplets at the beginning of the reaction and, since the droplet size decreases during the reaction, for the whole course of the polymerization. Moreover, it is true for polymer particles, which have much smaller diameters. Therefore, droplets and particles behave like rigid spheres in a still medium, as far as mass transport is concerned. The layer mass transport coefficients can then be calculated from eq. (F.14) as:

$$k_{do} = \frac{D_w}{r_d} \quad (\text{F.18})$$

for the droplets and

$$k_{po} = \frac{D_w}{r_P} \quad (\text{F.19})$$

for the particles. Thus, the transport coefficients h_d and h_p defined in eqs (F.8) and (F.9), respectively, which appear in expression (F.11) for the monomer flux J_m become:

$$h_d = 4\pi D_w r_d N_d V_w \quad (\text{F.20})$$

$$h_p = 4\pi D_w r_P N_P V_w \quad (\text{F.21})$$

where N_d is the number of droplets per unit volume of water. These expressions require the knowledge of droplet and particle radius and number.

Droplet and Particle Radius and Number

The droplet radius was calculated by use of the empirical relation (F.16). From the radius the average volume of a single droplet is calculated. To calculate the droplet number, the volume of the overall droplet phase must be known. This can be calculated by writing an overall mass balance for the monomer in the droplets, involving its depletion by mass transport to the particles:

$$\frac{dn_g}{dt} = -J_m \quad (\text{F.22})$$

where n_g are the moles of monomer in the droplets. The initial condition for this equation is defined by equilibrium conditions. In the case of a seeded reaction, this is true if enough time is waited for particle swelling before starting the reaction.

To calculate the monomer concentration in the particles, which allows to evaluate J_m on one hand and particle radius on the other, an overall mass balance has to be written for the monomer in the particles, involving mass transport from the droplets and depletion by reaction:

$$\frac{dn_p}{dt} = J_m - (k_p + k_{fm})\bar{n}C_mN_PV_w/N_A \quad (\text{F.23})$$

Finally, the particle number N_P is determined by the rate of nucleation and of aggregation (if the system is instable). In a seeded reaction where secondary nucleation is negligible and the particles are well stabilized, N_P is constant and defined by the recipe.

Once the droplet and particle radius and number are known, it is possible to evaluate the exchange coefficients h_d and h_p according to eqs (F.20) and (F.21). It may be verified that, in ordinary conditions, the product r_dN_d is much smaller than the product r_PN_P . For instance, for a typical BA seeded polymerization reported in Chap. 6, the equations above permit to calculate at the start of the reaction: $r_dN_d = 3 \cdot 10^3 \text{ cm}^{-2}$ and $r_PN_P = 9 \cdot 10^7 \text{ cm}^{-2}$. Therefore $h_d \ll h_p$, i.e., the limiting step in the monomer transport is represented by the droplet-water diffusion. Since the droplet size decreases with conversion, while particle size increases, this will be true during the whole reaction. Even using a particle radius corresponding to micellar dimension, the same result is obtained. It may therefore be concluded that in the system examined the transport of monomer from the droplets to the water phase is always the limiting step in the process of monomer transport (at least under ordinary agitation rates and after the very few per cent of conversion, i.e., when enough polymer particles are formed). According to this finding, the final form of the monomer flux is:

$$J_m = 4\pi D_w r_d N_d \frac{V_w}{m'} (C_m^* - C_m) \quad (\text{F.24})$$

Results

Using the equations above, it can be analysed if the monomer diffusion from the droplets to the particles is rate determining in the BA polymerization. To this aim, a seeded reaction with intermediate initiator concentration, namely, reaction BA6, was taken in exam. The entry rate coefficient was taken to be $k_e = 1 \cdot 10^{-13} \text{ cm}^3 \text{ s}^{-1}$. The result is shown in Fig. F.1 in terms of released heat and monomer volume fraction in the particles vs. conversion. Comparing the curves obtained assuming monomer equilibrium with the curve obtained

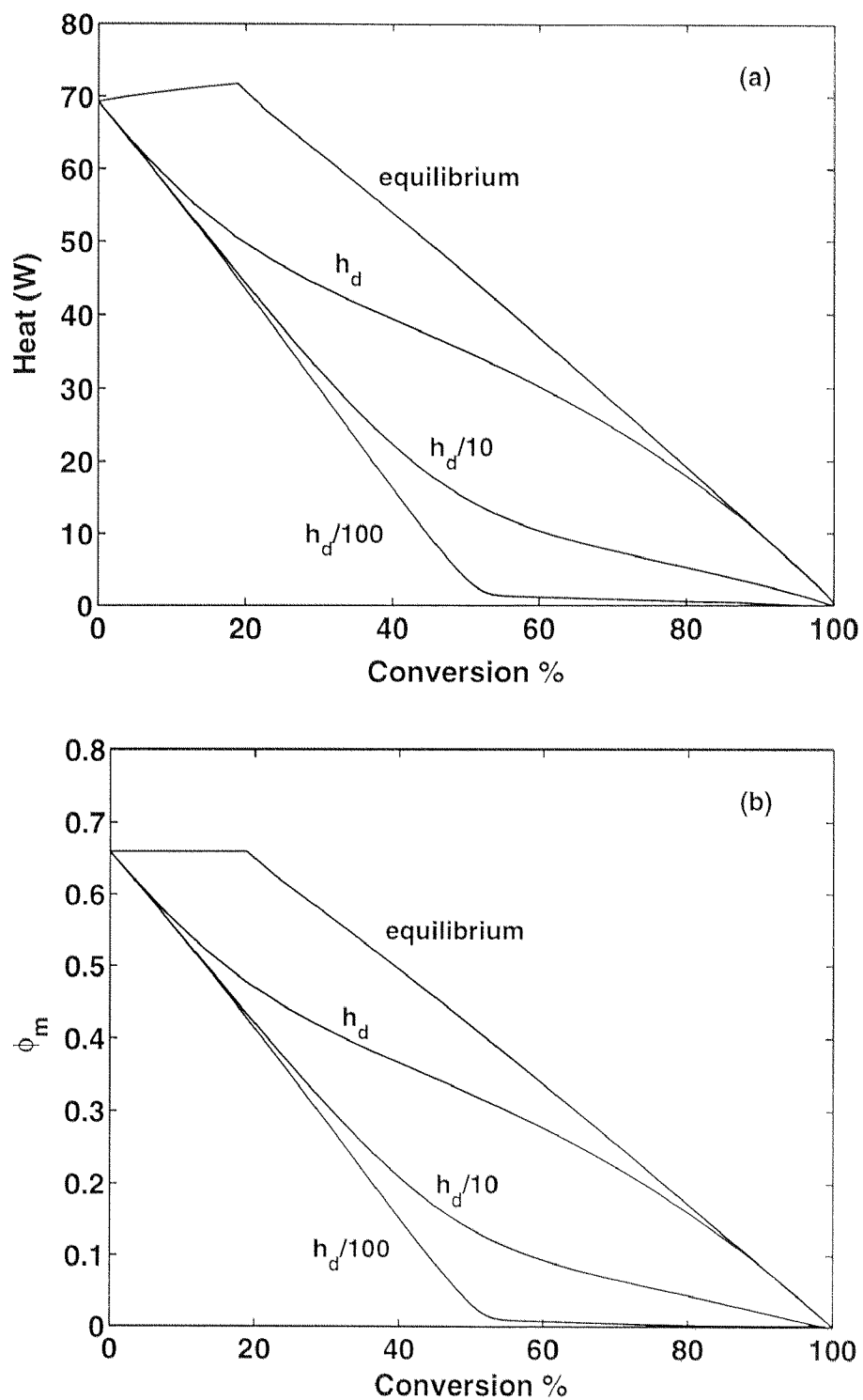


Figure F.1: (a) Heat of reaction and (b) volume fraction of monomer in the particles calculated for reaction BA6 assuming equilibrium conditions for the monomer or transfer limitations (h_d). The curves marked with $h_d/10$ and $h_d/100$ have been calculated by artificially enhancing the transfer resistances by 10 and 100 times, respectively.

calculating the resistance to monomer transport (h_d) according to the equations above, the diffusion limitations appear to be significant. However, also accounting for diffusion limitations, the calculated behavior is markedly different from the experimental one (see Fig. 6.17), even when correcting for the fact that the experimental curve has a zero value at the beginning, due to the thermal inertia of the system (which is overcome only after the first few per cent of conversion). The convex shape of the experimental curve is actually predicted after ca. 50% conversion when including the description of monomer diffusion, but the same cannot be said of the extended region of reaction rate changing only slightly at lower conversions, and of the presence and position of the maximum. The same conclusions are obtained also using different k_e values in the range which give calculated rates of reaction of the same magnitude as the experimental ones.

In order to analyse if even stronger mass transfer limitations would improve the agreement, the calculations were repeated decreasing artificially the transfer parameter h_d (i.e., the monomer flux J_m) by 10 and 100 times, respectively. The results correspond to the curves marked with $h_d/10$ and $h_d/100$ in Fig. F.1 and show that the agreement gets worse. Therefore, assuming stronger mass transfer limitations than calculated does not improve the description of the experimental behavior.

The same results are obtained when analysing reactions at different initiator and particle concentrations. Monomer transfer limitations are calculated to be important also at lower initiator concentrations, i.e., lower rates (e.g. reaction BAs7 and BAs9). This is somehow unexpected, since the behavior of reaction of reaction BAs9, exhibiting a plateau, is easily interpreted as a typical situation where the reaction proceeds in equilibrium conditions, the rate at the plateau being determined by the saturation monomer concentration.

Summarizing, the theoretical calculations show that monomer diffusion limitations are important in BA emulsion polymerizations under all experimental conditions examined. This is to be attributed to the high reactivity and low water solubility of the monomer. However, accounting for monomer transfer limitations in the equations does not improve the agreement of the model predictions with the experimental data.

Seite Leer /
Blank leaf

Appendix G

Publications Derived from this Work

Chapter 2, with the exception of Section 2.4, has been published in: A.Ghielmi, S.Fiorentino, G.Storti, M.Morbidelli, Molecular Weight Distribution of Crosslinked Polymers Produced in Emulsion, *J. Polym. Sci.: Part A: Polym. Chem.*, **36**, 1127-1156 (1998)

Chapter 3 has been published in: A. Butté, A. Ghielmi, G. Storti, M. Morbidelli, Calculation of molecular weight distributions in free-radical polymerization with chain branching, *Macromol. Theory Simul.*, **8**, 498-512 (1999)

Chapter 4, with the exception of Section 4.6, has been published in: A.Ghielmi, G.Storti, M.Morbidelli, W.H.Ray, Molecular Weight Distribution in Emulsion Polymerization: Role of Active Chain Compartmentalization, *Macromolecules*, **31**, 7172-7186 (1998)

The part of **Chapter 5** dealing with vinyl chloride polymerization has been published in: S. Forcolin, A.M. Marconi, A. Ghielmi, A. Butté, G. Storti, M. Morbidelli, Coagulation Phenomena in the Emulsion Polymerization of Vinyl Chloride, *Plast., Rubber Compos. Process. Appl.*, **28**, 109-115 (1999)

Seite Leer /
Blank leaf

Curriculum vitae

Alessandro Ghielmi

- | | |
|-------------|--|
| 1971 | Born on 9th of August, Milan, Italy |
| 1977 – 1985 | Primary school at the International School of Milan. |
| 1985 – 1990 | Liceo Scientifico Argonne, Milan.
Scientific high school degree with full marks. |
| 1990 – 1995 | Politecnico di Milano.
Degree in Chemical Engineering with full marks and honor. |
| 1995 – 1999 | Doctoral studies at the Chemical Engineering Department,
Swiss Federal Institute of Technology (ETH), Zurich. |

List of publications

1. M.Mazzotti, G.Storti, S.Fiorentino, A.Ghielmi, M.Morbidelli, Kinetics of branching in emulsion polymerization, *5th International Workshop on Polymer Reaction Engineering, DECHEMA Monographs*, **131**, 19-34 (1995)
2. M.Mazzotti, S.Fiorentino, A.Ghielmi, M.Morbidelli, G.Storti, Kinetics of long-chain branching in emulsion polymerization, *Macromol. Symp.*, **111**, 183-193 (1996)
3. A.Ghielmi, S.Fiorentino, G.Storti, M.Mazzotti, M.Morbidelli, Long Chain Branching in Emulsion Polymerization, *J. Polym. Sci.: Part A: Polym. Chem.*, **35**, 827-858 (1997)
4. S.Fiorentino, A.Ghielmi, G.Storti, M.Morbidelli, Nonlinear Chain-Length Distributions in Free-Radical Polymerization, *Ind. Eng. Chem. Res.*, **36**, 1283-1301 (1997)
5. A.Ghielmi, S.Fiorentino, M.Mazzotti, G.Storti, M.Morbidelli, Long Chain Branching and Crosslinking in Emulsion Polymerization, in *Proceedings of the First European Congress on Chemical Engineering*, Vol. 1, 113-116 (1997)
6. A.Ghielmi, S.Fiorentino, G.Storti, M.Morbidelli, Molecular Weight Distribution of Crosslinked Polymers Produced in Emulsion, *J. Polym. Sci.: Part A: Polym. Chem.*, **36**, 1127-1156 (1998)

7. A.Ghielmi, G.Storti, M.Morbidelli, W.H.Ray, Role of Radical Compartmentalization in Chain Branching and Gel Formation in Emulsion Polymerization, *6th International Workshop on Polymer Reaction Engineering, DECHEMA Monographs*, **134**, 327-337 (1998)
8. S.Melis, A.Ghielmi, G.Storti, M.Morbidelli, Aggregation Phenomena in Emulsion Polymerization of Vinyl Chloride, *Entropie*, **212/213**, 65-72 (1998)
9. A.Ghielmi, G.Storti, M.Morbidelli, W.H.Ray, Molecular Weight Distribution in Emulsion Polymerization: Role of Active Chain Compartmentalization, *Macromolecules*, **31**, 7172-7186 (1998)
10. A.Butté, A.Ghielmi, G.Storti, M.Morbidelli, Calculation of molecular weight distributions in free-radical polymerization with chain branching, *Macromol. Theory Simul.*, **8**, 498-512 (1999)
11. S.Forcolin, A.M.Marconi, A.Ghielmi, A.Butté, G.Storti, M.Morbidelli, Coagulation Phenomena in the Emulsion Polymerization of Vinyl Chloride, *Plast., Rubber Compos. Process. Appl.*, **28**, 109-115 (1999)